AN EXPERIMENTAL STUDY IN THE WETTING OF POROUS POWDERS

by

THOMAS ALAN WOOD

A thesis submitted to the University of Birmingham for the degree of

DOCTORATE IN ENGINEERING EngD

School of Chemical Engineering
College of Engineering and Physical Sciences
The University of Birmingham
B15 2TT
UK

Abstract

Manufacture of emission control catalysts involves preparation of concentrated washcoat slurries, which are coated onto monoliths. This thesis considers the early stages of washcoat preparation, involving the wetting and dispersion of highly porous catalyst support powders into suspension.

An optimal geometry for powder incorporation in mechanically agitated batch mixing vessels is found experimentally using a design of experiments approach. The effect on this optimal geometry of increasing solid concentration in the slurry is shown to have a significant impact on the energy required to incorporate powder. Scaling criteria are also suggested to maintain incorporation performance between different scales of mixing vessel. Multivariate regression modelling is used to determine which powder properties are most significant in determining how easily a powder is incorporated into concentrated suspensions.

Two industrial case studies are presented in this thesis. The first involves design and scale up of a continuous powder incorporation process to prepare base catalyst washcoat slurries. This study presents a detailed design for a manufacturing scale production process. The second case study considers a powder mixing process for the pre-treatment of support powders prior to their incorporation into slurry, comparing the efficiency and capability of three separate mixers for this duty.

Acknowledgements

The four years of my EngD have been a great experience and I would like to thank the EPSRC, Johnson Matthey, and the University of Birmingham for the opportunity. I would also like to thank my supervisors Professor Mark Simmons, Professor Hugh Stitt, and Dr Richard Greenwood.

Mark – Thank you for all your ideas and enthusiasm throughout my project. Your help has been invaluable in structuring the project and your feedback for all my writing and presentation has been incredibly helpful. Also thank you for your great company in Quebec, Nice, and all the numerous trips between Birmingham and The Wynyard.

Hugh – Thank you for all your help, ideas, support, enthusiasm and humour over the course of my EngD. I am incredibly grateful for the opportunities you provided for me to get involved with different aspects of the business, which helped show the impact this work could have within the business. Thank you also for your great company, I hope another beer (or two) in the Jesters will be on the cards at some point in the future!

Richard – Thanks for all the beer! Also thank you for all your help, support, and contributions throughout these five years, all of which have been invaluable to helping me through this project.

A big thank you to my friends at Johnson Matthey, without whom I don't think this project could have been anywhere near as fun or as successful. Firstly – Steph, thank you to you, D, and Penny for your friendship, company, ideas, help, and so much more. Also thank you for convincing me statistics isn't boring! Thank you to the JMTC Italians (Michele, Giuseppe, Giuseppe, Domenico, Andrea) for your company, enthusiasm, ideas, and converting me to the brilliance of coffee. Thank you to so many more people at JMTC (too many to mention!) for just being awesome and making it a fun place to be.

Finally thank you to my loved ones. To all four of my parents; Susannah, Frazer, Caroline, and Steve who have helped make me who I am and for their endless support. Lizzie thank you for being my bear!

Contents

List of Figures

List of Tables:

Nomenclature

B – Vessel baffle width

C – Impeller off-bottom clearance (stirred vessel dimensions)

C – Carrs Index (Powder material property)

CoV – Coefficient of variance

D – Impeller diameter

g – Acceleration due to gravity (9.81 $m.s^{-2}$)

G – Greyscale value in image analysis

h – Height of liquid rise for capillary rise measurements

h – Number of latent variables in PLS models for VIP score calculations

H – Hausner ratio

H – Vessel liquid height

H_0 – Initial liquid height

k – Latent variable in PLS models for VIP score calculations

M - Mass

N – Impeller rotation speed

N_{JI} – Impeller speed required to achieve just incorporation condition

P – Impeller power draw

P_{JI} – Impeller power required to achieve just incorporation condition

$\bar{r}$ – Mean capillary radius for contact angle calculation

Re_{JI} – Reynolds number required to achieve just incorporation condition

RMSE – Root mean squared error

s – Standard deviation

S – Impeller submergence

t - Time

T – Tank diameter

V - Volume

X – Solid fraction

X_{max} – Maximum solid packing fraction

Z – Normalised value during Z-score normalisation

α – Impeller tilt angle

γ – Surface tension

$\dot{\gamma}$ – Shear rate

Γ – Impeller shaft torque

θ – Three phase contact angle

μ – Fluid dynamic viscosity

μ_{app} – Apparent dynamic viscosity

$[\mu]$ – Viscosity factor used in Krieger Dougherty equation

ν_k – Variance explained by latent variable k in VIP score calculations

ρ – Density

ρ_T – Powder tapped bulk density

ρ_P – Powder poured bulk density

σ – Standard deviation

σ_C -

τ – Shear stress

ω_{ki} – Covariance weighting of variable i in latent variable k for VIP score calculations

1.

Introduction

1.1. Project Background

1.1.1. History of Vehicle Emission Control Catalysts

The first legislation governing the after treatment of vehicle exhaust emissions was passed in California, USA in 1975, shortly followed by the rest of the USA, Canada, and Japan, as shown in Figure 1-1 (Acres and Harrison 2004). Since then the concept of the catalytic converter has become ubiquitous with the road vehicle, with more than 98 % of cars sold worldwide fitted with a catalyst of some design, amounting to over 50 % of the world demand for platinum group metals (IPA 2014).

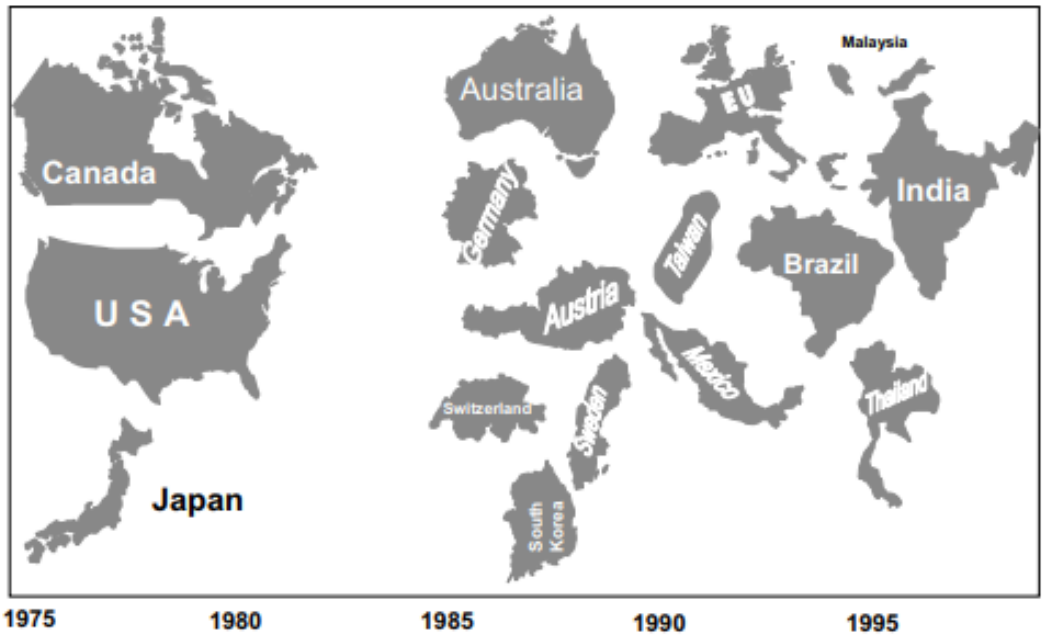

Figure 1-1: Global introduction of vehicle emissions legislation (Acres and Harrison, 2004)

The main reason for this huge increase in use of automotive catalysts is their effectiveness, with harmful vehicle emissions reduced by more than 90 % since 1960 (Twigg 2007). This reduction has tracked ever more stringent legislation regarding the acceptable levels of emissions from road vehicles. Since 1992 the EU has released six emission standards (Euro 1-6), with the most recent

(Euro 6) controlling the acceptable levels of carbon monoxide, NO_x gases, hydrocarbons, particulate matter, and total number of particles (European Commission 2012).

1.1.2. Vehicle Emission Control Catalyst Design

The design and functionality of emission control catalysts is specific to their application. However, the basic structure is that of a metal or ceramic monolith coated with support and active catalyst material sat in the exhaust train, examples of which are shown in Figure 1-2 (Johnson Matthey 2018).

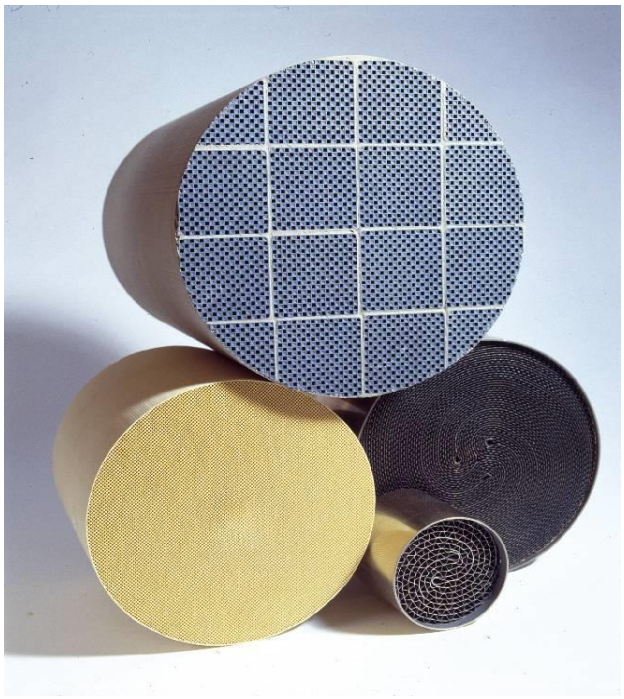

Figure 1-2: Ceramic SiC (top), ceramic flow through (bottom left) and two metallic (front and right) catalyst monoliths (Johnson Matthey, 2018)

There are benefits to either type of monolith; metal monoliths, generally made from Fecralloy® (S. Adegbite 2010) tend to have thinner walls, giving them a lower thermal mass, allowing them to heat up quicker on start-up. This is important because as much as 75 % of harmful emissions are produced in the first few minutes of vehicle operation, before the catalyst sufficiently warms up (Cybulski and Moulijn 2005). Ceramic monoliths tend to be cheaper than metallic monoliths,

generally made from extruded cordierite (Avila *et al.* 2005). Ceramic monoliths also tend to be more porous than metallic monoliths, facilitating better adhesion of the support and catalyst materials to the monolith walls (Agrafiotis *et al.* 1999).

Three-way catalysts, used to reduce harmful emissions from gasoline engines, are based on a honeycomb monolith, with straight channels that air can flow through. These catalysts are responsible for three simultaneous reactions (Acres and Harrison 2004):

Reduction of nitrogen:

$$2NO_x \rightarrow xO_2 + N_2$$

Oxidation of carbon monoxide:

$$2CO + O_2 \rightarrow 2CO_2$$

Oxidation of unburnt hydrocarbons:

$$4HC + 5O_2 \rightarrow 4CO_2 + 2H_2O$$

Treatment of diesel engine exhaust emissions requires more complex catalysts than those for gasoline engines due to the excess levels of oxygen, higher levels of particulate matter, and lower gas temperatures than in a gasoline engine (Twigg 2015). Thus, alternative catalyst technologies have had to be developed for diesel exhaust emissions using combinations of soot filters and NO_x traps. More recently selective catalytic reduction (SCR) catalysts have been developed. These rely on the addition of urea to provide a source of ammonia which is used to reduce NO_x present in the exhaust gases.

The full process of preparing a monolith for use as a vehicle emission control catalyst is described in section 1.3.1. However, at its simplest it involves preparing a catalyst washcoat slurry, which is then coated onto the monolith which is then canned, ready for use in an exhaust train (Avila *et al.*

2005). The formulation of the washcoat slurry can vary dramatically depending on the ultimate use of the catalyst.

Figure 1-3 and Figure 1-4 show SEM and optical micrograph images respectively of a monolith cell wall coated in catalyst washcoat (Cooper 1983).

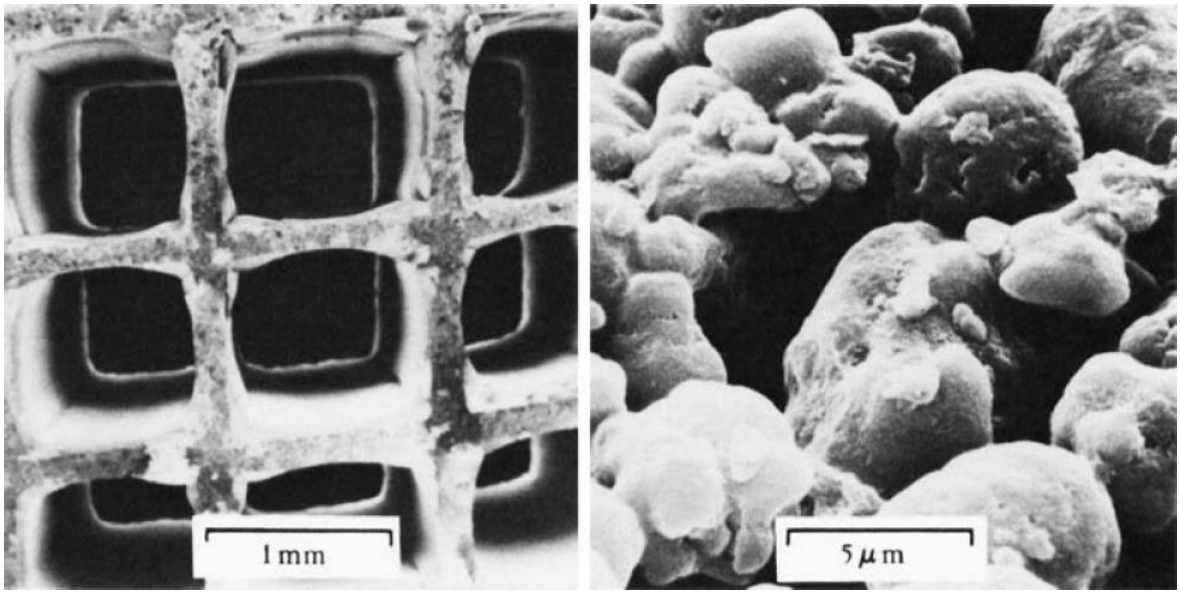

Figure 1-3: SEM images of catalyst washcoat on monolith cell wall (Cooper, 1983)

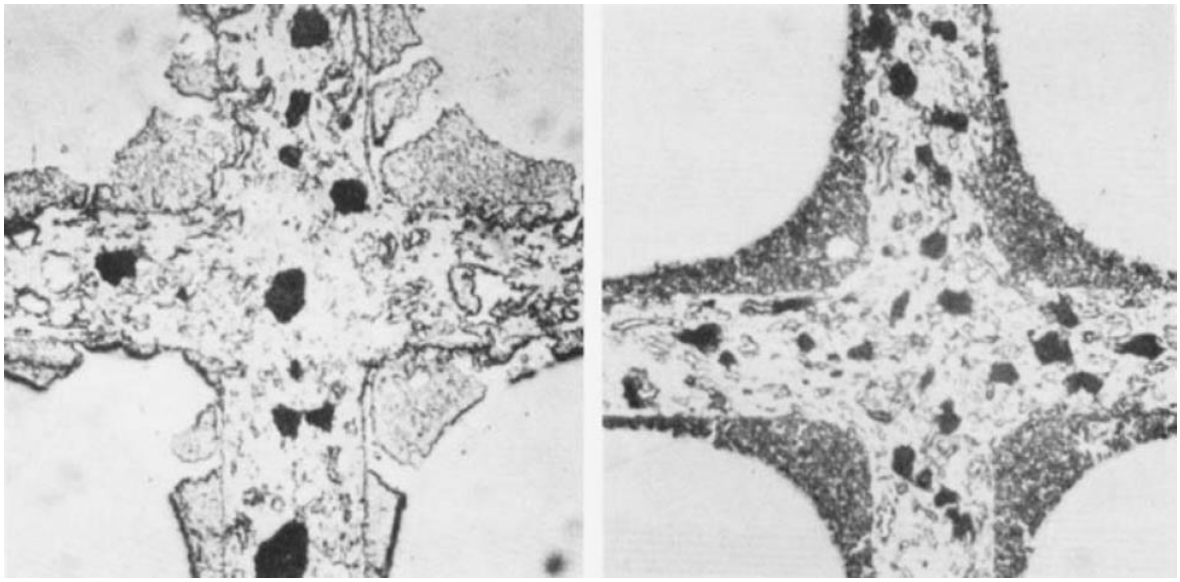

Figure 1-4: Optical micrograph images of catalyst washcoat on monolith cell wall (Cooper, 1983)

1.1.3. Catalyst Washcoat

Ultimately the key quality determining characteristics of a catalyst washcoat are the activity, selectivity, and lifetime of the catalyst produced once it is coated onto a monolith. The impact of the coating on the exhaust backpressure is also of high importance as this inherently affects the compression ratio, and so, the engine performance. These parameters are affected by the thickness and homogeneity of the washcoat coated onto the monolith, the quality of the adherence to the monolith, and the quantity and accessibility of catalytic material loaded into the washcoat. The primary aim in optimising each of these criteria is to maximise the number of active sites presented to exhaust gases as they pass through the monolith (Park and Regalbuto 1995; Agashe and Regalbuto 1997; Spieker and Regalbuto 2001).

Optimal coating of monoliths requires a careful balance of each of these parameters. Excess loading of catalyst material may increase selectivity and activity, but not only would it dramatically increase the cost of the catalyst but it will likely also reduce the quality of adhesion to the monolith, and increase back pressure in the exhaust. Therefore, much of the excess PGM will be lost as the catalyst is loaded during its lifetime on a vehicle (Agrafiotis and Tsetsekou 2000).

This balance of parameters is achieved through formulation engineering in designing and preparing the washcoats used before they are coated onto monoliths. Many of the key properties of washcoat slurries that are controlled to achieve optimal coating and catalyst performance are described below.

1.1.3.1. Support Material

Many different materials are used as the support material initially dispersed into suspension to prepare a base washcoat. The most commonly used support material is γ-alumina. However, other inorganics including α-alumina, silica, titania, and ceria are also used, as are mixed oxides

such as ceria-zirconia and zirconia silicate, and zeolite materials (Bodke *et al.* 1998; McCarty *et al.* 1999; Williams 2001). This thesis primarily focusses on γ-alumina as a main product for study. However, other powders are studied where relevant and important for the sponsor company.

Alumina exists in several polymorphs, with α-alumina being the thermodynamically stable structure at all temperatures up to its melting point (Andersson 2005). However, there are many metastable polymorphs of alumina, examples of which include η-alumina and γ-alumina, both of which have found use as catalyst supports (Maciver *et al.* 1963).

γ-alumina is highly effective as a catalyst support material due to its high surface area, 204 $m^2 g^{-1}$ compared to 40 $m^2 g^{-1}$ for α-alumina (Maciver *et al.* 1963; Kiyohara *et al.* 2000), high porosity, and high thermal stability, all of which make it ideal as a support in automotive applications (Musil *et al.* 2010). The structure of γ-alumina is considered as a cubic defect spinel type. In this the oxygen atoms are in close cubic packing, with the aluminium atoms occupying the tetrahedral and octahedral sites (Samain *et al.* 2014), as shown schematically in Figure 1-5 (Ionescu *et al.* 2002).

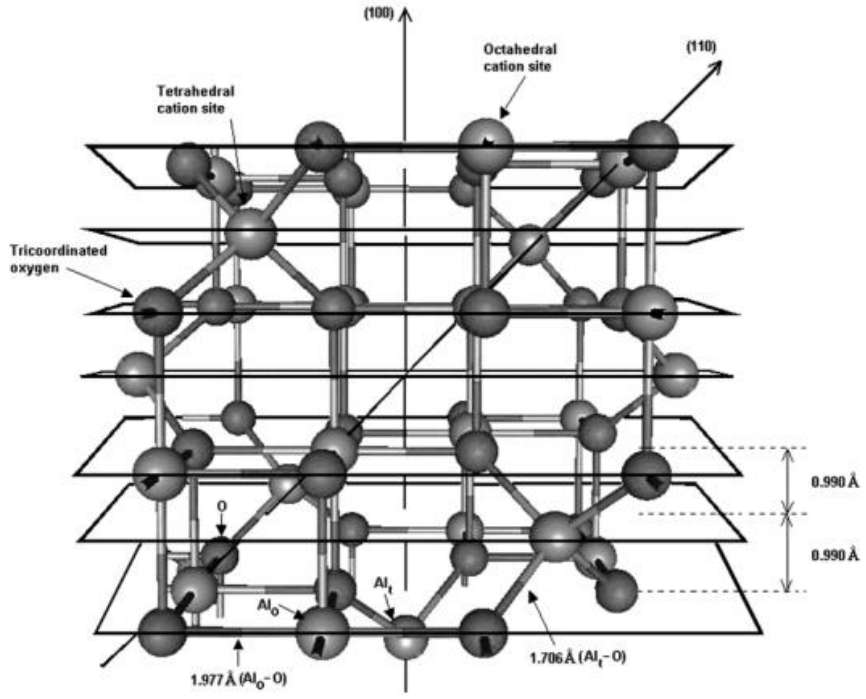

Figure 1-5: Schematic of γ-alumina structure (Ionescu et al., 2002)

1.1.3.2. Particle Size Distribution

The particle size distribution of support material particles in a catalyst washcoat slurry plays a hugely important role in determining both the adhesion of the washcoat to the monolith walls and the performance of the final catalyst (Germani *et al.* 2007; Jia *et al.* 2007). Adhesion is shown to improve with decreasing particle size, this is why it is important to mill the initial slurry prepared by addition of the support material to liquid (Agrafiotis *et al.* 1999). This milling action can be affected through a variety of methods including ball milling (Yang *et al.* 2015), bead milling (Nam *et al.* 2011), and jet milling (Chauruka *et al.* 2015). However, the milling stage of the washcoat preparation process is not studied in this thesis.

Particle size can be measured through a number of different techniques. One of the most common methods is laser diffraction, for example using a Malvern Mastersizer (Malvern, UK). This technique measures the angular variation in the intensity of a laser beam scattered as it passes through dispersed particles. Small particles scatter light at large angles, whereas larger particles scatter light at much lower angles (Eshel *et al.* 2004). Other optical techniques are used to measure particle size. For example, the Sympatec QICPIC (Sympatec GmbH, Germany) measures the area of silhouettes cast by pulsed visible light. Focussed beam reflectance measurement (FBRM) uses a rotating laser beam to measure linear distances across particles. FBRM is described more in section 4.3.1.3.3.

These techniques will not give identical results, however they will generally show similar trends when comparing powders (Bontha *et al.* 2000). Much of this discrepancy between techniques comes from the fact that each is applying characteristics of a sphere to an inherently non-spherical object. This is reflected in the variety of ways in which particle size can be presented. The most common nomenclature for describing particle size is to use D_{10}, D_{50}, and D_{90} values. These represent sphere equivalent diameters (i.e. the diameter of a sphere with the same volume

as the particle measured) below which 10 %, 50 %, and 90% of the particles measured fit. This can be weighted by the number of particles or the volume of particles, depending on whether it is preferable to have high resolution at the small size fraction (number) or the large size fraction which dominate the solid volume (volume) (Kemper and Rosenau 1986). In this thesis all particle size measurements quoted are volume weighted.

1.1.3.3. Slurry Properties

There are a number of washcoat slurry properties that are key to determining coating and adhesion quality. Some of the most significant properties include the support material solid content, pH and rheology (Agrafiotis and Tsetsekou 2000; Cybulski and Moulijn 2005; Germani *et al.* 2007; Jia *et al.* 2007).

The solid concentration of the washcoat is important, with higher solid concentrations giving better coating adhesion to the monolith (Mogalicherla and Kunzru 2011). However, the solid concentration has a significant impact on other aspects of the slurry. For example, increasing solid concentration has a very significant impact on the slurry rheology. This was investigated by (Krieger and Dougherty 1959) who showed that the apparent viscosity of a slurry can be modelled by the following equation:

$$\frac{\mu}{\mu_0} = \left(1 - \frac{X}{X_{max}}\right)^{-[\mu]X_{max}} \quad (1)$$

where μ_0 is the viscosity of the liquid medium, in this case water, X is the volumetric volume concentration of solid, X_{max} is the maximum packing fraction and [μ] is a viscosity specific to the size, shape, and type of particles being studied.

Washcoat viscosity is also affected by the pH of the slurry. This is partly due to the nature of metal oxides to develop surface charges when suspended in aqueous suspension (Brunelle 1979; Brown *et al.* 1999). These surface charges change how individual particles interact with one

another as they are forced past one another as the fluid flows (Kumar *et al.* 1975). This charge is often measured as the zeta potential, i.e. the electrokinetic potential at the slipping plane, the radius from a particle at which ions are not electrostatically bound to the particle (Hunter 2013). The iso electric point (iep) of a slurry is the pH at which the zeta potential is zero. At this point particles can become very close and bind at the double layer, causing gelling of the slurry. This dramatically increases the slurry viscosity; generally making it un-processable (Gulicovski *et al.* 2008). The iep of γ-alumina slurries is generally regarded as being at pH 7.7-7.9 with the pH for best suspension found around pH 3.8 – 4.5 (S. A. Adegbite 2010).

The slurry rheology is critically important to coating performance. The slurry must be thin enough that during the coating process it can be evenly distributed across the entire monolith, whereas it must also exhibit a yield stress or sufficiently high apparent viscosity that it does not simply flow off whilst the monolith is being dried. Therefore it is essential that all of the above parameters are carefully controlled during washcoat preparation to ensure good quality coating onto the monolith is achieved. For the washcoats studied in this thesis the most common product is a γ-alumina with a solid concentration of 50 wt% and pH in the range of 4 – 4.5.

1.2. Company Background: Johnson Matthey plc

Johnson Matthey plc (JM) is a leading science and technology company with a core focus in precious metals, catalysis, and process technology. JM is a FTSE 100 company with more than 14,000 employees across 30 sites in North America, Europe, and Asia. In 2017/18 JM had a revenue of £3.85 billion (excluding precious metal sales) and an underlying profit of £525 million (Johnson Matthey 2018). JM operates in a number of sectors, including emission control technologies, process technologies, novel materials, pharmaceuticals, and battery technologies split across its four main divisions. During the course of this project JM underwent a major business restructuring, with divisions moving and changing. Each of the new sectors is described below, with reference to previous structure where relevant to this thesis. The work for this project was carried out within Johnson Matthey Technology Centre (JMTC), a centrally funded research centre that works with and for all business divisions.

1.2.1. Clean Air

The Clean Air sector, previously Emission Control Technologies (ECT), focusses on applications of catalysts for reducing emissions from vehicles and other sources. Primarily the Clean Air Division produces catalysts for the automotive industry, including light duty vehicles and heavy duty diesel catalysts. Johnson Matthey has supplied one third of all automotive emission control catalysts ever made (Acres and Harrison 2004). Clean Air also produce stationary emission catalysts for reducing emissions in industrial effluent flows, such as during energy generation and storage.

The Clean Air division is the primary funder within JM for this EngD project, with the main focus on the manufacturing process for both light duty vehicles and heavy duty diesel catalysts, as described in section 1.3.1.

1.2.2. Efficient Natural Resources

The Efficient Natural Resources (ENR) sector in JM focusses on using advanced science and technology to achieve greater efficiency and yields in the use of natural resources. The main areas of ENR include:

- *Catalyst Technologies* with a focus on supply of catalysts and licences processes to the petrochemical and process industries, specialising in applications including hydrogen plants, ammonia production, methanol synthesis, formaldehyde, biorenewable synthesis of bulk chemicals, Fischer-Tropsch, etc.
- *Platinum Group Metals Services* with a focus on refining and recycling of platinum group metals (PGMs), producing PGM based products such as salts, wires, sheets etc., and precious metal management services.
- *Advanced Glass Technologies (AgT)* with a focus on production of functional glass-based materials, primarily for the automotive glass, electronic, and tableware sectors. Main products include black obscuration enamels for use in the automotive sector, coatings, precious metal inks, and decorative enamels.
- *Diagnostic Services* through Tracerco, a world leading detection, diagnostic, and measurement business, primarily serving the oil and gas industry.

1.2.3. Health

The Health sector of JM is involved in many stages of pharmaceutical production. The main areas where JM operates in this sector include production of complex active pharmaceutical ingredients (APIs), supply of catalysts for the pharmaceutical industry, and in providing the solid form and particulate engineering expertise required to tackle challenges in scale up and product development.

1.2.4. New Markets

The New Markets sector of Johnson Matthey is a focus for future major growth areas for the business. The main sectors of focus for New Markets include alternative powertrain technologies for vehicles, such as battery materials, battery technologies, and fuel cells. JM is the world's leading manufacturer of Fuel Cell catalysts and membrane electrode assemblies as well as one of the leading manufacturers of battery cathode materials.

1.3. Formulation Processes Studied

As stated in section 1.2.1 the main driver for this EngD project came from the Clean Air business, specifically in the vehicle emission control catalyst area. Therefore, the main focus of this project considered manufacturing processes and materials specific to this division, as described in section 1.3.1. However, it was recognised than many of the learnings and developments for Clean Air products and processes during this project were transferrable to other business units, one of the major benefits of operating in a central research centre in JMTC. Therefore, work was also carried out as part of this project studying the manufacturing process of an automotive obscuration enamel for AgT and for fluid catalytic cracking additives for INTERCAT, an operating unit within the catalyst technologies business within the ENR sector.

The existing manufacturing processes for each of these products are described below.

1.3.1. Vehicle Emission Control Catalysts

Figure 1-6 shows a process flow diagram describing the basic process of preparing a vehicle emission control catalyst.

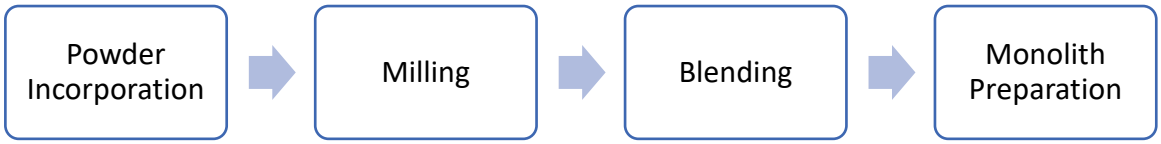

Figure 1-6: Process flow diagram for production of emission control catalyst

The initial stage of the process, known within the business as 'batching', involves the incorporation of dry powdered support material into a slurry. This slurry generally contains between 40 – 50 wt% solid material and is prepared in large stirred tanks of various design across the business. The specific formulation is highly dependent on the final application of the catalyst being produced. The main support materials added at this stage include γ-alumina and zeolite powders. However, other support materials such as α-alumina or mixed oxide powders (ceria, zirconia, etc.) may also be added. Generally the liquid phase is deionised water, into which a pH modifier is usually added: often acetic acid or ammonium hydroxide to adjust the pH downwards or upwards respectively. This pH modifier is added to ensure the solution stays away from the isoelectric point of the slurry: preventing gelling of the slurry which would make it un-processable or that the pH falls too low leading to peptisation and dissolution (denaturing) of the alumina. This stage has classically been seen as the 'cheap' end of the process, as it is before any of the high value active catalyst compounds are added to the slurry. Therefore, it has seen less innovation within JM than latter stages of the manufacturing process. This stage is the main focus for this EngD project.

This initial slurry is then milled to reduce the particle size of the support material in suspension. Again, the level of milling is highly dependent on the formulation and final application of the product but generally the solid phase is milled from a D_{50} of particle size of 50 – 100 µm to <<10 µm. Across the business this process is done in-situ (i.e. in the same vessel as the batching occurred), in recirculation mode, where the slurry is repeatedly pumped from a storage tank through a mill until the desired specification is reached, and in single pass mode, where the slurry is pumped from the batch tank to a storage vessel through a milling operation, which each element of the slurry only passes through once. This slurry is known as 'base washcoat'

The base washcoat product of the milling process is then mixed with the active catalyst components, such as platinum, palladium, and rhodium, in a large batch stirred vessel with a high shear impeller. Other components may also be added at this stage including rheology modifiers, to ensure the slurry has the correct rheology for coating, and pH adjusters.

The final washcoat slurry following blending is coated onto monoliths in a continuous coating production line. In this line slurry is added to the monoliths and drawn inside the matrix of the structure. This is then dried to remove the water from the slurry before being calcined to break down the precursors (nitrates, organic acids) and to improve adhesion of the support and catalyst materials to the monolith.

1.3.2. Automotive Glass Enamel

The highest volume product made by AgT is a black enamel used in the automotive industry on windscreens to protect the glue used to adhere windscreens to vehicles from UV degradation as well as to obscure the electrical connections associated with heated windshields and automated wiper control. Figure 1-7 shows a simple process flow diagram for the manufacturing route used to prepare this product. Initially the raw materials are prepared: These are a powdered glass frit and pigment, made by powdering glass, which is then roll and jet milled to give fine particles. The

solvent is prepared through synthesis of a complex organic mixture, primarily composed of pinene oil.

Following this the powder is added to the solvent in a batch mixing vessel to a solid concentration of 80 wt%. This mixing vessel uses a complex 'butterfly' impeller geometry to deliver high shear to break up clumps of powder, whilst operating at a low power number in the highly viscoelastic slurry made at these high concentrations (Ramsay *et al.* 2016).

After the slurry is prepared the suspension is the passed twice through a triple roll mill to reduce the maximum particle size, a key quality determining parameter of the final enamel mixture.

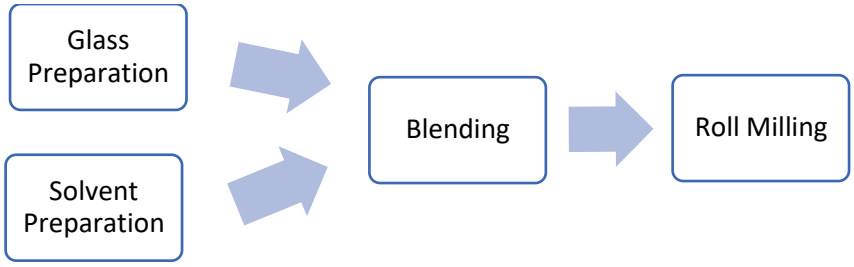

Figure 1-7: Process flow diagram for production of automotive glass enamel products

1.3.3. Fluid Catalytic Cracking Catalysts

INTERCAT produces spray dried products that are used as additives (impurity and catalyst poison scavengers) in fluid catalytic cracking (FCC) reactors. Figure 1-8 shows a simple process flow diagram describing this manufacturing process for one of the main products. Initially magnesia and alumina slurries are prepared in batch mixing vessels to solid contents of 14 wt% and 30 wt% respectively. Following this the two streams are pumped to a very large (8 m^3) mixing vessel, where the mixture is heated to near 100°C, at which temperature the magnesia and alumina react to form a hydrotalcite (magnesium aluminate) -like product (HTLp) structure. The HTLp is blended with further functional components and the concentration (and rheology) are adjusted to allow the product to be spray dried; the final product form.

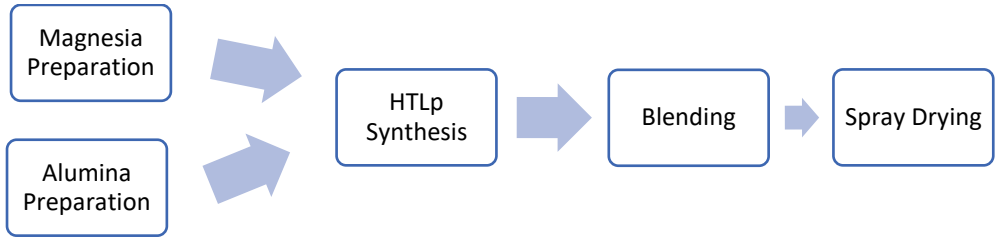

Figure 1-8: Process flow diagram for production of FCC catalysts

1.4. Business Case

There are multiple areas where an increased scientific understanding of the processing stages in wetting porous powders is advantageous for Johnson Matthey:

- As already shown, a wide range of products and processes within JM contain a powder incorporation stage, where a slurry or suspension is prepared by addition of powder to liquid. Often this is not deemed a high value process and so has generally seen little attention for research and development programmes in the past. However, multiple JM facilities are production limited due to the space required for the large batch mixing vessels used for this duty, which can take exorbitantly long amounts of time relative to the rest of the process. Any improvement and optimisation of these stages of manufacture can lead to reductions in the equipment footprint, energy requirement, or time requirement for this stage, leading to a reduction in manufacturing costs and/or an increase in manufacturing capacity and, therefore, increased profit.
- Due to the similar nature of many JM processes learning from one product/process can be applied to a wide variety of products across the entire company, facilitating knowledge transfer between different manufacturing groups and increasing the impact of this study.

Academically this project is part of an important relationship between the University of Birmingham and Johnson Matthey, building on previous EngD and PhD projects. Journal papers

and conference presentations arising from this project demonstrate the impact of this work to the wider scientific community.

1.5. Thesis Objectives

- To use experimental techniques to deliver scientific understanding of powder incorporation processes. Including:
    - How powder drawdown and incorporation scales from the laboratory to production scale in stirred vessels;
    - Understanding of how changes in the slurry affect processing as the slurry becomes more concentrated;
    - Understanding of how various powder properties affect their behaviour when being wet.
- Deliver a step change in manufacturing processing to increase the output of powder incorporation processes.
- Describe the design space and optimisation criteria for a range of powder wetting processes, including an understanding of scale up from laboratory to manufacturing scale.
    - Powder drawdown and incorporation in stirred vessels;
    - Incipient wetness impregnation of dry powder with catalyst solution.

1.6. Structure of the Thesis

This thesis is split into four main sections. Initially the existing Clean Air batch drawdown and incorporation mixing vessel is studied to deliver scientific understanding and optimisation criteria in Chapters 2 and 3, these Chapters are related and should be treated as a pair. In Chapter 4 a step-change in manufacturing from batch to continuous operation is designed and scaled up and presented as an industrial case study. Chapter 5 describes an exploratory study based on observations in Chapters 2-4 that different powders behave significantly differently on wetting. This Chapter is designed to inform and improve all results and recommendations delivered in Chapters 2-4. Chapter 6 is a detailed optimisation and comparison of three techniques available for the incipient wetness impregnation of dry powder. This is separate to the previous Chapters which all focus on adding solid as a disperse phase to a liquid continuum, whereas this Chapter focusses on adding liquid to a solid continuous phase. However, readers unfamiliar with the concepts of multivariate statistics are advised to read Chapter 5 before this Chapter, where the background and principles of these techniques are described. A roadmap for this thesis is presented in Figure 1-9.

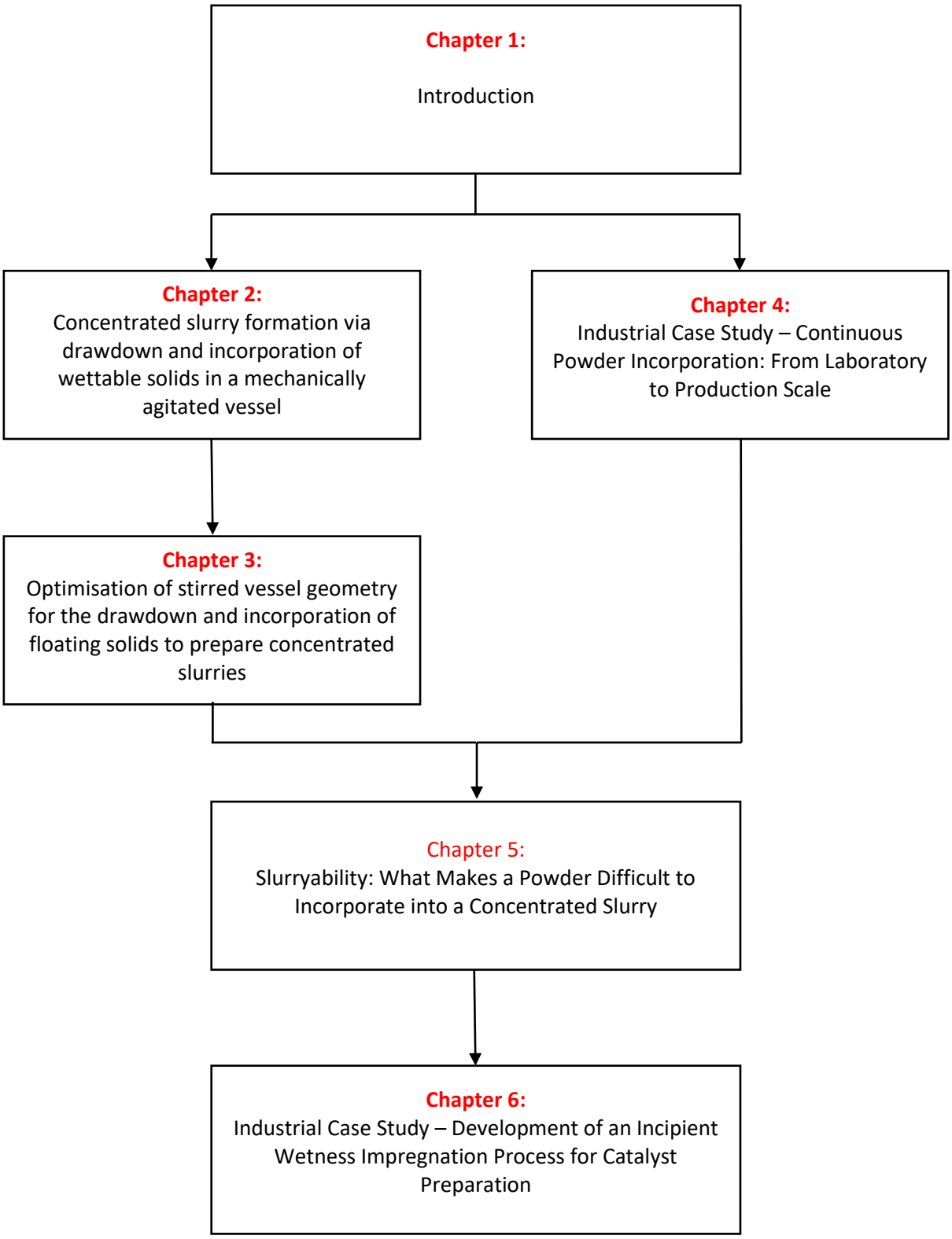

Figure 1-9: Thesis roadmap

1.7. List of Publications and Conferences

Publications (chronological):

a. Wood, T., Simmons, M. J. H., Greenwood, R. W. and Stitt, E. H. (2018), Concentrated slurry formation via drawdown and incorporation of wettable solids in a mechanically agitated vessel. AIChE J., 64: 1885-1895. doi:10.1002/aic.16121

b. Wood, T., Simmons, M. J. H., and Stitt, E. H. (2018), Optimisation of stirred vessel geometry for the drawdown and incorporation of floating solids to prepare concentrated slurries. ChERD, 133: 70-78. doi: https://doi.org/10.1016/j.cherd.2018.03.002

c. Wood, T., Simmons, M. J. H., Greenwood, R. W., Turnbull, S. A., Stitt, E. H. (2018), Slurryability: What Makes a Powder Difficult to Incorporate into a Concentrated Slurry. **Submitted for review**

Conferences (Chronological)

a. 10th European Congress of Chemical Engineering; held at Nice, France, 27th September – 1st October 2015.

b. Mixing XXV North American Mixing Forum, held at Quebec City, Canada, June – July 2016.

c. 9th International Symposium on Mixing in Industrial Processes, held at Birmingham, UK, 25th June – 28th June 2018.

2.

Concentrated slurry formation via drawdown and incorporation of wettable solids in a mechanically agitated vessel

This Chapter describes the effect of vessel configurations upon the drawdown and incorporation of floating solids to prepare concentrated alumina slurries in stirred tanks. The impeller speed and power draw required to incorporate all dry powder within four seconds, N_{JI} and P_{JI}, are used to evaluate incorporation performance. The effect of impeller type is assessed, with pitched blade impellers proving to be the most effective across the full range of solid contents considered.

At higher solids content the energy demand is shown to increase dramatically, with a 100-fold increase in energy required to add 1% w/w more solid at 50% by weight compared to 1% by weight. Analysis of impeller power numbers show this coincides with a transition from constant power number to a region where power number increases linearly with decreasing Reynolds number. Contrary to studies at low solids content, the presence of baffles is shown to inhibit drawdown.

2.1. Chapter Preface

This Chapter is published in the American Institute of Chemical Engineers Journal (AIChE J) in the following paper (Wood, Simmons, Greenwood, *et al.* 2018):

Wood, T., Simmons, M. J. H., Greenwood, R. W. and Stitt, E. H. (2018), Concentrated slurry formation via drawdown and incorporation of wettable solids in a mechanically agitated vessel. AIChE J., 64: 1885-1895. doi:10.1002/aic.16121

2.2. Introduction

The drawdown of floating solids is a widely-used operation across the process industries, whether for dissolution, reaction or simple suspension involving the incorporation of solid into liquid. The process of incorporating solids into liquid can include some or all of the following steps, depending on the specific properties of the particles and unit operation in question (Freudig *et al.* 1999):

1. Wetting
2. Drawdown or submersion of the particles
3. Dispersion
4. Off-bottom suspension
5. Deagglomeration
6. Dissolution

Due to the nature of the system the solid may float for a number of reasons (Waghmare *et al.* 2011). The first and most obvious of these is the case where the solid has a lower density so the buoyancy force upon the solid particles will be greater than the gravitational settling force and cause them to float. Drawdown of these particles is a steady-state phenomena and thus they will rise back to the surface if agitation ceases. Another possibility is that an agglomerate containing

multiple particles with a solid envelope density higher than the liquid may have a lower bulk (overall) density than the liquid due to trapping of air between individual particles. Finally, high liquid surface tension or poor solid wettability leads to a high interfacial tension, which can result in sufficient force to overcome the gravitational settling force. In the case of these latter two phenomena, which can both occur simultaneously, incorporation is an irreversible process as the particles will be dispersed into suspension and will not rise to the surface unless the first case is also true.

Previous studies (Joosten *et al.* 1977; Hemrajani 1988; Thring and Edwards 1990; Takahashi and Sasaki 1999; Özcan-Taşkin and McGrath 2001; Özcan-Taşkin and Wei 2003; Özcan-Taşkin 2006; Khazam and Kresta 2009) have largely focussed on finding an optimum geometry or set of conditions to achieve the most effective drawdown performance. This performance is generally measured by observation as the impeller speed to just drawdown the particles (N_{JD}), ensuring that none spend longer than four seconds on the vessel surface (Khazam and Kresta 2008). This is analogous to the Zwietering condition used in the suspension of sinking solids (Zwietering 1958). Although it is possible to make this analogy, it is worth noting the abundance of literature available studying the suspension of solids, whilst there is a relative dearth of works looking at the incorporation of floating solids. This is likely because the deformable free surface at the top of a stirred vessel significantly complicates the situation compared to the vessel bottom. Particles also have a tendency to clump and agglomerate when not dispersed in a continuous phase, which can significantly complicate the force balance on the solid (Xie *et al.* 2007).

All these previous studies conclude that radial impellers are not effective for the drawdown of floating powders, being outperformed by axial and mixed flow impellers; this is another similarity to work on suspension. Generally, mixed flow pitched blade impellers (PBTs) outperform hydrofoils and other axial flow impellers, with the majority of focus on down-pumping mode of

operation. Özcan-Taşkin *et al* (2006) show that up-pumping impellers required a significantly lower power to achieve the same drawdown performance as down-pumping impellers. This is attributed to the different drawdown mechanisms, with stronger surface turbulence giving drawdown with the up-pumping mode compared to the large vortex or recirculation loops for the down-pumping mode. Khazam and Kresta (2008) also suggested different mechanisms of drawdown including the central vortex; which was shown to trap solids just below the liquid surface, turbulent engulfment; where eddies pull particles into the flow, and mean drag; where strong liquid circulation drags particles to the walls or impeller shaft where they are drawn down. Turbulence is shown to be the main mechanism of drawdown for low submergences and mean drag for higher submergences for both up and down pumping impellers.

There is a general consensus amongst previous work that baffles improve drawdown performance, although there is some variation in choice of baffle type. Hemrajani (1988) recommended the use of four full length narrow baffles with width B/T of 0.02. Özcan-Taşkin and McGrath (2001b) show that four full baffles out perform a single or two baffles, as did Karcz and Mackiewicz (2009), specifically for up-pumping impellers. Khazam and Kresta (2009) developed a novel geometry specifically for drawdown with four surface only baffles, which increase surface turbulence. This was done to promote drawdown whilst minimising recirculation flows lower in the vessel, greatly reducing the power requirement for drawdown. Siddiqui (1993) also recommended the use of surface only baffles, but used three rather than four.

Many researchers have considered the effect of impeller diameter, specifically the impeller diameter to tank diameter ratio (D/T). Özcan-Taşkin and Wei (2003) demonstrated that impellers with a D/T of 0.33 required a higher impeller speed than larger impellers to achieve the same drawdown performance, but achieved this at lower power draw. This was true except for cases where the larger impellers drew a very large vortex, where the air entrainment lowered the

power draw of the impeller. Khazam and Kresta (2009) found that larger impellers (D/T = 0.5) outperformed smaller ones both in terms of N_{JD} and P_{JD} for their system involving slightly higher solid contents.

Scale up of mixing duties generally considers measurements made by keeping geometric similarity between two scales and comparing the measured data whilst maintaining constant dimensionless numbers. These dimensionless numbers show the difference between the relative importance of the impeller diameter (D) and impeller speed (N) (Stitt 2016). Hemrajani (1988) and Joosten *et al.* (1977) both considered the effect of scaling on low solid content drawdown processes using a down-pumping PBT with specific baffling; using one or two surface only baffles. Both works conclude that scaling at constant Froude Number is the most reliable method to predict scale up. Özcan-Taşkin (2006) studied the scale up of a drawdown process from T = 0.61 m to T = 2.67 m for both up- and down-pumping impellers. They found that Froude Number was the most accurate predictor for down-pumping mode, although only within ±30% and it could not predict effects of other geometric parameters. Constant power per unit volume was shown to be the best predictor for upward pumping impellers.

Most information available in the literature focuses on cases with low solid concentrations of low particle density solids, as this is the simplest case for drawdown and most likely to give meaningful correlations. This allows measurement of N_{JD} and P_{JD} at steady state. Khazam and Kresta (2009) considered the effect of increasing the amount of solids present in the system, up to a maximum of 10 % by volume, using expanded polystyrene. They demonstrated a significant increase in N_{JD} from 2 % to 10 % although trends between impeller types were preserved as the solid content increased with both up- and down-pumping impellers requiring a similar increase in impeller speed. The solids studied were non-wettable, low density solids so it was not possible to ascertain the effect of incorporated solids at higher solid contents.

The effect of solid concentration on rheology has been shown to be very significant. For rigid spheres the relative apparent viscosity of suspension increases exponentially with increasing solid concentrations up to the maximum packing fraction according to the Krieger Dougherty model (Krieger and Dougherty 1959). Concentrated monodisperse suspensions of spherical particles have also been shown to display yield stresses above volume concentrations of 0.5 (Heymann *et al.* 2002). Both these phenomena have been shown in less regular solid suspension, although the degree to which they occur and point of onset highly depends on the type, shape and size of the particles considered (Mueller *et al.* 2010).

In this paper, the drawdown of floating solids up to 50% weight is studied for five different common impeller types at two scales (5 L and 25 L, a five-fold volume increase) and four different baffle geometries. A similar approach to many of those works described above is used. However, rather than low true density particles and steady state drawdown conditions, alumina powder is used; for which drawdown and wetting is an irreversible process as the powder is incorporated into a slurry. The alumina powder is porous and floats initially on the liquid surface and must be mechanically drawn down and incorporated. Once this happens the impeller disperses agglomerates, freeing trapped air and the pores fill with fluid. Once fully incorporated the powder sinks if agitation ceases. This allows measurement at increasing solid contents as the concentration of the slurry is increased, demonstrating both the effect of higher solids on drawdown and interactions between solid content and impeller or geometry choice. The novelty and importance of this study is that it enables understanding of industrially relevant slurry systems where the drawdown of floating powders acts as a significant technical challenge in formulation preparation. For example; many coating formulations such as decorative paints, catalyst washcoats and fuel cell electrodes commonly use high solid content slurries, often up to and above 40 wt%.

2.3. Experimental

Two scales of flat bottomed cylindrical vessel with diameters, T = 0.17 m (5 L) and T = 0.32 m (25 L) were used in this study. These were both filled to an initial height, H = T, geometrical parameters are shown in Figure 2-1. At the smaller scale, five different impellers were used with Torrance sawtooth and 6 bladed Rushton disc turbine (RDT6) impellers as example radial flow impellers, up- and down-pumping pitched blade impellers (UP-PBT4 & DP-PBT4) as mixed flow impellers and a down-pumping Lightnin A310 hydrofoil as a purely axial flow impeller as shown in Figure 2-2 (Post Mixing Optimizations and Solutions 2017). Four baffle configurations were considered: unbaffled, full, surface and bottom half. In all configurations with baffles the baffle width, B/T = 0.1. At the larger scale only the unbaffled case was considered for up-and down-pumping PBTs. The effect of moving the impeller to an eccentric (off-axis) position by 0.1T was also considered as a way of reducing full body rotation without using baffles (Hall *et al.* 2005).

For all five impeller types, three sizes of impeller were used, corresponding to a D/T of 0.25, 0.33 and 0.5. The impeller blade thickness was kept constant between scales at 1 mm. The effect this has on power number has been shown to vary for impeller type, being significant for RDT impellers although not for PBT impellers (Chapple *et al.* 2002). However, this effect will be minimal with the relatively small change in scale, especially compared to the significant change in power draw due to changing solid content.

The majority of results presented are for unbaffled, centrally mounted impellers with an initial submergence, S_o of 0.5T unless otherwise stated. Submergence is measured to the middle of the impeller, as shown in Figure 2-1.

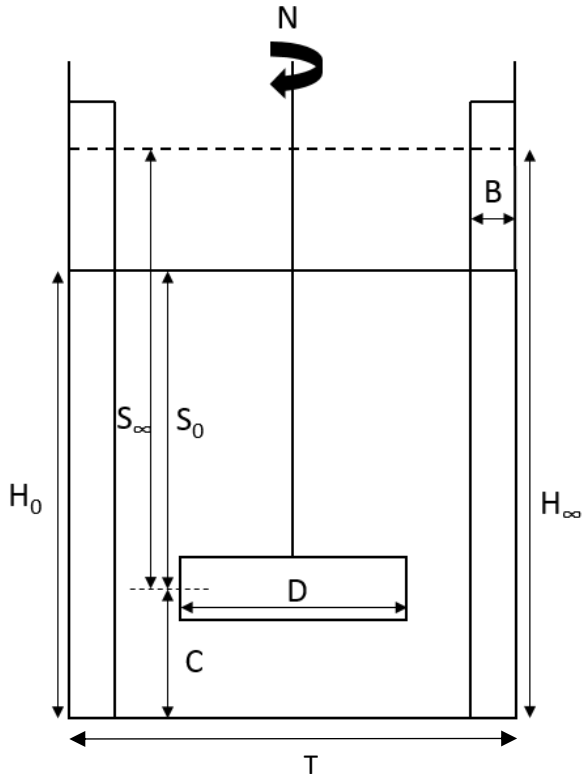

Figure 2-1: Vessel Schematic

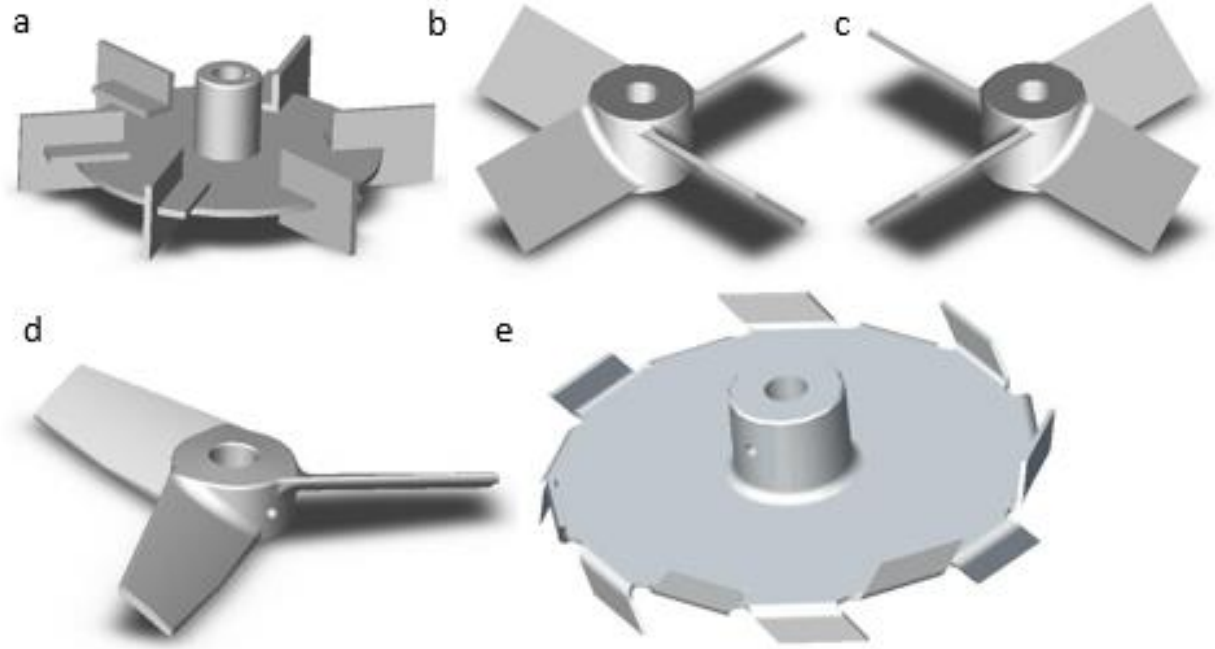

Figure 2-2: Selection of impellers studied. 6 bladed Rushton disc turbine (a), down pumping pitched blade (b), up pumping pitched blade (c), Lightnin A310 hydrofoil (d) and sawtooth impeller (e) (Post Mixing Optimizations and Solutions, 2017)

To give an initial fill height of H = T the vessel was filled with 3.86 L solution at the small scale and 25.7 L at the large scale. An equal mass of solid was used to give a final solid concentration (X) of 50 % w/w. The solid used was Sasol Puralox SCFa-140, a γ-alumina, added up to 50 % in 50 aliquots, this allowed measurement at increasing solid concentration. These aliquots were 77 g at the small scale and 514 g at the larger scale and were prepared prior to the start of the experiment using a KTron KT20 loss in weight powder feeder set to deliver a fixed mass. Solid was added in this manner to give sufficient measurements to show the effect of increasing solids content. It also ensured enough solid was added in each aliquot to completely cover the liquid surface when the impeller was at rest. Each aliquot was added quickly all in one motion to the centre of the vessel, by adding in this way the powder spread on hitting the surface to cover the entire surface. The alumina is a porous ceramic material and initially floats on the liquid surface. However, once wetted and fully incorporated, if the slurry is not agitated, the solid will sediment to the bottom of the vessel, rather than return to the surface. Properties of the powder are given in Table 2-1. Full details on the measurement of these properties is given in section 5.3.1, where powder characterisation for all powders studied in this thesis is described.

Table 2-1: Properties of γ-alumina used in study

Powder Name	d_{10} (μm)	d_{50} (μm)	d_{90} (μm)	Skeletal density (kg m^{-3})	Poured density (kg m^{-3})	Tapped density (kg m^{-3})	Mean pore size (A)	Pore volume ($cm^3 g^{-1}$)
γ-alumina 1	4.02	18.8	39.3	3352	662	793	107	0.415

The powder envelope density, defined as the density of a particle, including the skeletal mass and porous volume, can be estimated from the pore volume and the skeletal density by calculating the ratio of pore volume to solid volume in a fixed mass of solid. For this specific powder the envelope density is approximately 1400 kg m^{-3}. This means that, in the absence of surface tension forces or inter-particle occluded air in agglomerates the particles will be negatively buoyant and

sink with time. It also means the volume concentration of fully incorporated solid will be less than the weight concentration (41.7 vol% at 50 wt%).

The maximum packing fraction for this specific powder can be estimated as the ratio between the tapped bulk density and the envelope density, assuming the powder is approaching maximum packing when fully tapped. This gives a maximum packing fraction at 56.5 % for this specific powder. It is worth noting that the powder is unlikely to be perfectly at maximum packing when tapped so the fraction is likely to actually be slightly higher than this.

The liquid used in these experiments was a dilute (initially 6 % by weight) aqueous acetic acid solution to give a final (50 wt%) slurry pH of <5. This was required to prevent the pH approaching the isoelectric point of the slurry at high solids content; this would have a very significant impact on the viscosity, causing the slurry to gel and so it was necessary to avoid this. The isoelectric point for the γ-alumina is in the range 7.7 - 7.9 (S. A. Adegbite 2010).

The point at which the solid is just drawn down and incorporated was measured visually by observing the point at which no solid remains dry on the liquid surface for longer than four seconds. This operating condition is termed *Just Incorporated* (N_{JI}) and is similar but distinct from the *Just Drawdown* (N_{JD}) condition reported in other works (Joosten *et al.* 1977; Hemrajani 1988; Thring and Edwards 1990; Takahashi and Sasaki 1999; Özcan-Taşkin and McGrath 2001; Özcan-Taşkin and Wei 2003; Özcan-Taşkin 2006; Khazam and Kresta 2009). This distinction is made as, in this case N_{JI} does not represent a steady state condition as once the powder is incorporated it will not become dry and float again, as is the case with solids in previous studies.

The H/T in the vessel increased as solid was added to a maximum of approximately 1.2 at 50 % by weight of solid. Thus, the submergence of the impeller increased throughout the duration of the experiment and so a control was carried out to determine the extent to which any effects seen at high solids were caused by the solid content, rather than the increased submergence. To do this,

N_{JI} was measured for the first addition of powder in the small scale vessel with H/T = 1.2 and S/T = 0.7 (equivalent to S_0/T = 0.5 in the normal experimental procedure). The results in Table 2-2 clearly demonstrate that, while increasing the liquid height and submergence will have a negative impact on drawdown, the presence of solid dominates over this, even with the change in liquid height. This control experiment was done using a down-pumping PBT with D/T = 0.5.

Table 2-2: N_{JI} & P_{JI} for initial and final H/T & S/T for high and low solid contents demonstrating the relatively small impact of final submergence vs solid content

Condition	N_{JI} (RPM)	P_{JI} (W)
H/T = 1, S/T = 0.5, X = 0%	210	0.11
H/T = 1.2, S/T = 0.7, X = 50%	590	23.1
H/T = 1.2, S/T = 0.7, X = 0%	275	0.19

Torque (Γ) was measured using a calibrated Binsfield TorqueTrak 10k wireless strain gauge attached to the impeller shaft. Torque was then used to measure the power dissipation in the vessel as:

$$P_{JI} = 2\pi N_{JI} \Gamma \tag{2}$$

The slurry rheology was measuring using a TA AR2000 rheometer with a 28 mm diameter vane and 44 mm diameter cup geometry. Measuring the rheology of quickly sedimenting solids is very difficult due to settling and it was not possible to measure the full flow curve with either geometry without the slurry separating. Thus, in place of a full flow curve the apparent viscosity of the slurry was measured at a fixed shear rate of $200s^{-1}$ for 3 minutes. The shear rate used was estimated as the effective shear rate in the stirred vessel using the approach described by Metzner and Otto (1957). They suggested that the effective shear rate is proportional to the impeller rotation speed:

$$\dot{\gamma}_{eff} = k_s N \tag{3}$$

where k is an impeller specific constant, ranging in this case from 10 for the PBTs to 11.5 for the RDT (Nienow *et al.* 1997). The highest effective shear rate seen in these experiments was using the RDT impeller at N = 1000 RPM. This gives an effective shear rate of approximately 200 s^{-1}. For this reason the slurry apparent viscosity was measured at a constant shear rate of 200 s^{-1}; using the highest shear rate as it was also the most likely to prevent sedimentation during the rheological measurement.

This apparent viscosity was used to calculate the Reynolds number of the vessel at the Just Incorporation condition such that:

$$Re_{JI} = \frac{\rho N_{JI} D^2}{\mu_{app}} \tag{4}$$

The root mean square error (RMSE) is used to compare the reliability of the different scaling parameters studied calculated as:

$$RMSE = \sqrt{\frac{1}{50}\sum\left(N_{Large,measured} - N_{Predicted}\right)^2} \tag{5}$$

where the measured and predicted impeller speeds are specific to each of the 50 powder additions.

2.4. Results and Discussion

2.4.1. Effect of Pumping Mode, Impeller Type & Solid Concentration

In Figure 2-3 the impeller speed for just incorporation for the five impeller types tested at a D/T of 0.5 is shown. In all cases N_{JI} increases with increasing solid content as it becomes harder to draw down and incorporate more solid from the surface at higher solid loadings. This effect becomes particularly pronounced at around 40 % by weight solids for all impellers of this size. It is also

around this point that there is a significant increase in the impeller power draw, as shown in Figure 2-4. It was observed that this dramatic increase in N_{JI}, typically at 40±5 % w/w solids that generally also coincided with the collapse of the vortex pulled by the impeller. At this point the incorporation mechanism changed. At low solid contents with a large vortex the dry powder was pulled down through the vortex to the impeller, from which it is then dispersed into the suspension. As the vortex collapsed at higher solids, added solid tended to clump on the liquid surface and form agglomerates which would partially wet, becoming sufficiently dense to sink below the surface and physically hit the impeller to become dispersed, this is much more akin to the mean drag mechanism of drawdown described by Khazam and Kresta (2008). Example images of this transition are shown in Figure 2-5.

The sawtooth, as the impeller with the lowest pumping number and having a radial flow pattern (Kresta *et al.* 2015), required the highest N_{JI} at low solids concentration. The mixed flow PBT impellers are shown to be the best performing, requiring both the lowest speed and power draw across the full range of solid contents tested. The PBTs significantly out-perform both the radial flow impellers, in terms of speed and power required for drawdown, and marginally out-perform the more axial flow hydrofoil, regardless of pumping direction. This result is similar to the low solid concentration studies described above and seems to hold true even at the higher solid contents studied here.

The RDT was most significantly affected by the presence of solids in the vessel, with significant increases in N_{JI} being seen above ~37 % w/w solids, whereas in contrast, the PBTs only started to show significant increases above 45 % w/w. The sawtooth impeller showed the highest resilience to solid concentration. This is especially true in terms of power consumption where, although at low solids it performed similarly to the RDT (also a radial impeller) it did not demonstrate the very significant rise in N_{JI} and P_{JI} until a significantly higher solid content. This suggests that as the

suspension becomes more rheologically complex with higher solids loadings the high shear rate imparted by the sawtooth in the impeller region has a beneficial effect, despite the low pumping number. This is likely caused by more effective breakup of the agglomerates forming at the surface after the vortex collapses.

Although this demonstration that mixed flow impellers outperform their radial and axial counterparts is similar to previous works it is important to note the dramatic increase in P_{JI} with increasing solid content. The increase in N_{JI} combined with this significantly larger impeller shaft torque means that increasing the solid content of a slurry by a further 1 % requires almost 100-times as much energy for a 50 % by weight slurry compared to a 1 % by weight suspension as seen in Figure 2-6.

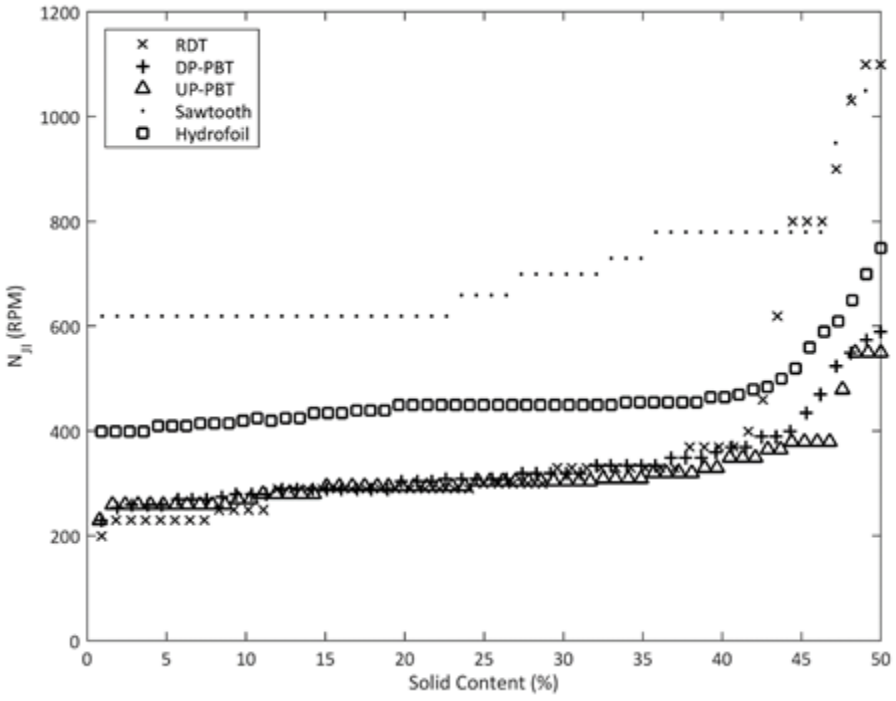

Figure 2-3: N_{JI} with increasing solids content for different impeller types, all with D/T = 50 %, S_0/T = 50 %, no baffles, and T = 0.17 m

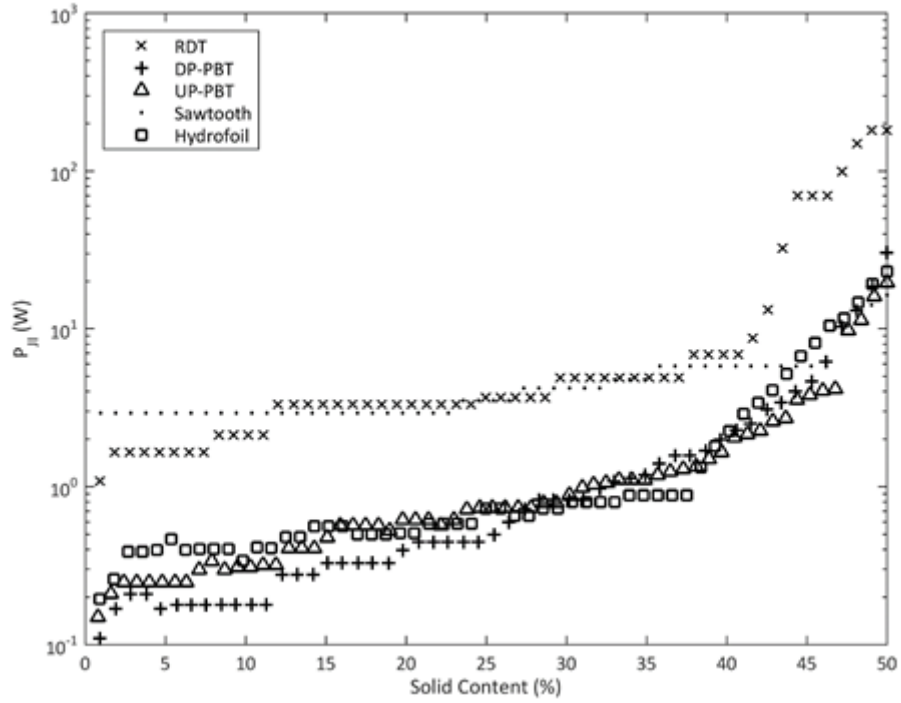

Figure 2-4: *P_{JI} with increasing solids content for different impeller types, all with D/T = 50 %, S_0/T = 50 %, no baffles, and T = 0.17 m*

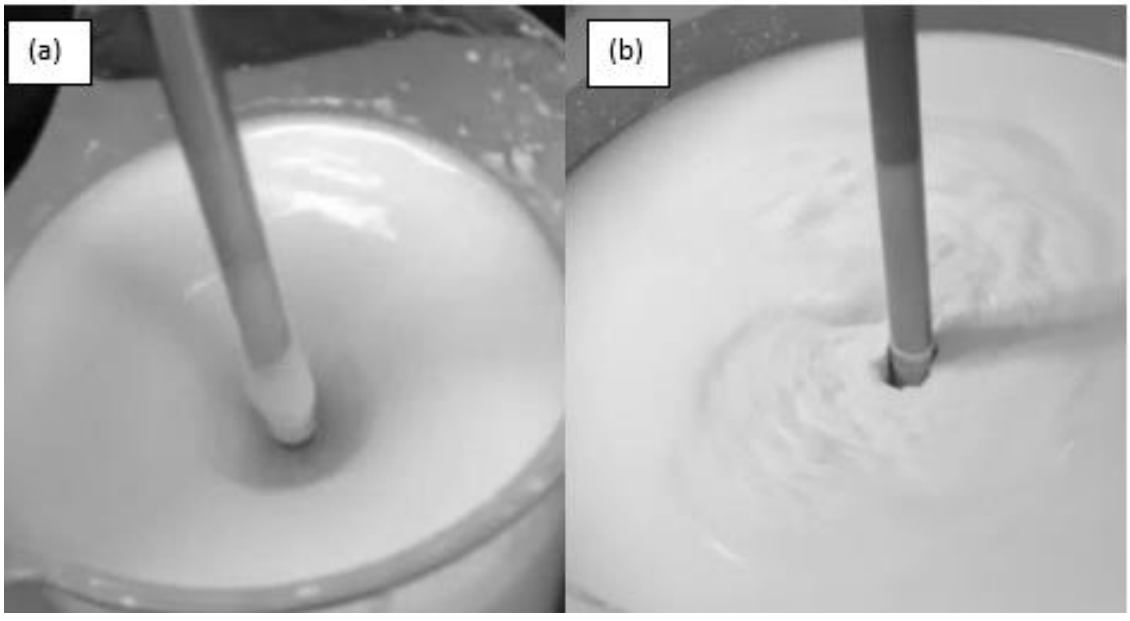

Figure 2-5: *Vessel surface showing incorporation via a vortex (a) and large agglomerate at impeller after vortex collapse (b)*

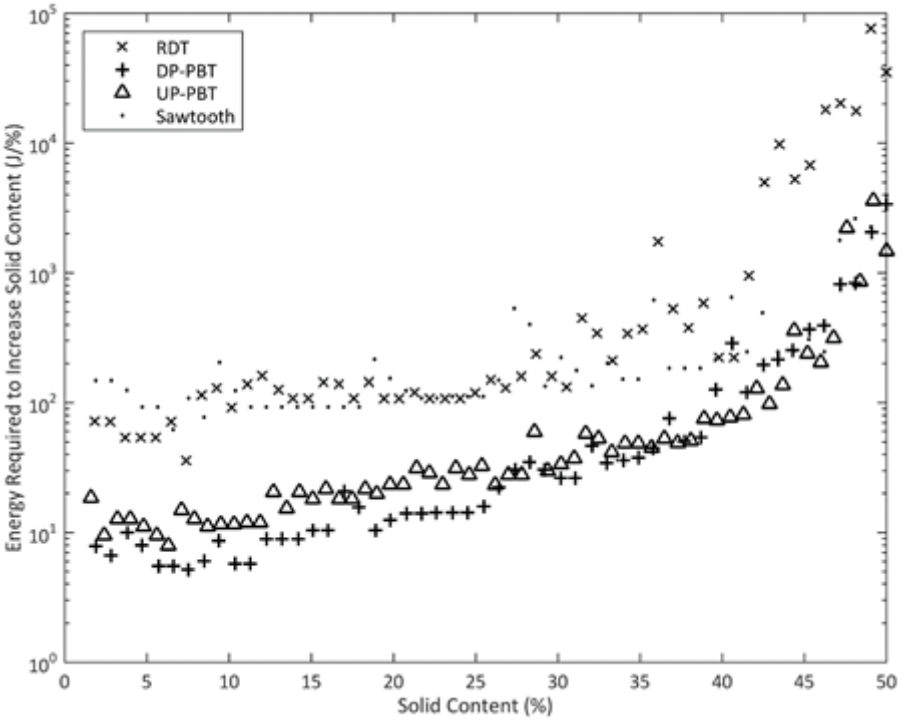

Figure 2-6: Energy required to increase slurry solid content by 1 % with increasing solid content for different impeller types, all with D/T = 50 %, S_0/T = 50 %, no baffles, and T = 0.17 m

The dramatic increase in impeller shaft torque is a combined effect of the increased impeller speed and the dramatic increase in viscosity, as expected due to the Krieger Dougherty relationship (Krieger and Dougherty 1959). Figure 2-7 shows an estimate of the slurry viscosity based on this relationship (equation 1) with intrinsic viscosity, [μ] = 3.2, a suitable estimate for powders of this type (Pavlik 2011). This predicts a significant increase in viscosity (almost 10-fold increase between 32 – 42 wt%) which aligns with the significant increases in both power and impeller speed required for drawdown, suggesting the increase in fluid apparent viscosity is a significant cause of the increased difficulty in powder incorporation.

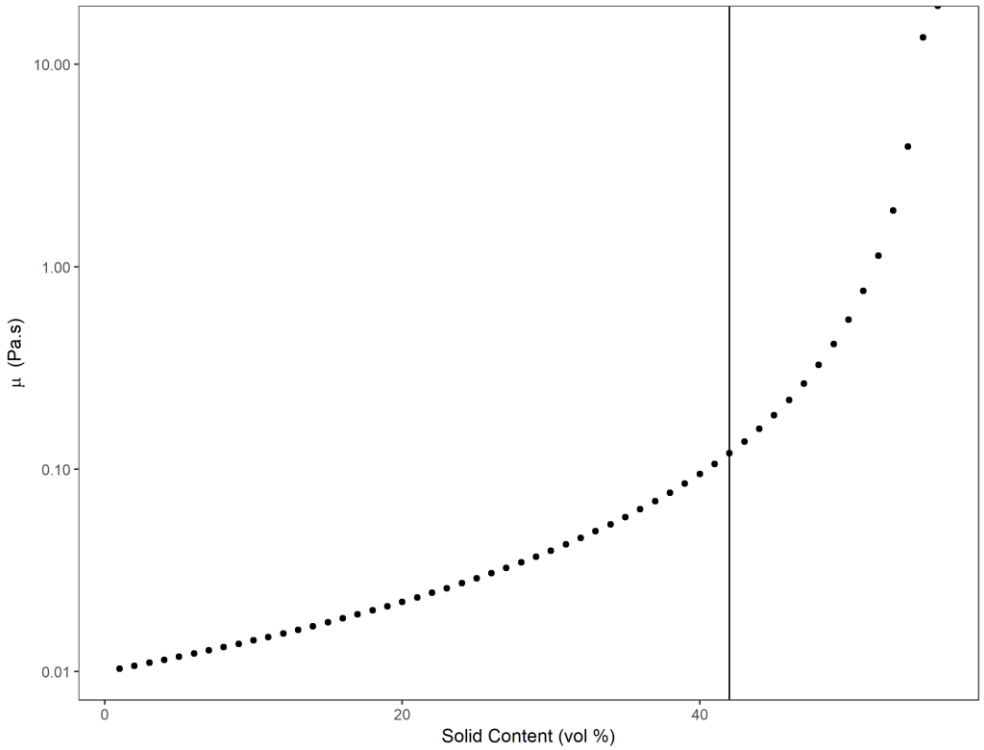

Figure 2-7: Estimated slurry viscosity based on Krieger-Dougherty relationship with [μ] = 3.2. The line shows 50 wt% for this powder

2.4.2. Effect of Impeller Size

For all impeller designs tested the smallest impellers struggled to maintain incorporation of powder at the highest solid contents. The measured impeller speed required for incorporation increased faster for the smallest impellers than for the larger impellers, as shown for a down pumping PBT in Figure 2-8. This was so extreme that for all D = 0.25 T impellers the impeller speed required to maintain drawdown and incorporation within four seconds exceeded 2500 RPM, which was the maximum speed possible with available motors, before the target of 50% w/w solid was attained.

The impeller power draw from shaft torque measurements, shown in Figure 2-9, showed very similar performance between different impeller sizes across most solid contents. The largest impeller required less power at the lowest solid contents (<20 wt %), matching observations by Khazam and Kresta (2009). This suggests that, within normal size ranges, larger diameter

impellers are likely to outperform smaller ones as they will require a lower impeller speed to maintain the same incorporation performance. This, generally, will give more flexibility in a process to increase the speed further to push to higher solids content if required.

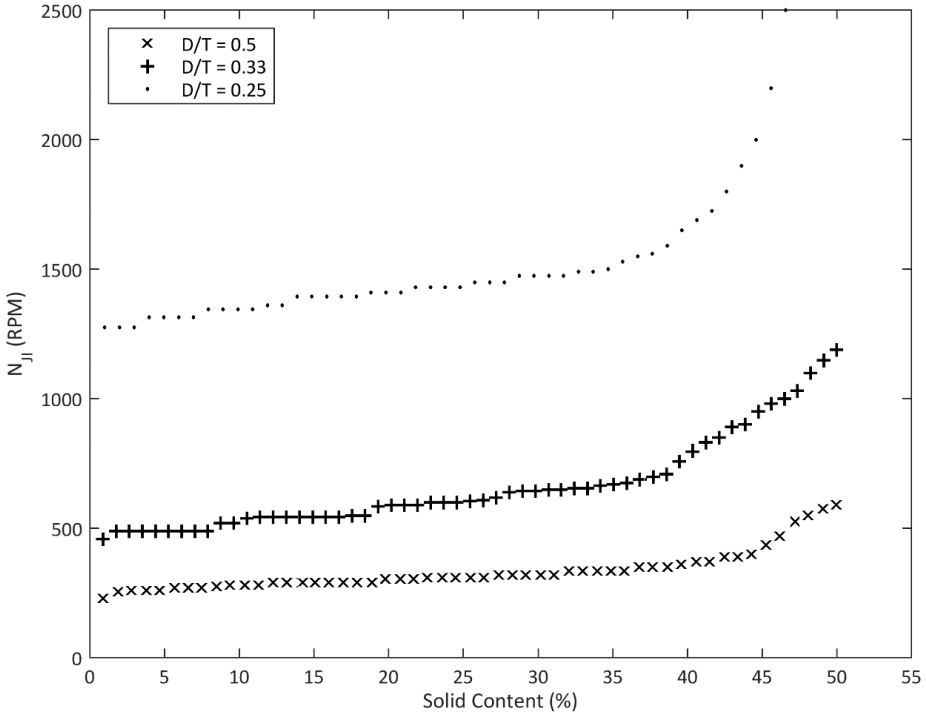

Figure 2-8: Comparison of N_{JI} with increasing solid content for three sizes of down pumping PBT all with S_0/T = 50 %, no baffles, and T = 0.17 m

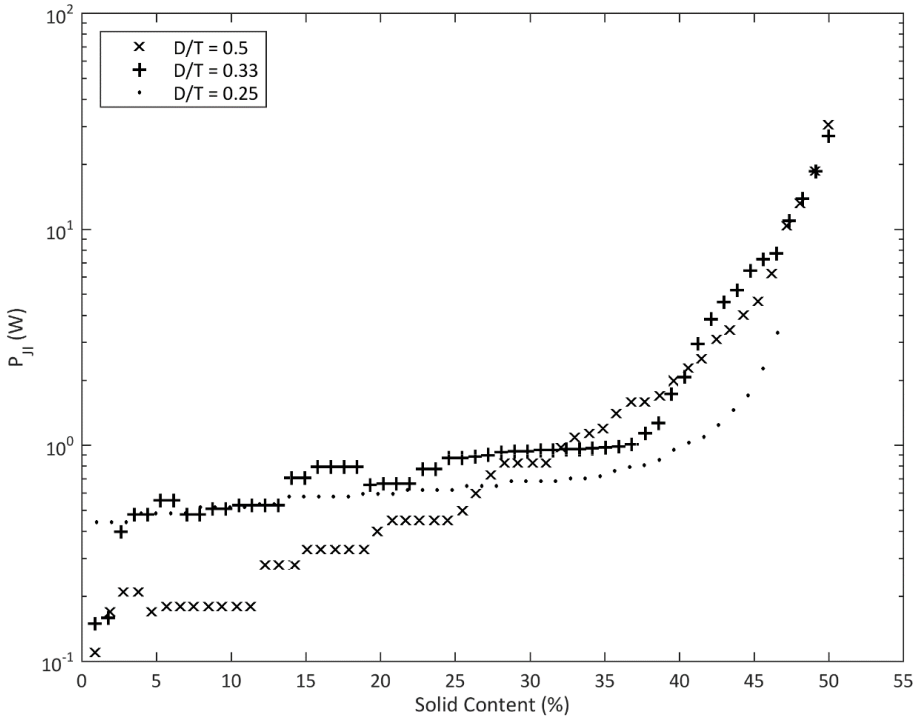

Figure 2-9: Comparison of P_{JI} with increasing solid content for three sizes of down pumping PBT all with S_0/T = 50 %, no baffles, and T = 0.17 m

2.4.3. Effect of Baffles and Eccentricity

In many previous studies considering drawdown of low density, non-incorporable solids, baffles were found to improve drawdown performance. However, as shown in Figure 2-10, this was not found to be the case with solids that are incorporated. Adding baffles provided extra surface area at the surface to which the dry powder became caught behind. This dry powder acted as a site of agglomeration for more powder on the surface, forming a motionless semi-wet mass that could not be drawn down. This was especially true in the dead zones behind the baffles; where, for additions above approximately 20% by weight, dry powder quickly collected. This dry powder then became partially wetted by the liquid and formed a large stationary agglomerate which became very difficult to drawdown for incorporation to occur. This meant that maintaining the

Just Incorporation condition quickly became impossible for both full and surface baffles, where metal protruded above the liquid surface.

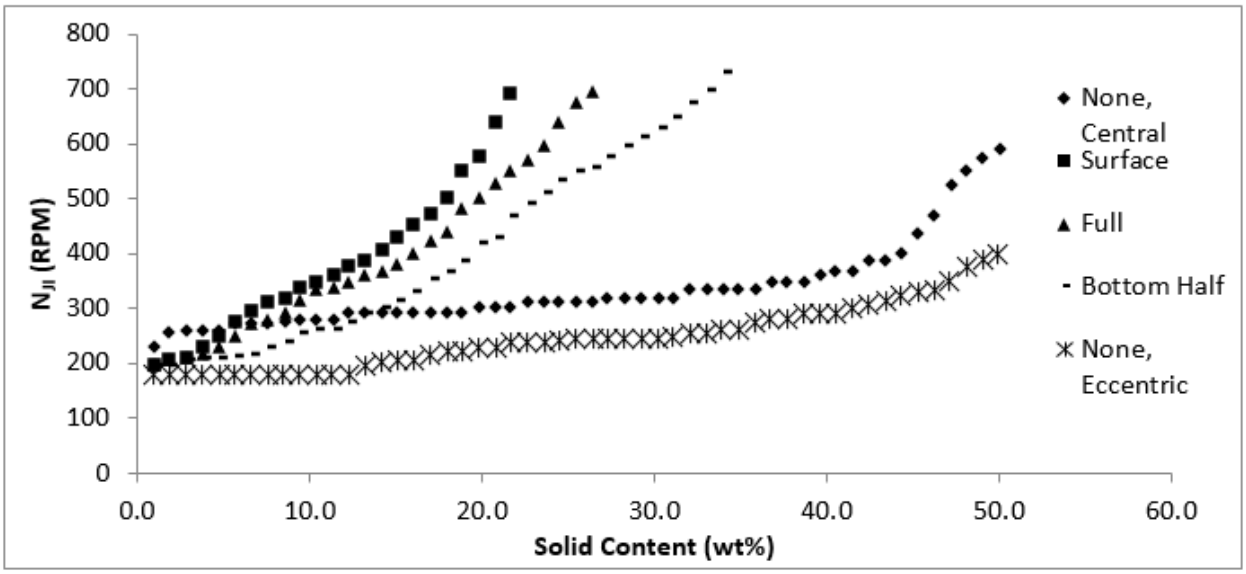

Figure 2-10: Effect of baffle geometries and impeller eccentricity on N_{JI} for down pumping PBT with D/T = 0.5, S_0/T = 50 %, and T = 0.17 m

Bottom half baffles marginally improved the drawdown performance at the lowest solid contents. However, as the solid content increased the impeller speed for drawdown increased much more significantly than in the unbaffled cases, again decreasing drawdown efficiency as the solid content was increased further. This is due to the fact that the presence of baffles prevented vortex formation within the vessel, which inhibited wetting and incorporation of the powder.

Significantly higher shaft torque was also seen in the eccentric, full, and bottom half baffle cases at the low solids contents studied, this is to be expected as the centrally mounted impeller showed a high degree of bulk rotational flow, which will reduce the energy delivered by the impeller due to a lower power number. This is not true in the fully baffled case. This has implications for the mixing performance as it is possible that, although drawdown efficiency is increased in the unbaffled cases, the mixing performance will be reduced, increasing the chances

of inhomogeneity in the vessel. This limitation was overcome through use of an eccentric impeller, which gave a noticeably higher power draw (with a measured power number of 1.3 at low solid contents, whereas the central impellers had a power number in the region 0.3-0.4) and better drawdown performance. These observations were observed for both up and down pumping PBTs at a variety of submergences.

2.4.4. Flow Regimes

There is a significant change in drawdown behaviour at around 40 % solids by weight, although the exact concentration at which this happens is impeller specific. In order to explore this observed step change in behaviour the apparent flow regime within the vessel was studied by considering the Reynolds and power numbers of the system around the transition.

The apparent viscosity of the slurry was measured as described above. As seen in Figure 2-11 the slurry apparent viscosity increased exponentially with the solid content. Both the hatched plate and vane geometries give similar apparent viscosities to ±15 %. Fitting an exponential to these measurements gives the apparent viscosity at 200 s^{-1} as a function of solid content for 0 % ≤ X ≤ 50 %:

$$\mu_{app} = 0.0006e^{0.0994X} \quad (6)$$

The rheology of the slurry was measured in this manner because it is extremely difficult to measure full rheology curves. This is because at low shear rates the slurry separated within seconds, displacing the water and causing the solid to dry out during measurement. However, it was observed during mixing that, even at the highest solid contents and large initial submergence, a dry particle placed near the wall at the free surface would move, tracing the liquid flow. As the point in the vessel furthest from the impeller motion of fluid to the impeller from the wall at the surface shows that the slurry was fully mobile, with no caverns forming.

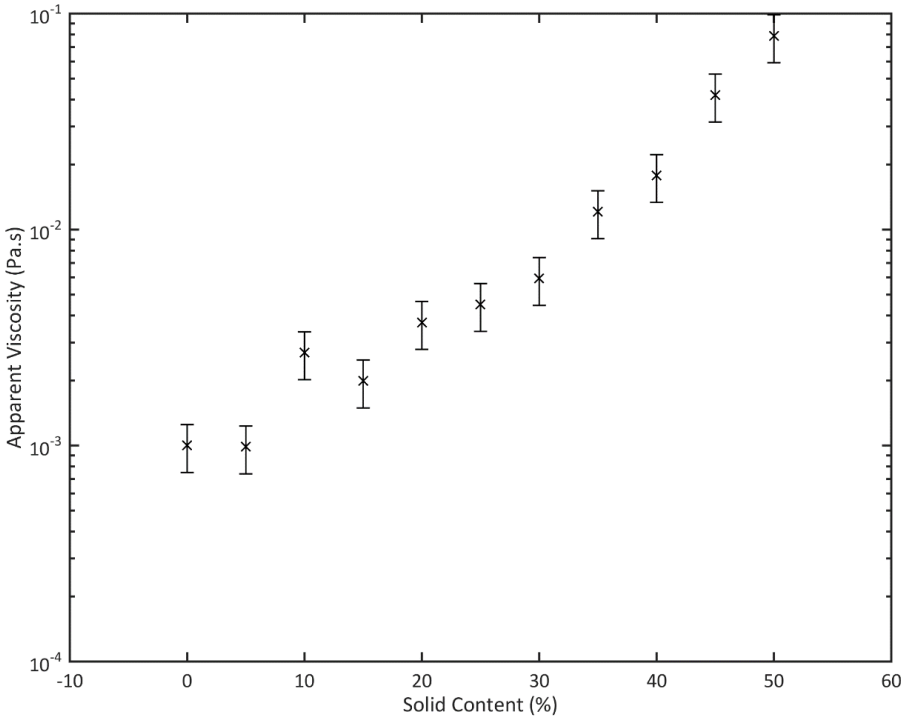

Figure 2-11: Evolution of slurry apparent viscosity for increasing solid content. Measured at 200s^{-1}

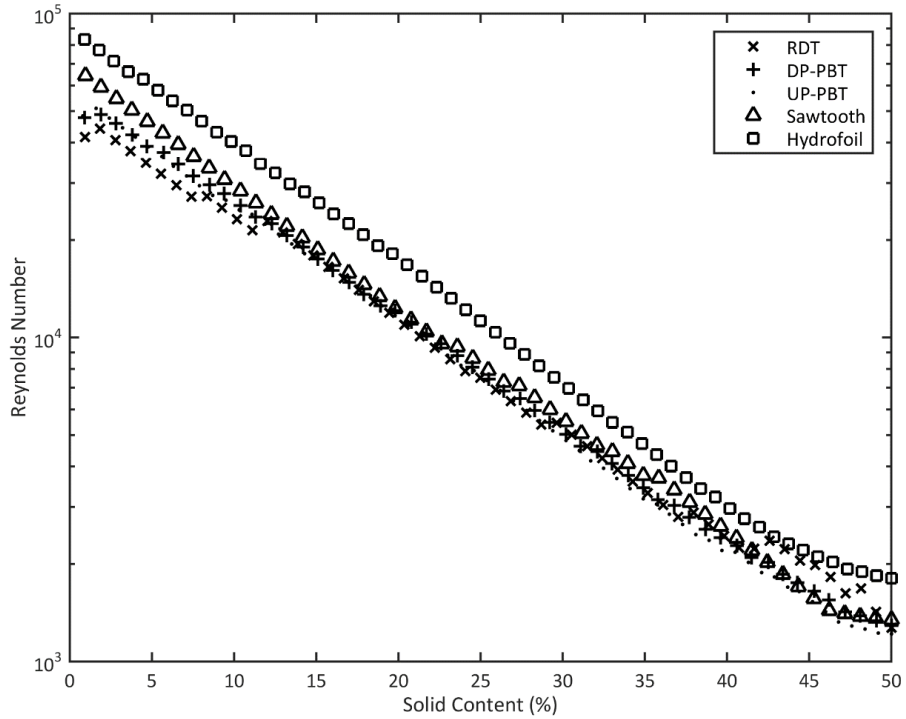

Figure 2-12: Evolution of Reynolds number in the vessel as the solid content increased for all impellers studied with D/T = 0.5, no baffles, T = 0.17 m, S_0/T = 50 %

Figure 2-12 shows that the Reynolds number steadily decreases with increasing solid content as the slurry becomes more viscous, despite the increasing impeller speed. At ca. 40 % w/w solids, where the apparent change in incorporation mechanism occurs, all impellers seem to have a Reynolds number in the order of 2000-3000. This would classically be considered to be inside the transitional regime but not close to the laminar transition, which is generally accepted to occur at around Re = 10. The transition from full turbulence to transitional flow, based on the commonly assumed boundary of ca. Re = 10,000, would occur between 25-30 % w/w solids.

The impeller power number can be calculated from the measured power draw as:

$$Po = \frac{P}{\rho N^3 D^5} \tag{7}$$

Figure 2-13 shows that the power number remained constant as the Reynolds number dropped from its maximum, at the start of the experiments, with no solids present to a Reynolds number of 2000. This constant Po with changing Re is indicative of fully turbulent flow. The value of the power number is also approximately 1.3 for the PBTs and 5 for the RDT, the power numbers expected for a fully turbulent pitched blade impeller and Rushton turbine (Rushton *et al.* 1950; Nienow *et al.* 1997). From Figure 2-12 this Reynolds number value coincides with a solid content of approximately 40 %. At solid contents above this (and lower Reynolds numbers) the power number increases with decreasing Reynolds number, indicative of laminar flow, explaining the collapse of the vortex and massive increase in requirement to maintain effective drawdown and incorporation.

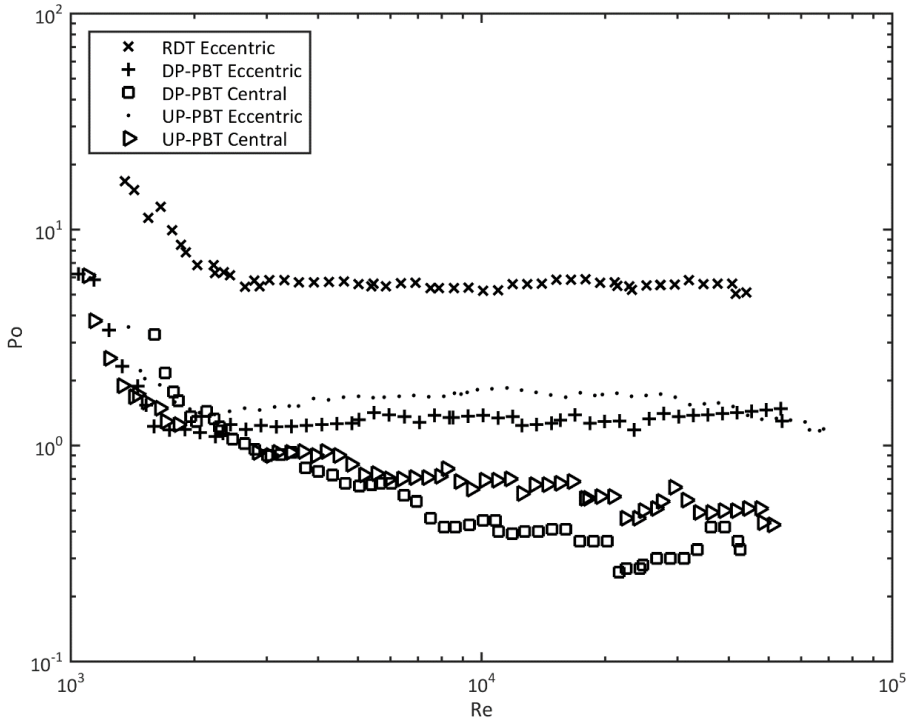

Figure 2-13: Change in impeller power number for change in Reynolds number & solid content for RDT, up & down pumping all at D/T = 50 %, PBT S_0/T = 50 %, no baffles, and T = 0.17 m

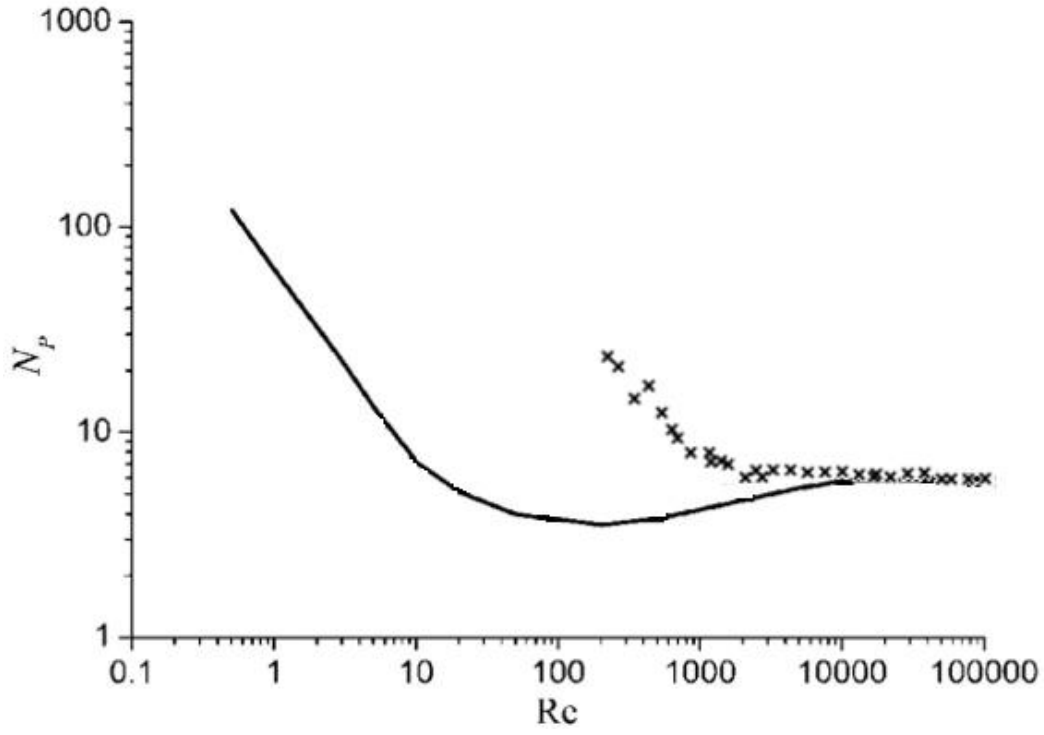

Figure 2-14: Measured power numbers for Rushton turbine compared to standard values (24)

Figure 2-14 compares the measured power numbers to standard values for a Rushton turbine (Rushton *et al.* 1950). The figure illustrates that the presence of the solids appears to suppress the transitional regime, causing elongation of the "laminar" flow regime, where a linear increase in power number with decreasing Reynolds number is observed.

Possible reasons for this phenomenon are local or bulk changes in the rheology of the fluid due to complex dynamic interactions between the liquid and solid particles (as well as possible particle-particle interactions) or that the solids particles act to suppress turbulence within the continuous phase. Suppression or augmentation of turbulence within solid-liquid and liquid-liquid systems is an observed phenomenon which has been the studied by many workers at low dispersed phase concentrations (Gore and Crowe 1989; Mandø *et al.* 2009; Gabriele *et al.* 2011; Unadkat *et al.* 2013), though mechanistic understanding at high solids concentrations remains elusive with little study (Agrawal 2016).

Evidence exists in the rheology data of unstable behavior at high solid loadings. This is shown in Figure 2-15a where crude slurry was held in the vane rheometer for one minute at 200 s^{-1}. For slurries with solid content ≥ 40 wt% the rheology evolved with processing time, and the apparent viscosity decreased; this is likely due to deagglomeration of small agglomerates that remain after large agglomerates are broken up directly by the impeller. These small agglomerates contain occluded air, and so give the slurry a temporary artificially high solid volume concentration. The apparent viscosity values used to calculate Reynolds number above were once the slurry reached a steady μ_{app} after more than a minute.

Figure 2-15b shows that the same rheology change occurred in the vessel when the slurry was left stirring on the impeller, as seen by a decrease in torque measurement with constant impeller speed. For all impellers the torque decayed to around 75% of the torque immediately after the final powder addition within 20 minutes.

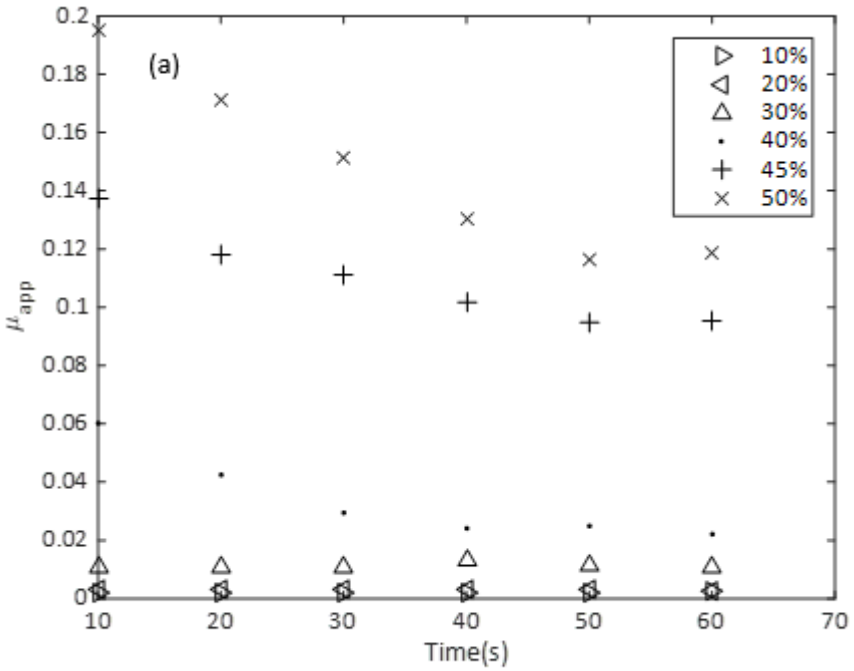

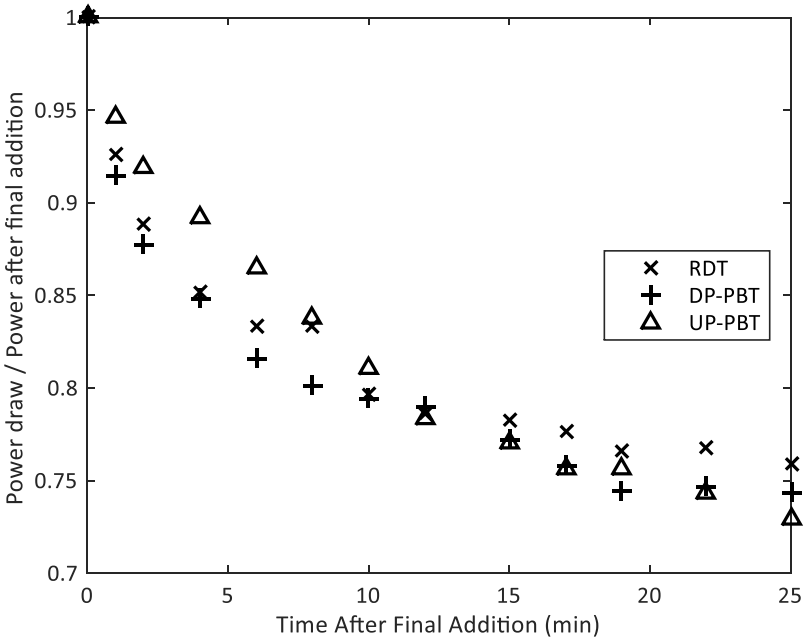

Figure 2-15: Rheology evolution shown by apparent viscosity measurements of freshly made slurry held in a 40mm vane rheometer for one minute at 200 s^{-1} (a) and shaft torque changes in the mixing vessel (b).

This artificially high solid volume concentration due to occluded air causes the slurry to act as a more concentrated slurry, moving further to the right in the mixer torque rheometry curve for this powder, shown in Figure 2-16. This means the slurry acts more like a paste and so has a higher Reynolds number whilst deagglomeration is still occurring, releasing the occluded air.

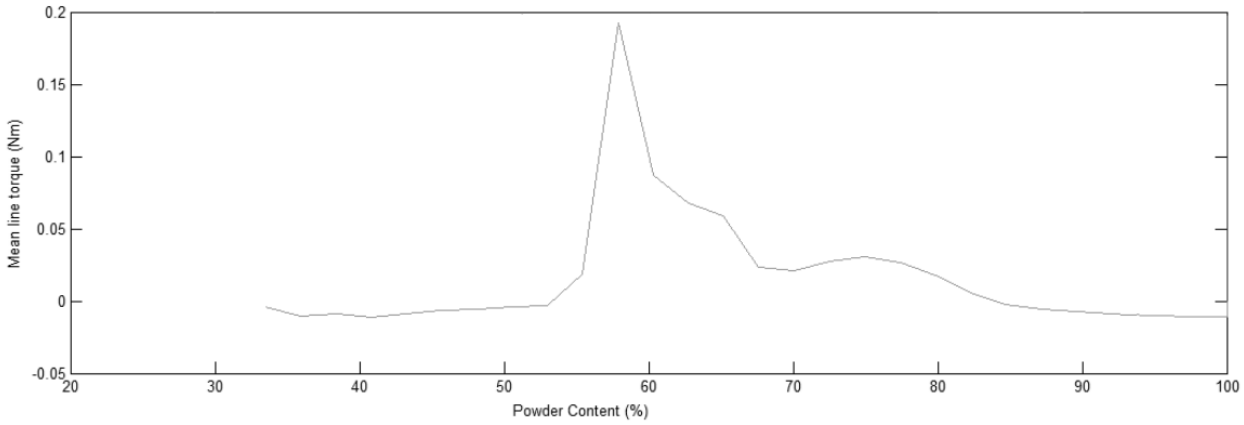

Figure 2-16: Mixer torque rheometry plot for alumina slurry

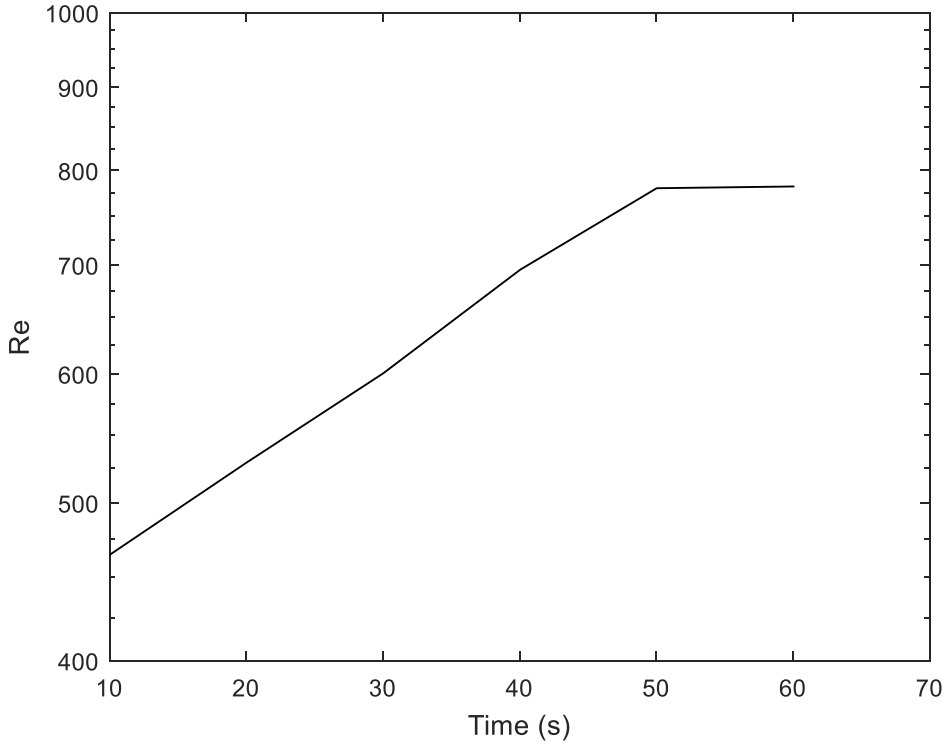

Figure 2-17: Calculated Reynolds number change due to evolution in apparent viscosity with processing time for 50 wt% slurry held in vane rheometer

2.4.5. Scale Up

Six scale up protocols were considered: Constant N^3D, constant tip speed, constant impeller discharge, constant Froude Number, constant Reynolds number, and constant power per unit volume, the dependencies of which are shown in Table 2-3.

Table 2-3: Scaling protocols considered

Scaling Protocol	Constant	Assumed Inter-Scale Constants
Froude number*N	N^3D	-
Froude number	N^2D	-
Power per unit mass	N^3D^2	Impeller power number
Tip speed	ND	-
Reynolds number	ND^2	Fluid viscosity & density
Flow	ND^3	Impeller flow number

The approach used was to measure the value of N_{JI} with increasing solids for down pumping PBTs at both large and small scale. The small scale values were then used to predict large scale values based on each of the above scaling parameters. The predicted and measured values were then compared.

Figure 2-18 shows that maintaining a constant N^3D between scales is the best scaling protocol for the lowest solid contents, giving the lowest RMSE shown in Table 2-4. However, as the solid content of the slurry is increased the ability of any of the parameters to predict scale up fails. This point corresponds to the regime transition at 40% by weight solid observed above.

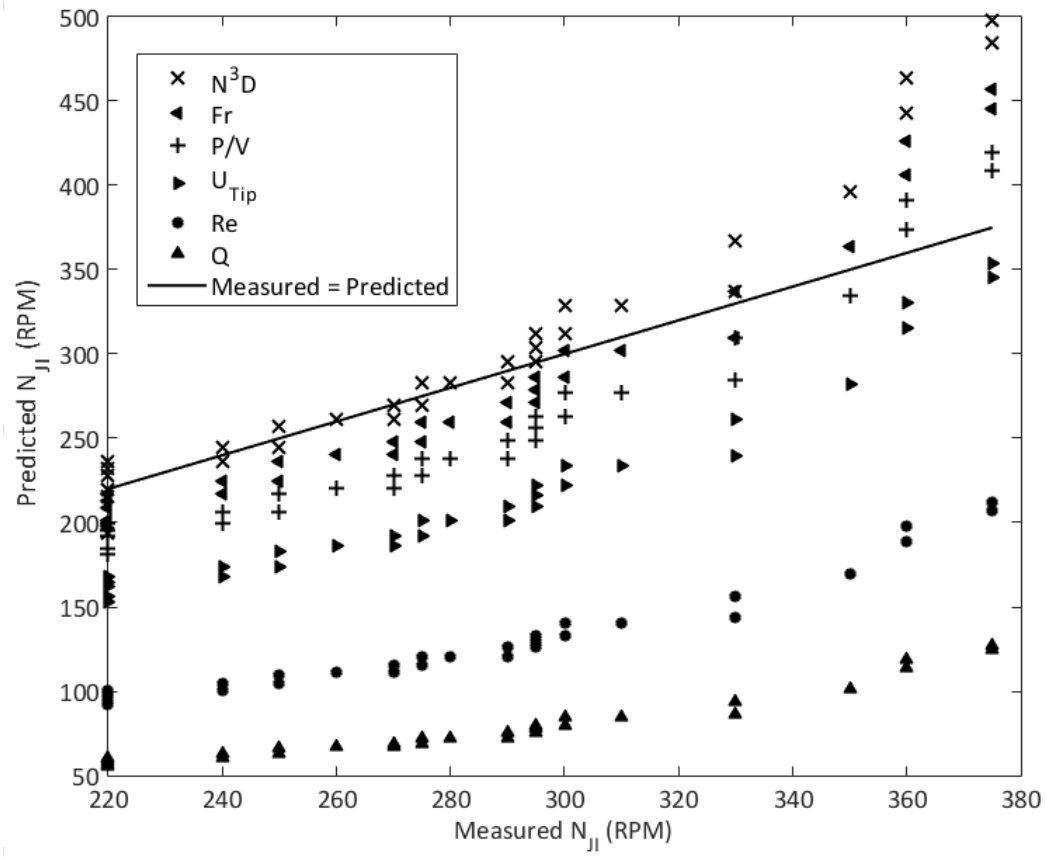

Figure 2-18: Predicted vs measured N_{JI} values for scaling protocols considered

Table 2-4: Error from measured and predicted N_{JI} values for scale up from 5L to 25L for down pumping PBT

Scaling Protocol	RMSE - Full	RMSE - < 40%
Froude number*N	32.29	7.44
Froude number	27.67	22.12
Power per unit mass	39.09	40.95
Tip speed	72.20	74.65
Reynolds number	152.66	147.59
Flow	202.03	191.40

This is a different result to previous studies (Joosten *et al.* 1977; Hemrajani 1988; Özcan-Taşkin 2006) which generally showed a constant Froude number to be the best scaling protocol for drawdown. This result shows extra dependency on the impeller rotation speed compared to Froude number: thus the scaling parameter proposed is N.Fr. While it is not surprising to find that

the Froude number is an important parameter (Joosten *et al.* 1977; Hemrajani 1988; Özcan-Taşkin 2006) the extraneous "N" deserves a little more discussion.

There are two possible explanations, both of which are essentially variants on a similar theme:

1. Average Shear (Metzner and Otto), and Equation 3 above) = K_S.N. Given the same impeller is used at both scales, then K_S = constant so the average shear α N
2. Whole vessel pumping: Q = Fl. ND^3 so vessel turnover frequency is proportional to Fl. ND^3/T^3.

   Given that D/T = constant as geometric similarity is maintained and that Fl = constant as the same impeller is used at both scales, then scale independent whole vessel turnover frequency α N

Scaling of N.Fr therefore considers not only the drawdown, courtesy of Fr, but also the ability to to distribute the incorporated solids around the vessel, or alternatively the ability to maintain average shear rates that could reflect the disruptive forces on the drawn down agglomerates or the suppression of cavern formation.

Figure 2-18 shows that none of the scaling protocols suitably predict scale up after the regime change when considered as part of the full range of concentrations. However, it is possible to predict the change in impeller speed after the regime change where:

$$N_{2,\ Predicted} = \left(\frac{\left(N_{1,\ Measured} - N_{1,\ Transition}\right)^a D_1^b}{D_2^b} \right)^{\frac{1}{a}} + N_{2,\ Transition} \qquad (8)$$

where 1 and 2 represent the two scales considered.

The impeller speed at the regime transition is specific to the power and liquid system considered and so must be measured experimentally. The exponents a and b are determined by the scaling

constant that most reliably predicts the change in impeller speed after the transition, i.e. gives the closest to a gradient of 1 for measured vs predicted $N_{JI.}$

Figure 2-19 shows how the scaling protocols predict the change in impeller speed as opposed to the absolute value of N_{JI} after the regime change using Equation 8 above. From this a constant Reynolds number most accurately predicts the ΔN_{JI}, which is also reflected in the RMSE values shown in Table 2-5.

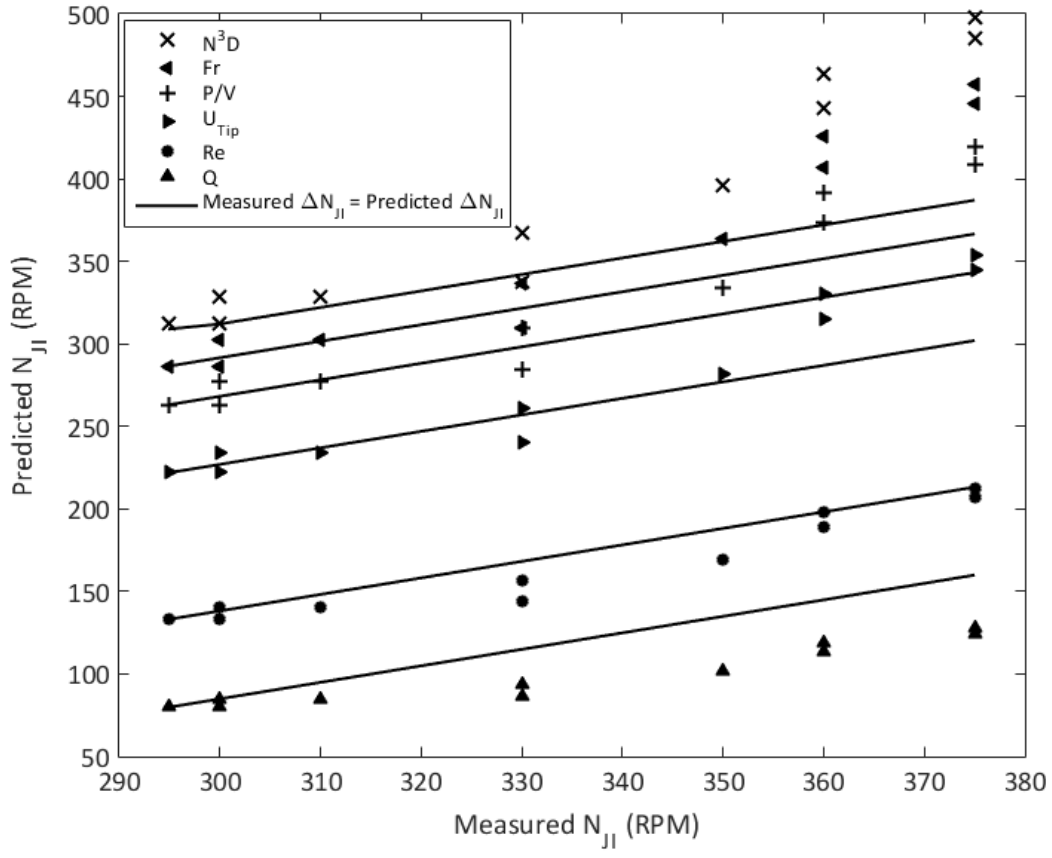

Figure 2-19: Predicted vs measured N_{JI} values for down pumping PBT at >40 wt% solids with lines showing how each scaling protocol predicts ΔN_{JI}

Table 2-5: Error between measured and predicted ΔN_{JI} values for different scaling protocols

Scaling Protocol	RMSE – ΔN_{JI} at > 40%
Froude number*N	58.30
Froude number	46.68
Power per unit mass	39.19
Tip speed	26.28
Reynolds number	10.85
Flow	24.34

This is a new observation, showing that the regime change observed above also changes the scaling dependence of the system. Where the impeller speed required for effective drawdown is calculated as:

For constant Po (turbulent) regime:

$$N_{JI,2} = \sqrt[3]{\frac{{N_{JI.1}}^3 D_1}{D_2}} \tag{9}$$

For changing Po regime:

$$N_{JI,2} = N_0 + \frac{\Delta N_{JI,1} {D_1}^2}{{D_2}^2} \tag{10}$$

where 1 and 2 represent the two scales considered, ΔN is the change in impeller speed with increasing solids after the regime change, and N_0 is the impeller speed at the regime change.

This change in scaling dependency is likely caused by the change in incorporation mechanism that happens at the regime change. As stated above; below the transition loose particles are drawn down and incorporated through a vortex. After the transition mean drag of larger agglomerates, that form on the surface due to gentle surface motion, becomes the main incorporation mechanism. These two mechanisms are significantly different and therefore give rise to these two scaling regimes.

2.4.6. More Design Considerations

Whilst this chapter has focussed on improving the performance of the drawdown of floating solids in terms of minimising both the impeller speed and power draw there are multiple other factors that may be important in specific mixing and incorporation duties.

For example, in this study it was noticed that the mechanism for drawdown and incorporation below 40 wt% solid content was via a central vortex in the vessel. Whilst this is effective for drawdown and incorporation it also leads to significant amounts of air being entrained during mixing. For many processes this may cause significant problems. For example, if the fluid exhibits a yield stress it is possible that small bubbles of occluded air will get trapped in the suspension, resulting in negative performance of the product or downstream processes. This is not a problem for the suspensions studied in this chapter.

The suspensions in this study do not exhibit a yield stress and therefore, there is little or no risk of cavern formation within the vessel and therefore the relatively small impellers studied in this chapter are suitable. However, if the fluid does exhibit a yield stress the conclusions in this chapter are unlikely to hold true and much larger impellers, such as anchor or paddle impellers, may be more suitable than the pitched blade turbines studied here.

2.5. Conclusions

This work demonstrates the effect of high solid content systems on the drawdown and incorporation of floating solids in stirred vessels. Similarly to low solid systems in previous works, the mixed flow impellers out performed either radial or axial flow impellers tested. This is true for the entire range of solid contents studied (up to 50 % by weight). However, at the very highest solid contents (40 %+) the mechanism of powder incorporation changed; the central vortex collapses at this point such that solid is no longer brought directly to the impeller. Instead clumps of semi-wetted powder tend to form into agglomerates, these then sink below the surface as fluid

motion wets them to a sufficient density to overcome buoyancy forces on them. At this point the sawtooth impellers studied went from being the worst impeller at low solids to one of the better performing ones, this suggests that high shear is beneficial in achieving very high solid contents.

Generally larger impellers (up to a max D/T of 0.5) out performed smaller ones. This was especially true for the smallest impellers studied at D/T = 0.25, which were often too small to produce sufficient surface motion at higher solids to sufficiently wet power to incorporate it.

Contrary to many works at low solid contents baffles were found to significantly inhibit the incorporation of powder as the solid content was increased. This was true for all types of baffles tested, with submerged half baffles being the best but still performing significantly worse than the unbaffled system. It would be interesting in further work to see the effect of moving the impeller eccentric or tilting the impeller on incorporation performance. These are generally ways to prevent full body rotation in systems where baffles are not suitable.

Scaling on a constant N^3D is found to predict most accurately the scale up from a 5 L vessel to 25 L with geometric similarity for both up and down pumping PBTs up to around 40 % by weight solid content. This was the maximum concentration before the vortex collapsed in all systems tested and coincides with a constant Reynolds Number better predicting the change in impeller speed required to maintain drawdown. This concentration, approximately 40 % by weight solids for this specific powder, is also where a flow transition from turbulent (or constant power number) to laminar seems to occur, which has been demonstrated by analysis of the apparent power number of the impeller at that point, which shows very little transitional flow behaviour.

3.

Optimisation of stirred vessel geometry for the drawdown and incorporation of floating solids to prepare concentrated slurries

This Chapter reports on a Design of Experiments (DoE) approach to optimise the geometric configuration for effective drawdown and incorporation of floating solids to prepare high solid content slurries. The main parameters considered were the impeller pumping direction (up versus down), impeller submergence, eccentricity, and angle of tilt. DoE was used as this allows not only the independent effects of the main parameters but also their interactions to be considered.

Pumping mode was found to be the most significant parameter, with down-pumping impellers providing the best incorporation performance. This is related to the strong interaction between pumping mode and other parameters. Adding tilt or eccentricity reduced drawdown performance for up-pumping impellers yet caused improvement in the case of down-pumping impellers.

The optimal geometry was found using a down-pumping PBT, 10^{o} tilt, 10% of the vessel diameter eccentricity and placed at an initial submergence of half the liquid height. This geometry is shown to reduce the time required to prepare a 50 wt% slurry by two thirds compared to a general Rushton turbine design, emphasising the benefits of rational impeller and vessel design.

3.1. Chapter Preface

This Chapter is published in the Chemical Engineering Research and Design Journal (ChERD) in the following paper (Wood, Simmons and Stitt 2018):

Wood, T., Simmons, M. J. H., and Stitt, E. H. (2018), Optimisation of stirred vessel geometry for the drawdown and incorporation of floating solids to prepare concentrated slurries. ChERD, 133: 70-78. doi: https://doi.org/10.1016/j.cherd.2018.03.002

3.2. Introduction

Drawdown of floating solids in stirred vessels is a common process operation for many industries to incorporate solids for dissolution, reaction, or suspension and slurry preparation. Examples of drawdown processes can be found throughout the polymer, paint, food, and catalyst industries, amongst others. The specific requirement of the drawdown duty is highly dependent upon the solid and liquid phase composition. For example the drawdown, incorporation and suspension of small particle ceramic materials in concentrated slurries for paints or catalyst washcoats will behave differently to the drawdown of low solid concentration buoyant particles for dissolution, mass transfer, ion exchange, or reaction processes (Siddiqui 1993).

Solid particles may float for a variety of reasons (Waghmare *et al.* 2011). Firstly, if the density of the solid particles is lower than the fluid they will float if not agitated. Using agitation to draw these particles down into the fluid forms a dynamic equilibrium where, if agitation ceases, they will return to rest at the top surface. Secondly, if the interfacial tension between the solid and liquid is sufficiently high, this causes a force at the surface with a larger magnitude than the gravitational settling force which prevents the particles from sinking, even if they have a higher density than the fluid (Rouquerol *et al.* 2013). Thirdly, particles can agglomerate at the surface, with liquid bridges between particles, forming a large semi-wet mass with occluded air. The presence of this air gives this agglomerate a lower envelope density than the original particles and

so it may float until it is broken up. An important distinction between the three cases is that while the first is reversible, the latter two are not. Once the particles are either pulled through the surface and/or fully wetted they will become non-buoyant and will not return to the surface once agitation is stopped; rather they will most commonly sediment.

Each of the above phenomena does not necessarily happen in isolation. For example, in the case of porous ceramic powders all three can potentially occur. Initially, the pores of the particles are filled with air and so the envelope density will be low. As the pores fill with fluid (a process that depends on the interfacial tension between the two phases) the envelope density will increase until it rises to above that of the fluid. However, the particles may also agglomerate as they hit the liquid surface, leading to a very complex force balance on the system.

Due to the complexity of the problem, previous studies have largely focused on simple systems. For example, large, low density buoyant particles have been used to isolate the phenomena (Hemrajani 1988; Özcan-Taşkin 2006; Khazam and Kresta 2008; Khazam and Kresta 2009). The effect of various geometric parameters on the impeller speed (N_{JD}) and power (P_{JD}) to just drawdown the solid from the liquid surface have been explored. The just drawdown criterion, N_{JD}, first proposed by Joosten et al. (1977), is the impeller rotation rate at which no solid spends more than four seconds at the free surface. This is an analogue to the well-known Zwietering "just suspended" criterion (Zwietering 1958) which is the impeller rotation rate at which no particle spends more than 2 seconds in contact with the vessel bottom.

Whilst N_{JD} is a useful parameter to study the effect of geometry at a given solids concentration, it relies upon the reversibility of the drawdown process. This is of course only true for the first of Waghmare's three conditions given above. In the context of the present study, all three apply and hence the drawdown process is not reversible. Therefore a similar condition, the "just incorporation" condition proposed in Chapter 2 for non-buoyant solids that can be incorporated

into slurries. This measurement is very similar, measuring the impeller speed required, N_{JI}, to ensure all powder added is drawn down and incorporated within four seconds of addition, where a fixed amount of solid is added at a time at a fixed frequency, allowing measurement of drawdown to be carried out for concentrated systems.

Amongst previous studies there is a general consensus that mixed flow pitched blade turbine (PBT) impellers give the best performance, with significant power and speed savings compared to radial flow impellers (Joosten et al., 1977; Khazam and Kresta, 2009; Özcan-Taşkin, 2006; Özcan-Taşkin and McGrath, 2001; Özcan-Taşkin and Wei, 2003; Takahashi and Sasaki, 1999; Wood et al, 2018). The majority of these works have focussed on down-pumping impellers, although Özcan-Taşkin and Wei (2003) demonstrated that up-pumping impellers ran at lower N_{JD} and P_{JD} when placed close to the surface than down-pumping impellers. Given the consistent conclusions within previous literature, only pitched blade turbines are considered in this study; both up- and down-pumping.

The effect of submergence on drawdown performance has been considered by several researchers, with conflicting conclusions. Özcan-Taşkin and McGrath (2001) reported good performance at high impeller submergences, specifically for radial flow impellers and downward pumping PBTs. Khazam and Kresta (2009) showed that the cloud depth within the vessel improved with a higher submergence at the cost of increasing both the impeller speed and power required for drawdown for a novel geometry using a down-pumping impeller, regardless of baffle configuration. Özcan-Taşkin and Wei (2003) showed that whilst drawdown performance, in terms of N_{JD}, improved as the submergence was increased for down-pumping impellers, the opposite was true for up-pumping impellers. Khazam and Kresta (2009) made a similar observation that up-pumping impellers are much more sensitive to the effect of submergence than down-pumping impellers.

Previous studies focussing on low solid contents and solids that cannot be incorporated demonstrated an improvement in drawdown performance when using baffles. Various baffle geometries have been studied and generally show improved performance over the unbaffled case; this includes the use of one, two and four baffles that can either be full vessel height or surface only baffles (Hemrajani 1988; Siddiqui 1993; Özcan-Taşkin and McGrath 2001; Karcz and Mackiewicz 2009; Khazam and Kresta 2009). However, baffles have been shown to inhibit the drawdown and incorporation of incorporable solids (i.e. those that, once wetted, incorporate to form a slurry rather than returning to the surface) during slurry preparation, especially as the slurry solid content is increased above 10%, as shown in Chapter 2. Therefore, it is important to examine non-standard geometries to reduce quasi-solid body rotation and improve mixing performance within the vessel. The use of eccentric impellers is a common technique to improve mixing in unbaffled systems, shown to give equally efficient mixing as a baffled vessel (Hall *et al.* 2004; Hall *et al.* 2005). Waghmare et al. (2011) demonstrated some promise in the use of a tilted impeller for drawdown, a practice that has been shown to potentially improve mixing performance over unbaffled systems (Chung 2008).

There are limited studies considering the effect of increasing the concentration of the solid phase on the mixing system. Xie et al. (2007) studied the deagglomeration of fumed silica agglomerates up to 10 wt % and found that drawdown requirement (in terms of drawdown time) increased exponentially with increasing solid concentration for all impellers studied. Khazam and Kresta (2009) studied a system up to a maximum 10 % by volume expanded polystyrene and found the drawdown requirements (in terms of N_{JD} significantly increased with increasing solid concentration. (Özcan-Taşkın (2012) studied the incorporation of nanoscale clusters into suspension using a proprietary design mixer and found that the drawdown requirement (in terms of incorporation time) increased with increasing solid concentrations, especially above solid concentrations of 10 wt% up to a maximum concentration of 20 wt%.

The effect of D/T is significant on drawdown performance and has been studied by multiple authors (Joosten *et al.* 1977; Takahashi and Sasaki 1999; Özcan-Taşkin and McGrath 2001; Özcan-Taşkin and Wei 2003), again with varying conclusions. Generally larger impellers require lower speeds to achieve the same drawdown performance at the cost of increased power draw. However, in Chapter 2 it was demonstrated that a larger diameter PBT (D/T = 0.5) provided much better incorporation at higher solids content (> 40%) and this outweighed the lower power of smaller D/T at low solids content (< 20%) in overall process terms.

Design of Experiments (DoE) is a useful tool to ensure the maximum information is obtained from a process using a minimised set of experimental conditions. In a factorial DoE approach, process parameters are varied systematically within an orthogonal design space in order to assess efficiently the effect of each considered parameter on an output, or response, variable. This approach also allows the consideration of interactions between the process variables while minimising aliasing between them, allowing optimisation of that response for a given system (Montgomery 2012).

This study considers the effect of increasing solid concentrations on the geometric parameters in a 5 dm^3 cylindrical stirred vessel. This allows optimised vessel designs to be found for industrially relevant high solid content systems with incorporable solids. This study also considers the interactions between different geometric parameters rather than considering each in isolation; something not previously examined. Non-standard parameters, such as impeller tilt and eccentricity, are also considered as a method of reducing quasi-solid body rotation, while avoiding the use of baffles, which have previously been shown to inhibit the drawdown of incorporable solids above approximately 10 wt.% solids in Chapter 2.

3.3. Experimental

All experiments were carried out in a flat bottomed cylindrical 5 dm^3 vessel with diameter, T = 0.17 m and initial liquid height, H_0 = T. The geometric parameters considered were impeller pumping mode (up- versus down-pumping PBTs), impeller eccentricity, impeller tilt, and impeller submergence, shown in Figure 3-1. No baffles were used in the vessel. The impellers studied had a diameter, D = 0.085 m (D/T = 0.5). This diameter was selected based on previous studies indicating that this would outperform smaller impellers in terms of required impeller speed and power at higher solid contents, as shown in Chapter 2.

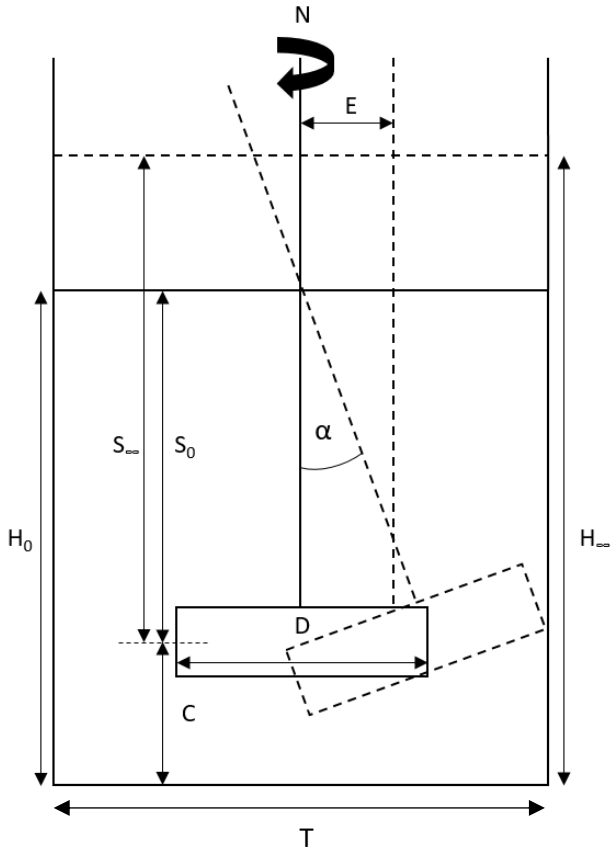

Figure 3-1: Vessel Schematic

The vessel was filled to an initial height, H_0/T = 1, with 3.86 dm^3 of liquid. An equal mass of solid was pre-weighed into 50 aliquots of 77 g using a KTron KT20 loss in weight powder feeder set to deliver a fixed mass. Each aliquot was poured in one motion to the centre of the vessel to remove

disturbance effects due to addition location or rate. An aliquot was added every two minutes. The impeller speed was adjusted upwards as required to ensure that the "just incorporated" condition was maintained throughout the experiment.

The total mass of powder added was 3.85 kg, giving a final slurry concentration (X) of 50 wt.%. A porous γ-alumina, Sasol Puralox SCFa-140, was used as the dispersible solid. This alumina is the same porous ceramic as used in Chapter 2, with a poured bulk density of approximately 560 kgm^{-3} and D_{50} of 30 µm, that initially floats. Once incorporated however, the pores fill with fluid and the particles sediment if not agitated. Powder was added in 50 aliquots to allow the effect of increasing solid concentration to be seen on drawdown performance. It also ensured each aliquot was sufficiently large to completely cover the liquid surface when at rest.

An aqueous acetic acid solution, initially 6 wt% acetic acid and pH 3, was used as the liquid. This was done in order to maintain a low viscosity, Newtonian liquid throughout the experiment by ensuring that pH remained well below the isoelectric point of the alumina slurry. The pH of a final 50 wt% slurry was in the range 4.8 - 5, whereas the isoelectric point for this powder is in the range 7.7-7.9 (S. Adegbite 2010). This increased pH not caused by dissolution of the particles, which are insoluble. Rather it is due to the amphoteric nature of alumina particles which, when suspended in water, due to the reaction of surface hydroxyl groups (Yokosawa *et al.* 2002). The vessel was double walled with a cooling water flow through the outer jacket. The cooling water was kept at 5^0C. This was used to reduce the effect of slurry temperature on viscosity.

The incorporation performance is defined as the impeller speed and power required to ensure the *Just Incorporation* condition where no fresh powder spent longer than four seconds at the vessel surface, *see* Chapter 2. These measures are termed N_{JI} and P_{JI} respectively and are similar to the *Just Drawdown* condition used in reported studies by other workers. However, the conditions are distinct as just drawdown is a steady state, reversible condition, whereas just incorporation is not.

An initial H/T = 1 was used in all experiments. As solid was added to the vessel the liquid level increased to give a final H/T = 1.2, meaning the initial and final submergence of the impeller is different. This increase in liquid level and submergence does have a detrimental effect on the drawdown and incorporation of powder from the surface with all other geometric parameters remaining constant, as in Chapter 2. However, this effect is considerably smaller than the effect of the increasing solid content.

The impeller shaft torque (Γ) was measured using a calibrated Binsfield TorqueTrak 10k wireless strain gauge attached to the shaft. The impeller power draw (P) was then calculated from the torque using equation 11.

$$P = 2\pi N\Gamma \tag{11}$$

The measured torque, and so impeller power draw was found to fluctuate by ±5 % of the reading value. All values quoted are the mean value recorded over time at a sampling frequency of 10 Hz.

A full factorial design of experiments (DoE) with centre points approach was used to design an experimental matrix to maximise the information captured regarding the effect of individual variables and the interactions between different variables. The high, centre point, and low values for each of the variables considered is shown in Table 3-1.

Table 3-1: Design of Experiments: Variable high, centre point, and low values

Variable	High	Centre Point	Low
Pumping Mode	Up	-	Down
Eccentricity	0.2 T	0.1 T	0
Tilt (^{o})	20	10	0
Submergence	0.3 T	0.5 T	0.7 T

The design, with four variables and two centre points (one for each pumping mode) gives rise to 18 trials, as shown in Table 3-2. Each experiment was repeated three times. Measurements were found to be repeatable to ±5 RPM. The average value of the three runs is reported herein. For

trials outside of the DoE design space described in Table 3-2 each of the other variables were kept constant, at a standard value. The standards used in these cases were taken as the "low" values from Table 3-1 for all parameters. These further non-orthogonal trials were added following the orthogonal DoE to probe further behaviour of a single parameter at a time.

Table 3-2: List of trials

Run Order	Pumping Mode	Eccentricity	Tilt	Submergence
1	Down	0.2	20	0.3
2	Up	0.2	20	0.7
3	Down	0.2	0	0.7
4	Down	0.2	0	0.3
5	Down	0	0	0.3
6	Down	0	20	0.3
7	Up	0	0	0.7
8	Down	0	20	0.7
9	Up	0	0	0.3
10	Up	0	20	0.7
11	Up	0	20	0.3
12	Down	0.1	10	0.5
13	Down	0	0	0.7
14	Down	0.2	20	0.7
15	Up	0.2	0	0.7
16	Up	0.2	0	0.3
17	Up	0.1	10	0.5
18	Up	0.2	20	0.3

Following this initial scoping factorial design, each of the numeric factors were further probed with additional data points both inside the initial design space, and outside where appropriate. This was done to find turning points in behaviour to find optimal configurations. This involved measuring at submergences between 0.1 T – 0.8 T in 0.1 T increments, at tilts of 5° and 15°, and at eccentricities of 0.5 T, and 0.15 T as well as the initial scoping set points.

In order to validate the effect of optimising the vessel geometry, a trial was carried out. During this trial powder was added to the vessel as quickly as possible (as soon as the previous aliquot had been drawn down) at a fixed impeller speed of 450 RPM (the maximum speed required to

maintain N_{JI} for the optimum configuration up to 50 wt%). The time and energy required to prepare a 50 wt% slurry was measured in this manner for both the optimal geometry and a six bladed Rushton turbine with D/T = 0.5, S_0/T = 0.7, with no baffles, eccentricity or tilt.

3.4. Modelling Approach

A general linear model (GLM) was built using stepwise regression using the 18 data points described in table 3-2 and all the extra non-orthogonal trials. This GLM is designed to give the N_{JI} and P_{JI} required to incorporate solids at a fixed solid content as a function of the geometric conditions studied. The stepwise approach used involved bidirectional elimination, where variables are tested to see whether they improve the fit of the model or not, as indicated by the Akaike information criterion (AIC), with low AIC values indicating a better model fit to the data. Both main effect and interaction terms were used to build the models used in this chapter. Quadratic terms were not used.

3.5. Results and Discussion

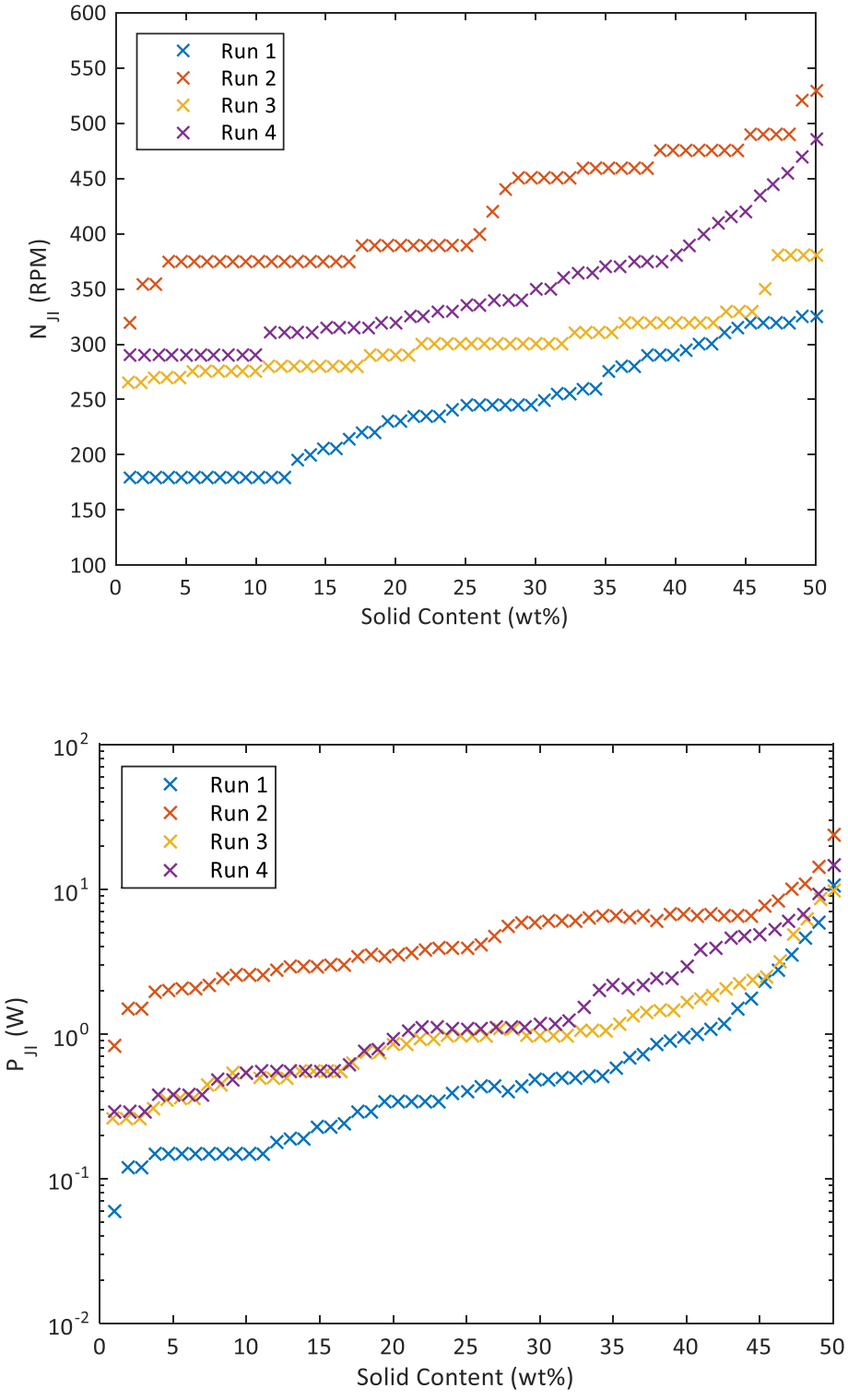

Figure 3-2: (a) N_{JI} evolution with increasing solid content for first four runs; (b) P_{JI} evolution with increasing solid content for first four runs (only four runs shown for clarity)

Figure 3-2 shows the measured N_{JI} and P_{JI} data respectively for the first four trials in the experimental matrix. Better drawdown and incorporation performance is characterised by lower N_{JI} and lower P_{JI} at a given solids content. At low solid contents (<30 wt%) N_{JI} increases approximately linearly with solid content and so can be modelled as a straight line with the intercept and gradient values shown in Table 3-3. In Chapter 2 it was observed that there is a significant increase in both impeller speed and power draw required to maintain just incorporation as the solid content increases. It was also observed that, for the most part, impeller selection ranking does not change with increasing solids content; what is good at low solids remains good at high solids and *vice versa*. The above sample of results indicates that the same is largely true for geometrical designs. Thus, poor performing geometries perform poorly at low and high solids content. The difference in power draw between the best and worst does become less significant at highest solids, as the effect of the high viscosity dominates over geometry considerations. The impact of the specific geometric design parameters will be discussed in the context of the statistical analysis of the data.

Table 3-3: N_{JI} results for 30 wt% slurries and linear model parameters for each trial

Run Order	N_{JI} at 30 wt%	Gradient	Intercept
1	240	3.0	163
2	450	2.6	345
3	290	1.3	264
4	320	2.5	278
5	300	2.4	275
6	250	2.1	222
7	305	0.8	281
8	260	1.1	241
9	295	1.9	267
10	440	0.6	418
11	330	2.3	295
12	250	2.1	203
13	320	1.5	294
14	265	1.8	226
15	335	2.9	271
16	320	1.3	289
17	350	1.2	314
18	360	1.3	321

3.5.1. Main Variable Effects

When using a Design of Experiments approach, the simplest method of looking at the effect of each variable is the Main Effects plot. This takes the mean value of all measurements for a variable at each set point. For example the Main Effect value for 'down' for pumping mode would be the average of runs 1, 3-6, 8, 12-14. The main effects plot, shown in Figure 3-3, uses the mean value of N_{JI} for each variable under each condition studied and can be used to see high level trends from each of the variables considered. This approach allows consideration of both categoric and numerical variables. The importance of each primary variable is reflected simply by the ranges of the output variable responses: pumping mode is the most important, tilt and eccentricity have similar (non-monotonic) but minor effects while submergence seems to become important at higher values (where the impeller is in the lower half of the vessel). Simply considering the main effects suggests that using a down pumping PBT with 10° tilt, E/T = 0.1, and

a low submergence will give the best drawdown performance, as this is the set of variable conditions which each give the lowest value of N_{JI} and therefore best incorporation performance.

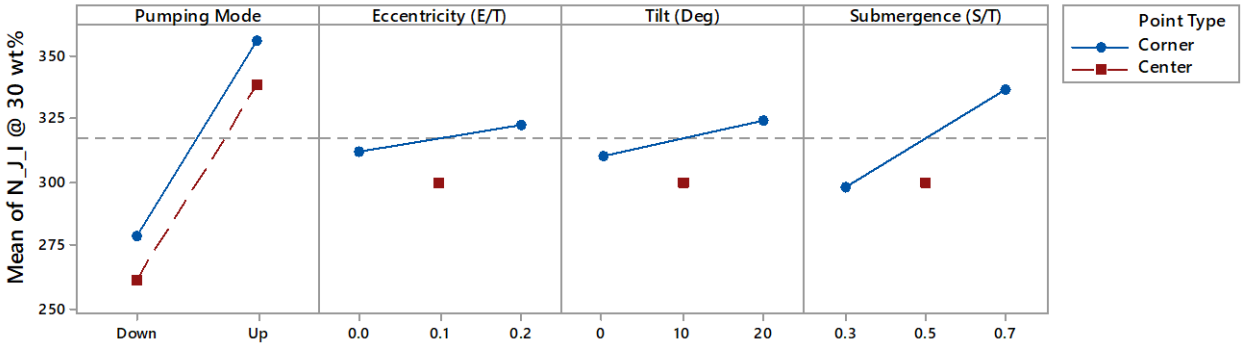

Figure 3-3: Main Effects Plot at 30 wt% for impeller speed at just incorporation condition

3.5.2. Variable Interactions

The above discussion and results presentation considers only the uni-variate impact of each design parameter. Stirred vessel design is however a multi-variate problem, where changing one parameter may impact the influence of another. It is therefore important to assess any inter-dependency of the primary parameters. Figure 3-4 is the interaction plot and presents a more detailed breakdown of the Main Effects Plot, separating the design parameters to assess the interactions between them. Each point on the interaction plot represents the mean value of all runs with both variables considered, held at a specific set point. To aid interpretation of these plots, converging lines in the Interaction Plot, Figure 3-4, indicate the presence of interactions between variables whereas parallel lines suggest those two variables are substantially independent.

There is a strong interaction between pumping mode and every other variable, as seen in the first column. This means there is a significantly different response when changing tilt, eccentricity, or submergence depending on whether the impeller is in an up- or down-pumping mode. For each of these interactions the best performance for the up-pumping impeller is the low value for each

variable, whereas for the down-pumping impeller it is the center point of each value. Each of these interactions is considered in more detail below.

There is also a slight interaction between impeller tilt and submergence, with tilting the impeller proving to be detrimental to drawdown performance at higher impeller submergences. This matches with experimental observation that at high submergence and high tilt the impeller shaft passes through the liquid surface close to the vessel wall resulting in a very narrow gap where dry or semi-wetted powder agglomerates would adhere to the wall and shaft, creating a static site for further agglomeration which could not be easily drawn down and incorporated.

There is no interaction between eccentricity and impeller tilt. This is probably because they both achieve similar effects on the flow pattern; reducing quasi-solid body rotation and increasing axial and radial flows in the vessel and increasing the impeller power delivery.

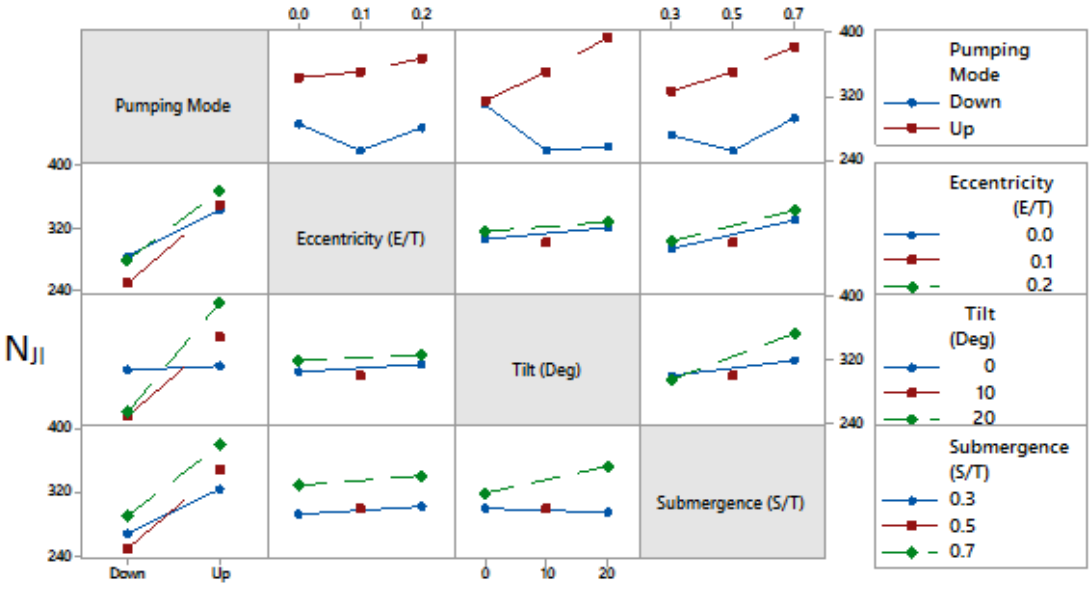

Figure 3-4: Interaction Plot at 30 wt% for impeller speed at just incorporation condition

3.5.3. Complex Variable Effects

Some of the main effects and interactions present complex and non-linear trends that require further investigation, such as the interaction between pumping mode and tilt and the impact of submergence. These are explored in more detail below.

Figure 3-5 shows a more detailed view of the interaction between pumping mode and impeller tilt, where each measurement is represented by a single point. It also includes extra measurements at tilts of 5° and 15° to further probe the linearity of the system response to impeller tilt. The spread of points at 0° and 20° show the presence of an effect from other variables. It is important to note that this spread is significantly larger for the up-pumping impeller than for down-pumping. This indicates that when pumping upwards the system is much more sensitive to the effect of the variables changing.

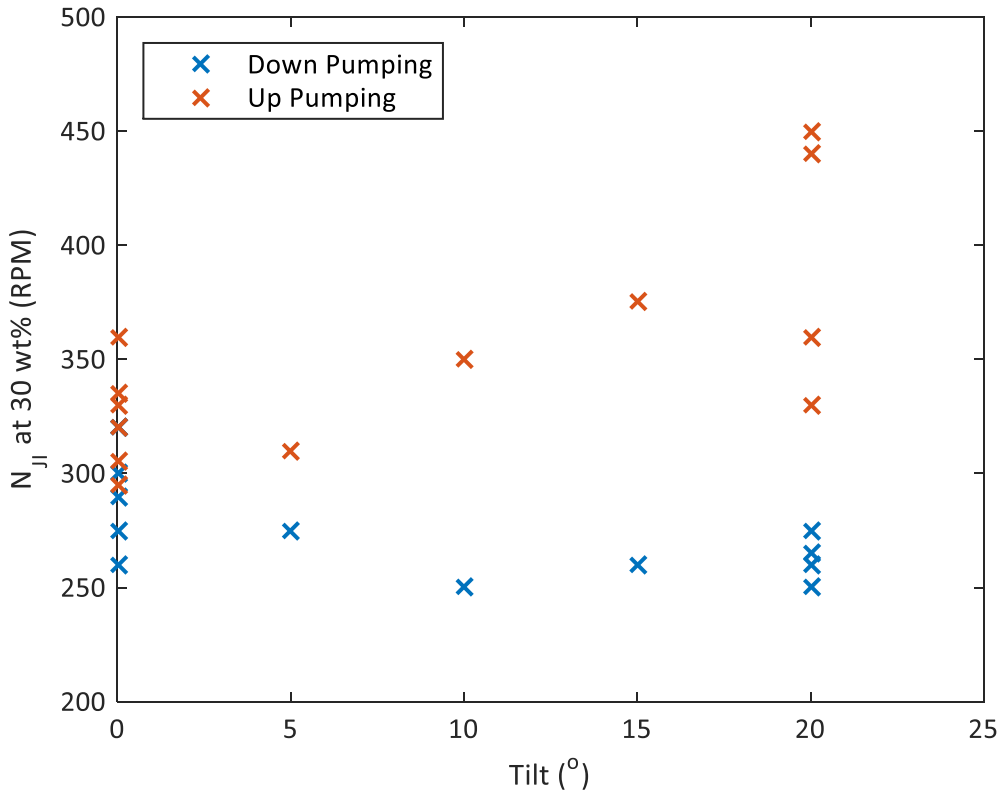

Figure 3-5: Effect of interaction between impeller tilt and pumping mode on N_{JI} at 30 wt% solid content

There is a different response to impeller tilt depending on pumping mode, with a small improvement in drawdown performance generally seen with tilting a down-pumping impeller. Conversely, there is generally a decrease in drawdown performance with increasing impeller tilt for an up-pumping impeller.

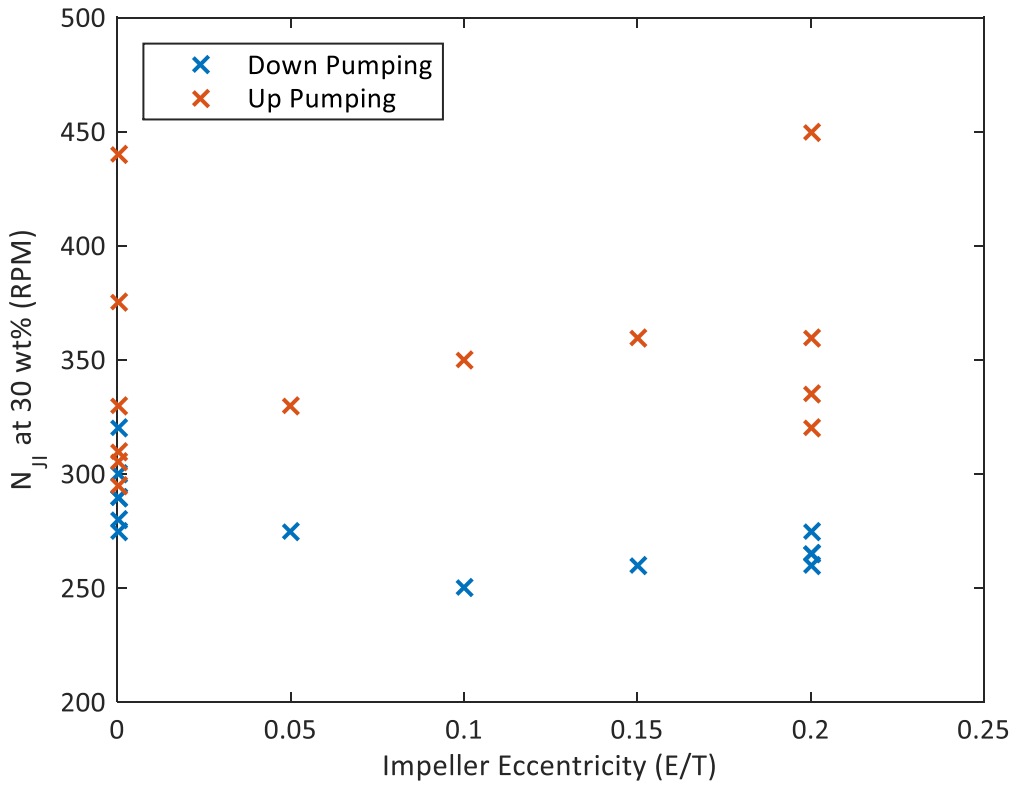

Figure 3-6: Effect of interaction between impeller eccentricity and pumping mode on N_{JI}

In Figure 3-6, the effect of eccentricity is minimal regardless of pumping direction. Again, each individual point represents a single measurement with extra trials on top of the DoE at E = 0.05 T and E = 0.15 T to probe the linearity of the system response to eccentricity. There is evidence of a slight negative correlation between tilt and N_{JI} for the down-pumping impeller, suggesting that eccentricity can marginally improve drawdown performance. This is not the case for the up-pumping impeller where there is no obvious effect of eccentricity.

The up-pumping impeller again shows a significantly larger spread of values than the down-pumping impeller, showing a greater dependency on geometry interactions than the down-pumping impeller for effective drawdown to occur. The minimum impeller speed required for the down-pumping impeller is seen at a slight eccentricity of 0.1 T. However, the minimum for the up-pumping impeller is found at zero eccentricity.

Figure 3-7a shows the three-way interaction between submergence, solid content and pumping mode. Each set of points is a single experiment, where solid content was increased for a constant geometry, using "low" values for eccentricity and tilt for three different submergences for each impeller. Again; there is a different response to submergence depending on pumping mode. For the down-pumping impeller the best performance was at an initial submergence of $S_0/T = 0.5$ whereas, for the up-pumping impeller best performance was as close to the surface as possible at $S_0/T = 0.3$. This difference is explained by visual observations when conducting the experiments as the down-pumping impeller entrained air from the surface straight to the impeller, reducing the effectiveness of the impeller whereas the flow pattern in up-pumping mode prevented this. Both impellers gave their worst drawdown performance when in the bottom half of the vessel with an $S_0/T = 0.7$.

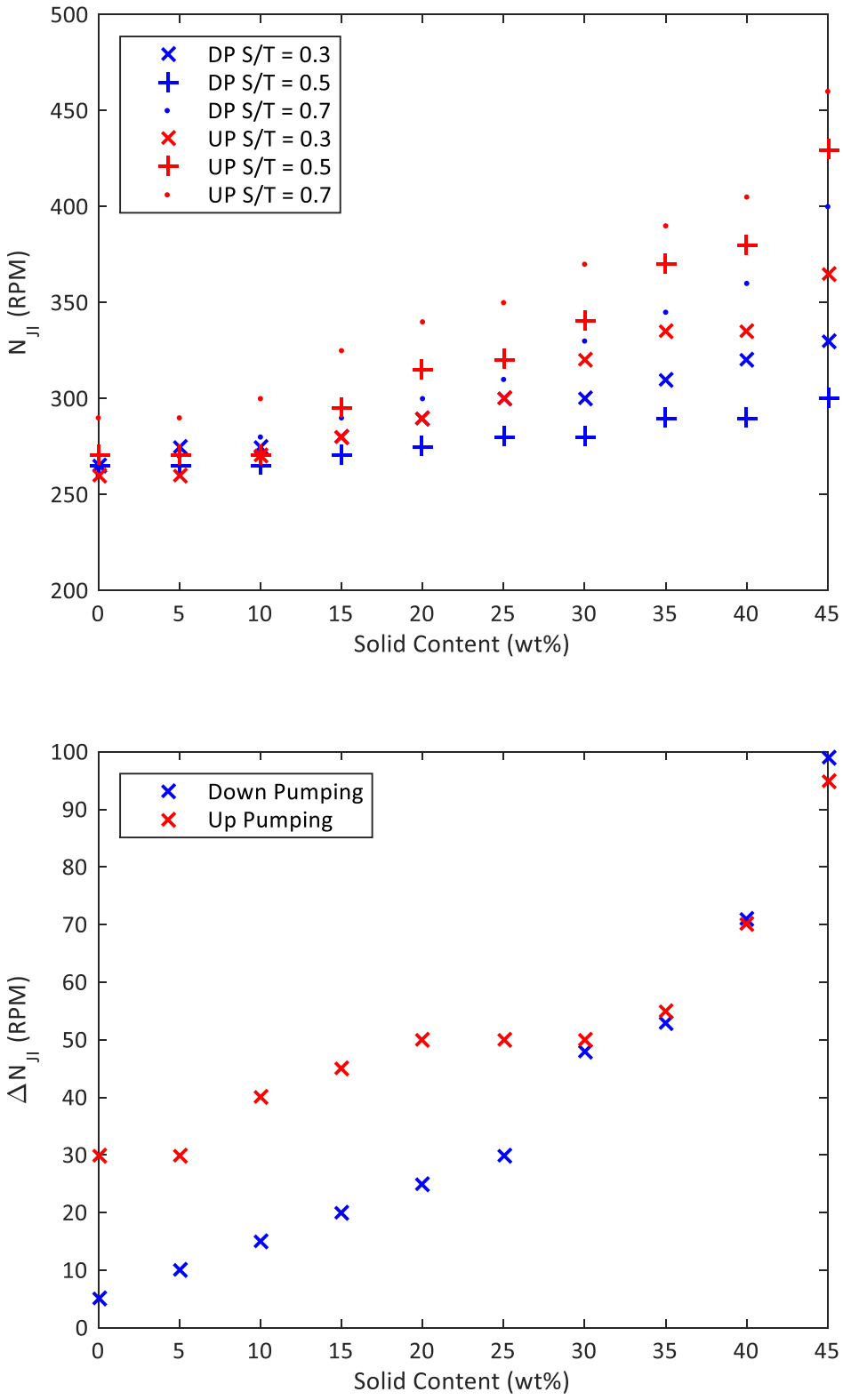

Figure 3-7: (a) Change in N_{JI} with increasing solid content and varying impeller initial submersion (b) Difference between highest and lowest required N_{JI} across all submergences measured

At the lowest solid contents studied the up-pumping impeller was more sensitive to impeller depth, with a larger difference between the impeller speeds required at the best and worst performing depths, as shown in Figure 3-7b, which shows the difference between the best and worst performing submergence in Figure 3-7a. This is a consistent with the observations of Khazam and Kresta (2008). However, as the solid content increases this difference between pumping mode becomes less marked, a new result since this phenomenon has not previously been studied at higher solid contents.

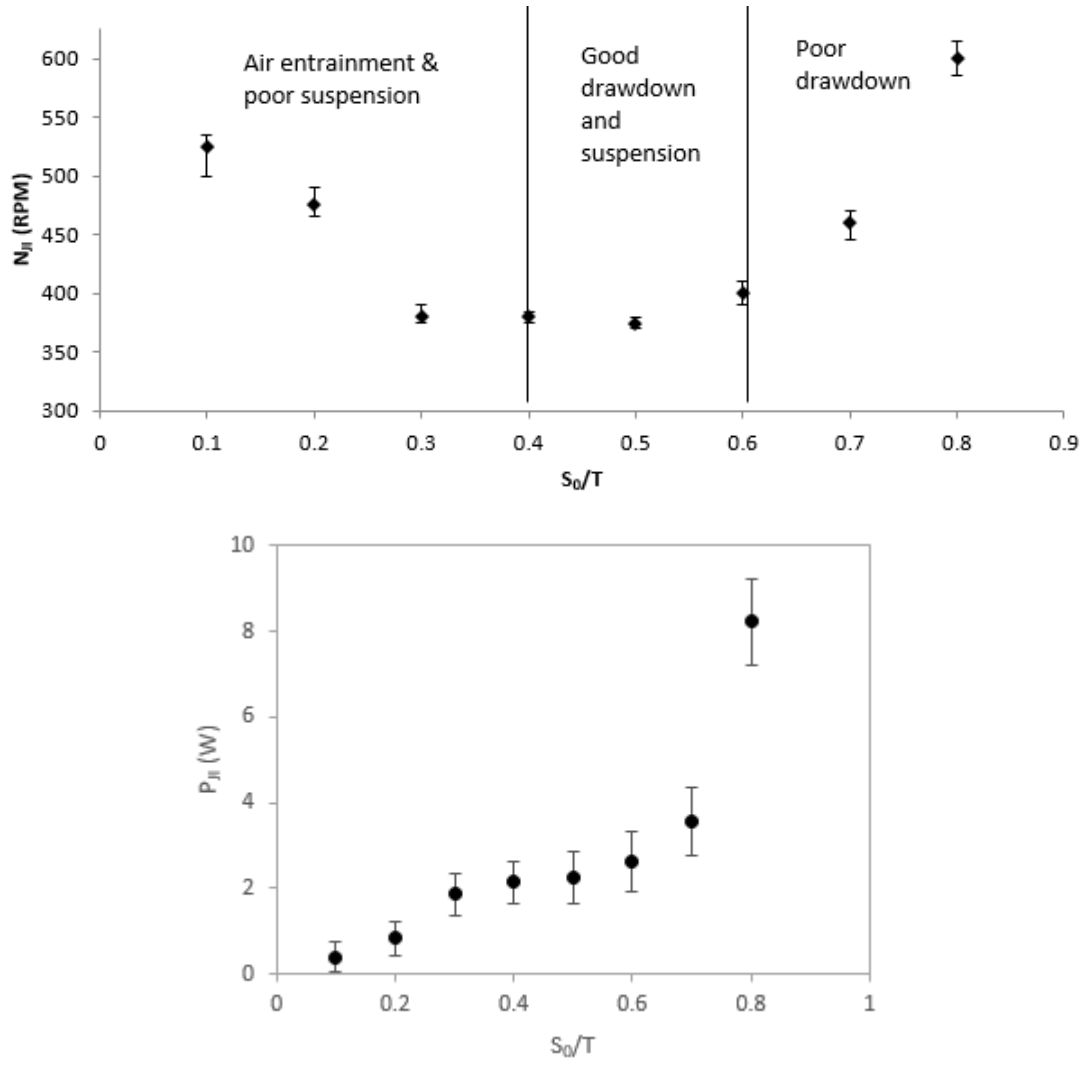

Figure 3-8: *(a) N_{JI} at 40% by weight solids with varying initial impeller submergence for up pumping PBT with D/T = 0.5 (b) P_{JI} at 40% by weight solids with varying initial impeller submergence for up pumping PBT with D/T = 0.5*

Figure 3-8a shows the effect of submergence on impeller speed required for drawdown for an up-pumping impeller with no tilt or eccentricity. As seen in other studies on low solid contents; increasing the impeller submergence above ~ 0.6 T has a negative impact on drawdown and incorporation performance. However, in contrast to many of these other works, performance does not continue to increase indefinitely as the impeller is brought closer to the surface. At submergences less than 0.4 T there was significant air entrainment, causing semi-permanent bubbles to form at the liquid surface. These bubbles provided surface area for dry or semi wet solid to bind to, increasing buoyancy force and preventing full incorporation into the slurry. Figure 9b shows the P_{JI} values as a function of S_0/T and indicates that the power draw fall off significantly at S_0 below 0.3 T; despite an increasing N_{JI}. A gassed system would draw significantly less power than an un-gassed system (Middleton 1992). This fall off in power draw thus confirms that surface aeration is significant and the probable cause of the loss of incorporation performance. Although good drawdown performance was seen for a submergence of 0.3 T, once the vessel was drained a significant amount of sediment was found on the base of the vessel. This was not true for greater impeller submergences, suggesting that for submergences of 0.3 T and below, the impeller is too far from the base of the vessel to provide sufficient vessel turnover to ensure complete suspension at the Just Incorporation condition.

This was not true at submergences above 0.3 T, suggesting that for drawdown and incorporation processes there is an optimum range of impeller submergences between 0.4 – 0.6 T, as shown in Figure 3-8a. This observation was true for both up- and down-pumping impellers.

3.5.4. Optimal geometry and Validation

The DoE can be used to specify the best conditions for each of the impellers studied and then to design an optimal geometry. This optimum geometry is found using the general linear model built using all the datapoints described above. The model performance is shown in Figure 3-9, it gives decent predictive performance with an r^2 on the training data of 0.78 and r^2 for test data of 0.74 and RMSE = 33.5. The optimum point is highlighted to show that it is well predicted by the model.

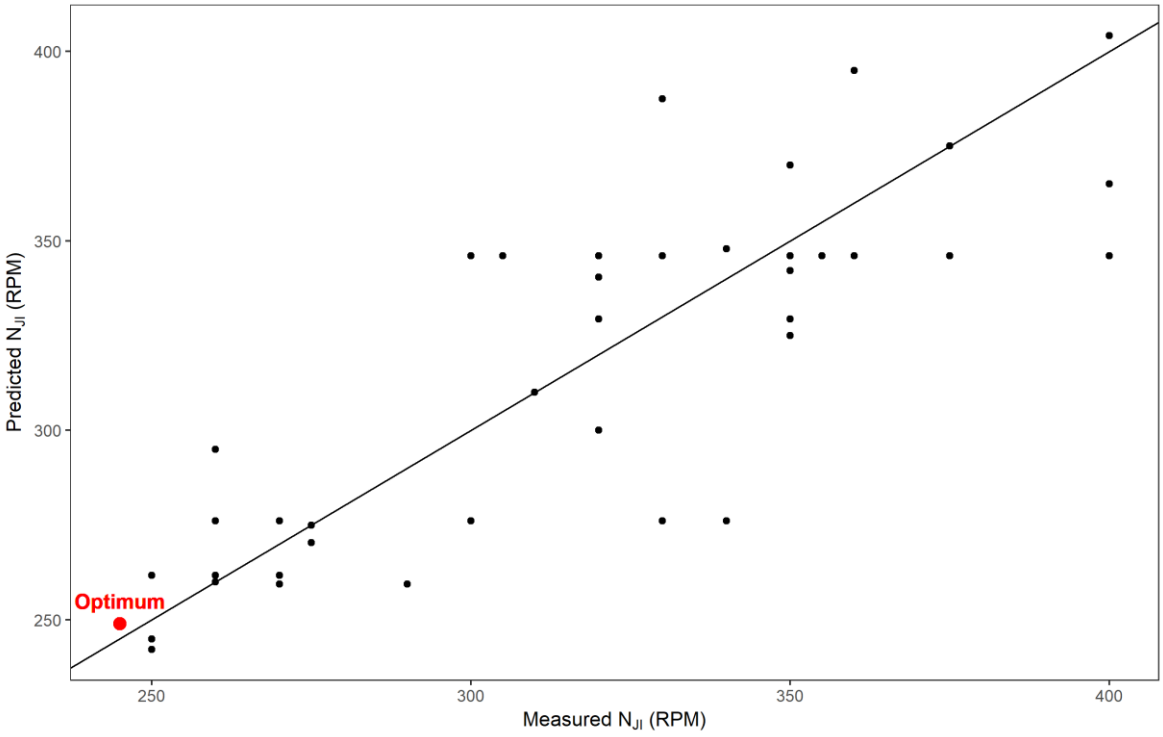

Figure 3-9: Performance of general linear model, with r^2 = 0.78 and the optimum point highlighted

For the down-pumping impeller the optimum submergence occurred at S_0 = 0.5 T, the optimal tilt was 10°, with a slight eccentricity of 0.1 T, this happened to be the central point of the design.

For the up-pumping impeller the best conditions were as close to the surface as possible, whilst maintaining suitable suspension (S_0 = 0.4 T), with no tilt or eccentricity. The down-pumping impeller was much less sensitive to changes to other aspects of the geometry and capable of

giving a better drawdown performance, so the full optimised geometry design uses a down pumping impeller, as shown in Table 3-4.

Table 3-4: Optimal geometry configuration

Property	Value
Impeller Type	PBT
Pumping Mode	Down
Impeller Diameter	0.5 T
Baffles	None
Impeller Submergence	0.5 T
Impeller Tilt (°)	10
Impeller Eccentricity	0.1 T

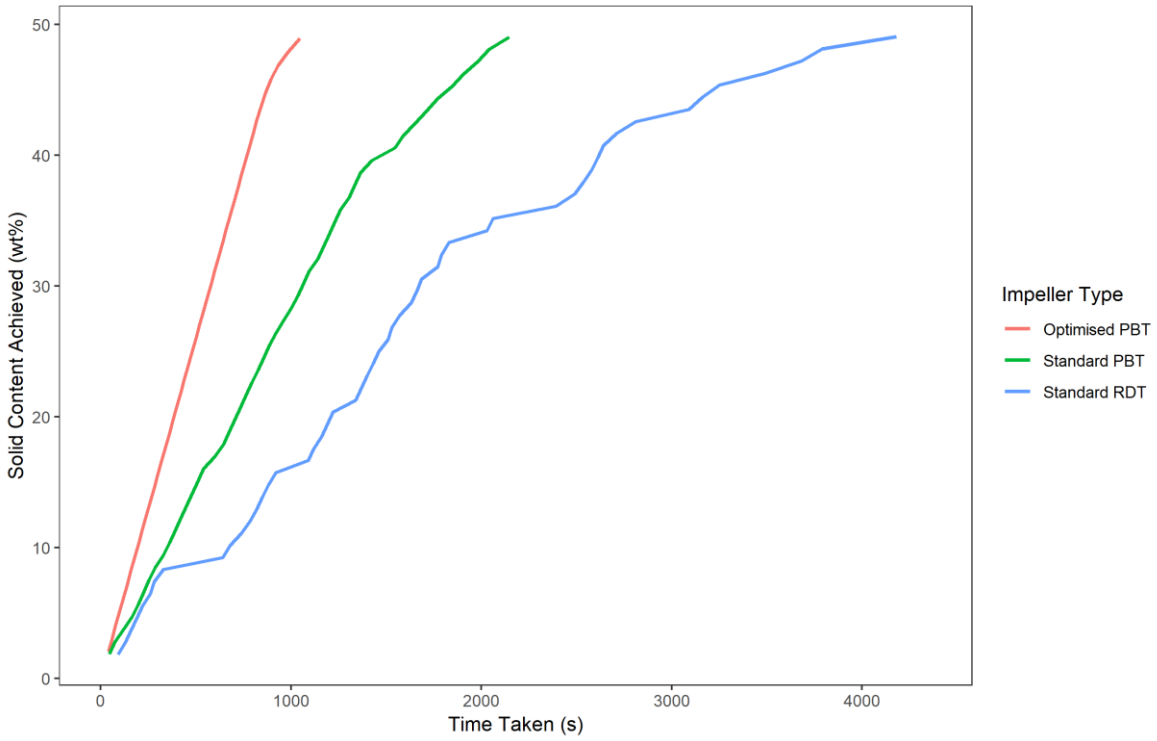

Figure 3-10: Minimum time required to prepare a 50 wt% slurry with the optimised geometry vs a standard Rushton turbine and down pumping PBT, all at 450 RPM

Figure 3-10 shows a comparison of the time taken to prepare a 50 wt% slurry using this optimal geometry against a Rushton turbine and an unoptimized down pumping PBT, all running at the same impeller speed. Whereas the Rushton required over an hour to prepare the slurry, the

optimised geometry only took 17 minutes. This demonstrates the effectiveness of an optimised geometry design for the drawdown and incorporation of floating solids to prepare concentrated slurries. It also serves to emphasize the importance of good impeller and vessel design in achieving effective powder incorporation.

3.6. Conclusions

This work uses a design of experiments approach to fully optimise a geometry for the drawdown and incorporation of floating solids to prepare high solid content suspensions. The use of a full factorial orthogonal DoE enables an analysis of the effects of key geometric variables and the interactions between these variables. The variables specifically focussed on are impeller pumping mode, tilt, eccentricity, and submergence within the mixing vessel.

The most significant variable is impeller pumping mode with down-pumping impellers generally out performing up-pumping impellers in terms of drawdown performance. Down-pumping impellers perform better both in terms of the best possible performance in terms of the smallest possible N_{JI} required under optimal configuration, but also in terms of sensitivity to interactions with other variables. The up-pumping impeller showed significant decreases in performance if moved eccentric, tilted or at higher initial submergences whereas the down-pumping impeller showed improvements with tilt and eccentricity.

The best performing set of conditions involved using a down-pumping PBT with no baffles and D/T = 0.5 at an initial submergence halfway down the vessel ($S_0/T = 0.5$; $H_0/T = 1$), a 10° tilt and eccentricity of 0.1 T. The best set of conditions for using an up pumping impeller were as close to the surface as possible ($S_0/T = 0.4$), no impeller tilt, or eccentricity. However, there was a significant amount of sedimentation at the lowest submergences for both up- and down-pumping impellers therefore it is not recommended to operate at an $S_0/T < 0.4$ in order to maintain both effective drawdown and incorporation, and suspension.

A comparison of the optimised geometry against a completely unoptimised mixing system shows a dramatic reduction in processing time required to prepare a 50 wt% slurry. The optimised system took less than one third the time required by a Rushton turbine to prepare the same slurry, demonstrating the effectiveness of simple geometry optimisation for this process.

4.

Industrial Case Study – Continuous Powder Incorporation: From Laboratory to Production Scale

This Chapter describes the development of a production scale continuous powder incorporation process. The process is studied at lab, pilot, and production scales with positive results for preparation of multiple different slurries. Alumina, zeolite, mixed oxide, magnesia, and glass ink slurries are all successfully produced to specification at production scale for three different products spanning three different business units within the sponsor company.

The final continuous process is based around an IKA MHD continuous powder incorporation mixer, fed by a KTron loss in weight powder feeder. Of all powder studied only one posed any problem to the designed process, a stabilised γ-alumina. However, design of a post processing operation showed that this could be overcome, enabling a system to be designed that can produce all products studied to specification at production scale.

4.1. Chapter Preface

The work in this Chapter was part of several projects within Johnson Matthey, in collaboration with multiple other people and business units. The lab scale work was primarily done by Thomas Wood, however much of the work on ink formulations was assisted by Ajay Tharakan (JMTC), Timothy Addison (JMTC), and Fred De Munck (JM Advanced Glass Technologies). The lab scale work on aluminas and other emission control support materials was done by Thomas Wood and Simon Hackett (JM ECT). All lab scale work on magnesia was done by Thomas Wood alone.

The pilot scale rig at JMTC Chilton was designed by Timothy Addison and Thomas Wood with the assistance of Billingham Research Engineering at JMTC Chilton. All work at this scale was performed by Thomas Wood and Timothy Addison, with assistance from Simon Hackett and Sylvester Mudaly (JM ECT) when working on emission control support materials.

The production scale trials performed at IKA, Germany, were carried out as a group project by Thomas Wood, Timothy Addison, Simon Hackett, Sylvester Mudaly, Fred De Munck, and Sandra Cabanas (JM AGT) from Johnson Matthey with support from Diego Sanchez and Christof Maier (IKA Process GmbH).

4.2. Introduction

The work described within this Chapter describes the proof of concept, scale up, and design of a manufacturing process for the continuous incorporation of powdered solid into liquid to produce high solid concentration slurries. This work initially focuses on the preparation of slurries for the incorporation of glass frit and pigments into an oil based medium for Johnson Matthey Advanced Glass Technologies. However, due to the success of this project within the business, it was also implemented for the emission control catalyst support material described in Chapter 2, and for incorporation of magnesia powders for the production of hydrotalcite. Each of these processes is described in detail in Chapter 1. The work for all three of these applications is described here.

Continuous processing has been successfully implemented across a wide range of process industries, including the pharmaceutical (Poechlauer *et al.* 2012; Poechlauer *et al.* 2013; Badman and Trout 2015), bioprocessing (Konstantinov and Cooney 2015), chemicals (Calabrese and Pissavini 2011), and manufacturing (Anderson 2001; Gonnissen *et al.* 2008) industries amongst others.

The main drivers in making this step change are generally the belief that continuous manufacture provides more consistent product, enables a smaller plant footprint as large batch vessels are not required and leads to reduced capital cost and operator involvement (Konstantinov and Cooney 2015). However, continuous manufacture is often negatively associated with issues in batch tracking (continuous online quality control is needed) and a reduced flexibility in the manufacturing system once fully designed (Plumb 2005).

There are numerous studies considering the continuous handling of powders (Pernenkil and Cooney 2006). For example Laurent and Bridgwater (2002) used PEPT tracer particles to assess the effect of agitator design on mixing performance in continuous paddle mixers. Sherritt *et al.* (2003) also used PEPT to study continuous powder blending in a rotary drum, considering design

parameters such as the rotation rate of the drum, fill level, drum size, and particle size. Portillo *et al.* (2008) used NIR spectroscopy to assess levels of powder mixing in a continuous high shear powder mixer, whilst varying design parameters such as mean residence time, impeller speed and design, and number of passes through the mixer. These studies and many others give a good empirical understanding of important factors in designing continuous powder blending processes. These processes are discussed more in Chapter 5.

Similar approaches have been carried out to study continuous delivery of powdered solids using powder feeders (Pernenkil and Cooney 2006). Powder feeding can generally be performed volumetrically or gravimetrically, with gravimetric feeding generally accepted as the more reliable of the two approaches (Harwood *et al.* 1975; Weinekötter and Gericke 2006). Wang *et al.* (2017a) studied the effect of powder properties on the performance of a loss in weight powder feeder, using multivariate statistics to show that the flow properties of the powder strongly determined the accuracy of feeding performance.

However, continuous powder incorporation into suspension is a much less studied system than continuous powder blending. Despite this, numerous devices are available to achieve this duty, both at the lab and manufacturing scale. Examples include the IKA MHD 2000, a dedicated continuous powder incorporation system made by IKA Process GmbH. This device is based on creating a high shear mixing environment comprised of a series of alternating up and down pumping impellers, rotating at high tip speeds (nominally 23 m s^{-1}). Liquid is sprayed into this environment horizontally whilst powder is conveyed vertically down into by a screw, generally fed by a screw powder feeder directly into the top of the mixing unit. The resultant mixture is very quickly forced through a stator. The MHD is made at seven different scales, with product throughputs of 60 L hr^{-1} to 40,000 L hr^{-1}, each of which operates at the same tip impeller speed. An example device is shown in Figure 4-1 (IKA Process GmbH 2017).

Figure 4-1: IKA MHD

YTRON make two continuous mixing devices designed for incorporation of hard to wet powders: the YTRON-XC and the YTRON-ZC. The YTRON XC works by drawing powder into a mixing chamber directly from a big bag by creating a strong negative pressure. Liquid is pumped into the mixing chamber, where it is contacted with the powder. Immediately after contact the mixture is pumped against impact plates, designed to promote mixing of the two phases. After this the mixture is discharged. The XC is designed to be a low shear mixing device, with the energy dissipation created by a high frequency of collisions with impact plates instead of a high shear zone seen in many similar systems. The YTRON ZC is similar to the XC in that it draws powder into the mixing zone by creating a negative pressure. However, it utilises a rotor stator system in the mixing chamber to create high shear to mix the powder and liquid together. Schematics for the mixing chambers of the YTRON XC and ZC are shown in Figure 4-2 (YTRON Process Technology GmbH 2018).

Figure 4-2: (a) YTRON XC mixing chamber; (b) YTRON ZC mixing chamber

The Silverson Flashblend™ is a high speed, high shear continuous mixer designed for powder incorporation into liquids up to high solid concentrations. Similar to the YTRON ZC it works by drawing powder into a venture chamber by creating a negative pressure. The powder is contacted with water in this chamber, after which it is forced through a rotor stator at high speeds to create high shear. There are four scales of Flashblend™ operating at powder flowrates from 900 kg hr^{-1} to 15,000 kg hr^{-1}. Similarly to the IKA MHD, these are designed to be scaled on a constant tip speed as a standard according to the manufacturer. Figure 3 shows a representation of the Silverson Flashblend™ (Silverson Machines Inc. 2018)

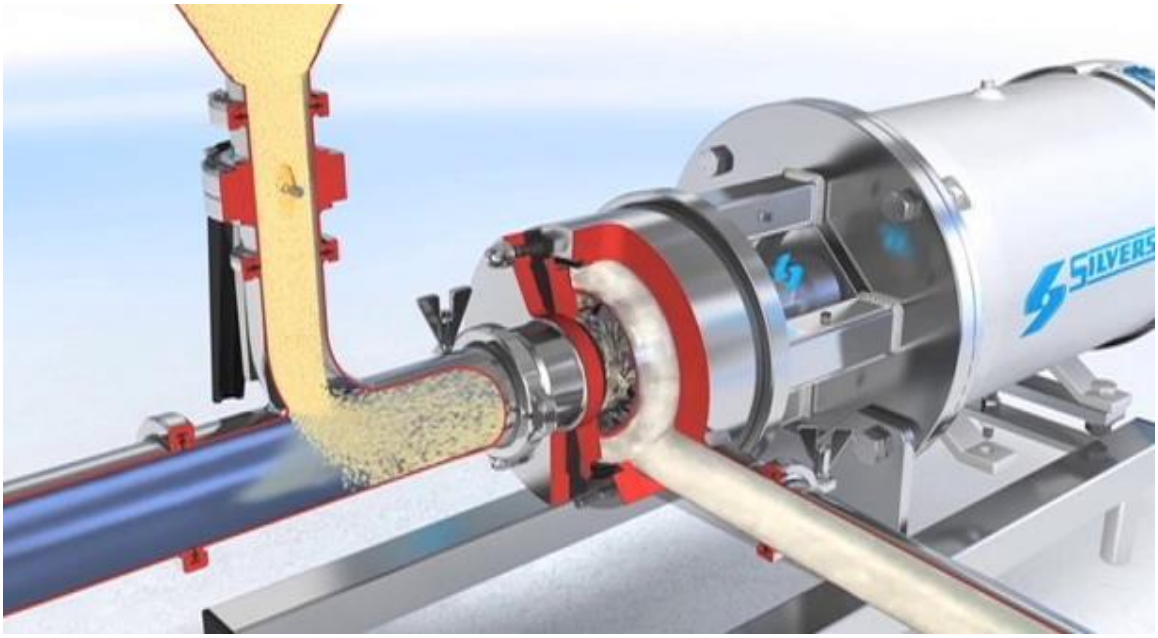

Figure 4-3: Silverson Flashblend™

The Admix Fastfeed™ system is a system designed to induce dry powder into a liquid flow using the Venturi effect. This is generally coupled with an Admix Dynashear™ in line high shear device to blend the powder into the liquid. Figure 4-4 shows an example of the Admix Fastfeed™ system.

Figure 4-4: Admix Fastfeed™

Despite the large variety of devices available for the continuous incorporation of powders they have received little academic attention; thus it appears that development on these devices has been kept in house with no publication of results. Prior to the start of this project each of these

devices were analysed by Johnson Matthey Technology Centre (Ajay Tharakan, 2013). This study was primarily focussed on the ink formulation process, described above, and found that the IKA MHD was the device best suited to the needs of the business at the time. Both YTRON and Admix advised that their devices would struggle to handle the high solid contents (<80 wt%) required. Even the smallest Silverson device was too large for the small-scale studies required for proof of concept and so a small scale IKA MHD was purchased on the recommendations of this study.

Chapter Structure

This Chapter describes a scale-up case study of an IKA MHD for continuous powder incorporation of a number of different catalyst and ink formulations. This device was studied at lab, pilot, and production scales throughout the course of the project. The experimental design and results at each of these scales is described in turn. Initially the lab scale studies are presented, where a small MHD device was assessed for feasibility. Following success of the feasibility studies the small scale device was investigated further to explore the design and operability window for each of the main formulations studied. Following this the pilot scale trials are described, where a larger rig was built at JMTC to understand how the continuous incorporation process scaled from the small lab-scale device for each of the formulations studied. Finally the production scale trials carried out at the IKA GmbH test facility are described, leading into a description of the final detailed process design for a full scale production line, which was the ultimate outcome from this project.

4.3. Lab Scale

4.3.1. Materials and Methods

4.3.1.1. Materials

The work presented in this Chapter is done in support of three business units, each of which produce different products through different production processes. However, all processes share a common stage; powder incorporation to produce slurries of varying concentration. The three products considered are emission control washcoat slurries which are primarily alumina and zeolite slurries (as described in previous Chapters), magnesia slurries for use in hydrotalcite production for INTERCAT, and glass ink slurries for Johnson Matthey Advanced Glass Materials (AGT).

Table 4-1: Selection of powders studied during continuous incorporation scale up

Slurry Name	Business Unit	Powder	Liquid	Solid Content Specification (wt%)	Reason for study
P0 (γ-alumina 1)	ECT	Sasol SCFa-140	3% Aqueous acetic acid	50 %	General alumina (same as Chapter 2)
PA (stabilised γ alumina 1)	ECT	Rhodia MI365	3% Aqueous acetic acid	39 %	Problem powder
Copper Zeolite	ECT		Water	40 %	Important product
AZM9 Zeolite (Zeolite 1)	ECT		Water	40 %	Important product
Magnesia 1	INTERCAT	MgO 93 HR	3% Aqueous acetic acid	14 % (Higher if possible)	Production limited
Magnesia 2	INTERCAT	MgO 98 LR	3% Aqueous acetic acid	14 % (Higher if possible)	Production limited
Ink (glass frit 1)	AGT	Glass frit + pigment	Organic medium (pinene)	80 %	Key product

Table 4-1 shows the selection of powders and slurry formulations considered for the design and scale up work for the continuous incorporation of powders. Various powders were considered at

different stages of the design and scale up process for reasons described throughout this Chapter. However, P0, PA and the ink slurry were always used as standards across all scales to ensure comparison between scales and to batch processes described in Chapter 2.

Table 4-2: Properties of powders used in continuous incorporation studies

Powder Name	d_{10} (µm)	d_{50} (µm)	d_{90} (µm)	Skeletal density (kg m^{-3})	Poured density (kg m^{-3})	Tapped density (kg m^{-3})	Mean pore size (A)	Pore volume ($cm^3 g^{-1}$)
γ-alumina 1	4.02	18.80	39.30	3352	662	793	107	0.415
Stabilised γ-alumina 1	3.20	21.00	62.40	2731	380	498	181	0.7014
Magnesia 1	2.02	15.46	31.21	3580	651	883	307	0.241
Magnesia 2	1.98	16.42	33.12	3620	510	690	318	0.251
Glass frit 1	0.40	3.00	479.60	5389	1124	1337	0	0
Copper zeolite	1.99	5.02	10.89	2210	450	570	150	0.416

Table 4-2 shows the properties of each of the powders used in this study. Full details on the measurement of these properties is given in section 5.3.1, where powder characterisation for all powders studied in this thesis is described.

4.3.1.2. Equipment

The mixer studied at lab scale was the IKA MagicLAB (IKA Process GmbH, Germany) using an MHD head, one specifically designed for continuous powder incorporation. Figure 4-5 and Figure 4-6 (IKA Process GmbH 2017) show the design of the MHD head, intended to receive powder through gravity from the top and liquid pumped into the side of the mixer. These are then blended in a small chamber by the three four-bladed impeller turbines before passing through a stator.

The device generates very little pumping so the effluent is collected in a bucket below the open exit of the effluent orifice. The impeller is capable of operating between 5000 - 20,000 RPM, the ability to vary the speed is unique to the lab scale device, which is designed to use heads other than the MHD, many of which run at different speeds. This is not true for larger models, which run at a fixed speed. Powder delivery was achieved through a Coperion KTron KT20 (Coperion

GmbH, Germany), calibrated before use for each powder studied using the built in calibration tool. The KT20 is a loss in weight twin screw powder feeder with minimum powder flow rate of 1 kg hr^{-1} and a nominal maximum of 10 kg hr^{-1}. For trials on the MagicLAB the feeder was always operated in loss in weight mode to minimise error in powder delivery rates. Liquid was pumped to the MagicLAB using either a peristaltic or gear pump, always calibrated before use for each specific liquid. Details of the calibration are given in Appendix 1. A photo of the assembled test rig minus liquid feed and product collection buckets is shown in Figure 4-7.

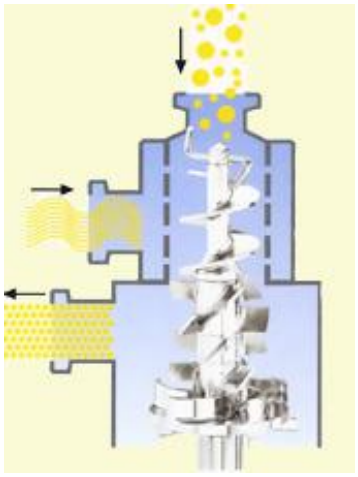

Figure 4-5: Schematic of MHD module for MagicLAB

Figure 4-6: Photo of IKA MagicLAB MHD head moving parts

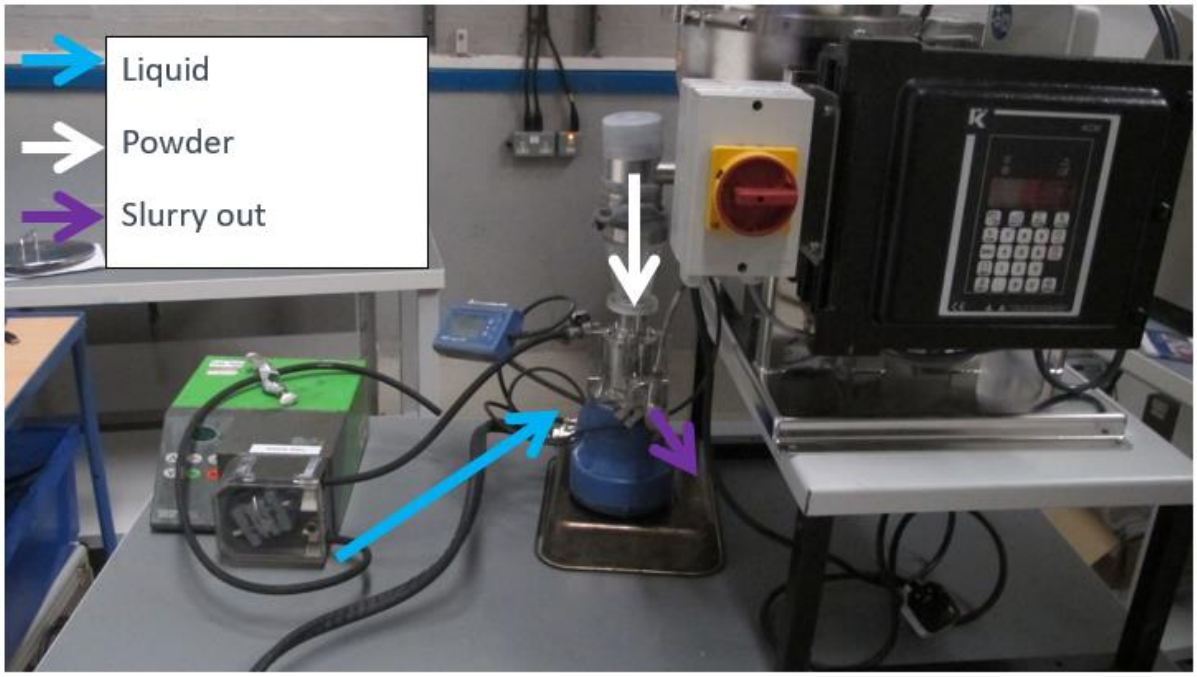

Figure 4-7: Photo of test set up for IKA MagicLAB

4.3.1.2.1. Start-Up and Shutdown Procedures

Start-up and shutdown procedures at the lab scale are complicated by the fact that the MagicLAB is a small piece of equipment and therefore not suitable for the use of a double mechanical seal between the motor and moving parts. This is not a limitation in larger models studied below, which are capable of running dry without suffering damage. Because of this the device is designed to always run wet, necessitating a specific start-up and shutdown procedure to prevent damage to the equipment. The start-up procedure was therefore described as:

- Connect all hoses and chutes
- Switch on pump at design speed for experiment
- Once liquid is flowing out of effluent pipe switch on MagicLAB
- Switch on KTron at 1 kg hr^{-1}
- Step up mass flow in 1 kg hr^{-1} increments until desired solid content achieved

The shutdown procedure was simply the reverse of this (although the powder feeder could be switched off immediately, not in increments). The liquid was pumped through the unit until running clear from the effluent to remove any remaining solid.

4.3.1.3. Trials

4.3.1.3.1. Scoping Tests

The primary success criterion for proof of concept for a continuous process was whether it would handle successfully the high solid concentrations required by the various slurry specifications. Therefore, the first test for each powder was simply to start up as described above and then run the rig at the desired solid content for five minutes to ensure that slurry could be produced in specification. The standard scoping test was run at a powder flowrate of 5 kg hr^{-1} and impeller speed of 12,000 RPM; both values in the middle of the available ranges. Liquid flowrate was

matched to the powder flowrate to give the desired slurry powder concentration. Samples were taken at three minutes and five minutes.

The solid content of the slurry was measured by taking a small sample and measuring the mass loss over 20 minutes at 500 ^{o}C in an oven. This was done to ensure consistent solid concentration at three and five minutes.

PA alumina was especially hard to prepare within the MagicLAB and so extra scoping trials were carried out. These involved increasing the powder flow in very small increments (0.1 kg hr^{-1}) every 1 minute to find the maximum achievable solid content. This was repeated for a variety of flowrates to assess the effect of mean residence time on this.

4.3.1.3.2. Stability Tests

Longer trials were run for both the ink formulation and P0 alumina, both of which are products where the process would be designed to run for extended periods of time. Therefore, testing the stability of the process over extended periods (> 1 hour) was required.

During these tests, the motor torque was measured by the device and recorded at a frequency of 10 Hz. The torque trace could then be used to investigate the stability of the process, with stable traces showing comfortable operation and unstable traces with significant peaks or troughs instabilities in the process, indicating unstable product flow, something not allowable in the final process. The motor torque was also used to calculate the power delivered to the slurry using Equation 11.

During these extended trials samples of slurry were taken every ten minutes for comparison.

4.3.1.3.3. Parametric Study

For both P0 alumina and MgO 93 HR the device was run at a wide range of production rates and impeller speeds to see the effect of these process variables on the quality of the slurry produced, as shown in Table 4-3 and Table 4-4.

Table 4-3: Parametric study conditions for MgO 93HR trials

Trial no	Powder flow (kg hr^{-1})	Liquid flow (ml min^{-1})	RPM
1	2	204.76	12000
2	3	307.14	3000
3	4	409.52	12000
4	3	307.14	15000
5	3	307.14	6000
6	6	614.29	12000
7	5	511.90	12000
8	3	307.14	9000
9	1	102.38	12000
10	3	307.14	18000

The slurry was analysed for both particle (chord) size, measured using a Lasentec focused beam reflectance measurement (FBRM) probe, and rheology, measured using a TA AR2000 rheometer.

FBRM is a measurement technique to measure particle size in-situ. The instrument is comprised of a probe and a measurement unit. The front of the probe is made of a sapphire window, through which a focussed laser beam is fired. This laser beam is rotated around the circumference of the window at a scan speed of 2 m s^{-1}. As the beam strikes particles in the slurry the light is backscattered. The duration and count of backscattered light is measured by the measurement unit and the size of a particle is found as the product of the backscatter pulse duration and the scan speed. FBRM measures the chord length of a particle, a measure of the linear distance between two edges of a particle (Kumar *et al.* 2013). This length is highly dependent on the orientation of the particle to the laser and so it is important to differentiate it from particle size distributions measured by equipment using laser diffraction techniques such as

a Malvern Mastersizer. However, FBRM measurements have been shown to be useful in qualitatively describing changes and differences in particle size distributions when compared to actual particle size distributions (Bontha *et al.* 2000). When using P0 the slurry had to be diluted from 50 wt% to 20 wt% for FBRM measurements. This was because at solid concentrations above 20 wt% the sapphire window would become covered in solid and fail to give a measurement.

Table 4-4: Parametric study conditions for P0 trials

Trial No	Powder Feed (kg hr^{-1})	Liquid Feed (mL min^{-1})	RPM
1	1	13	3000
2	1	13	5000
3	1	13	9000
4	1	13	12000
5	2	26	3000
6	2	26	5000
7	2	26	9000
8	2	26	12000
9	3	39	3000
10	3	39	5000
11	3	39	9000
12	3	39	12000
13	4	52	3000
14	4	52	5000
15	4	52	9000
16	4	52	12000
17	5	65	3000
18	5	65	5000
19	5	65	9000
20	5	65	12000
21	6	78	3000
22	6	78	5000
23	6	78	9000
24	6	78	12000
25	7	91	3000
26	7	91	5000
27	7	91	9000
28	7	91	12000

For the ink formulations two different residence times were tested by varying the material flowrate at three different impeller speeds, as shown in Table 4-5. A sample of made up ink formulation was also passed through the MagicLAB a second time at a series of different impeller speeds, as shown in Table 4-6. This was done to see if secondary processing would further reduce the maximum particle size.

Table 4-5: Parametric study conditions for ink formulations

Exp. #	Powder Flow (kg hr^{-1})	RPM
1.	1	5,000
2.	1	12,000
3.	1	19,000
4	3	5,000
5	3	12,000
6	3	19,000

Table 4-6: List of ink formulation second pass trials

Trial #	2^{nd} Pass RPM
1	5000
2	12,000
3	18,000

4.3.1.3.4. Cleaning in Place Tests

The ease of cleaning the equipment is an important consideration for the viability of continuous operation mode for production plants, especially in plants that make multiple formulations in one manufacturing line. Therefore, a simple full factorial DoE was performed to compare the effects of both material flow rate and impeller speed on the cleaning in place performance. The experimental matrix is shown in Table 4-7. These trials involved switching off the powder flow and recording the time taken for liquid to run clear from the effluent pipe by visual inspection. The powder flow is used to describe the material flowrate for each trial for simplicity however, during cleaning there is no solid flowing through the device. The MagicLAB was then taken apart to ensure there was no stuck paste inside the device. The number of residence times used to

compare cleaning performance is based on a mixer chamber volume of 27 mL. This number is hard to assess accurately as it is not supplied by IKA and depends on how full the chamber is whilst in operation. However, it was measured as 27 mL by submerging the assembled impeller in water and measuring the mass of displaced fluid. The corresponding volume was then subtracted from the void volume of the mixing chamber to give a mixing volume.

Table 4-7: Cleaning trials experimental matrix

Trial no	Powder flow (kg hr^{-1})	Liquid flow (ml min^{-1})	RPM
1	1	102.38	6000
2	1	102.38	18000
3	5	511.90	6000
4	5	511.90	18000
5	3	307.14	12000

4.3.1.3.5. Slurry Quality Assessments

The specific method of assessing slurry quality and consistency varied with product and application. The alumina powders were measured for crucible solids at 500^{o}C as described above, with small variation in solid concentration with sample time being a key parameter. Rheology was also assessed using an acrylic hatched 40 mm flat plate geometry on a TA AR2000 rheometer. The rheometry protocol involved a logarithmic sweep down from a high shear rate to low shear rate. This is a fairly crude method of measuring the slurry rheology but it was necessary to attempt to minimise sedimentation of the solid particles in the sample during the bulk of the test, something that inevitably occurred during low shear measurements. As described above the particle size distribution was also assessed using FBRM.

For the ink formulations the critical process parameter was the slurry maximum particle size. This was measured using a Hegman gauge, as shown in Figure 4-8. To measure maximum particle size on a Hegman gauge a small sample (5 – 10 mL) of the made up ink is placed at the top end of the size scale. A straight metal scraper is then used to spread the ink along the channel along the

centre of the tool. This channel gradually reduces in depth from 100 µm to 1 µm. Therefore the maximum particle size is measured as the first 'scratch' seen in the line of ink in the channel, when a particle is too large to fit between the scraper and the bottom of the channel and so is dragged along the surface by the scraper, disrupting the ink (Leyland *et al.* 2002).

Figure 4-8: Example of a Hegman Gauge

For the magnesia formulations the prime requirement was stability of production. However, there was also a secondary aim to produce a slurry as warm as possible to reduce the heating duty required in downstream processing.

4.3.2. Results

4.3.2.1. Sample Data

Figure 4-9 shows a sample torque trace from the IKA MagicLAB for a scoping trial run on P0 alumina. It is very clear to see the points in time where the powder flow was started and ended, as seen by the significant change in the torque trace at these times. This demonstrates that a significant amount of the energy delivered by the device is used for the incorporation of powder as the peak value of torque is double the initial value.

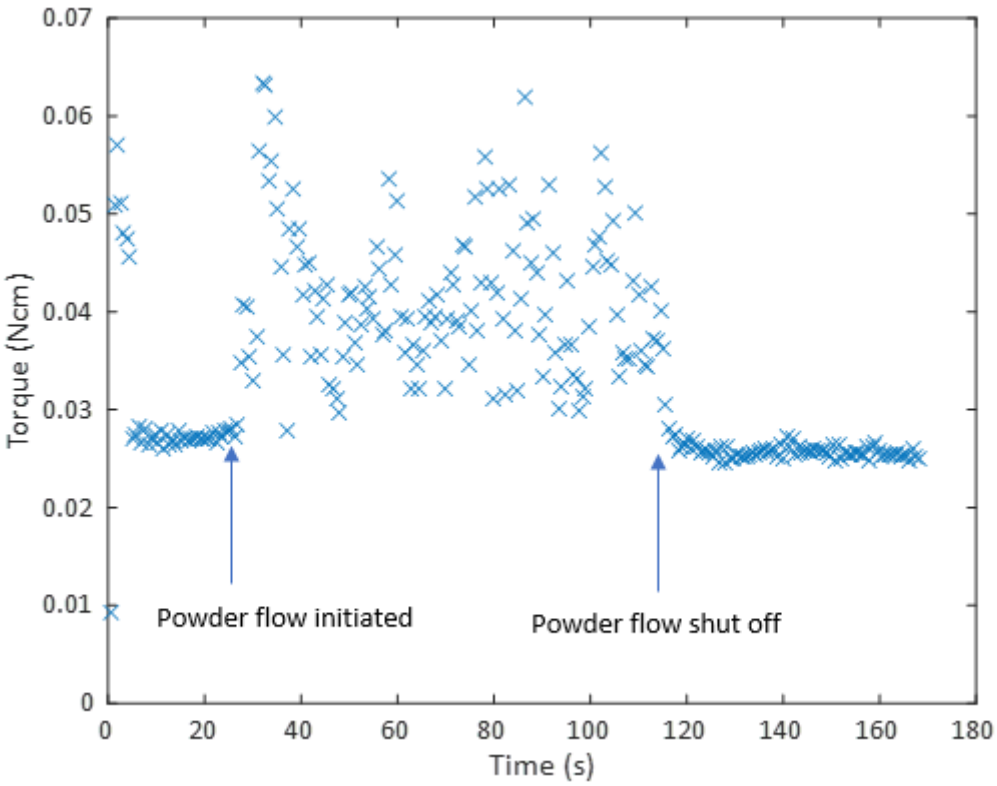

Figure 4-9: Example torque trace from simple run using P0 alumina, highlighting times when powder flow was initiated and ended

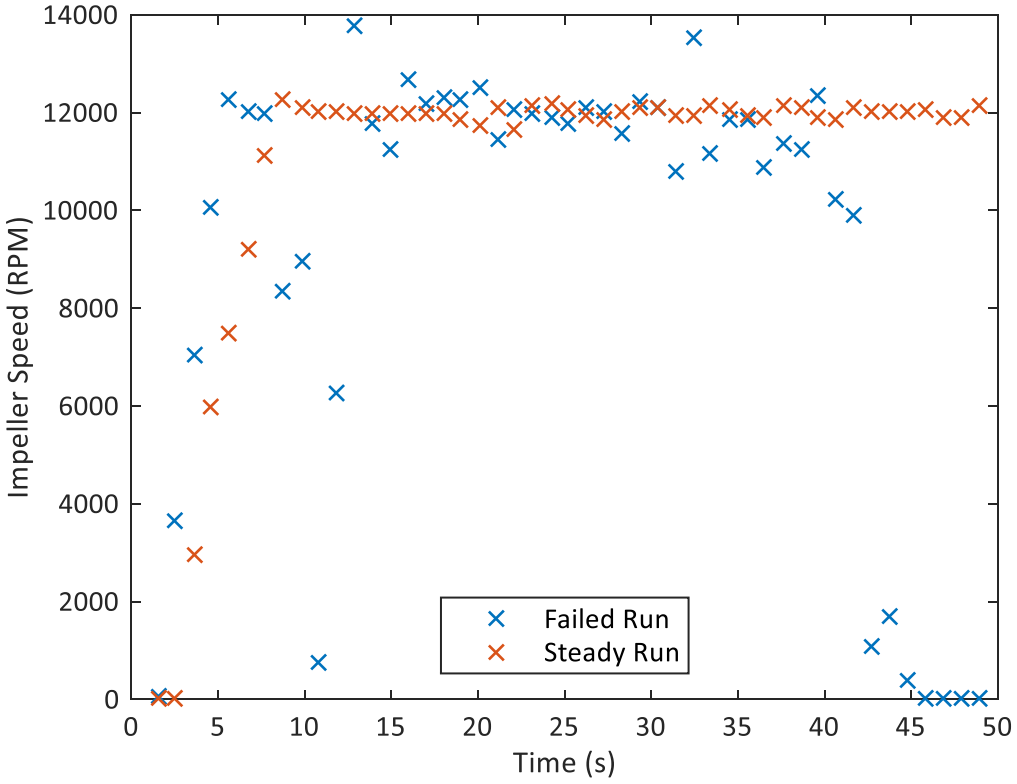

Figure 4-10: Comparison of the recorded impeller speed traces for runs where the IKA did and didn't block. Both for P0

Figure 4-10 shows the recorded impeller speed of the MagicLAB for two runs making P0; one that failed and blocked quickly and one that ran stably for five minutes. As the first powder was added in the failed run a large build-up occurred in the connection between the MagicLAB and powder feed unit almost as soon as the powder was turned on. This lump was drawn into the mixing chamber, at which point the impeller speed dropped to well below 2000 RPM. From this point onwards the mixer never achieved stable operation, with the impeller speed constantly fluctuating around the set point of 12,000 until it eventually blocked. However, in the stable run the impeller reached the set point and remained there with very little variation for the entire run. This demonstrates the important of accurate powder dosing to the mixing chamber, where a very brief moment of over dosing causes a prolonged instability in operation that eventually leads to blocking.

4.3.2.2. Scoping Tests and General Observations

Table 4-8 shows the outcome of the scoping trials for each of the powders considered. The majority of powders studied were incorporated to specification slurries very easily using this set up. The main exception to this was PA which failed during the initial scoping trials. P0 and the ink formulations were possible to prepare to specification for five minutes. However, the ink showed consistently high torque and P0 gave frequent torque spikes which, during repeats, occasionally led to the device blocking.

Table 4-8: Outcome of scoping trials

Slurry Name	Business Unit	Successful Scoping Trial?	Notes
P0	ECT	Yes	Occasional jamming
PA	ECT	No	Jammed at approximately 30 wt%
Copper Zeolite	ECT	Yes	Easy
AZM9 Zeolite	ECT	Yes	Easy
Magnesia 1	INTERCAT	Yes	Easy
Magnesia 2	INTERCAT	Yes	Easy
Ink	AGT	Yes	High torque

It was observed using P0 and PA that blockages tended to occur immediately after a build-up of powder was seen in the hose connecting the KTron powder feeder to the IKA MagicLAB. This build-up tended to then drop into the MagicLAB as a plug, which was then followed by a blockage. This build up was filmed so it could be observed off-line in more detail and was seen to happen across the full circumference of the connection simultaneously for both alumina powders. The two powders with the highest critical arching diameter, D_C, were P0 and PA with measured values of 145 mm and 175 mm respectively. The critical arching diameter is the maximum diameter of an opening over which a powder will form a stable bridge and is defined for a conical hopper as (Brookfield Ametek 2018):

$$D_C = \frac{2000\sigma_c}{\rho_{tapped}\, g} \tag{12}$$

where σ_C is the powder unconfined yield strength found by measurement in a shear cell. The full details of this test method and how it was used to measure all powders in this study are given in section 5.3.1.1.1.

The diameter of the orifice at the bottom of the connection was 120 mm, larger than or in the range of the critical arching diameter of most powders studied but lower than that of PA and P0. Therefore, it appears that the connection hose is acting as a temporary hopper between the powder feed and MagicLAB units. This hopper is not correctly designed for some of the more extreme powders studied and therefore causes instability in the flow to the MagicLAB, even if the flow from the powder feeder is uniform. This is an issue that will become less significant as the scale of operation is increased and orifices inevitably become larger.

As stated above, PA was significantly harder to incorporate by this continuous process than any of the other powders tested. Figure 4-11 shows the effect of varying the material flowrate through the MagicLAB on the maximum achievable solid concentration. At the lowest flowrates there was not sufficient flow to fill the mixing chamber of the device and so the mixing was inefficient and it was not possible to produce slurry. As the liquid inlet concentration reached approximately 10 mL per minute it was possible to produce slurry stably for five minutes with a maximum solid concentration of 38 % ± 1 %. As the liquid concentration increased further this then dropped back to the 30 % measured during the initial scoping trials for the full range of solid contents studied.

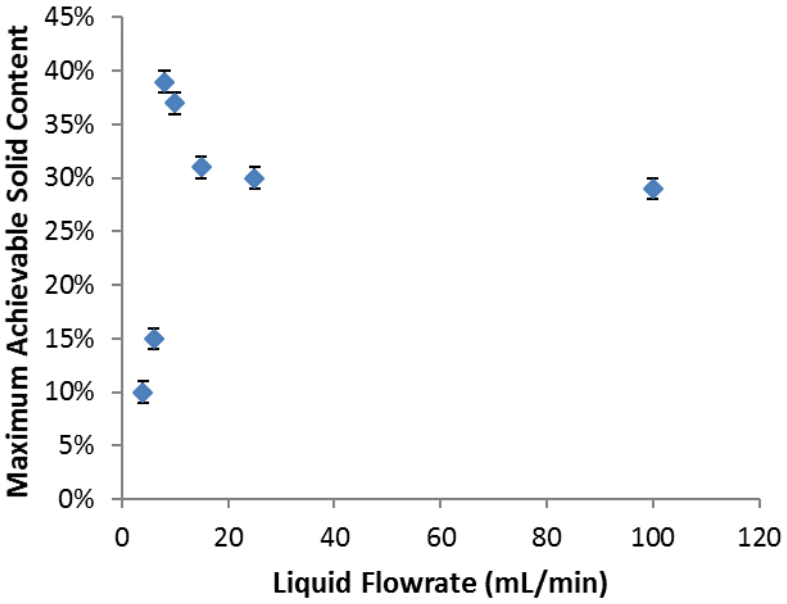

Figure 4-11: Effect of material flowrate through MagicLAB on maximum achievable solid concentration

4.3.2.3. Stability Tests

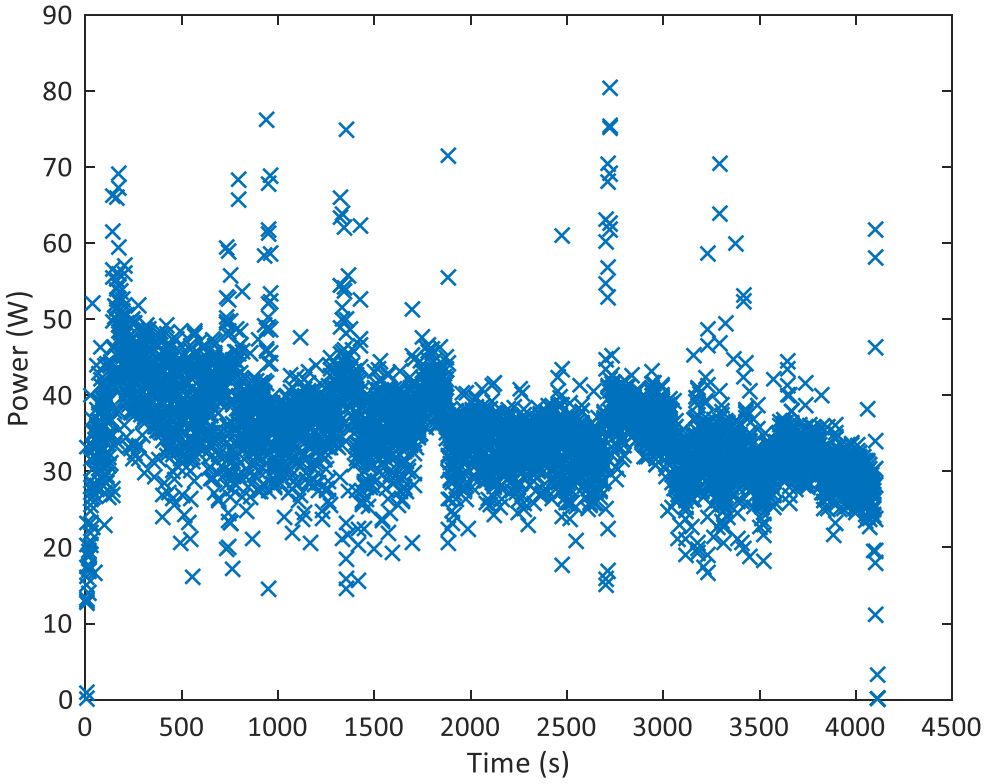

Figure 4-12: Torque trace for a > 1 hour run making the ink formulation

Figure 4-12 shows the torque trace for an extended run producing the ink formulation for greater than one hour without any blockages. There were periodic jumps in torque due to small build ups of powder in the connection between the MagicLAB and the powder feeder that then dropped into the mixing chamber. However, for this formulation the shock to the system did not destabilise operation sufficiently to cause blockages. This is a significant result to demonstrate the long term stability of the MHD which is shown to be capable of producing specification slurry for greater than one hour. This provides a sufficient proof of concept of viability as a possible replacement to existing manufacturing processes. Table 4-9 shows that the ink produced throughout the extended run maintained a steady maximum particle size.

Table 4-9: Measured maximum particle size with time for extended ink formulation run

Sample time (minutes)	d_{max} (1,2,3) µm	d_{max} Avg. µm
0	27, 27, 26	27
15	26, 26, 32	28
30	34, 28, 32	31
45	29, 30, 33	31
60	29, 29, 32	30

4.3.2.4. Parametric Study

Figure 4-13 and Figure 4-14 show the effect of material flowrate and impeller speed on the particle (chord) size distribution of the slurry produced for P0 slurry. It is clear that neither parameter has any effect on the slurry particle size. Three different samples were measured using a Malvern Mastersizer as a double check: All three gave identical distributions, as shown in Figure 4-15, confirming that the P0 slurry particle size was not modified by action of the MagicLAB.

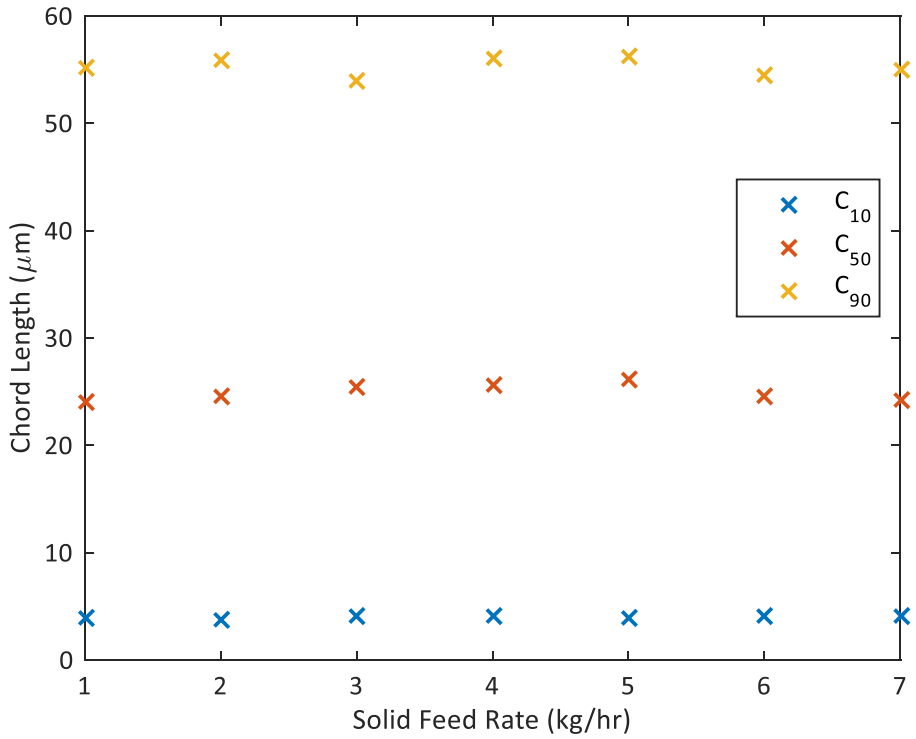

Figure 4-13: Effect of P0 flowrate on particle size distribution of slurry produced

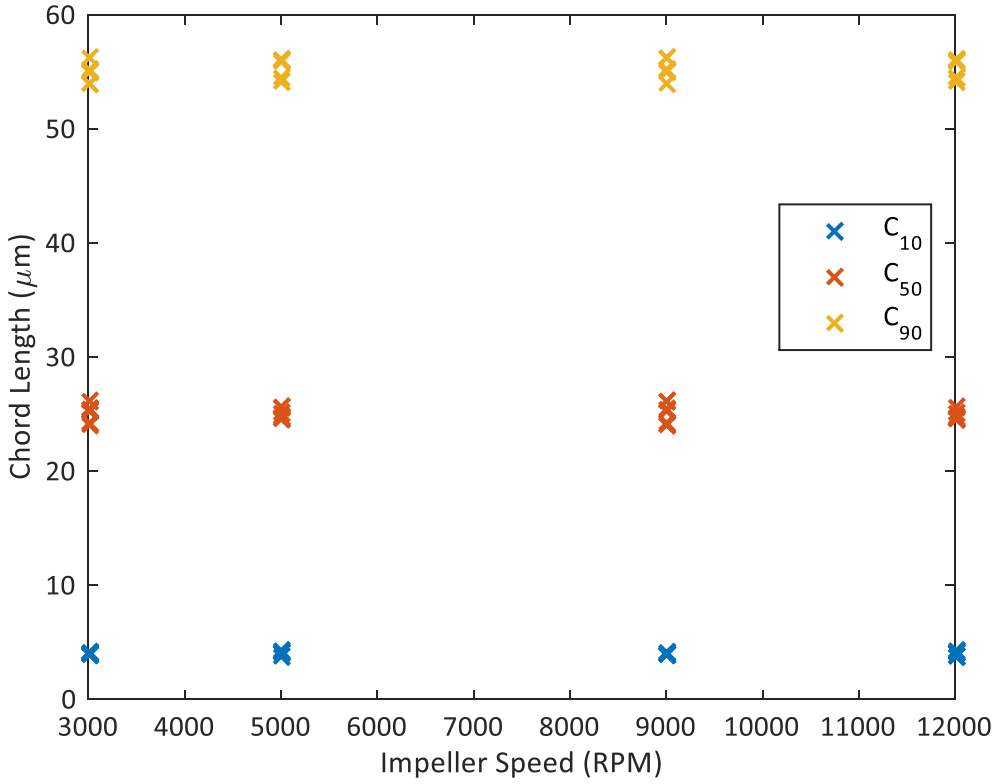

Figure 4-14: Effect of Impeller speed on P0 slurry particle size distribution

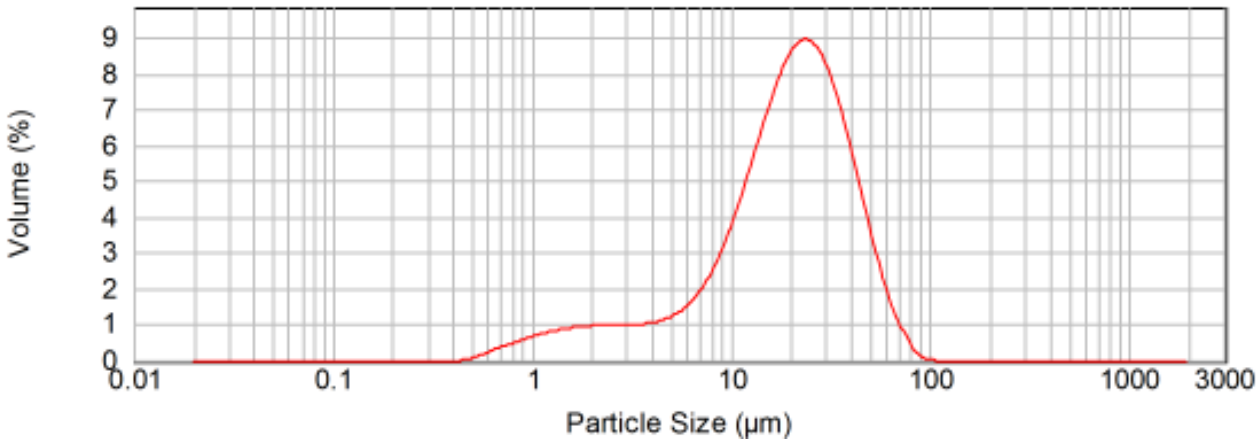

Figure 4-15: Malvern Mastersizer measurement for P0 slurry produced in IKA MagicLAB

Figure 4-16, Figure 4-17, and Figure 4-18 show the effects of MagicLAB impeller speed, material flowrate through the mixer, and energy delivered per unit mass of slurry on the final slurry particle size for the magnesia slurries. The size used is the C_{50} measured using FBRM, however

both the C_{10} and C_{90} showed similar trends. Contrary to the measurements for P0 slurry above; each of these Figures show a change in slurry C_{50} from 21.5 µm at the largest to 17.8 µm at the smallest. Figure 4-16 shows that this change in particle size is proportional to the impeller tip speed with smaller particles produced at higher tip speeds. This suggests that the action of the impeller is causing particle breakage as the slurry is produced. Figure 4-17 shows that the flowrate of material, and therefore mean residence time of the material in the mixing chamber, has no effect on the final slurry particle size and Figure 4-18 shows minimal relationship between the slurry particle size and energy per unit mass delivered. This is an important result: demonstrating that the particle size is being changed by action with the impeller and can be controlled simply through controlling the impeller speed.

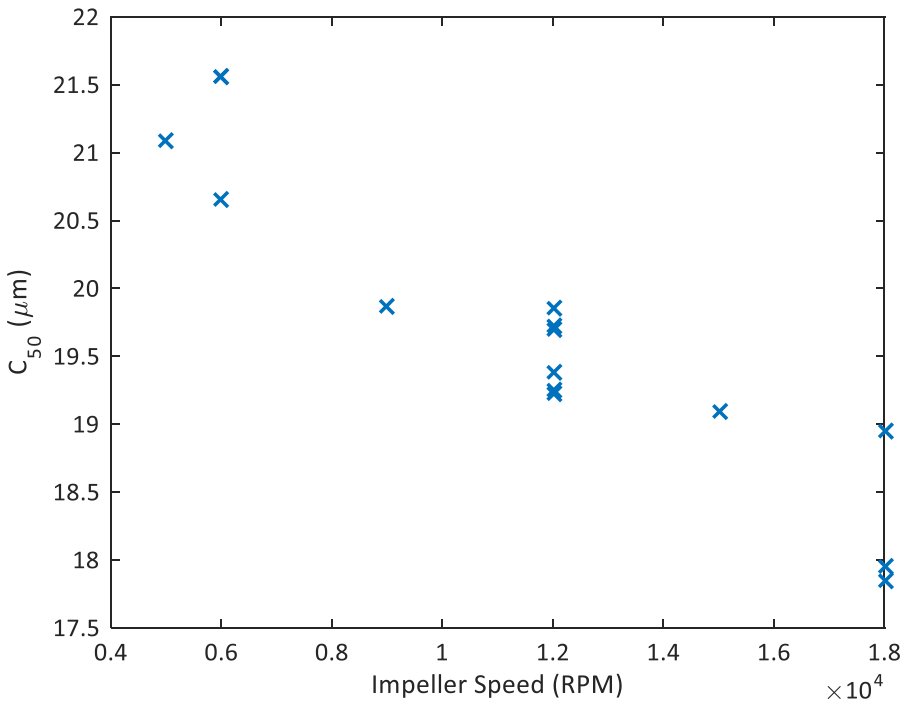

Figure 4-16: Effect of MagicLAB tip speed on MgO slurry particle size

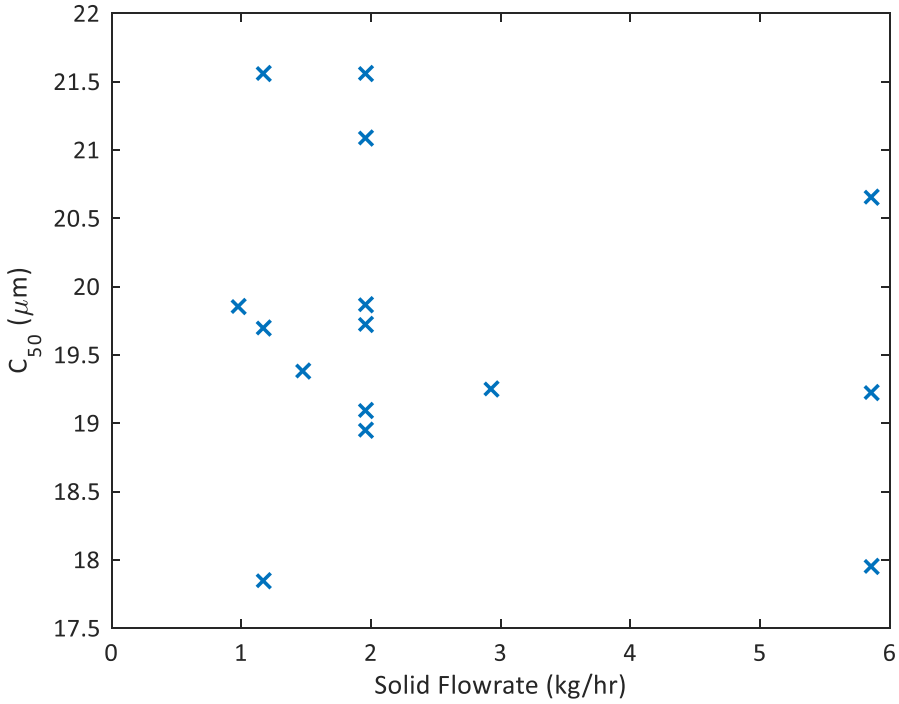

Figure 4-17: Effect of material flowrrate through MagicLAB on MgO slurry particle size

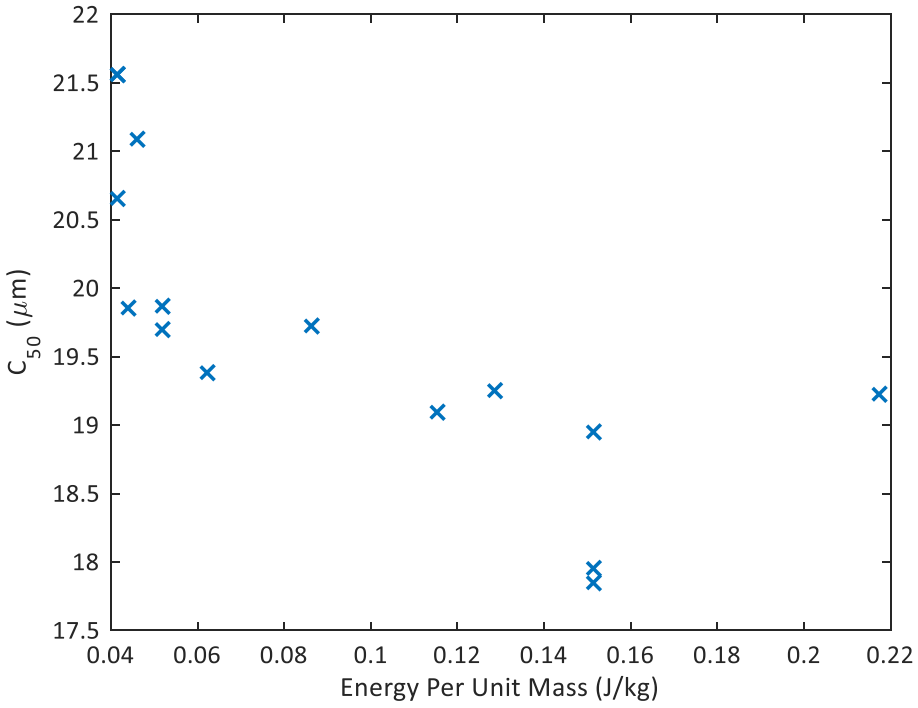

Figure 4-18: Effect of energy per unit mass delivered during mixing on MgO slurry particle size

Table 4-10: Maximum particle size for ink formulation slurries during parametric study with individual repeats listed

Exp. (Residence time)	RPM	d_{max} (1,2,3) µm	d_{max} Avg. µm
1 (High)	5000	32-, 29, 28	30
2 (High)	12,000	28, 34, 30	31
3 (High)	15,000	30, 29, 32	30
4 (Low)	5000	27, 27, 32	29
5 (Low)	12,000	28, 31, 29	29
6 (Low)	15,000	26, 33, 29	29

Table 4-11: Maximum particle size for ink formulation slurries using a second pass with individual repeats listed

RPM	D_{max} (1,2,3,4) µm	D_{max} Avg. µm
1 Pass material	29, 29, 32	33
5,000 (2nd pass)	38, 28, 36, 30	33
12,000 (2nd pass)	39, 28, 30, 28	31
18,000 (2nd pass)	29, 32, 28,29	30

Table 4-10 and Table 4-11 show that varying the residence time, impeller speed or using a second pass through the MagicLAB had negligible effect on the maximum particle size of the slurries produced. There was also no measurable difference in the viscosity of the product slurry, as shown in Figure 4-19.

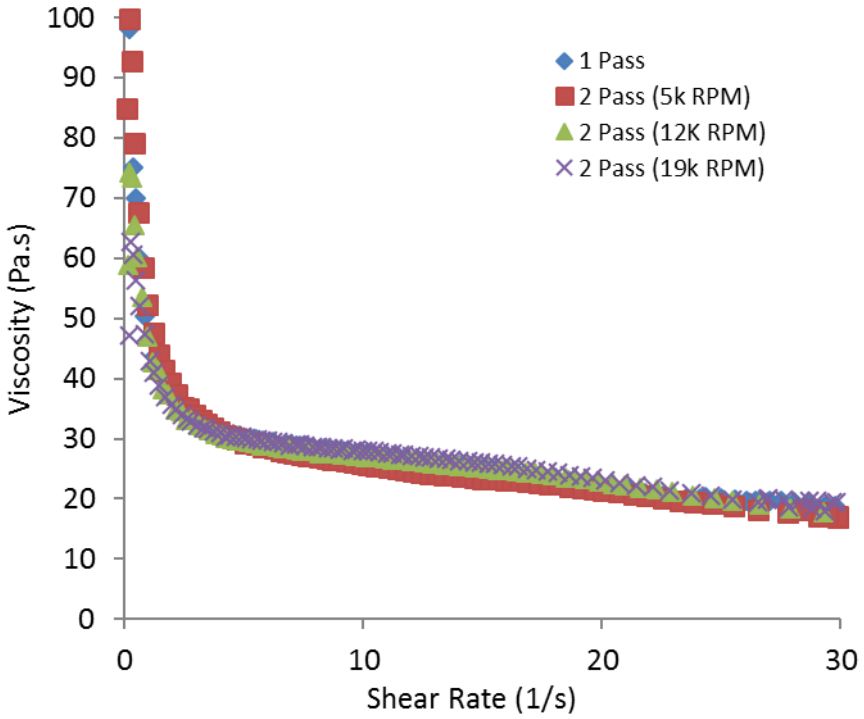

Figure 4-19: Measured rheology of ink formulation slurries before and after second pass through the MagicLAB

4.3.2.5. Cleaning in Place

Figure 4-20 and Figure 4-22 show the main effects plots for the time and number of residence times required for cleaning. These plots use the mean of every trial run at a specific value for each variable. From Figure 4-20 it is clear that the impeller motor speed has negligible effect on the time required for cleaning in place to occur, with all significant change in cleaning time resulting from changes in the material flowrate. Therefore, to clean the device quickly, flowing material through it as fast as possible is advised. However, Figure 4-22 shows that the number of residence times, and therefore volume of cleaning water required, increases linearly with the material flowrate. It is therefore likely that ideal cleaning conditions will be dependent upon the process and formulation applied to. For example: a process where wash water cannot be reused as a process feedstock or where expensive materials are used it would be ideal to spend longer cleaning with less fluid. Whereas, the reverse would be true for high throughput, lower value products where wash water can be reused in the process. Figure 4-24 demonstrates that material

flowrate through the mixer is the only statistically significant variable in affecting the cleaning time and so running the impeller slowly is recommended to reduce wear and energy consumption during cleaning.

Figure 4-21 and Figure 4-23 show interaction plots for the time and number of residence times required for cleaning. In these plots converging lines suggest the presence of interactions between variables, whereas parallel lines suggest they are totally independent. In Figure 4-21 there is little to no interactions between the two variables considered: again showing that material flowrate is the only important variable to control cleaning time. However, in Figure 4-23 there is evidence of an interaction suggesting that for high material flowrates running at a low impeller speed reduces the amount of cleaning fluid required, whereas at high flowrates lower impeller speeds give better performance. This may suggest a minimum level of turbulence is required to clean within the mixer chamber: achieved either through high flowrates or agitation. However, once this is achieved further increases to the impeller speed reduce performance, possibly as air is entrained into the mixer chamber which may reduce the contact time between the cleaning fluid and mixer surfaces.

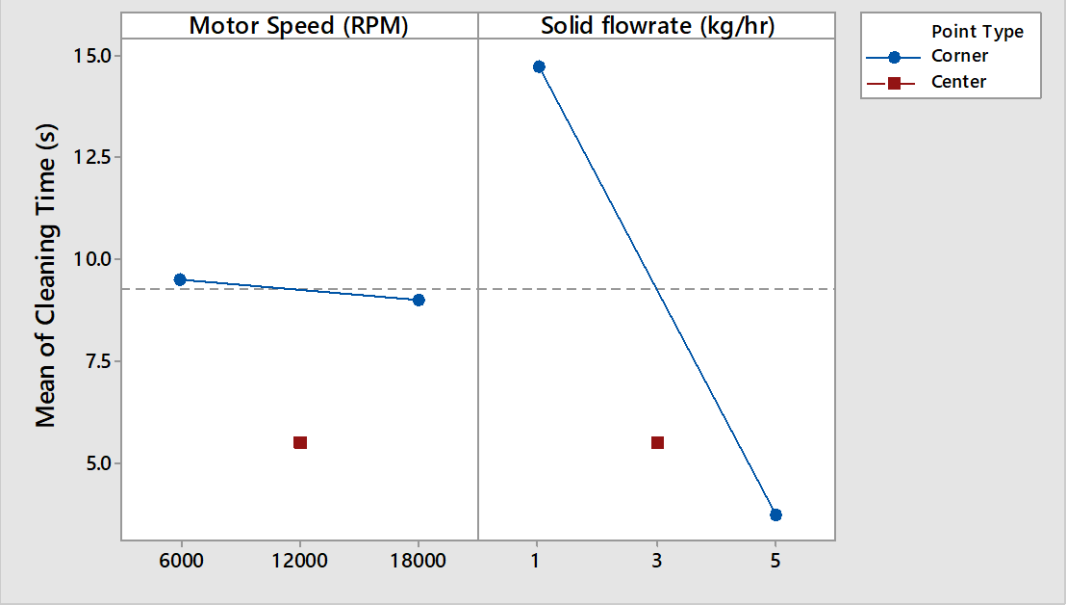

Figure 4-20: Main effects plot for cleaning time

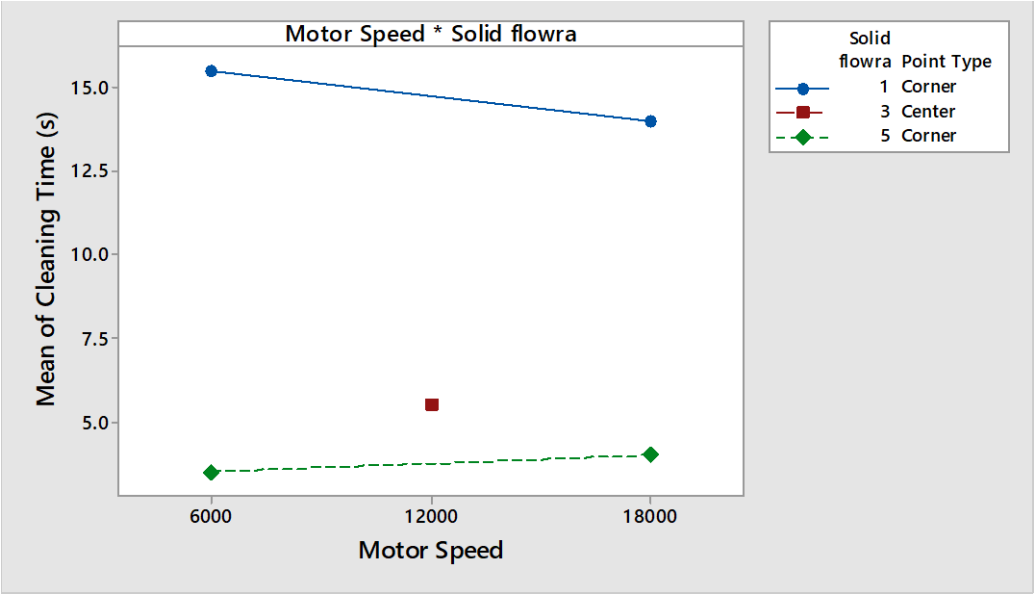

Figure 4-21: Interaction plot for cleaning time

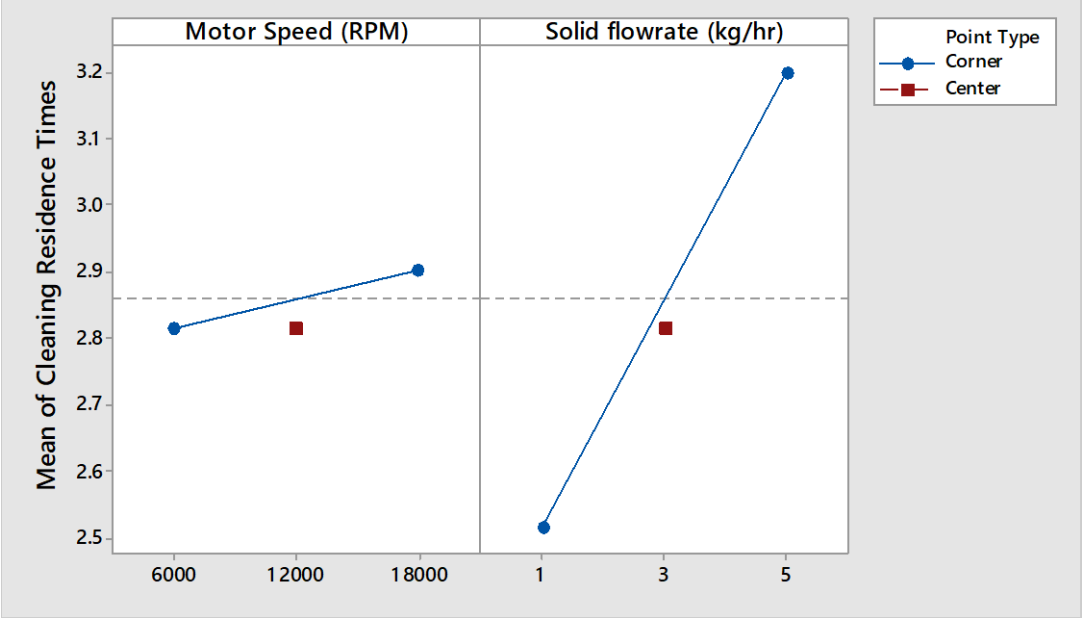

Figure 4-22: Main effects plot for number of residence time for cleaning

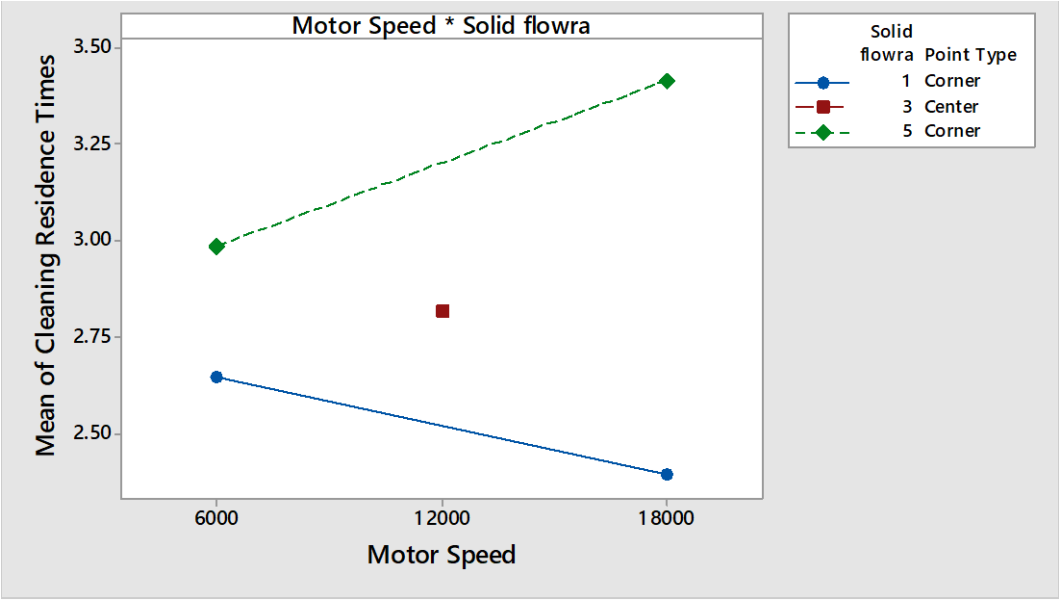

Figure 4-23: Interaction plot for number of residence times for cleaning

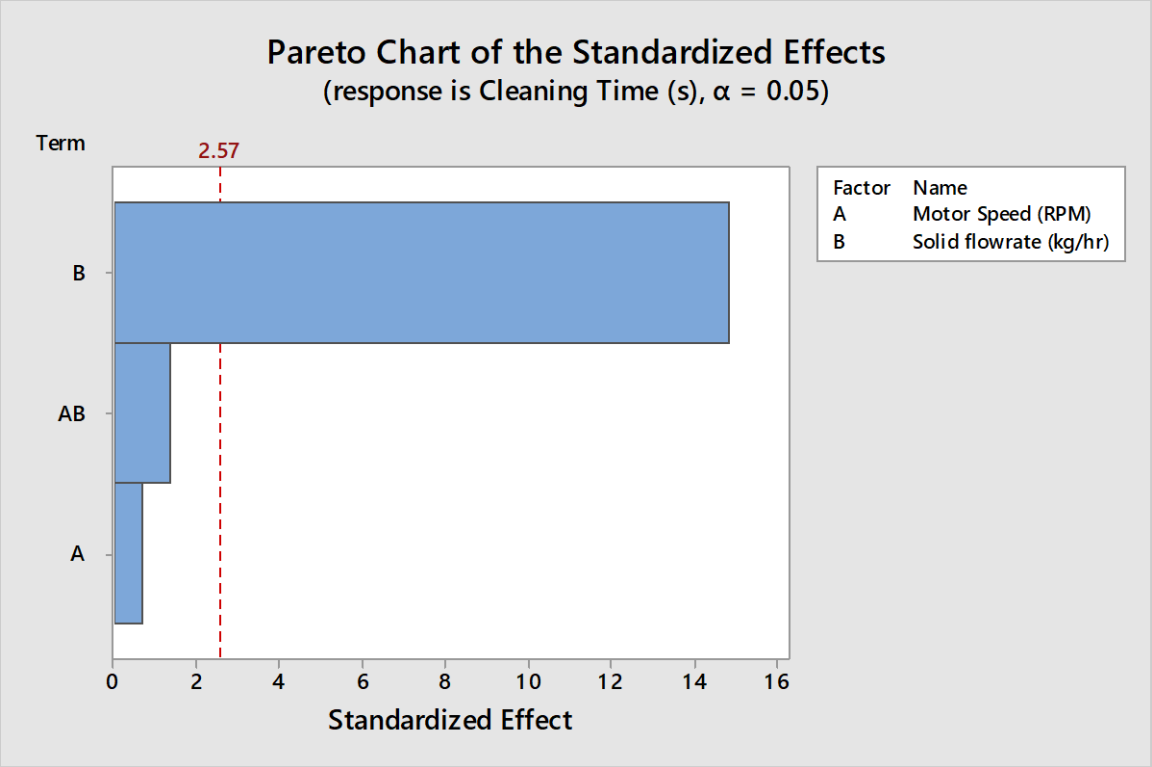

Figure 4-24: Pareto plot showing variable significance for cleaning time

4.3.3. Conclusions

Trials run on the IKA MagicLAB with the MHD head at small scale suggest that the device is capable of producing the vast majority of slurries for all Johnson Matthey products tested. PA alumina is the one major exception to this, where significant effort was required to run the device for five minutes without blocking. Blockages were seen using other powders too, especially the other alumina powders, which were inevitably caused by unstable powder flow into the IKA caused by the connection of the IKA and the powder feeder rather than instability in operation of the powder feeder itself. This problem is expected to be minimised as the scale of mixer is increased: where linear distances become larger so the connection will act more like a chute than a hopper. The orifice at the top of the IKA will be also be larger as equipment scale increases, making this orifice size greater than the critical arching diameter of all powders used will greatly reduce the changes of powder forming arches over the orifice and not entering the mixer.

For the majority of powders studied there is no measurable effect of any operating variables on slurry characteristics; either the slurry can be made or it cannot. This is a positive result for scale up of the device where power delivery per unit mass of slurry will, inevitable, reduce as scale increases when the mixer is scaled on tip speed. The one major exception to this was the magnesia slurries tested, where there was a small decrease in particle size with increasing mixer impeller speed. This is important to consider for processes using softer materials than alumina or glass frit if the slurry particle size is a critical process parameter. However, the drop in particle size is proportional to impeller tip speed, rather than energy delivered per unit mass. As these mixers are scaled at a constant tip speed it is likely that the change in particle size will be constant across mixer scales. However, if this is important for the specific application it should be considered during the scale up process.

4.4. Pilot Scale

4.4.1. Background

A pilot scale process rig was built at JMTC Chilton to run scale up experiments of a continuous powder incorporation process. This rig was built by Billingham Research Engineering on designs developed by the author of this thesis (Thomas Wood) and Timothy Addison.

4.4.2. Materials and Methods

4.4.2.1. Equipment

The rig was built on a trolley to enable mobility of the process and the use of dust booths for dealing with the large quantities of powder required. This pilot scale rig centred around an IKA MHD 2000/04 continuous powder liquid mixer. This was fed from the top by a KTron KT35 loss in weight powder feed unit. A SEEPEX progressive cavity pump was used to feed the liquid, a simple calibration was carried out on this pump for each liquid tested. Images of the rig are shown in Figure 4-25 and Figure 4-26.

Figure 4-25: Photo of pilot scale continuous incorporation rig

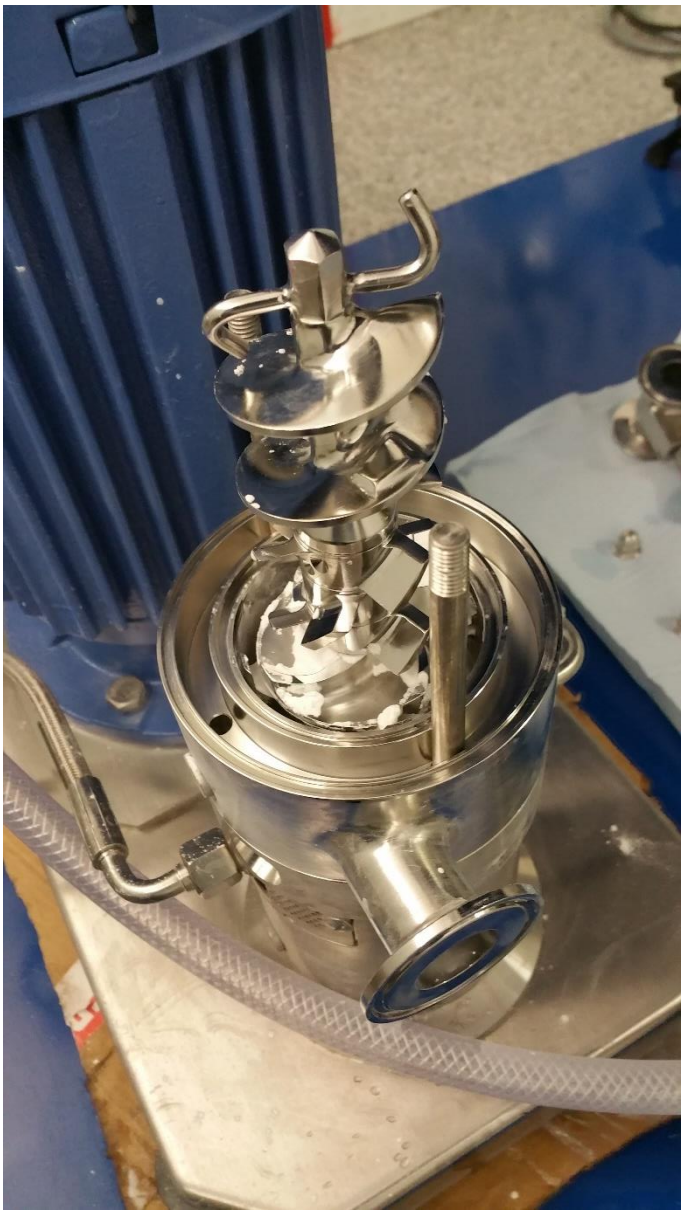

Figure 4-26: Close up of impellers inside the IKA MHD 2000/04

The MHD 2000/04, being significantly larger than the MagicLab, contained a double mechanical seal and so start up and shut down procedures were slightly less important than at the smaller scale. At the pilot scale the only important consideration was that powder flow was last on and first off: ensuring that liquid flow and the impeller were always on if powder was being delivered. This was done both to protect the equipment from abrasive powder and to prevent blockages due to overly high solid content pastes being formed inside the mixing chamber.

4.4.2.2. Trials

The primary aim of pilot scale trials on the MHD were to test the ability of the rig to produce the various formulations required by the three business units stably over a long period of time. The secondary aim was to push the limit of the pilot plant to find the maximum production rates possible at this scale to inform the next stage of scale up to production scale. Table 4-12 shows a summary of all the powders tested for each business unit.

Table 4-12: Summary of trials at pilot scale

Slurry Name	Business Unit
P0	ECT
PA	ECT
Copper Zeolite	ECT
AZM9 Zeolite	ECT
J43 mixed oxide	ECT
Magnesia 1	INTERCAT
Magnesia 2	INTERCAT
Ink	AGT

The PA paste produced by the pilot scale continuous incorporation rig was found to thin under shear. Therefore, 25g samples of paste were taken fresh from the MHD and placed in a TA AR2000 rheometer with a 28 mm diameter vane and 44 mm diameter cup geometry which was then run at a constant shear rate to measure the energy and shear required to thin the paste. The apparent viscosity was measured with time to track thinning of the paste when subjected to a constant shear.

4.4.3. Results

All slurries were produced to specification easily by the pilot scale rig at the maximum slurry flow rates shown in Table 4-13. The only exception to this was PA slurry, which was successfully produced by the rig but the effluent ran as a thick paste/solid foam rather than as a thin slurry as required, as shown in Figure 4-27.

Table 4-13: Summary of pilot trial results

Slurry Name	Business Unit	Max slurry production rate (kg hr^{-1})	Notes
P0	ECT	120	
PA	ECT	45	
Copper Zeolite	ECT	120	
J43	ECT	100	
AZM9 Zeolite	ECT	100	
Magnesia 1	INTERCAT	180	Pump limited
Magnesia 2	INTERCAT	180	Pump limited
Ink	AGT	50	

Figure 4-27: PA paste produced by pilot scale rig

When tested on the vane rheometer this paste was found to thin quickly when subjected to shear rates greater than 100 s^{-1}, as described in Table 4-14. The apparent viscosity measurements against time and energy input are shown in Figure 4-28 and Figure 4-29 respectively. Figure 4-28 shows that approximately 200 seconds are required to thin the paste at 100 s^{-1} applied shear rate and around 100 seconds when a shear rate of 200 s^{-1} is applied. Figure 4-29 shows that this thinning requires approximately 25 J (or 1 kJ kg^{-1}) of energy to thin the paste for shear rates of both 100 s^{-1} and 200 s^{-1}.

Table 4-14: Consistency of product after rheometer study

Shear Rate (s^{-1})	Pourable?
10	No
50	No
100	Yes
200	Yes

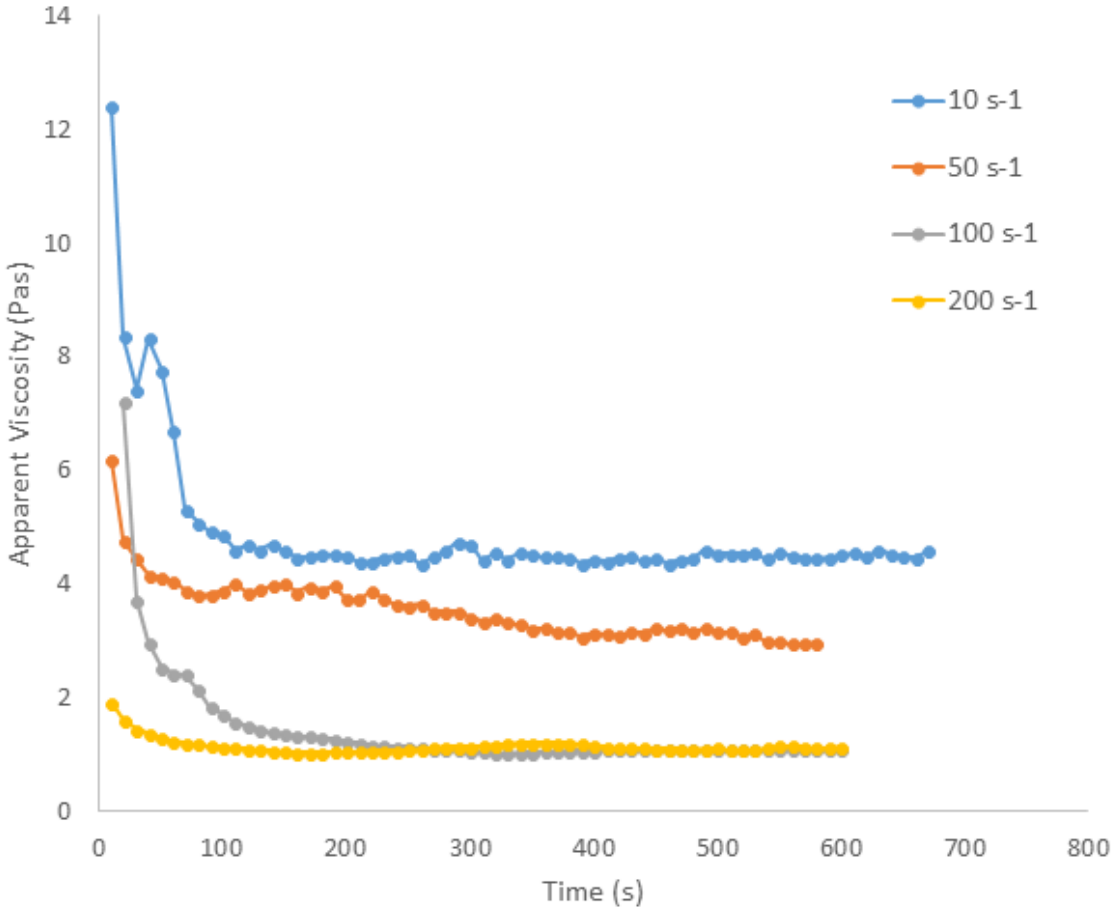

Figure 4-28: Viscosity of paste when subjected to constant shear rate in vane rheometer

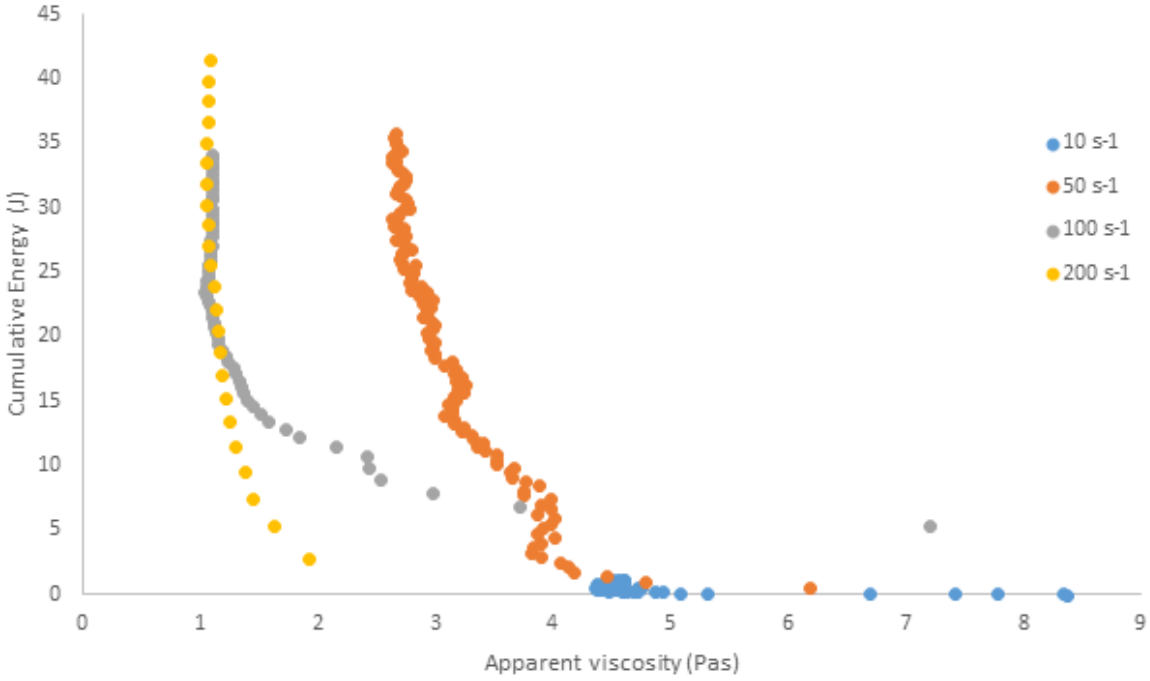

Figure 4-29: Change in apparent viscosity of paste with energy put into it by the rheometer

4.4.4. Conclusions

All slurries were able to be produced to specification at pilot scale for all businesses except PA alumina slurry. This was able to be produced at the desired crucible solid concentration but ran as a thick paste instead of as a thin slurry. Measurements on a vane rheometer showed that this paste could be thinned to a slurry through application of shear. A minimum shear rate of 100 s^{-1} was required for at least 100 seconds to thin the paste to a slurry, delivering a total energy input of 1 kJ per kg of slurry to achieve thinning. Pilot scale trials showed great promise for the feasibility of continuous powder incorporation for all of the products required and so continuing scale up to production scale was recommended.

4.6. Production Scale

4.6.1. Background

Production scale trials were carried out at the test facility at IKA Process GmbH, Staufen, Germany. The device used was an IKA MHD 2000/05: the smallest production scale unit they produce. The majority of trials run were performed on ECT materials (P0 and PA alumina) as P0 was seen as the easiest powder to generate data describing the effect of operating parameters, whereas PA was the most difficult to process.

4.6.2. Materials and Methods

4.6.2.1. Equipment

A diagram of the set-up is shown in Figure 4-30. A K-Tron screw feeder was placed above the MHD mixer. This delivers consistent powder flow at a specific RPM. This was calibrated before each new run with a new powder feed rate. Water with varying acetic acid concentration was delivered via a constant volume pump through a mass flow controller. The slurry-out nozzle is very short providing a very low backpressure on the system although some is needed to ensure the chamber is filled. A photo of the setup is shown in Figure 4-31 and close up images of the rotor and stator are shown in Figure 4-32 and Figure 4-33 respectively.

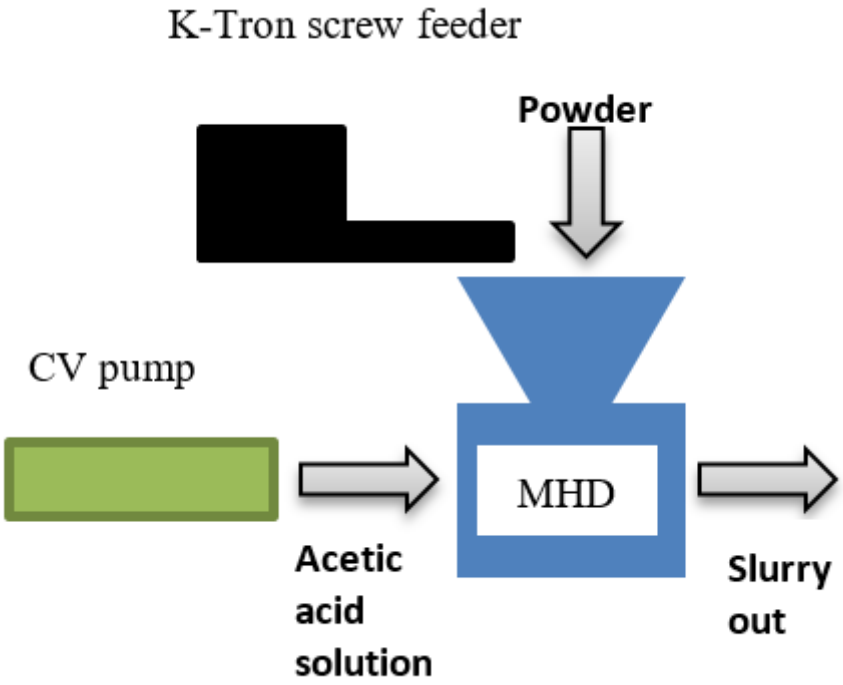

Figure 4-30: Experimental set up

Figure 4-31: Photo of Set up at IKA Process GmbH

Figure 4-32: Inside MHD module

Figure 4-33: Stator section of MHD module

4.6.2.2. Trials

4.6.2.2.1. ECT Trials

Table 4-15 shows a list of all the trials run using P0 alumina. These trials were designed to probe both the operability window of the MHD 2000/05 in terms of product flow rate and the effect of operating parameters such as impeller speed and mean residence time on the slurry produced.

Table 4-15: List of production scale trials on P0 alumina

Trial Name	Total flow (kg hr^{-1})	Liquid flow (kg hr^{-1})	Solid flow (kg hr^{-1})	Solid content (%)	Acid Conc (%)	Frequency (Hz)	Tip Speed (m s^{-1})	Notes
P0 1	300	153	147	49	3	50	23	
P0 2	300	153	147	49	3	40	18.4	
P0 3	150	76.5	73.5	49	3	50	23	
P0 4	150	76.5	73.5	49	3	40	18.4	Tap Water
P0 5	300	153	147	49	3	50	23	
P0 6	300	153	147	49	2	50	23	
P0 7	300	153	147	49	3	50	23	
P0 8	300	153	147	49	3	50	23	
P0 9	300	153	147	49	2.5	50	23	
P0 10	400	204	196	49	2.5	50	23	
P0 11	300	123	177	51	2.5	50	23	

Table 4-16: List of production scale trials on PA alumina

Trial Name	Total flow (kg hr^{-1})	Liquid flow (kg hr^{-1})	Solid flow (kg hr^{-1})	Solid content (%)	Acid Conc (%)	Frequency (Hz)	Tip Speed (m s^{-1})	Notes
PA 1	169	103	66	39	3	50	23	
PA 2	193	127	66	34.2	3	50	23	
PA 3	193	127	66	34.2	3	50	23	
PA 4	193	127	66	34.2	3	50	23	First Pass
PA 5	249	183	66	39	3	50	23	Second pass
PA 6	249	183	66	39	3	50	23	On small sawtooth after MHD
PA 7	169	103	66	39	3	50	23	
PA 8	169	103	66	39	3	50	23	On small sawtooth after MHD
PA 9	169	103	66	39	3	50	23	MHD - > Sawtooth
PA 10	169	103	66	39	3	50	23	MHD - > UTL
PA 11	169	103	66	39	3	50	23	MHD - > UTL
PA 12	169	103	66	39	3	50	23	MHD - > UTL

4.6.2.2.2. Other Formulations

Production scale trials on the ink and magnesia were carried out to ensure they could successfully be produced and what the maximum flowrate was for each formulation. For the ink slurry the maximum solid content was pushed to find the limit of the device. For the magnesia formulation water was preheated to assess the viability of preparing the slurry with warm water.

4.6.3. Results

4.6.3.1. ECT Formulations

PA1 – Initial single pass run

Initial trials trying to achieve true single pass slurry produced a very thick paste. This paste, if left for more than ~10 minutes, set hard and was not useable. Reduction in flow rate and therefore an increase in residence time in mixing chamber (shown to help at the lab level) was not possible as the powder feed was already at minimum setting. Changing to a smaller powder feed unit was not possible with the allotted time and equipment for these vendor trials. However, the MHD had no problem producing the paste for up to 15 min. No blockages were observed.

PA 2-6 – multi pass trial

A multi pass system, i.e. incorporating ~80% of total powder in single pass and then using that slurry as the aqueous feed for a second discrete pass where the final ~20% of powder is added worked at the lab scale. It was therefore decided that a run would be conducted to determine the max powder incorporation for a first pass yielding a free-flowing slurry by increasing the aqueous component flow rate. Due to a slight variation in acid concentration, the run was repeated to yield a 34.2% slurry.

This was then fed back into the system for a second discrete pass to take the solids up to 39%. The output was again a paste, similar to that of the single pass system., showing no advantage to a dual pass system.

PA 7-11 – Single Pass with post outlet high shear mixing

It was noticed that, although the single pass outlet slurry was a thick paste, application of shear from a simple sawtooth mixer in a collection vessel thinned out the slurry to manageable viscosity within 20 seconds and reduced in viscosity to a thin slurry within a minute.

A longer 10-15 minute trial was conducted using an IKA sawtooth mixer in a collection vessel just after the MHD outlet. This worked well, producing a thin slurry.

To mimic a fully continuous system, a high shear UTL 2000/05 in line mixer was placed on the outlet of the MHD. The set-up is shown in Figure 4-34. The slurry was delivered via a relatively long pipe to a funnel which fed into the UTL. This is not ideal as the backpressure created from the thick slurry having to make multiple 90^{o} turns and rising approximately 1m in height places strain on the system. A more realistic version of the set-up would be as shown in Figure 4-35 which would minimize the backpressure. Unfortunately, due to the available space this was not possible. The UTL outlet allows partial recirculation of the slurry. This is purely to help movement of the paste through the system.

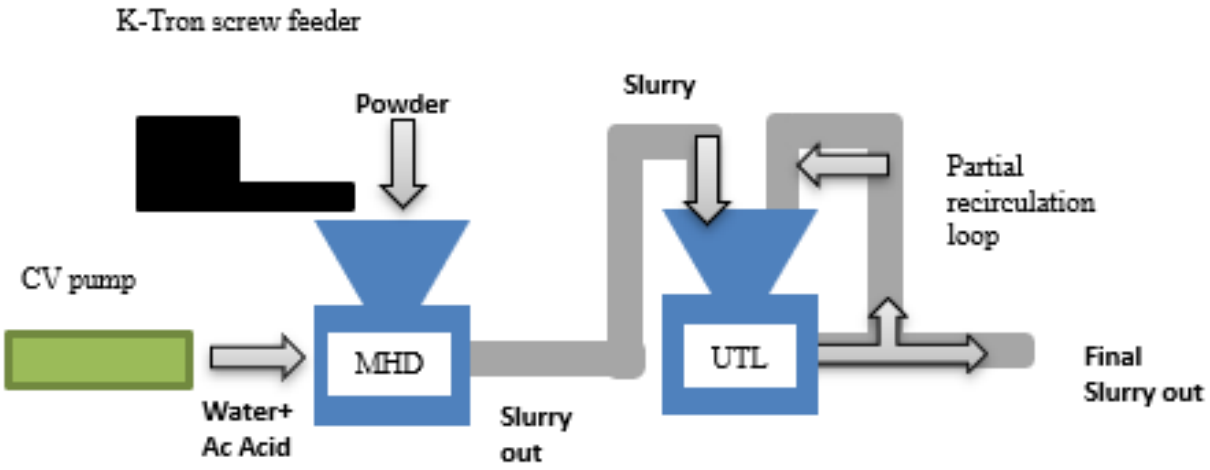

Figure 4-34: Diagram of setup including high shear UTL mixer

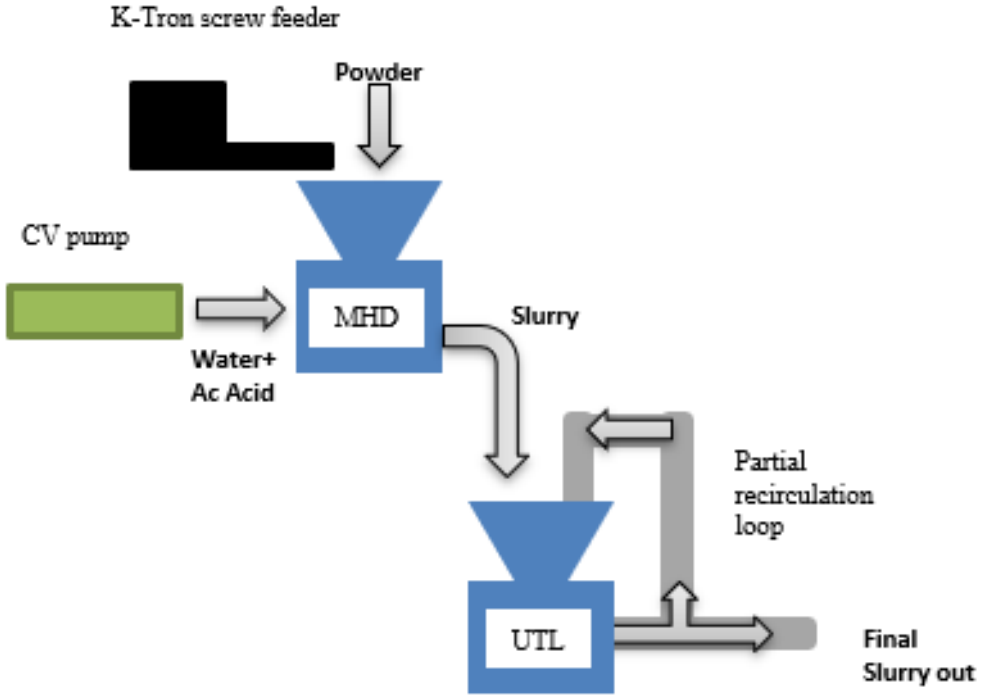

Figure 4-35: Diagram of low backpressure system

Figure 4-36: Hopper above UTL module

As with the P0 trial, the IKA MHD had no effect on slurry PSD although there was less variation in parameters and inlet feed conditions.

Blending of PA was attempted at 41% addition weight and ran for approximately 5 minutes before blocking. The blockage occurred in the outlet pipe between the MHD and UTL modules, not the MHD itself, and therefore is likely to be a false negative. The blockage was likely due to raising the thick paste through an extra-long pipe and a height of approximately 1 m. This is a problem because the MHD module produces very little pumping head at the exit to push the paste through this extra pipework.

A sample of the 39% paste was taken from the exit of the MHD module and mixed using a 36 mm diameter three bladed propeller impeller. The torque on the impeller was measured using the built in data-logging function of the IKA Eurostar 60 mixer motor. The power delivered by the impeller can be found from the measured torque using equation 11.

By studying the evolution of power draw on the impeller with time it is possible to infer the change in viscosity of the paste to a thin slurry as the power drops when mixing a lower viscosity fluid.

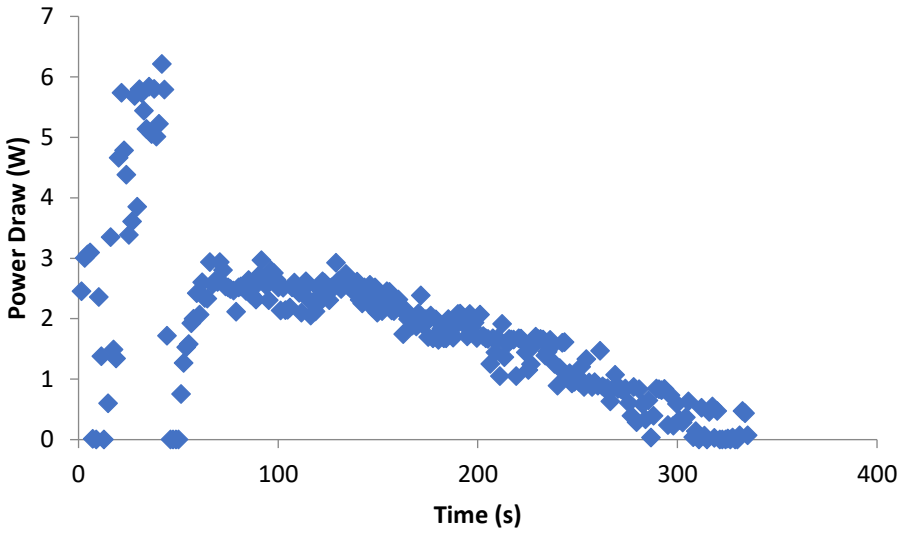

Figure 4-37: Evolution of power draw on mixer with time on thick paste produced by MHD

Figure 4-37 shows that the sample of paste taken from the MHD transitioned to thin slurry within 5 minutes of stirring on the impeller. The major transition from thick paste to thick slurry is clear when it occurred at approximately 30 seconds with a sudden drop in power draw. Numerical integration of this curve gives the energy required to achieve this change in state, as shown in Figure 4-38.

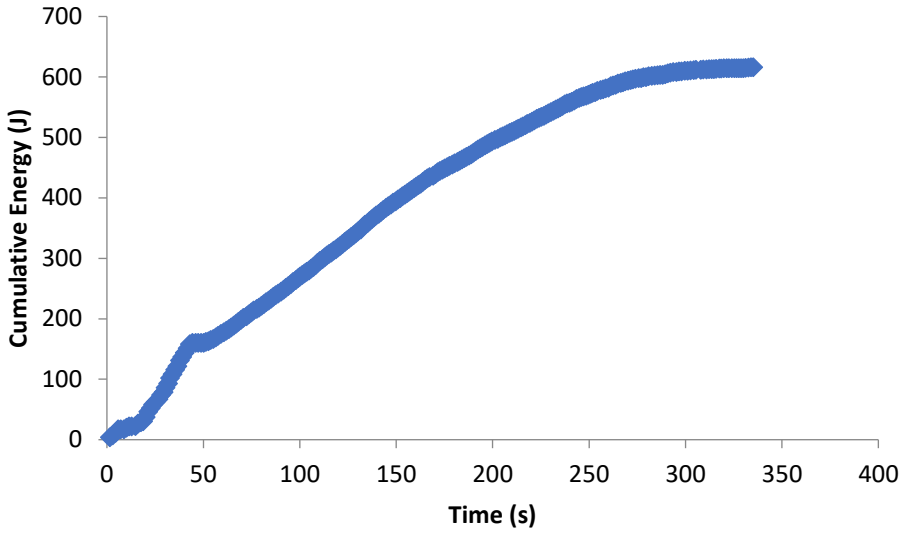

Figure 4-38: Cumulative energy required to reduce paste viscosity using an impeller

Figure 4-38 shows that approximately 6kJ kg^{-1} is required to change the paste to a thin slurry. This is a relatively low value and suggests that the UTL high shear mixer used was significantly overpowered for the duty.

4.6.3.2. Other Formulations

The production scale rig produced 80 wt% ink slurry with no problem at all with a maximum production rate of 284 kg slurry per hour. As seen at smaller scales, no combination in operating parameter had any effect on the maximum particle size of the slurry as measured by the Hegman gauge. As a stress test the solid content was increased to 85 wt%, which was produced with no problem by the device. However, this 'slurry' showed a very significant amount of elasticity and so was not a useful product.

The production scale rig produced both magnesia slurries with no problem whatsoever up to 30 wt% and 500 kg hr^{-1}. It was possible to preheat the liquid feed to 50 ^{o}C, giving a higher temperature product slurry. Figure 4-39 shows there was a small (approx. 5 ^{o}C) temperature increase inside the mixing chamber. This is significantly less than the exotherm seen when the

equivalent slurry is made in a batch tank. Therefore, the slurry was left stirring slowly on a propeller, just enough mixing to prevent sedimentation, and the temperature was monitored with time. As shown in Figure 4-39 it took approximately nine minutes for the slurry to reach its maximum temperature of 80°C. This is a significant result as it shows that for a final process design a buffer tank with mean residence time of at least ten minutes would be needed following the MHD to ensure the full wetting of magnesia has occurred before the next stage in the process.

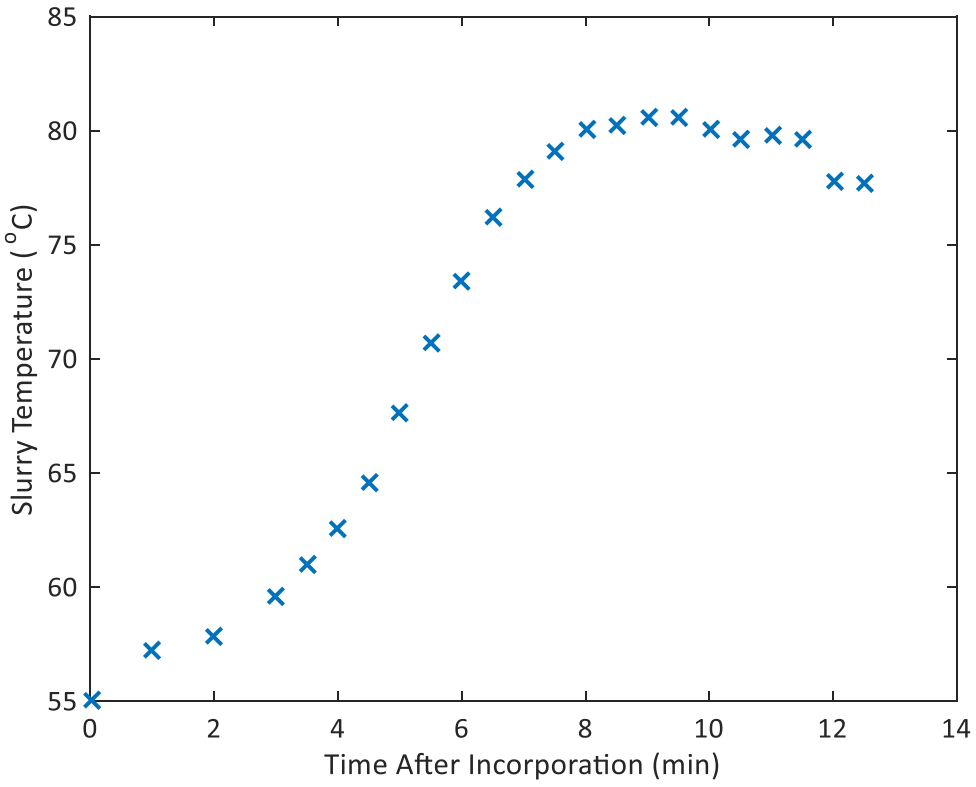

Figure 4-39: Temperature evolution of magnesia slurry after mixing in the MHD

4.6.4. Conclusions

P0 slurry was produced continuously at 400 kg h^{-1} (powder feeder limited) on a pilot scale IKA in line mixer. Variation in input slurry, water, acetic acid had little effect on the output slurry. Variation in machine parameters had little to no effect on the final slurry. It is possible to run for an extended period of time producing 39% (by addition weight) PA using a secondary high shear mixer to collapse the foam produced. The amount of shear needed to reduce the viscosity will be

calculated from the mixer torque rheology measurements as it is impossible to replicate the "paste" using the lab scale Magic Lab from IKA.

Both magnesia and ink formulations were successfully produced at production scale. Pre-heating of the water for the magnesia slurry was also shown to be possible, up to an initial liquid feed temperature of around 50^{o}C. The wetting of the magnesia produced a significant exotherm over approximately 10 minutes after initial slurrying in the continuous mixer, this means that any continuous design of this magnesia would require a 10 minute residence time buffer tank to allow this reaction to occur.

4.7. Production Process Design

4.7.1. Introduction

In order to ensure successful implementation of a pilot and production scale process a series of formal assessments were carried out at relevant stages in the scale up project. Relatively early in the project a technical risk assessment was carried out to highlight any aspects of the technology that were not fully understood technically. The outcome of this was used to inform the experimental plan during scale up. A second technical risk assessment was subsequently carried out to assess how well questions that arose in the initial assessment were answered and potentially to highlight any new areas where more understanding was needed. These studies were carried out by the full Emissions Control Technologies project team with additional personnel from operations to add extra expertise from outside research and development.

Following successful scale up trials at lab, pilot, and production scales and successfully answering the problems highlighted during technical risk assessments, a full detailed design was put together to plan for implementation of a full production scale production line.

Following successful proof of concept and detailed design of a production scale process a Hazard Study 3 was carried out to assess the design to ensure it met its design, environmental, health, and safety objectives. The HS3 was carried out by a full team including the research project team, representatives from operations, design, and chaired by a trained experienced Hazard Study leader.

4.7.2. Technical Risk Assessment

Johnson Matthey has developed a bespoke process for assessing the technical risk to the company involved in implementing new technologies. The process is designed to establish a semi-quantitative understanding of technical risks and uncertainties in a technology, allowing them to be systematically ranked. This 'risk register' provides priority areas for R&D resource allocation to answer specific high-risk areas of development. This technical risk assessment is designed to be run multiple times throughout the lifetime of a project, allowing tracking of technological risks (Stitt 2014).

The basic format of the assessment involves systematically working through a proposed process, assessing risks determining their likelihood, severity, and known mitigation strategies (Smith and Merritt 2002). This is done as part of a multidisciplinary project team, with representation from business and operations teams as well as the R&D project team. It is also preferred that the session is run by a trained facilitator, not part of the project team.

When risks are highlighted they are scored in terms of **likelihood, Impact,** and **(un)manageability** from 1 – 4, with guide definitions of 1 = low risk, 4 = panic (Stitt 2014). The total risk is then evaluated as the product of these three values. Risk scores greater than 20 are deemed significant and in need of study.

During the course of this project two technical risk assessments were carried out, the first in February 2015 and the second in August 2016. The results of each of these was used to direct the focus for R&D activities in this project and are shown in Figure 4-40.

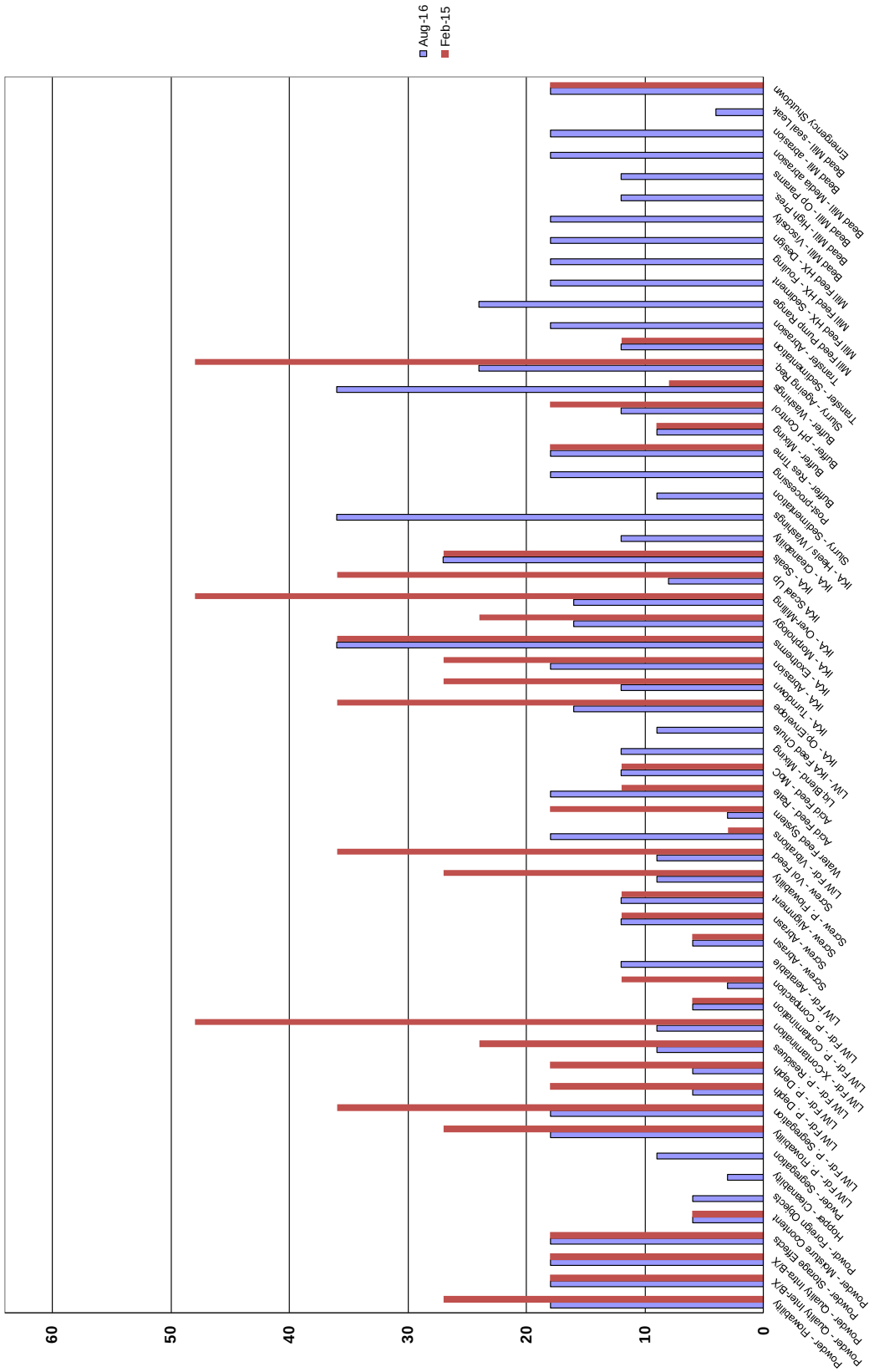

Figure 4-40: Technical risk assessment outcomes

4.7.3. Detailed Design

Following the three stages of the scale up project a full detailed design was prepared to which a full manufacturing scale production line could be built. This detailed design included an optional recirculation loop for PA slurries with an in line static mixer to achieve the work input required to thin the paste produced by the mixer to a slurry. A piping and instrumentation diagram for this full detailed design is shown in Figure 4-41. The full details of the design are not reported here.

4.7.4. Hazard Study 3

A Hazard Study 3 was conducted at Johnson Matthey on the detailed process design shown in Figure 4-41. This study involved a largely multidisciplinary group and was chaired by trained individuals who were not part of the project team. The results of the Hazard Study 3 are not reported here.

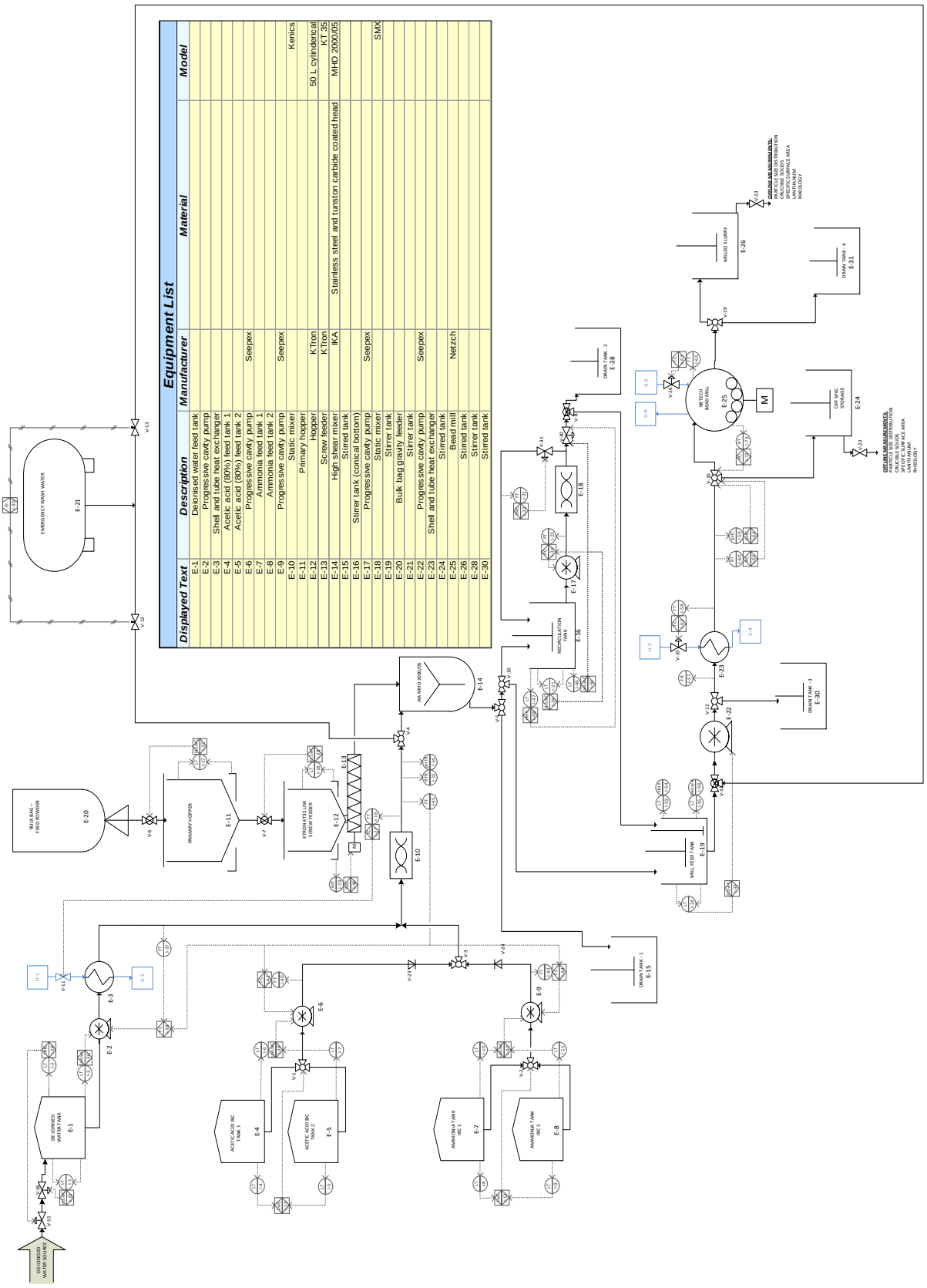

Figure 4-41: Full detailed design of production scale continuous incorporation process

5.

Slurryability: What Makes a Powder Difficult to Incorporate into a Concentrated Slurry

This paper investigates powder properties that are significant in determining how easily a powder may be incorporated into water to form a concentrated slurry. The slurryability of a powder is defined as the time and energy required to prepare a 50 wt% slurry, as well as a threshold concentration at which it requires 1 kJ to further increase the solid content by 1 wt% at the scale studied.

Partial least squares (PLS) models relating powder properties to their slurryability are built on a dataset of thirteen powders. The most significant properties determining slurryability are the particle pore volume, powder bulk density, and the results of permeability and aeration tests on a powder rheometer. The d_{50} particle size and powder cohesion measurements are also relevant in the models.

By measuring only these six properties the slurryability of two further powders, not included in the training dataset, were predicted within ±10 %.

5.1. Chapter Preface

At time of writing this Chapter has been submitted for publication as a research paper to the American Institute of Chemical Engineers Journal (AIChE J.)

5.2. Introduction

Throughout the process industries there is often a dichotomy between the formulation development and manufacturing stages of delivering a new product. This leads to issues with the 'manufacturability' of a new product as it moves from the laboratory scale into newly designed or existing manufacturing plants. This is inefficient, as useful data are either lost or not recorded during the formulation stage, which could be invaluable to the improvement and development of manufacturing processes. It can also be costly as new products may be sent to manufacture before they can be successfully made, either requiring extra development work or compromises in product quality or manufacturing cost. *In extremis*, the process may even fail due to unpredicted effects of manufacturing at scale. Such products can include concentrated high solids content slurries, created by the addition of large amounts of powdered solid (up to and above 50 wt%) to liquid media in a stirred vessel; these arise in a wide range of industries including paint (Braun *et al.* 1992), catalyst (Nowak, Robbins, *et al.* 2013), consumer goods (Fleming *et al.* 2006) and aerospace (Chou and Lee 2005).

Previously, in Chapters 2 and 3 an optimised geometry was designed to maximise the efficiency of powder incorporation to prepare concentrated slurries at laboratory and larger scales. However, it was noted that the scale up of this geometry was strongly affected by a step-change in incorporation performance that occurred at approximately 40 wt% for the alumina studied. This value of 40 wt% was observed to be specific to the type of powder studied and thus may be considered a powder characteristic for an individual liquid. This study considers a wide range of different powders and uses multivariate statistical modelling to determine which powder

properties drive the point at which this transition occurs: this should enable the prediction of this transition based on characterisation of new powders. The ease with which powders are incorporated, defined by how concentrated it is possible to make a slurry before reaching this transition, is referred to here as the *slurryability* of that powder. Raw material properties can significantly impact the behaviour of those materials through a manufacturing process (Prescott and Barnum 2000; Vasilenko *et al.* 2011). However, there are no previous studies considering the effect of raw powder properties on their ease of incorporation into high solids content dispersions.

The concentration of a slurry has so far been referred to on a wt/wt basis. This is generally how formulations involving powders are specified, weight being a considerably more reliable measure for powder quantity than volume, which is dependent upon the previous handling of the powder (Carr 1965; Hausner 1966; e Silva *et al.* 2013). However, volume concentration has been shown to be a better predictor of the slurry rheology, and therefore the effect of the powder on the behaviour of the system (Krieger and Dougherty 1959).

The flow behaviour of fine powders is not trivial, with multiple measurements being required to characterise powders sufficiently for even simple design calculations (Koynov 2015). In this study the powder is added to water to prepare a slurry. This adds further complication to the forces acting on individual particles. Due to the presence of three phases at the liquid surface, the interfacial tension between the liquid and the solid has a significant effect on the complex force balance on the solid. This value of the interfacial tension is specific to combination of the individual powder and liquid being studied and can give dramatically different powder wettability behaviour if different liquids or solids are studied (Chilekar *et al.* 2009). In highly hydrophobic solids the high interfacial tension with water can prevent particles from becoming wetted and thus being fully incorporated (Ruthiya *et al.* 2005). It can also promote agglomeration of particles,

where air becomes trapped within the agglomerate giving it a lower bulk density than the solid density, causing it to float even if the solid would sink. The formation of semi-wetted agglomerates may also lead to an increase in the apparent volume fraction of the dispersed phase, with resulting impact on the suspension rheology. This strong impact of wettability on the behaviour of particles in a solid-liquid system makes it a key parameter in many sectors. Examples where this is true include the pharmaceutical sector(Buckton 1988) and the food and personal care industries where the interfacial tension of solids used to stabilise colloidal interfaces is important (Binks and Whitby 2005; Dickinson 2010; Dickinson 2012). The wettability of a solid is generally indicated as the three-phase contact angle between the solid, liquid, and air given by Young's equation, below (Young 1805):

$$\gamma_{SL} = \gamma_{SV} - \gamma_{LV}\cos(\theta) \tag{13}$$

where θ is the three phase contact angle and γ is the interfacial tension between two phases, denoted as solid (S), liquid (L), and vapour (V).

This contact angle can be measured through several methods depending on the size and shape of the solid being studied and can generally be classified into three distinct categories: sessile drop, capillary rise, and direct measurement of the interfacial tension. This last category involves use of microcalorimetry (Yan *et al.* 2000) or inverse gas chromatography (Voelkel *et al.* 2009); expensive techniques that would only be available in a specialist research group or facility. Capillary rise methods, based on measuring the uptake of fluid through a powder bed with time, can be used to measure the contact angle through application of the Washburn equation (Washburn 1921):

$$h^2 = \bar{r}\frac{\gamma\cos(\theta)}{2\mu}t \tag{14}$$

where h is the liquid height at time t, μ is the liquid dynamic viscosity, and $\bar{r}$ is the mean capillary radius. This approach is used frequently for a wide variety of powders (Dang Vu and Jan 2005;

Galet *et al.* 2010; Kirdponpattara *et al.* 2013). However, researchers have reported issues when studying powders comprised of porous particles, demonstrating irreproducible results and effects of the particle porosity and shape on the liquid rise through the bed (Dang Vu and Jan 2005; Kirchberg *et al.* 2011; Nowak, Combes, *et al.* 2013; Nowak, Robbins, *et al.* 2013).

Sessile drop methods involve placement of a liquid drop onto the solid surface and directly measuring the angle between the solid and the liquid using a camera. This is simple for flat solids. However, it presents problems for powders, which do not present a flat surface and so the observed contact angle may not be the actual contact angle, as powder between the droplet and the camera can obscure the true measurement (Marmur 1996). Nowak *et al* (2013) compared various capillary rise and sessile drop approaches for measurement of the three phase contact angle for highly porous solids and found that the most consistent method involved placing a sessile drop onto a thin layer of powder dispersed onto a glass slide.

Two multivariate data analysis tools are used in this study. The first, principle component analysis (PCA), first developed by Karl Pearson in 1901 (Pearson 1901) is a tool used to reduce the dimensionality of a dataset. It is used herein as a data exploration tool to find powders with similar behaviour and to map the relationships between various powder properties and powder slurryability. PCA is frequently used in a wide variety of fields including stock market analysis and prediction in the finance sector (Ince and Trafalis 2007), image processing (Naidu and Raol 2008), and pharmaceutical formulation development (Bohidar *et al.* 1975). Wang *et al* (2017b) used PCA to study the effect of powder properties on the performance of a loss in weight powder feed system.

Partial least squares regression modelling (henceforth referred to as PLS) is a powerful multivariate statistical technique that looks for underlying latent structures within two datasets, a predictor dataset (X) and a response dataset (Y). These latent structures, or latent variables, are

similar to principle components in PCA, reducing the dimensionality of complex datasets to a smaller number of latent structures. A linear regression model is used to predict the maximum multidimensional variance in the Y space, explained by a multidimensional direction in the X space (Wold *et al.* 2001). PLS has found particular use in the field of chemometrics for spectral calibrations (Haaland and Thomas 1988; Sjöblom *et al.* 1998; Caporaso *et al.* 2018), where the ability of PLS to comfortably deal with highly co-correlated X variables (such as spectral bands) and more variables than observations make it a highly useful tool for building calibrations (Wold *et al.* 2001). More recently PLS is finding more use in study of process data, finding complex multivariate relationships between process and recipe formulation variables (Wise and Gallagher 1996; Gurden *et al.* 1998). There are multiple ways to consider the relative effects of different variables in the X space in PLS models. One of the simplest is the use of Variable Importance in the Projection (VIP) scores, which are defined as: (Tran *et al.* 2014).

$$VIP_i = \sqrt{d \frac{\sum_{k=1}^{h} \nu_k (\omega_{ki})^2}{\sum_{k=1}^{h} \nu_k}} \tag{15}$$

where d is the number of variables, h is the number of latent variables in the PLS model, ν_k is the fraction of explained variance in the X space by latent variable k, and ω_{ki} is covariance weighting for each variable, i, over all latent variables. A cut off threshold is often used for VIP scores, where a variable with VIP scores < 1 is deemed insignificant (Tran *et al.* 2014).

This study defines a measure to compare slurryability between a number of different powders. By measurement of a wide range of powder properties, PLS is used to build a predictive model for the slurryability of powders based on their bulk and particle properties. This model is validated through two additional powders which were not part of the datasets used to build the model. VIP scores are also used to find the most important powder properties dictating the slurryability of a given powder.

5.3. Materials and Methods

5.3.1. Materials

In this study 15 different commercially available porous and non-porous powders were studied to build and test the predictive multivariate models used. Thirteen of these were used to build the statistical model, listed in Table 1. The data from remaining two were used to test and validate the model. The powders were characterised by a variety of techniques which are described below.

Table 5-1: List of materials studied

Powder Name	d_{10} (µm)	d_{50} (µm)	d_{90} (µm)	Skeletal density (kg m^{-3})	Poured density (kg m^{-3})	Tapped density (kg m^{-3})	Mean pore size (A)	Pore volume ($cm^3 g^{-1}$)
Mixed oxide 1	7.65	25.10	57.30	2432	909	1109	206	0.321
γ-alumina 1	4.02	18.80	39.30	3352	662	793	107	0.415
α-alumina 1	11.80	116.00	245.00	2701	313	381	345	1.53
α-alumina 2	13.50	69.50	147.00	2688	465	567	271	0.78
Stabilised γ-alumina 1	3.20	21.00	62.40	2731	380	498	181	0.7014
Titania	0.03	0.96	3.00	3900	247	357	0	0
Magnesia 1	2.02	15.46	31.21	3580	651	883	307	0.241
Magnesia 2	1.98	16.42	33.12	3620	510	690	318	0.251
Glass frit 1	0.40	3.00	479.60	5389	1124	1337	0	0
Mixed oxide 2	3.31	15.01	30.20	6130	1100	1210	289	0.285
Copper zeolite	1.99	5.02	10.89	2210	450	570	150	0.416
γ-alumina 2	0.81	2.01	21.12	2698	492	679	68	0.147
γ-alumina 3	6.12	47.23	187.65	2701	736	879	71	0.358

Powder Characterisation

Particle size was measured by laser diffraction using a Malvern Mastersizer 3000 (Malvern Instruments, UK) using a dry dispersion module. The results are reported as D_{10}, D_{50} and D_{90} which represent the size at which 10 %, 50 %, and 90 % respectively of the solid volume in the powder sample is comprised of particles with an equal or lesser volume than a sphere of that diameter.

Multiple density terms are considered as no individual definition of density can describe all the necessary features of an individual powdered solid. The first density measurements considered are the poured and tapped bulk density measurements, bulk powder density values measured using a measuring cylinder with a known mass of powder carefully poured into it to give the poured density. This cylinder is then tapped 2000 times using a Tapped Density Tester (Copley Scientific, UK). These were used to calculate the Hausner ratio, H, (Equation 16) (Hausner 1966) and Carrs Index, C, (Equation 17) (Carr 1965) as:

$$H = \frac{\rho_T}{\rho_B} \tag{16}$$

$$C = 100\left(1 - \frac{\rho_B}{\rho_T}\right) \tag{17}$$

These values are often used as rule of thumb metrics to determine the flowability of a powder, with HR values > 1.25 and CI values > 25 indicating poor flow. These values are clearly related and will show a significant degree of co-correlation. However, this is easily handled by the multivariate statistical approaches used in this study so there is little reason to neglect either.

Skeletal density measurements, a measure of the density of the pure solid material, neglecting inter- and intra- particle pores, were taken using helium pycnometry. Mean pore diameters and pore volumes were measured using nitrogen adsorption BET. Using nitrogen adsorption BET is

not a perfect approach for this measurement as it generally measures small pores and is liable to miss large pores (i.e. those in the range 50-500 μm) and therefore mercury porosimetry would be the preferred technique and a possible improvement to this study. However, most of the powders in this study have a d_{90} < 100 μm, and so are unlikely to contain pores large enough to be missed by nitrogen adsorption BET, making the possible error caused by this measurement unlikely and small.

5.3.1.1. Powder Flow Characterisation

Powder flow characterisation was carried out in two different types of equipment: a shear cell for quasi-static behaviour and a powder rheometer for dynamic characterisation. The rheometer was used also to assess powder aeration and compressibility as well as permeability of a compact powder bed.

5.3.1.1.1. Shear Cell

A Brookfield Powder Flow Tester (PFT) (AMETEK Brookfield, USA) was used to perform shear cell measurements on the powders. The test consists of three steps: (1) pre-compaction of a pre-prepared uniform powder bed to an initial consolidation stress, (2) the powder is sheared until a steady state is achieved, this is the preshear point, (3) the normal stress is then reduced and the yield point is again found by applying a shear stress to the powder bed. This is repeated for five normal stresses to give a yield locus, as shown in Figure 5-1(Schulze 2008). This test is repeated at normal consolidation stresses of 15 kPa, 9 kPa, 6 kPa, and 3 kPa to give four yield loci.

A Mohr-Coulomb analysis approach is used, where a linear regression is fitted to the yield locus. The slope of this linear regression, ϕ, is an estimate of the powder internal angle of friction. Two Mohr circles are used to find the flow function of the powder. The first of which passes through the origin and is tangential to the yield locus defines the powder unconfined yield strength, σ_c, as shown in Figure 5-1(Schulze 2008). The second Mohr circle is drawn tangential to the yield locus

at the preshear point and defines the major principal stress, σ_1. The powder flow function (ffc) is defined as the gradient of a plot of the major principal stress against the unconfined yield strength. Figure 5-2 shows a guideline of how the flow function of a powder corresponds to how easily it is likely to flow.

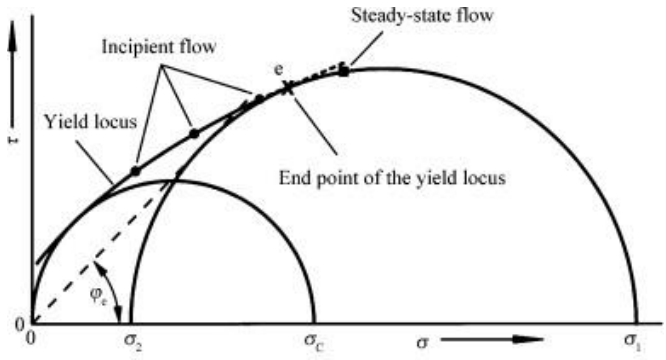

Figure 5-1: Example yield locus of a powder bed (Schulze 2008)

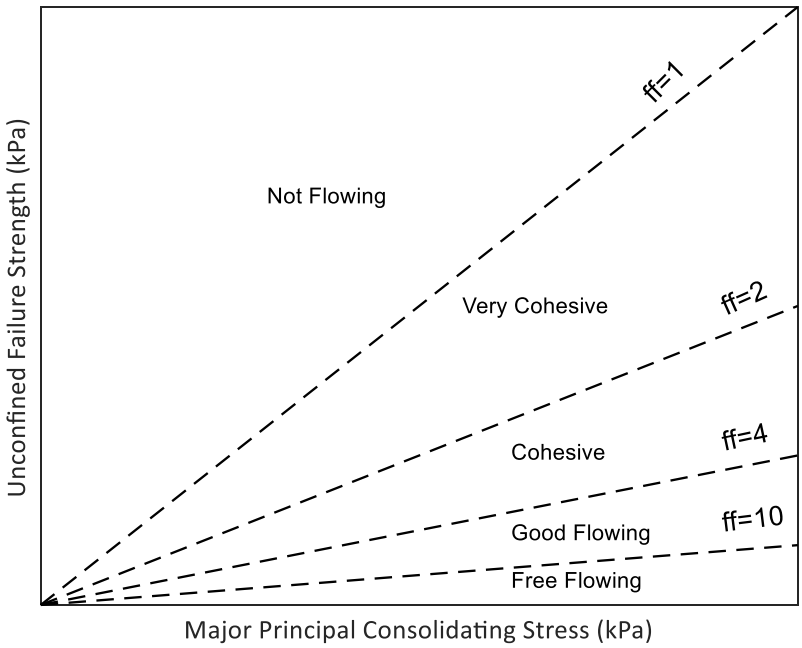

Figure 5-2: Guideline flow function values for different powder flow regimes

5.3.1.1.2. Freeman FT4 Powder Rheometer

A series of tests were carried out on a Freeman FT4 powder rheometer (Freeman Technologies, UK). For each test the powder is first conditioned in the rheometer by a helical blade, shown in Figure 5-3, moving up and down through the powder bed three times at a tip speed of 60 mm s^{-1} to give a uniform powder bed and to remove the handling history of the powder (Bharadwaj *et al.* 2010). Four different tests are carried out in the FT4, all of which are preceded by this conditioning stage: the compressibility test, the permeability test, the flow energy test, and the aeration test.

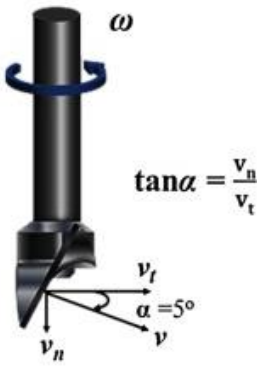

Figure 5-3: Freeman FT4 powder rheometer helical impeller blade used for conditioning and measurement

In the compressibility test the powder is subjected to a normal pressure up to 15 kPa for one minute. The powder compressibility is given as a function of the change in powder bed volume:

$$C\ (\%) = 100\frac{V_i - V_C}{V_i} \tag{18}$$

where V_i is the powder volume after conditioning and V_C is the compressed powder volume.

In the permeability test air is passed through the powder bed after the conditioning step at a flow rate of 2 mm s^{-1}. The powder bed is compressed at 15 kPa during this test. The permeability of the powder is indicated by the measured pressure drop across the powder bed, with a low

pressure drop indicating a high permeability powder bed. The permeability of a powder bed is proportional to the bed porosity and particle diameter squared using Darcy's law and the Kozeny-Carman equation respectively (Carman 1938; A. Alzaydi 1975).

In the basic flow energy dynamic test the powder is initially conditioned. Following this the impeller is passed down through the powder bed at a fixed velocity. The energy required for the powder to flow during this test is measured by the torque on the impeller and the normal force exerted on the base of the instrument. Higher flow energies indicate a higher level of mechanical locking and friction, this would indicate powders with higher angles of internal friction that are less likely to flow easily. This test is repeated three times with a conditioning stage in between each measurement.

The aeration test is similar to the basic flow energy test. In this test the powder is fluidised where possible, if not it is simply aerated, and the normal dynamic test is carried out. The test is repeated three times at air flows decreasing from 20 mm s^{-1} to 0 mm s^{-1}. At each air velocity the flow energy is measured three times, with a conditioning stage between each measurement. The aeration index is the ratio of flow energy under fixed bed conditions (Leturia *et al.* 2014), i.e. air velocity = 0 mm s^{-1}, and the flow energy under full fluidisation where possible, or at 20 mm s^{-1} where the powder will not fluidise. This measurement is used to give an indication of how the powder behaves when aerated, with high aeration indexes suggesting that the powder is easily aeratable and does not remain cohesive whilst aerated, allowing the impeller blade to easily move through the bed.

5.3.1.2. Powder Wetting Characterisation

5.3.1.2.1. Contact Angle

To measure the powder contact angle with water the method shown by Nowak *et al* (2013) to be most appropriate for use with highly porous powders was used. A thin layer of powder was

adhered to a flat surface using a spray adhesive. Particles not firmly attached to the slide 30 seconds after application were removed. The size of the liquid drop was chosen such that the mean capillary length, a, defined in Equation 19, was larger than the radius of the droplet. This is done to make the effect of gravity negligible when compared to capillary effects(Drelich *et al.* 1993). The capillary length of water is 2.7 mm so a 10 µL droplet was used for all solids, giving a droplet with radius approximately 2.3 mm (Kranias 2004).

$$a = \sqrt{\frac{2\lambda}{\rho g}} \tag{19}$$

A KRUSS Drop Shape Analyser (DSA) 100 (KRUSS GmbH, Germany) was used to place the droplets on the powder surface and measure the resultant contact angle. Each measurement was repeated 25 times for each powder due to the possible complications in contact angle measurement of powders, such as powder between the droplet and camera obscuring the true contact angle, described above. The values stated are the mean of all measurements. An example DSA image is shown in Figure 5-4.

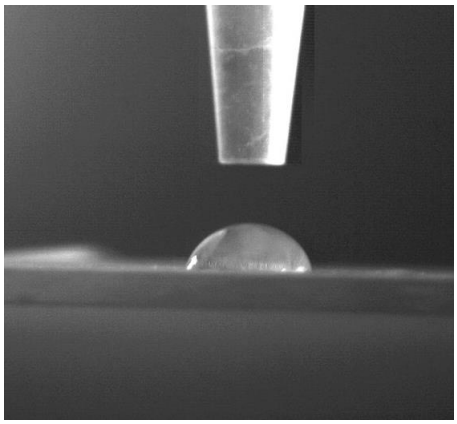

Figure 5-4: Example sessile drop sat on a thin powder bed

5.3.2. Slurryability Measurement

Slurryability was measured in a 5 L cylindrical stirred vessel with the geometric configuration that was found previously to incorporate powder most effectively into high concentration slurries in Chapters 2 and 3. This geometry is shown in Figure 5-5 and comprised a stainless steel flat-bottomed cylindrical mixing vessel with diameter, T = 0.17 m, a down-pumping pitched blade turbine (PBT) impeller with a diameter, D, of 0.085 m (D/T = 0.5). Off-bottom clearance, C, (measured to the middle of the impeller) was 0.085 m (C/T = 0.5; C = D). The impeller was placed off-centre, E, by 0.1 T (0.017 m) and tilted, α, by 10°. No baffles were used. The impeller speed, N, was fixed at 450 RPM.

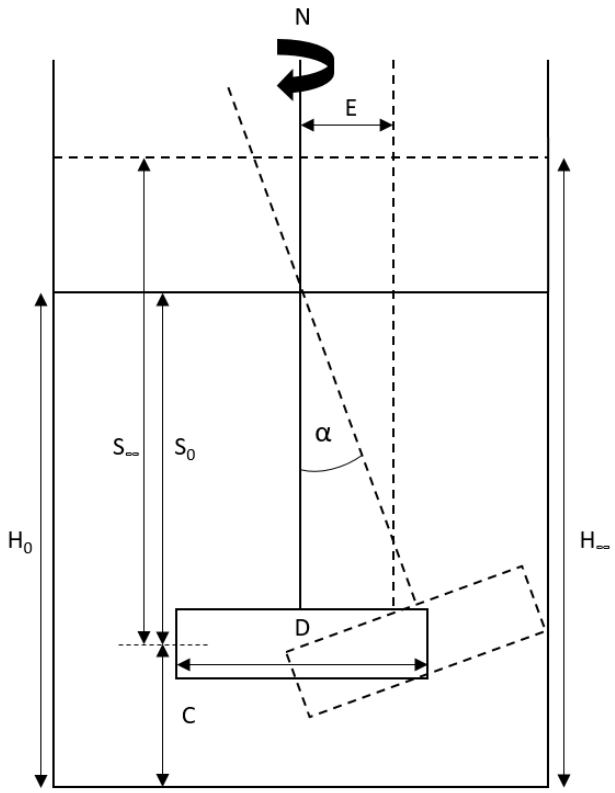

Figure 5-5: Mixing vessel schematic

Slurryability was assessed by measuring the time taken to add 50 wt% powder to a given vessel. Prior to the start of the experiment the vessel with filled with 3.86 L of water and 3.86 kg of powder was weighed out into fifty × 77 g aliquots using a KTron KT20 loss in weight powder

feeder configured to deliver a constant total mass. This allowed tracking of the amount of powder added to the vessel with time. The powder was added to water the stirred vessel described above up to 50 wt% as quickly as possible, adding each subsequent aliquot to the liquid surface as soon as the previous powder had been drawn down and incorporated into the slurry. The time and energy required to prepare a 50 wt% slurry was measured in this way for all powders studied. The slurryability of each powder was measured three times, the values used are the mean of these repeats.

The impeller shaft torque was measured using a calibrated Binsfield TorqueTrak 10k wireless strain gauge. The impeller power, P, was found from the shaft torque, Γ, using Equation 11.

The measured torque, and so impeller power draw was found to fluctuate by ±5 % of the reading value. All values used are the moving average value recorded over 1 s at a sampling frequency of 10 Hz.

5.3.3. Multivariate Analysis

Multivariate data analysis was carried out using JMP statistical software (SAS Institute Inc., UK). The data were first normalised using Z-score normalisation (or auto-scaling) as the different properties measured all have different units and scales. Z-score normalisation centres all the data around 0, with a standard deviation of 1 and is done simply by applying the following to all measurements:

$$Z_{i,m} = \frac{x_{i,m} - \bar{x}_i}{s_i} \tag{20}$$

where Z is the normalised value, x is the measurement of the ith property for the mth powder, $\bar{x}$ is the property mean for all powders, and s is the standard deviation of that property across all powders.

Principal component analysis is used as an exploratory tool to find trends and patterns within the dataset. PCA works by reducing the dimensionality of the dataset by orthogonal transformation, reducing the total number of variables to a set of orthogonal principal components (PC). The first PC (PC1) describes the largest possible variance within the dataset, with subsequent PCs describing less variance with increasing dimensions. Each subsequent PC is orthogonal to all preceding PCs.

Partial Least Squares regression (PLS) works in a similar manner, reducing the number of dimensions in both the predictor (X) and response (Y) datasets into a series of orthogonal structures. The Y structures are then regressed onto the X structures to give a covariance matrix relating the two using a Nonlinear Iterative Partial Least Squares (NIPALS) algorithm. Leave-one-out cross-validation was used during this analysis. This involves calculating potential models whilst leaving out one of the observations (in this case leaving out a powder). The response, based on each model, is predicted for the left-out observation to give a residual between the predicted value and the measured value. This is repeated for all observations, giving a total precision value, given as the root mean squared error of cross validation (RMSECV). This is repeated testing a different number of latent variables in the two structures. The optimum number of structures is determined as that which gives the lowest RMSECV value, whilst explaining as much of the variation in the Y block as possible (in terms of R^2). VIP scores are then calculated using Equation 15, shown above, to calculate the relative importance of each of the individual predictor variables studied.

PLS is a particularly effective technique for this application as it effective at handling co-correlation between predictor variables. This is important here due to the inevitable relationships between different powder properties. For example, as stated above, there is clearly a strong correlation between Hausner Ratio and Carr's Index. However, there will also be other significant

related variables such as particle porosity and bulk density, many of the various dynamic flow properties, and particle size values and pressure drop measurements.

PLS models can be improved by removing noise in the original dataset. VIP scores can be used as a variable selection method to indicate which of the initial variables are likely to contribute only noise, and which contribute useful variance. Therefore, the PLS algorithm is run over the dataset twice. Once to find an initial model, calculating VIP scores of all variables. Insignificant variables (those with a VIP score < 1) are then removed from the dataset and the model rebuilt. This will provide an improved model, with less overfitting (Akarachantachote *et al.* 2014).

The performance of the predictive models built using PLS can be considered by calculating the root mean square error (RMSE) between the predicted and measured values of slurryability. RMSE is calculated as:

$$RMSE = \sqrt{\frac{1}{N}\sum_{i=1}^{N}\left(Slurryability_{measured,i} - Slurryability_{Predicted,i}\right)^2} \qquad (21)$$

where N is the number of powders studied.

In order to validate the models built using partial least squares regression analysis two extra powders were studied, a zeolite material (zeolite 1) and another mixed oxide (mixed oxide 3). These powders were not included in the training sets used to build the models and so are used to study the applicability of the models outside of the original training set of powders.

5.4. Results and Discussion

5.4.1. Powder Characterisation

Table 5-1 gives the particle size, bulk density, skeletal density, and pore volume measurements for each of the thirteen powders studied in the training dataset. These powders were chosen to give a wide range of properties, as shown for all of these measures in Table 5-1.

Figure 5-6 shows the shear cell measurements at an initial consolidation stress of 15 kPa. The flow function coefficient is used to characterise how easily a powder will flow, with larger flow functions indicating easier flow, as shown in Figure 5-2. The glass frit showed the highest flow function coefficient, indicating it is the best flowing powder. The various alumina powders studied generally showed the lowest flow function values. The glass frit also showed the highest cohesion, with the magnesia powders and mixed oxides also showing reasonable cohesion. Again, the alumina powders showed the lowest cohesion values.

Figure 5-7 shows the basic flow energies and aeration energies of the initial 13 powders studied. The glass frit and mixed oxide 1 required the most energy to flow, whereas the titania powder sample required the least. Many of the powders were found possible to fully aerate during the test, with the glass frit, mixed oxides, and γ-alumina 2 being the only powders where it was not possible. This meant that most of the powders showed a significant aeration index as the energy required to make them flow dropped considerably when they were fully aerated.

Figure 5-8 shows the compressibility and pressure drop measurements from the Freeman FT4 powder rheometer. The magnesia and titania proved to be the most compressible, with the mixed oxides and alumina powders showing little tendency to compress.

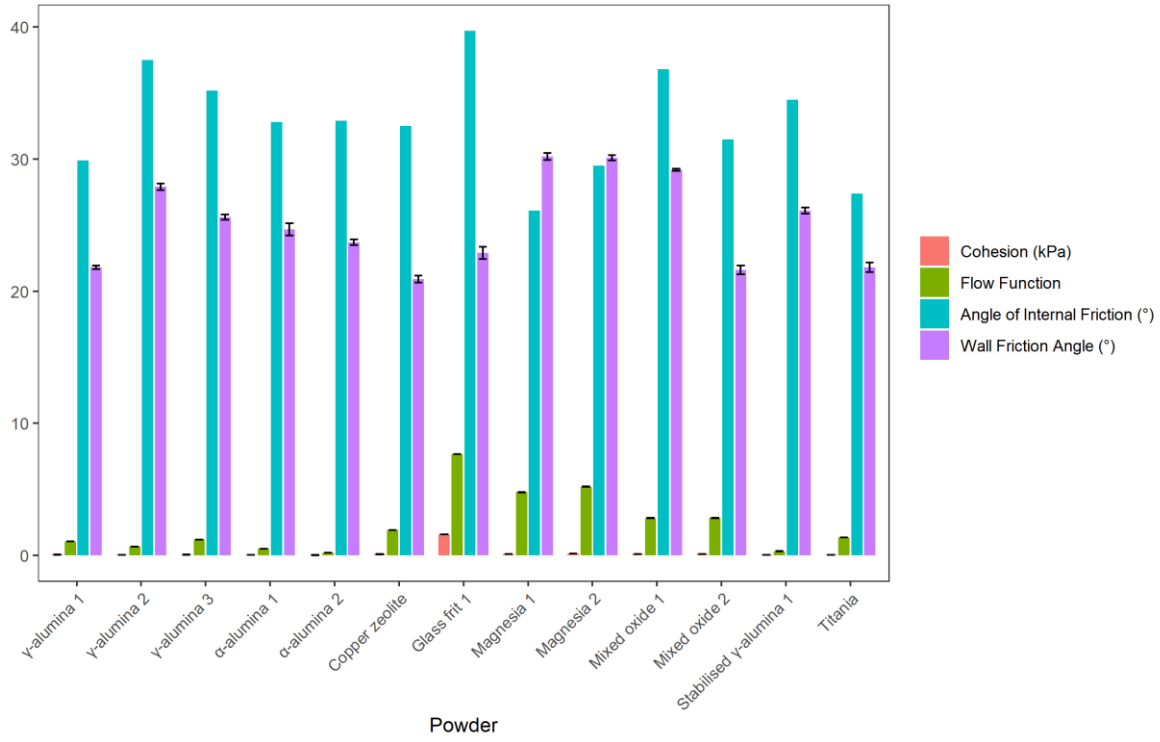

Figure 5-6: Shear cell measurements for initial 13 powders

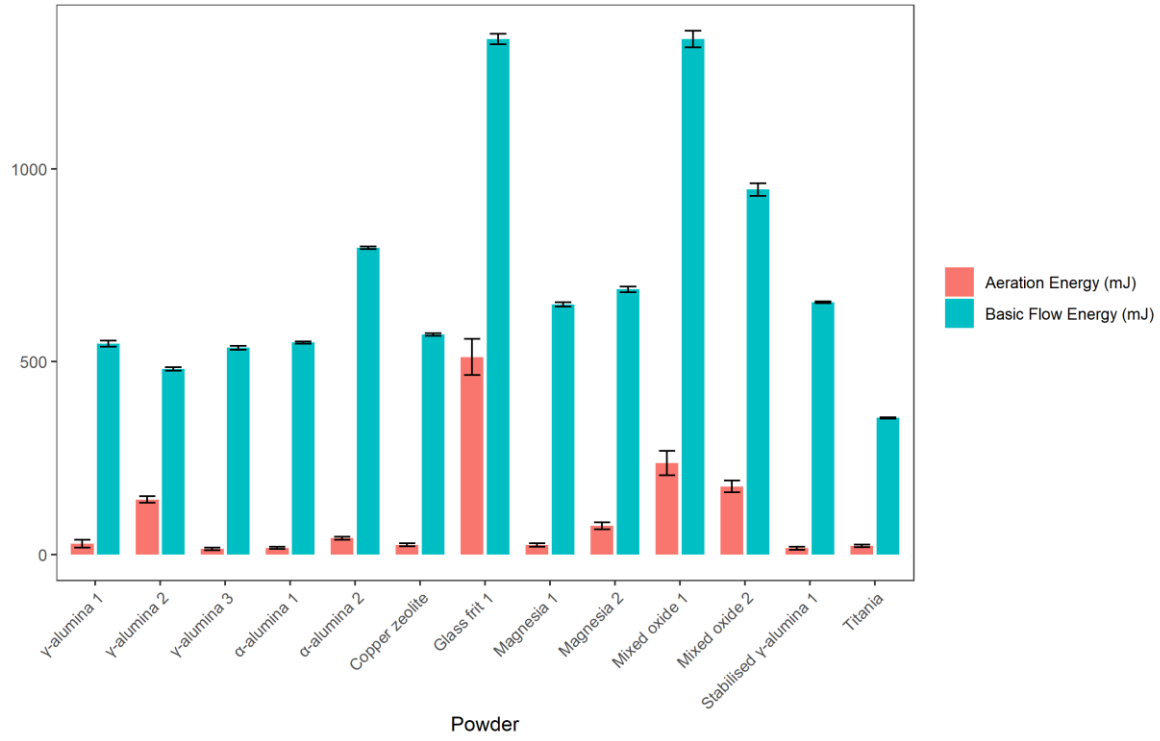

Figure 5-7: Basic flow energy and aeration energy test results from the Freeman FT4 for initial 13 powders

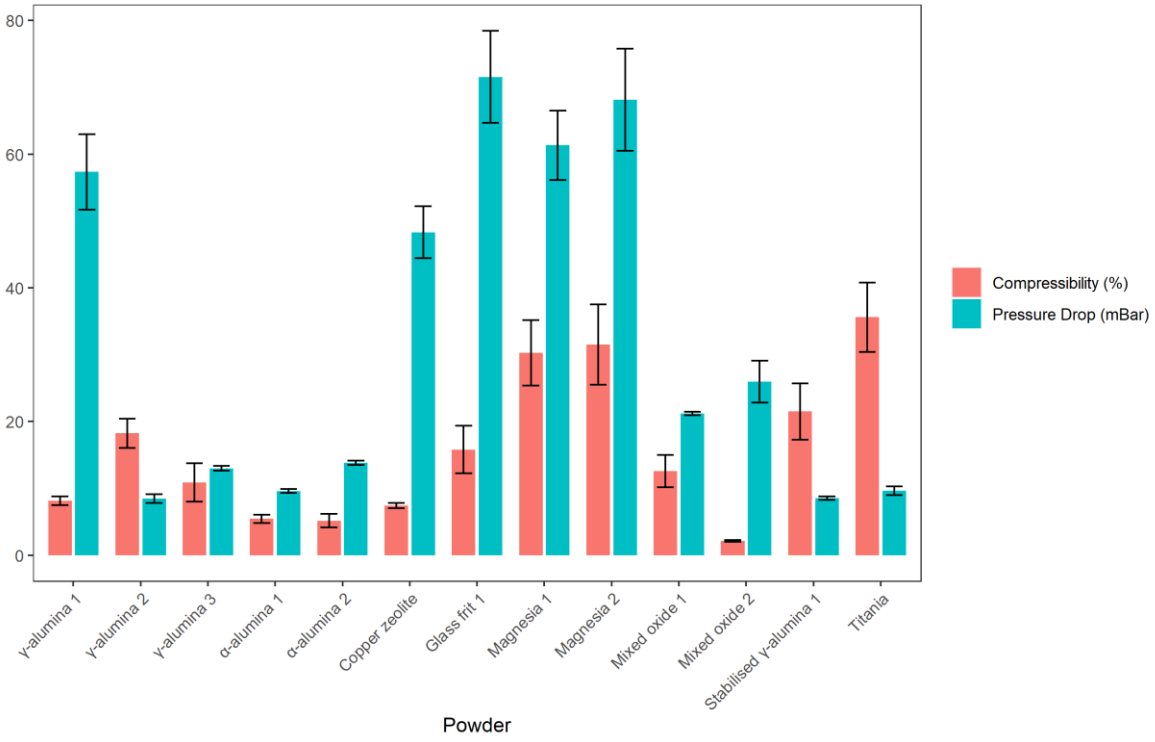

Figure 5-8: Compressibility and pressure drop tests from the Freeman FT4 for the initial 13 powders

5.4.2. Slurryability and powder ranking

In order to model the effect of powder and particle properties on the slurryability of a powder, a definition of powder slurryability is required that allows direct comparison between powders. The slurryability of a powder is defined in three ways:

1. t_{50} The time required to prepare a 50 wt% slurry.
2. E_{50} The cumulative specific energy required to prepare a 50 wt% slurry.
3. X_{11} The solid content at which it requires more than 1 kJ to raise the slurry solid content by 1 wt%.

These three approaches are shown graphically for three example powders in Figure 5-9, Figure 5-10, and Figure 5-11 respectively. Figure 5-9 shows the time taken to add powder to the vessel

up to the final solid concentration of 50 wt%. t_{50} is defined as the time value of the final point of the curve. Figure 5-10 shows the cumulative energy required to incorporate powder into slurry. This energy is calculated using the measured impeller torque and mixing time. E_{50} is defined as the cumulative energy value of the final point of the curve. Figure 5-11 shows how this energy requirement increases with increasing solid content and defines X_{11} as the solid content when the curve for each powder crosses 1000 J $\%^{-1}$.

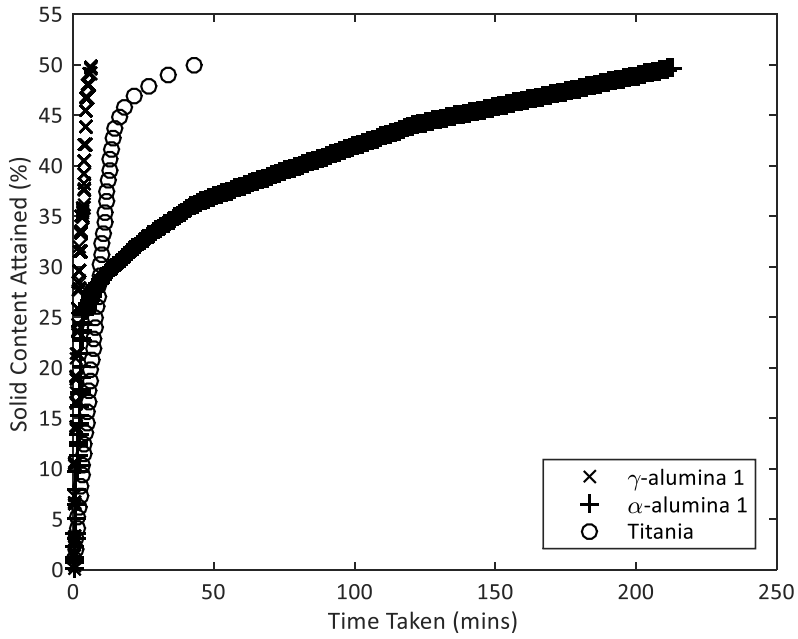

Figure 5-9: Slurryability approach 1 – time taken to prepare a 50 wt% slurry

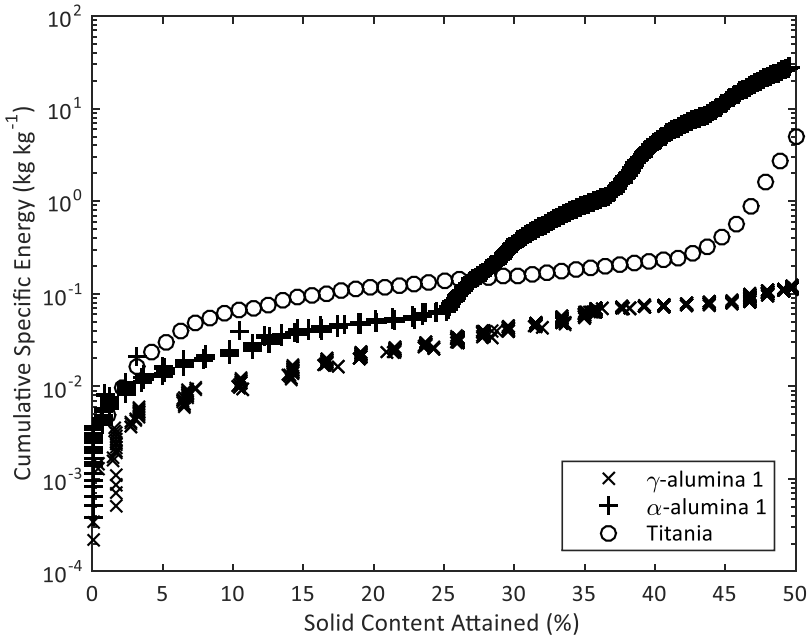

Figure 5-10: Slurryability approach 2 – total energy required to achieve a 50 wt% slurry

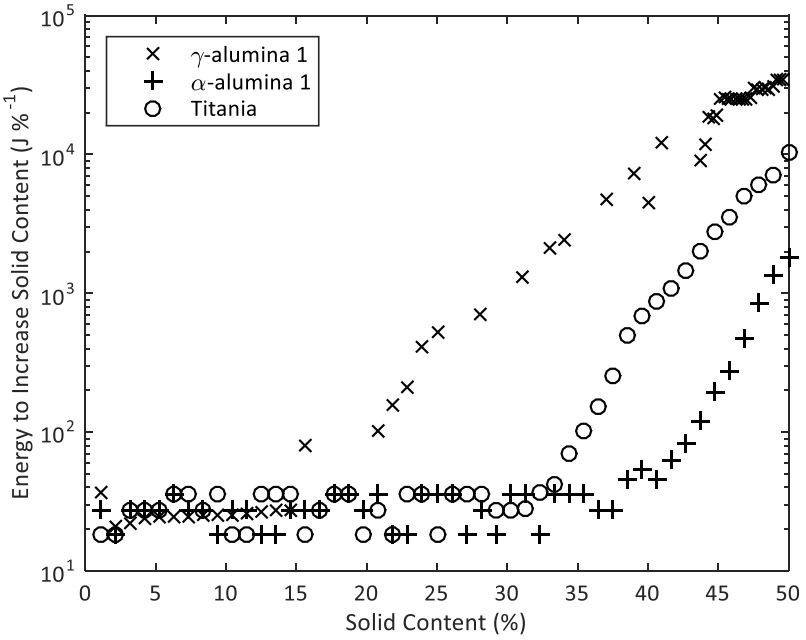

Figure 5-11: Slurryability approach 3 – solid content at which it requires at least 1 kJ to raise the solid content of the slurry by 1 wt%

Table 5-2 shows the slurryability measurements for each of the thirteen initial powders. There was a significant range in powder slurryability within the dataset with slurry time to prepare a 50 wt% slurry at 6 minutes for the easiest powders (γ-alumina 1 and Mixed oxide 1) and over four hours for the least slurryable powder studied (Stabilised γ-alumina 1).

Table 5-2: Measured slurryability values

Powder Name	**Slurry Time (mins)**	**Slurry Energy (kJ kg^{-1})**	**Threshold Concentration (wt %)**
Mixed oxide 1	6.2	0.12	48.2
γ-alumina 1	6.0	0.11	48.8
α-alumina 1	212.0	28.2	32.1
α-alumina 2	171.3	22.4	38.2
Stabilised γ-alumina 1	250.0	34.5	25.1
Titania	92.6	9.9	41.3
Magnesia 1	7.1	0.25	47.3
Magnesia 2	75.5	1.2	41.5
Glass frit 1	21.3	1.3	46.2
Mixed oxide 2	8.1	0.8	47.6
Copper zeolite	15.1	0.21	45.2
γ-alumina 2	131.2	17.8	39.2
γ-alumina 3	21.8	3.2	43.2

Figure 5-12 shows the relative rankings of each powder in terms of their slurryability ranked from most easily incorporated to most difficult for each of the three measures of slurryability described above. It is clear that for most cases all three metrics give similar rankings of each powder.

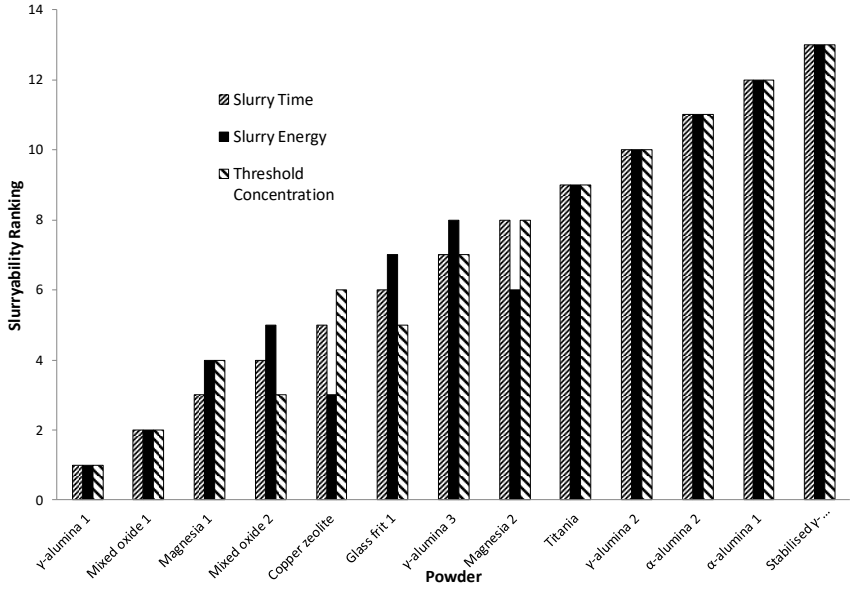

Figure 5-12: Relative rankings of each powder in terms of each slurryability measure with 1 being slurry time, 2 slurry energy, and 3 threshold concentration

5.4.3. Univariate Analysis

The most likely powder properties governing how easy a powder is to incorporate are the volume concentration and the interfacial tension with the liquid into which the powder is being added. Each of these can be studied in isolation.

5.4.3.1. Powder Density

Figure 5-11 shows the energy to increase the solid content of three slurries by 1 wt% of three powders with different slurryabilities as their solid content by weight is increased. Figure 5-13 shows the same three powders with the slurry solid contents expressed by tapped volume. The two alumina powders appear to behave similarly when normalised by their volume, with their X_{11} occurring at around 50 vol% for both powders. However, the titania powder does not, reaching a considerably higher solid content of 71 vol% before it requires 1 kJ to add an addition 1 wt% of powder.

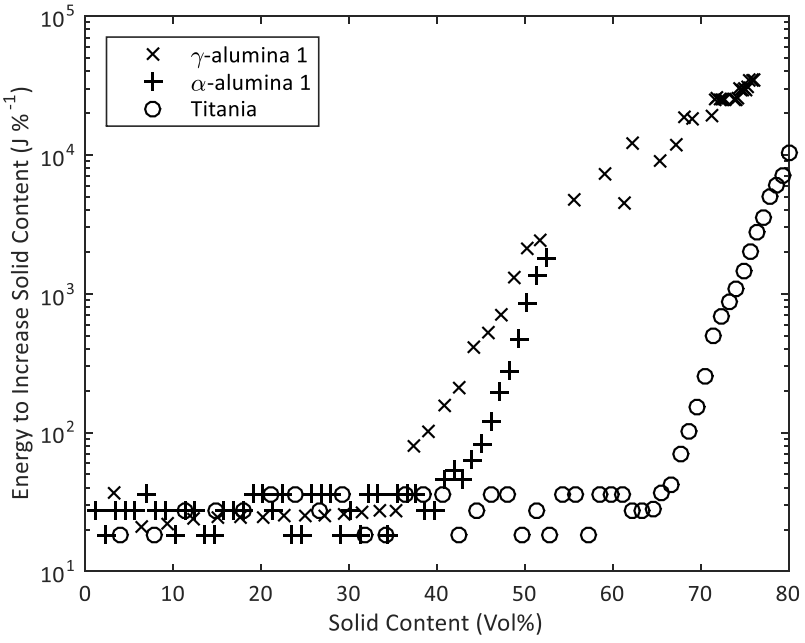

Figure 5-13: Energy to increase the solid content slurry by 1 wt% against the slurry solid volume

concentration

The powder envelope densities were also estimated from their pore volumes and tapped bulk densities, as described in section 2.3, and are shown in Table 5-3.

Table 5-3: Powder estimated envelope densities

Powder Name	Estimated Envelope Density (kg/m3)
Mixed oxide 1	1366
γ-alumina 1	1402
α-alumina 1	526
α-alumina 2	868
Stabilised γ-alumina 1	937
Titania	3900
Magnesia 1	1922
Magnesia 2	1897
Glass frit 1	5389
Mixed oxide 2	2231
Copper zeolite	1151
γ-alumina 2	1932
γ-alumina 3	1373

The Pearson's correlation index between the estimated envelope density and the slurryability was calculated using the R *cor* function, and found to be -0.065, suggesting there is very little correlation between the powder envelope densities and their slurryability.

5.4.3.2. Contact angle

Figure 5-14 shows the measured three phase contact angle plotted against the threshold slurry content slurryability measure. It is clear there is little trend between the contact angle with water and the slurryability of a powder, indicating that the interfacial tension between the solid and the liquid has little effect in how easy that powder is to incorporate. However, given that measuring the contact angle for porous powders is notoriously difficult, it is it is difficult to draw a firm conclusion. An improvement to this study would be to repeat this measurement using a number of different liquids, with a wide range of dispersive and polar surface tension components to find

the solid surface free energy for each powder, as described by Owens, Wendt, Rabel, and Kaelbe (Kaelble 1970; Rabel 1971; Owens and Wendt 2003).

It is clear that, although some differences in slurryability can be explained when looking at properties in isolation, there will always be exceptions. This is because the system being studied is complex and cannot be described by a single property. Therefore, a multivariate approach is needed.

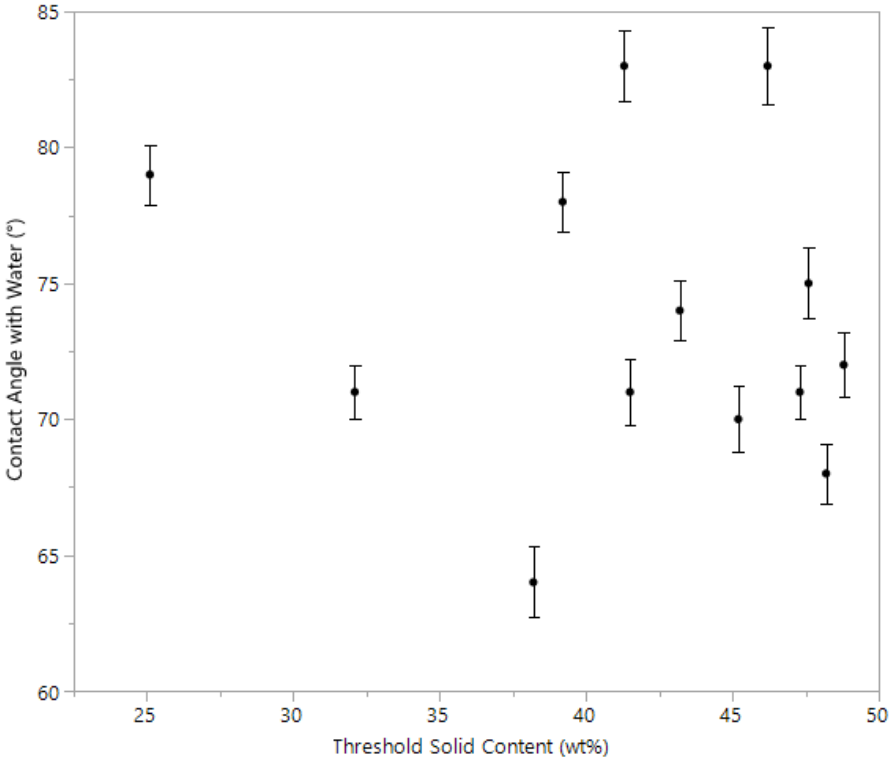

Figure 5-14: Three phase contact angles with water for initial 13 powders measured using a KRUSS DSA 100

5.4.4. Multivariate analysis

5.4.4.1. Simple Stepwise Regression

A simple regression model predicting threshold concentration as a function of particle size, pore volume, envelope density, and tapped bulk density is shown in Figure 5-15. This model shows a decent fit, suggesting that some of these variables and their interactions are important to the

powder slurryabilities. The most significant variables in the model are the pore volume, tapped density, and the interaction between tapped bulk density and pore volume.

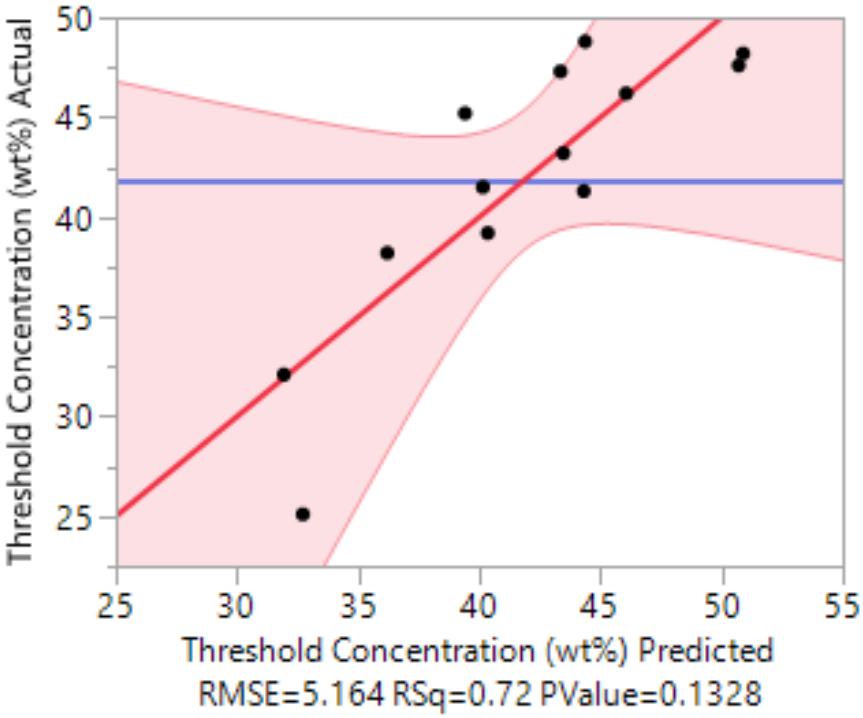

Figure 5-15: Simple regression model predicting threshold concentration as a function of particle size, pore volume, and envelope density

5.4.4.2. Principal Components Analysis (PCA)

Figure 5-16 shows a PCA scores plot for the first two principal components within the dataset, explaining the relationships between the samples in the first two principal components. Powders that are similar will be clustered in multivariate space, visualised by their similar score values. These first two components account for 58.6 % of the variation measured within the powder properties, with 74.3 % of the variation described by three principal components, and adding more principal components beyond three describes relatively little extra variation for each PC added. This suggests that three principal components are required to suitably describe the measured variation between the powders, with the first two describing the majority of the

variation. It is interesting to note that the different mixed oxides, magnesia, and α-alumina powders are clustered with one another in pairs, suggesting that these pairs are similar powders. The most unique powder of all appears to be the glass frit, which sits by itself with a high value in PC1.

Figure 5-17 shows the loadings plot of each of the measured powder properties. In the loadings plot, points close together suggest correlation whereas points in opposite quadrants (i.e. directly opposite one another through the centre of the plot) show anti-correlation. Points in adjacent quadrants show little or no correlation to one another. This is demonstrated clearly by the three slurryability measures, where slurry time and slurry energy are closely correlated and strongly anticorrelated to the threshold concentration (which responds in the opposite direction to slurry time and energy as powders become harder to incorporate). Some powder properties clearly cluster into sensible groups. For example particle size measurements cluster together with the pore volume, showing correlation, as do the Carrs Index and Hausner Ratio. Many of these are expected, as mentioned previously, showing strong co-correlation between measured variables. The angle of wall friction, powder flow function, and powder compressibility show little correlation with any other parameter. It is important to consider the standard deviation as well as the mean because more variable powders may behave differently than consistent powders, something not described by the mean value alone. However, most standard deviation and mean values appear strongly correlated due to their close proximity in Figure 5-17. This is likely because the value of the standard deviation is likely to scale in magnitude with the mean.

It is interesting to note the lack of correlation between the D_{10} and D_{50} values with the D_{90} values. This is likely because the PSD is being normalised by volume, where a single large particle can contain a significant amount of the measured volume, having a particularly strong influence on

the value of D_{90} but not on either the D_{50} or D_{10}. This is most strongly seen in the glass frit powder, which has the lowest D_{10} and D_{50} values of all powders studied but the highest D_{90} value.

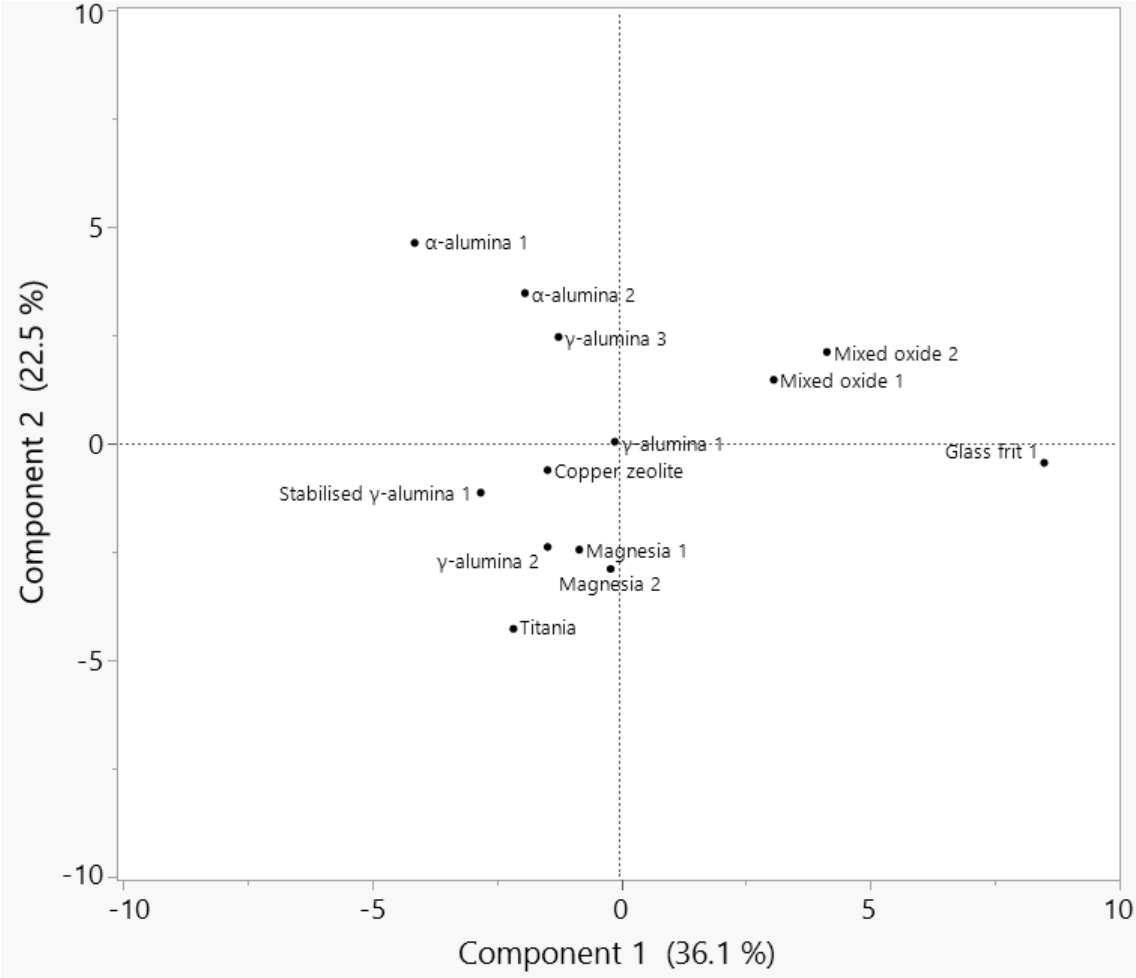

Figure 5-16: PCA scores plot

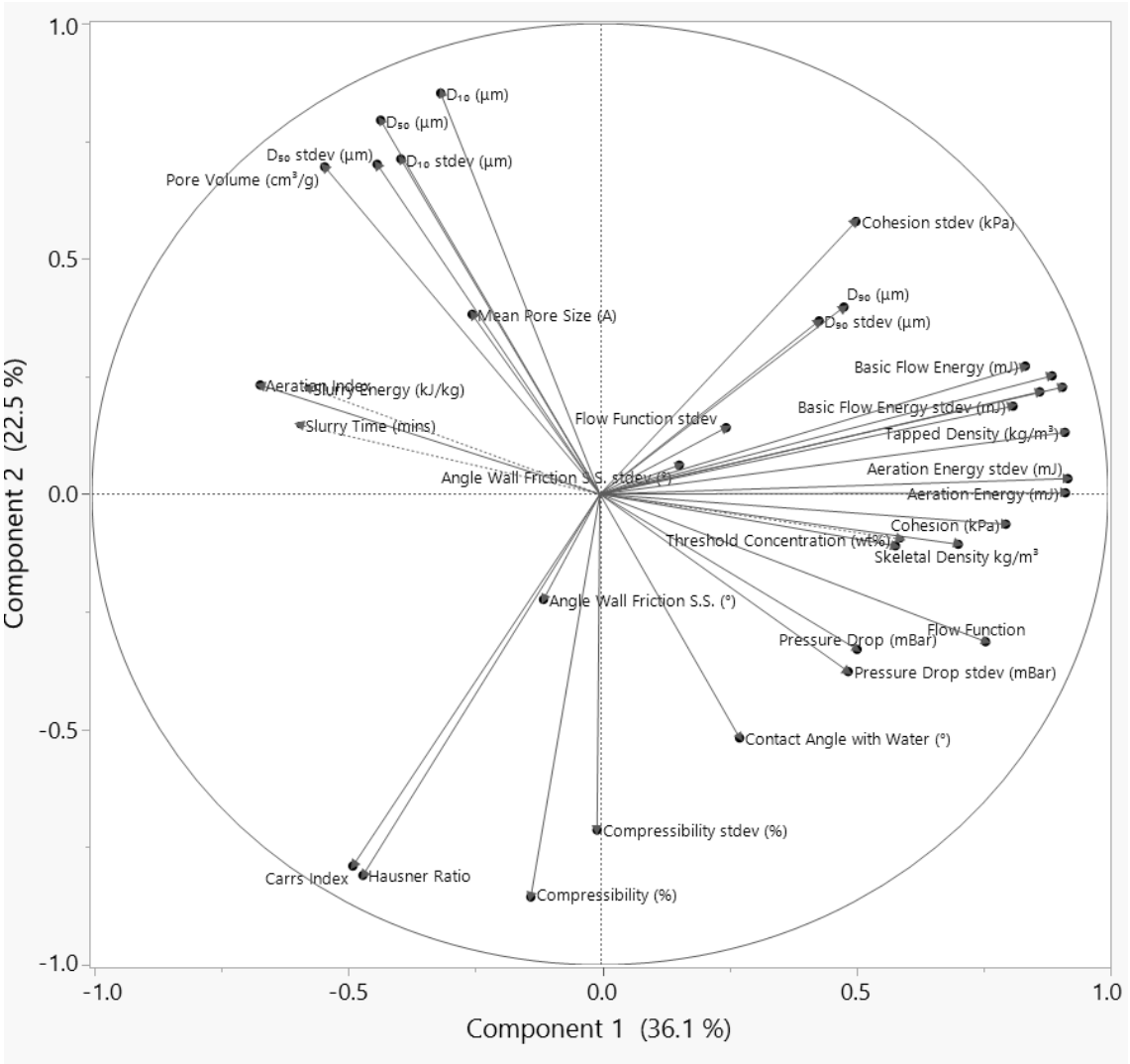

Figure 5-17: Loadings plot for first two principal components

5.4.4.3. Partial Least Squares (PLS)

Partial least squares regression modelling was applied to the entire training dataset of 13 original powders. This included 34 predictor variables, when factoring in both the mean and standard deviation values for repeats for each of the characterisation tests described above.

Initially a NIPALS PLS algorithm was carried out with two latent variables (cross-dimensional structures within the x-space that best describe the variation in the powders, as described in section 5.3.3), the number of latent variables giving the smallest RMSECV value during validation. Figure 5-18 shows the VIP scores for all variables in this initial PLS model, VIP scores of <1 are

considered insignificant within the model. The standard deviations for most predictors are unimportant in the model, this is because (as seen in Figure 5-17) they are strongly correlated with their corresponding means and so do not have additional significant contribution to the PLS models. The powder compressibility, wall friction angle with stainless steel, and Hausner ratio and Carrs Index are all also unimportant in the model. This is understandable as the powder is not in contact with a wall unless at the free liquid surface in the vessel and there is little compression of the powder during decanting and pouring onto the liquid surface.

The most significant variables in the projection include the pore volume, pressure drop test result, bulk densities, and powder cohesion. The plots in Figure 5-19 show the measured versus predicted values in terms of all three slurryability measures from this model. Slurry time and slurry threshold concentration show reasonable agreement at this stage, although there is clearly still error in the predictions. The prediction of the slurry energy does not show a strong correlation with actual measured values. In all three models the magnesia 2 powder is the least well predicted of all powders in the model. The VIP scores in Figure 5-18 can be used to inform the choice of which parameters can be removed to create a new model, with less inherent noise in the predictor dataset. This is done by rerunning the PLS NIPALS algorithm but only considering the variables with a VIP score greater than one in the original model (i.e. those larger than the blue threshold line in Figure 5-18).

X	VIP
Pore Volume (cm^3/g)	1.5178
Pressure Drop (mBar)	1.5147
Tapped Density (kg/m^3)	1.4404
Poured Density (kg/m^3)	1.3814
Pressure Drop stdev (mBar)	1.3260
Basic Flow Energy stdev (mJ)	1.2507
Aeration Energy (mJ)	1.2162
Flow Function	1.1951
Poured Density stdev (kg/m^3)	1.1806
Aeration Energy stdev (mJ)	1.1492
Tapped Density stdev (kg/m^3)	1.1260
Basic Flow Energy (mJ)	1.1182
D_{50} (µm)	1.0983
Aeration Index	1.0258
Cohesion (kPa)	1.0251
D_{90} (µm)	0.9987
Contact Angle with Water (°)	0.9654
Skeletal Density kg/m^3	0.9061
Angle Wall Friction S.S. stdev (°)	0.9051
D_{50} stdev (µm)	0.8910
D_{10} (µm)	0.8183
Flow Function stdev	0.8095
Contact Angle with Water (°) 2	0.7523
D_{90} stdev (µm)	0.7423
D_{10} stdev (µm)	0.7244
Cohesion stdev (kPa)	0.6262
Carrs Index	0.5631
Hausner Ratio	0.5166
Mean Pore Size (A)	0.4030
Compressibility stdev (%)	0.3549
Angle Wall Friction S.S. (°)	0.2218
Compressibility (%)	0.0587

Figure 5-18: Table for VIP scores for all variables in initial PLS model with two latent variables

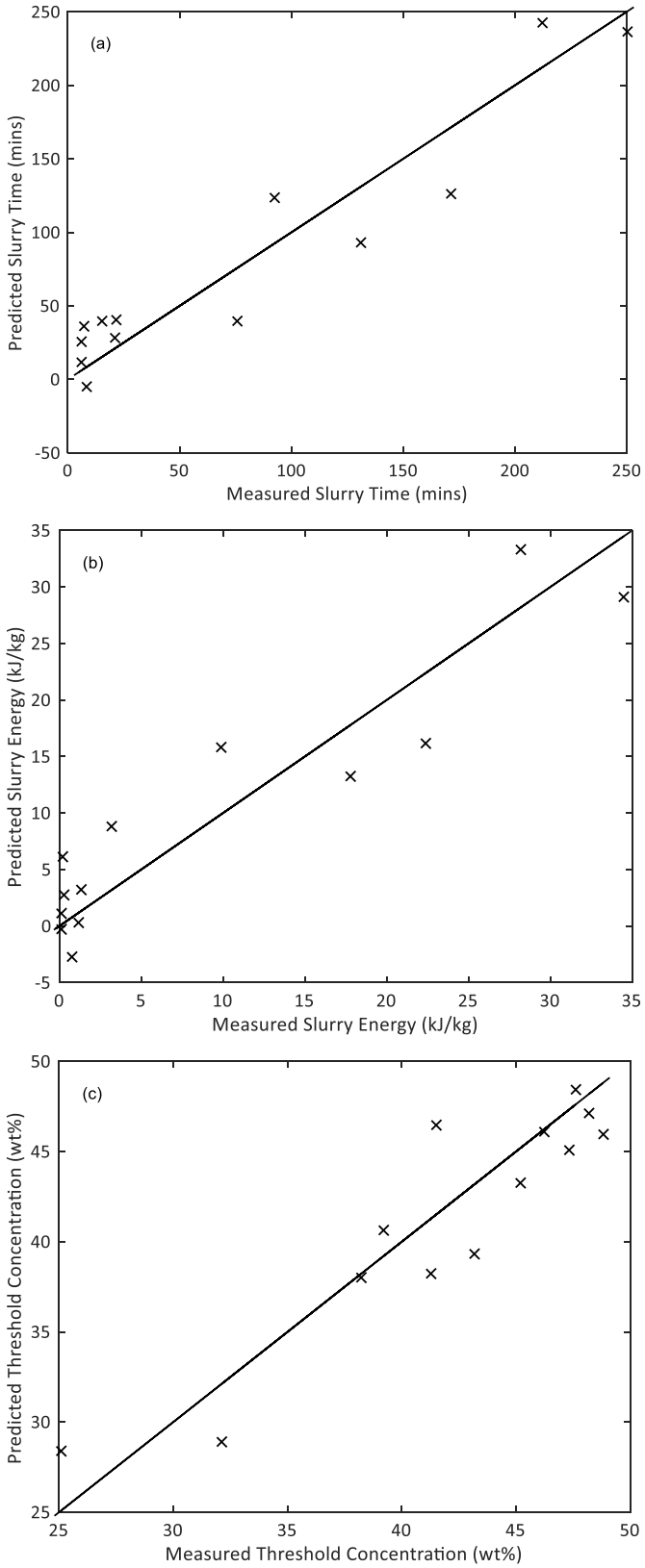

Figure 5-19: Measured vs predicted slurryability values in terms of slurry time (a), slurry energy (b), and threshold concentration (c) for initial PLS model with two latent variables

The resultant VIP scores for the new model are shown in Figure 5-20. The pore volume and pressure drop measurements remain the most significant parameters, with high importance still given to the bulk density measurements. In this new model, most of the bulk powder flow measurements, such as flow function, basic flow energy, aeration energy, and aeration index drop below the VIP significance threshold of 1.

Figure 5-21 shows the predictive performance of this new model for the three measures of slurryability. The prediction for the threshold concentration measure gives a strong performance for all powders studied. The slurry energy prediction also shows strong performance, although some of the very easiest to incorporate slurries show less strong predictions. The slurry time predictive performance is weaker than the other two. This is, again, most evident amongst the easiest to incorporate slurries, with magnesia 1 predicted as having a negative slurry time, which is obviously unrealistic. Table 5-4 shows RMSE values for both models, showing the error between measured and predicted slurryability values. As described above, the predictive performance improves when noise is removed in the second model for both the slurry energy and threshold concentration measurements. However, the slurry time predictive performance drops.

X	VIP
Pore Volume (cm^3/g)	1.1834
Pressure Drop (mBar)	1.1303
Aeration Energy (mJ)	1.0905
Tapped Density (kg/m^3)	1.0570
Pressure Drop stdev (mBar)	1.0527
Poured Density (kg/m^3)	1.0385
Cohesion (kPa)	1.0178
D_{50} (µm)	1.0134
Poured Density stdev (kg/m^3)	0.9620
Basic Flow Energy stdev (mJ)	0.9603
Aeration Energy stdev (mJ)	0.9406
Basic Flow Energy (mJ)	0.9295
Flow Function	0.9100
Tapped Density stdev (kg/m^3)	0.9047
Aeration Index	0.7231

Figure 5-20: VIP scores for all variables in second PLS model with three latent variables

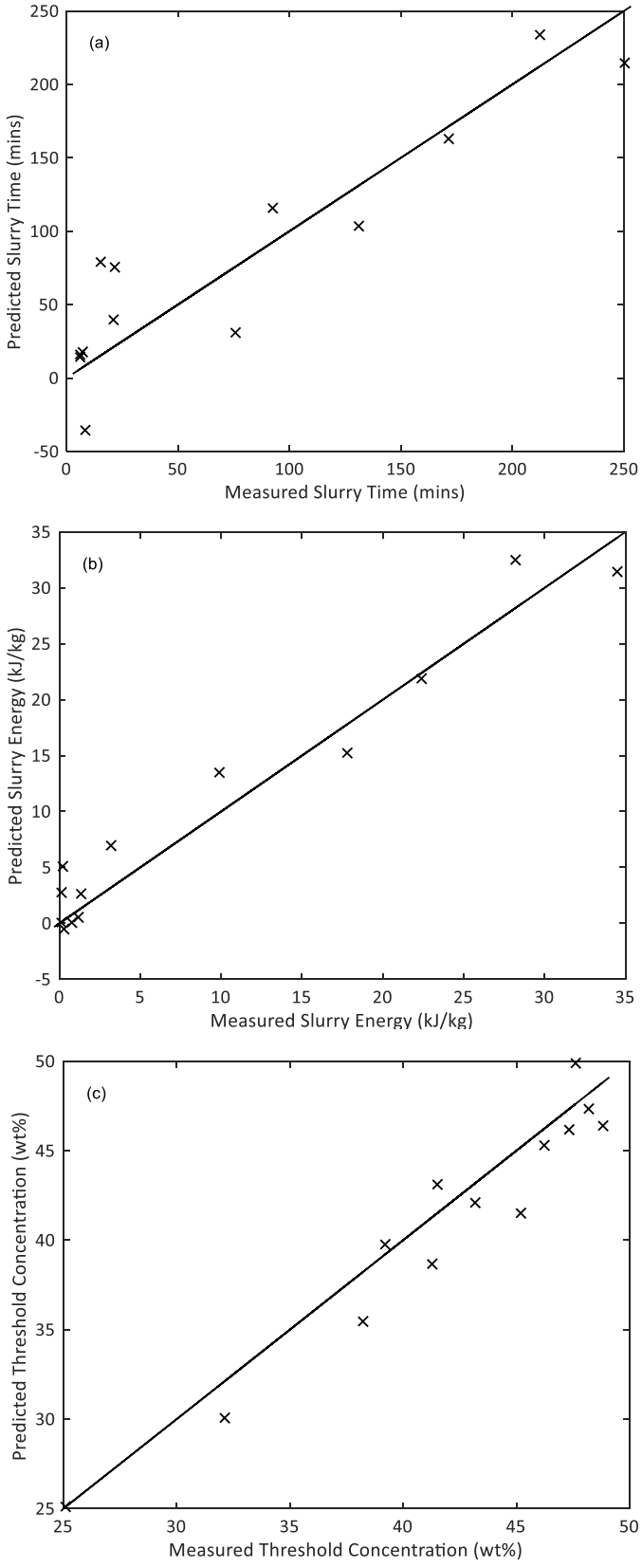

Figure 5-21: Measured vs predicted slurryability values in terms of slurry time (a), slurry energy (b), and threshold concentration (c) for second PLS model with three latent variables

Table 5-4: RMSE values for the two models

	Slurry time	Slurry energy	Threshold concentration
Initial model RMSE	26.6	4.28	2.64
Initial model r^2	0.841	0.871	0.852
Second model RMSE	33.4	2.72	1.96
Second model r^2	0.898	0.953	0.939

The VIP scores in Figure 5-18 show the key powder properties that affect how easily the powder may be incorporated. The four most important properties are the pore volume, pressure drop, aeration energy, and bulk density. Knowing this, it is possible to hypothesise some physical meaning behind why these properties are important.

As described above, the powder content is described in weight fraction as this is the easiest to measure and matches formulation specifications. However, volume concentration of the dispersed phase(s) is important in the behaviour of any multiphase system. This makes explaining the importance of the powder bulk density trivial, as powders with low bulk densities will ostensibly occupy a larger volume for the same weight content as powders with higher densities. This is clearly shown as powders with low bulk densities such as the titania, stabilised γ-alumina, and α-alumina 1 proved to be some of the hardest to incorporate powders, based on their slurryability measures shown in Table 5-2.

The significance of pore volume is also relatively simple to explain, as particles with significant porosity are likely to occupy a larger volume until the pores fully fill with liquid. This means the particle will act as a less dense particle initially. The presence of air inside the particle is also likely to increase the buoyancy force on the particle as it hits the liquid surface when initially added to the vessel. This increased buoyancy force will make it harder to draw the powder down into the fluid and incorporate it into a slurry. The presence of pores also generates the possibility of a

dynamic effect to occur, where even after the particles are incorporated, whilst the pores are still filling with liquid they occupy a larger volume in the slurry. This gives a temporarily higher solid phase volume concentration, increasing the slurry apparent viscosity and making it more difficult to add additional powder until the air inside the pores has been displaced. This effect is described in Chapter 2.

The importance of the aeration energy and pressure drop measurements in the models is slightly harder to explain physically. However, as the powder is poured onto the liquid surface, it is possible that less aeratable powders have a tendency to cluster as they are poured and aerated. The consequence of this is that as the powder hits the liquid surface and begins to wet, clustered particles are more likely to form semi-wet agglomerates on the free surface. In Chapter 1 it was shown that formation of large agglomerates on the free surface was one of the main hindrances to increasing the solid content of a concentrated slurry. Figure 5-17 shows that the pressure drop measurements are strongly anti-correlated with D_{10} and D_{50} values. The Kozeny-Carman equation indicates pressure drop is dominated by bed voidage and specific surface area. Wide size distributions will lead to lower voidages while increasing amounts of fines will lead to higher surface area; both of which contribute to an increase in pressure drop. It is apparent therefore that the presence of fine particles has a strong negative impact on the slurryability of a powder as the extra surface they provide increases the complexity of the slurry rheology. The presence of these fine particles may well be seen more effectively by measurements of low permeability than in volume weighted particle size distribution (light scattering-based) measurements, explaining why pressure drop and not D_{10} is significant in the models.

5.4.4.4. Model Validation

Another mixed oxide powder and a zeolite material not included in the original training set of 13 powders were studied to assess the applicability of this PLS model beyond outside of the original

data set and provide validation of the PLS model. The results from measurements of the identified key parameters for these powders are shown in Table 5-5.

Table 5-5: Relevant properties of the two validation powders studied

Property	Zeolite 1	Mixed oxide 3
D_{50} (µm)	33.2	60.4
Poured Density (kg m^{-3})	443.2	943.5
Tapped Density (kg m^{-3})	394.6	799.6
Cohesion (kPa)	0.121	0.095
Aeration Energy (mJ)	4.2	17.3
Pressure Drop (mBar)	10.3	29.6
Pressure Drop stdev (mBar)	3.54	7.21
Pore Volume (cm^3 g^{-1})	0.842	0.302

Figure 5-22 shows the plots from Figure 5-21 with these two validation powders added. In absolute terms all three slurryability metrics are well predicted, lying close to the measured = predicted line. Table 5-6 shows absolute and percentage error for both validation powders for all three metrics. The mixed oxide 1 powder showed high percentage error for both slurry time and energy, although this is because it is amongst the easiest to incorporate powders, where slurry time and energy requirements are low and so small absolute errors give large percentage errors. The threshold concentration slurryability is well predicted for both powders, with an error of less than ±10 %.

Table 5-6: Absolute and percentage error in predictions for the two validation powders

Powder	Slurry time error		Slurry energy error		Threshold concentration error	
	Absolute (mins)	Percentage (%)	Absolute (kJ kg^{-1})	Percentage (%)	Absolute (wt%)	Percentage (%)
Mixed oxide 1	11.3	77.3	0.7	99.2	2.3	5.3
Zeolite 1	-27.3	-16.3	-2.4	-12.4	2.9	-8.6

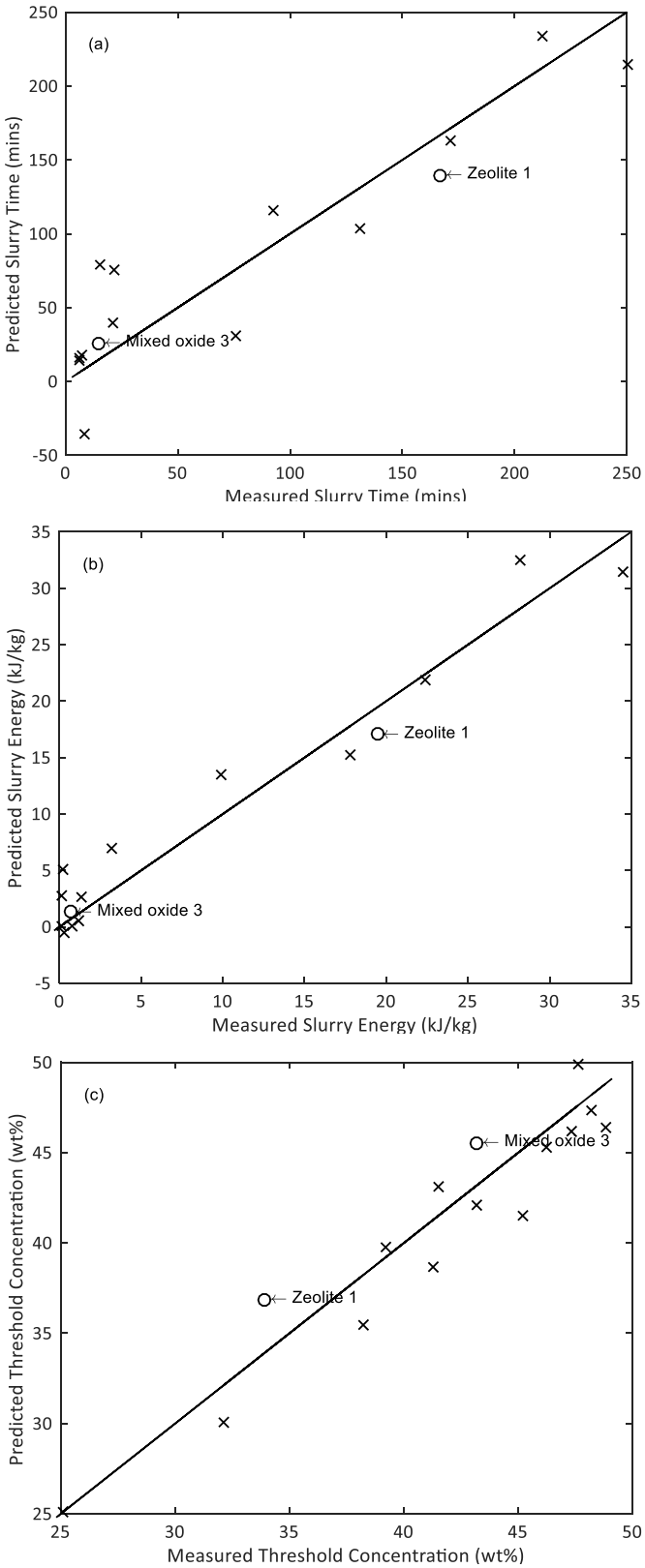

Figure 5-22: *Measured vs predicted slurryability values for two validation powders in terms of slurry time (a), slurry energy (b), and threshold concentration (c) for second PLS model with three latent variables*

5.5. Conclusions

This study has used multivariate statistical modelling techniques to elucidate the most significant powder properties determining how easily a given powder may be incorporated into a high solid content slurry in a stirred vessel. The ease with which a powder is incorporated into a slurry is defined here as the *slurryability* of the powder and is measured in three distinct ways: firstly, the time required to achieve a 50 wt% solid content slurry in a fixed vessel geometry configuration, secondly the energy required to achieve the same. The third metric considered is a threshold slurry concentration at which it requires more than 1 kJ to increase the solid content by a further 1 % in the vessel studied.

Partial least squares models are built which predict the slurryability of a powder based on its key properties. The most significant properties, based on variable importance in projection scores, are the particle pore volume, the pressure drop result of the Freeman FT4 powder rheometer permeability test, the powder aeration energy, again measured on the Freeman FT4 powder rheometer, powder tapped and poured density, and the d_{50} particle size of the powder. By measuring these six properties it is shown to be possible to predict the slurryability of two validation powders, not present in the original training dataset, to an error in threshold concentration of ±10 %.

6.

Industrial Case Study – Development of an Incipient Wetness Impregnation Process for Catalyst Preparation

This Chapter describes the study of the applicability and optimisation of three different mixers for their use in incipient wetness impregnation of aqueous solutions into dry zeolite powder. This is a new process step intended to add catalyst to the support prior to its incorporation into washcoat slurry.

The work described in this Chapter uses a holistic quality by design approach to probe the design space of both a ribbon and a double bowl blender powder mixers to find optimal operating windows to maximise both product yield and homogeneity. A d-optimal orthogonally designed experiment is used for both mixers to maximise the amount of information from a minimal number of trials. Multivariate statistics are used to find the key operating parameters for each mixer. A Vrieco-Nauta mixer is also studied, although in less detail.

The Nauta mixer showed the highest possible yields, and the ribbon blender the best homogeneities of the three mixers. The double bowl blender showed both the lowest yields and lowest homogeneities. It also showed the highest tendency to severely suffer in performance when poor process configurations were used.

Chapter Preface

This Chapter is based on work done as part of a group project within Johnson Matthey Technology Centre. The project team consisted of Thomas Wood, Michele Marigo (JMTC), Stephanie Turnbull (JMTC), Isabel Castro (JMTC), and Giuseppe Raso (JMTC & University of Edinburgh).

All experiments on the double down blender and ribbon blender were carried out by Isabel Castro. Those on the Nauta were done by Thomas Wood. The experimental designs and data analysis was all performed by Thomas and Stephanie. Development of the methodology using image analysis to determine mixing performance was done by Thomas Wood.

6.1. Introduction and Background

Whereas previous Chapters have focussed on adding powder to liquid to prepare a slurry, this Chapter focusses on incipient wetness impregnation (IWI) of dry powder with a solution. Commercially this process is designed to add catalyst to the support material before it is incorporated into slurry, as shown in Figure 6-1.

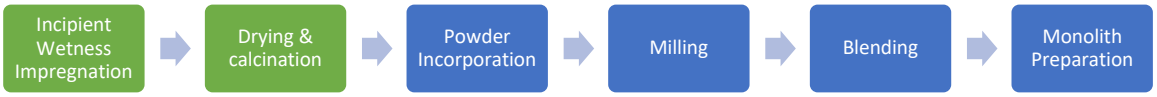

Figure 6-1: Process flow diagram for catalyst preparation with incipient wetness impregnation steps added (green)

This has been shown within Johnson Matthey to improve precious metal distribution within the catalyst compared to the traditional production process described in Chapter 1. This in turn produces emission control catalyst products with higher activity and selectivity.

6.1.1. Project Objectives

The three main objectives of this project were:

- Test and compare multiple equipment choices for incipient wetness impregnation to find the best available in terms of product yield, homogeneity, and lump size distribution.
- Develop optimal operating conditions for each piece of equipment studied using a dye solution as a mimic.
- Use understanding from optimisation studies to highlight critical process parameters for the incipient wetness impregnation process.

This Chapter describes the optimization of three separate pilot-scale convective powder mixers for incipient wetness impregnation. The experimental work for each mixer is described in turn before a final comparison of each of the three mixers is made.

6.1.2. Incipient Wetness Impregnation

Industrial metal based catalysts generally include a high surface area support material such as alumina, silica, or zeolite, onto which the active metal is placed. There are three main methods to achieve this: incipient wetness impregnation, ion exchange, and deposition techniques (Chang *et al.* 2003). Thus far focus has been on catalysts prepared by deposition. This Chapter focuses on optimising and scaling up an industrial process for the incipient wetness impregnation of palladium nitrate onto zeolite.

Preparation of IWI based catalysts is generally seen in the laboratory as one of the simplest catalyst preparation techniques (Bowker *et al.* 2007). This is because the general process is relatively simple, with little chemistry required. A liquid containing the active metal catalyst, often a metal salt solution, is sprayed onto a powdered support material to around a volume concentration equal to the porous volume of the support. The resultant impregnated powder is then dried and calcined to attach the metal to the support material (Munnik *et al.* 2015).

6.1.3. Industrial Scale Incipient Wetness Impregnation

At scales larger than the laboratory, IWI tends to be performed in large scale powder mixers, into which the catalyst salt is sprayed onto a moving powder bed. Powder mixers can be divided into two types: convective blenders and tumbling blenders. While convective blenders involve the use of a paddle, blade, or screw which stirs the powder inside an immobile vessel, tumbling blenders rely upon the action of gravity to cause the powder to cascade within a rotating vessel (Bridgwater 1976). This study investigates three convective blenders, which exhibit variations in both blade and bowl geometries.

Powder materials that have an average size of less than 20 µm in diameter are highly cohesive, and tend to form agglomerates because of strong van der Waals forces (Vanarase 2011). Cohesion in powder/granular systems is also caused by the capillary forces that exist due to the

presence of moisture in the system. Powders that tend to agglomerate are typically mixed in a high shear rate environment so that the agglomerates are de-lumped and a homogeneous mixture is created (Vanarase *et al.* 2013).

The disadvantages of convective mixers are that they often permit stagnant regions to form which lead to a variability in the concentration of the product. Also, they may allow pinch points, which are narrow spaces between the blade and the vessel walls that can cause the attrition of fragile particles. The pinch points may be beneficial when dealing with hard cohesive powders as the increased shear conditions around the blade are beneficial for disrupting agglomerates (Muzzio *et al.* 2008).

A number of research studies have been conducted considering the operating window of convective mixers for dry powders. For example (Muzzio *et al.* 2008; Yeow *et al.* 2011; Halidan *et al.* 2018) have all studied the operating window of ribbon mixers for a variety of dry powder systems. These studies show contrary results: with (Yeow *et al.* 2011) showing that better mixing is obtained at high rotation speeds and mixing time, whereas (Halidan *et al.* 2018) showed that mixing performance increased with impeller speed up to a point, beyond which it reduced with increasing impeller speed, an observation also seen by (Musha *et al.* 2013). They also found that mixing for a prolonged period of time decreased mixing performance, as segregation of the powder due to differing particle size occurs.

The lack of consensus between many of the studies considering the optimization of powder mixing processes demonstrates the complexity of the problem. Further complexity is added during the IWI process by the addition of another phase in the form of the liquid spray. This is partly shown by the comparisons between cohesive and non-cohesive powder mixing, where differing operating regimes are required depending on the cohesiveness of the powder (Hersey 1975; Carter *et al.* 1992). Increasing moisture content has been shown to affect the flow

properties of powders, increasing their cohesiveness (Sandler *et al.* 2010). However, addition of a liquid phase adds further complications, for example, porous powders have a tendency to swell on wetting, increasing their size, and so reducing the density of the bulk powder bed during mixing (Wangler and Kohlus 2017). This is significant as powder bulk density has been shown to strongly affect the behaviour and mixing performance of a powder in convective mixing processes (Vanarase *et al.* 2013). This means it is possible that during an IWI process changes to the powder properties caused by the increase in moisture concentration will cause the optimum operating window to shift throughout the operation of the process.

The discrete element method (DEM) is being used increasingly in the modelling of systems such as convective powder mixing for geometry optimisation. (Chandratilleke *et al.* 2018) used DEM studies to demonstrate that increasing the number of spokes inside a ribbon mixer increases mixing performance at the expense of the magnitude of contact forces between the blades and the powder. This means it is ideal to have many spokes for powders with low cohesiveness and less spokes as the powders being mixed become more cohesive, where higher forces are required to break apart the agglomerates that form. DEM has also been used to study flow patterns within powder mixers, with studies considering how powder moves in bladed paddle mixers (Remy *et al.* 2009), dry granulation pharmaceutical processes (Ketterhagen *et al.* 2009), V-shaped tumbling mixers (Lemieux *et al.* 2008), and ribbon mixers (Basinskas and Sakai 2016) amongst others. All authors of these studies comment how significant both powder property variables, such as density and cohesiveness, and process parameters such as fill level and rotation speed, significantly affect flow patterns and mixing behavior inside these devices.

6.1.4. Image Analysis

Optical visualisation techniques are frequently used in engineering applications to monitor flow patterns, mixing performance, and behaviour at phase boundaries. Visualisation techniques

utilise a visible difference that can be tracked to monitor variations within the process. Possibly the most basic example of this is the movement of a stick as it flows downstream on the surface of a river (Milne 1928).

There are numerous approaches to optical visualisation, but all are based around the principle of taking images of the system where there is variation in the visible light range that can be seen by the camera. These images are then processed based on the pixel values within the image to allow numerical quantification and analysis of the process being measured (Mewes 2015). How the variation in the visible light range is achieved is highly dependent on the system being studied.

The behaviour at fluid/solid boundaries can be measured in wind and water tunnels through use of surface films which are used to track mean shear stress lines on the surface. In this application the surface fluid must have a yield stress less than the shear stress imparted by the fluid flowing over it, but higher than the effect of gravity. This results in the fluid moving to track the fluid whilst in motion, but then remaining in the resulting pattern once the fluid flow is ceased (Maltby *et al.* 1962; Lu 2010). Generally the surface fluid consists of an oil containing suspended solids, which leave streaks as the oil flows, showing traces of the fluid flow over the surface which can be analysed (Benson 2009). The specific oil/solid mixture used is highly variable with different research groups having their own preferred recipe (J Pierce *et al.* 2010). Examples of this approach include a 10 % zinc oxide in 'Crisco' oil used to measure flow patterns over a plexiglass plate (Hunt *et al.* 1978), This technique has even been applied outside of wind/water tunnels on in flight vehicles (Meyer 1985).

Another optical visualisation approach for measuring fluid flow patterns involves use of tracer particles to track movement of the fluid in a 2D plane. By taking a sequence of images in time, with a known time step between images, it is possible to track particle, and so fluid, motion (Raffel *et al.* 2007; Adrian and Westerweel 2011). This technique is known as particle image

velocimetry (PIV). PIV has found widespread use for the measurement of flow behaviour in process operations from flow inside household appliances (Schröder and Willert 2008), stirred tanks (Sharp and Adrian 2001), high shear industrial mixers (Espinoza *et al.* 2018), to blood flows in microchannels (Pitts and Fenech 2013). Some drawbacks to PIV are that it requires mostly transparent fluids to allow visualisation, so mimic fluids are often used to estimate the performance of real industrial fluids, which tend to be opaque (Yousif *et al.* 2009). The choice of size, shape, and concentration of tracer particle is also key to getting good PIV results, as there needs to be sufficient concentration of particles per unit volume (based upon the resolution of the PIV apparatus) to give good results, whilst not interfering with one another due to collisions or changing the viscosity of the continuous phase (Einstein 1906). The particles must also trace the motion of the fluid as closely as possible, and so require a similar density to the fluid (Melling 1997).

Mixing performance of solids and fluids can be measured by optical visualisation where there is a significant colour or appearance difference between the phases being considered. There are numerous examples of this concept. For example, fast acting decolourisation using an acid-base indicator reaction can be used to monitor mixing time in a stirred vessel (Cabaret *et al.* 2007). The premise behind this is that the absorption (or fluorescence) of light by a chemical species is directly proportional to the concentration of that species according to the Beer-Lambert law (Svanberg 2003). In this study the reaction removes the coloured species and so a mixing time can be determined as the time required for all colour to be removed from the vessel.

Quantification of mixing is often a non-trivial problem, with mixing performance depending on both the intensity and scale of segregation within a system. These concepts can be measured using image processing techniques by considering the pixel values within the image. 8-bit images are captured in greyscale, with each pixel given a value of 0 – 255 based on its brightness, which

correlates to species concentration according to the Beer-Lambert law (Svanberg 2003). The intensity of segregation can be measured using descriptive statistics of the pixel values throughout the image. The coefficient of variance is a widely used metric to describe mixing performance, given by:

$$CoV = \frac{\sigma}{\bar{G}} \tag{22}$$

where the standard deviation is defined as as:

$$\sigma = \sqrt{\frac{1}{N-1}\sum_{i=1}^{N}(G_i - \bar{G})^2} \tag{23}$$

where N is the number of pixels considered, $\bar{G}$ is the greyscale value at perfect mixing, and G_i is the greyscale value of pixel i (Harnby *et al.* 1997). One issue that can arrive considering only the intensity of segregation is in cases where there is little or no diffusion of species but the scale of segregation between two species is decreased, as shown in Figure 6-2 (Kukukova *et al.* 2011).

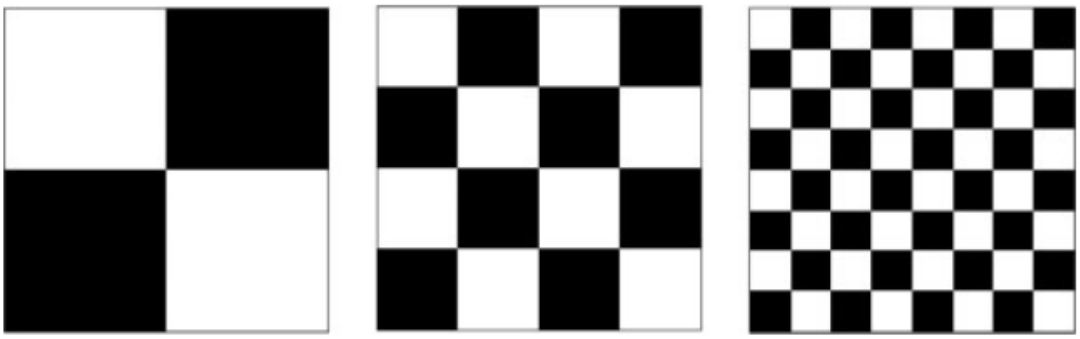

Figure 6-2: Decreasing scale of segregation with no change in intensity (Kukukova et al., 2011)

This concept has been applied to particulate solid systems by a number of researchers. The coefficient of variance was used to describe the level of mixing of two different coloured powders at the outlet of a continuous mixer in real time using on-line image analysis of greyscale images (Ammarcha *et al.* 2017). Koc et al. (2007) simply monitored the modal greyscale pixel value over

time in images of powder inside a mixing process and took the mixing time to be the time required for the modal greyscale pixel value to cease changing with time. (Realpe and Velazquez 2003) considered the mean greyscale value and frequency of greyscale pixel values of greyscale images. These were fed to multivariate models that were validated using near infra-red spectroscopy. All of these authors found optical visualisation an adequate technique to measure the mixing of powders in unit operations using the mean and frequency of pixel values in greyscale images.

Working with greyscale images is unquestionably simpler than working with full colour images, dealing with a two dimensional dataset, rather than a three-dimensional dataset obviously simplifying the situation. However, when images are recorded in colour there is a risk of loss of information during the conversion. This is especially true when studying colour change, which may not be apparent when dealing in greyscale alone (Kanan and Cottrell 2012). The most common format for colour information to be stored in images is in red, green, and blue (RGB) format where each pixel in an image contains three byte values of 0-255 for each of the red, green, and blue colour spaces. This gives a total number of combinations of 16.7 million different colours (Hirsch 2004). Other colour formats exist, with HunterLab LAB (Hunter 1958) and CIElab L*a*b* (Ansorena *et al.* 1997) being two of the most common. These colour formats are intended to give a wide three dimensional space to describe the difference in colours that the human eye can see, with a linear distance in L*a*b* describing a fixed 'difference' in appearance. Conversion to either of these colour spaces from RGB is possible with the use of calibration charts, where known colours in L*a*b* space are mapped to RGB values in captured images. However, any calibration is only valid under very specific lighting conditions (Lan *et al.* 2011).

6.2. Methods and Materials

6.2.1. Materials

The industrial product studied in this project is an aqueous palladium nitrate solution impregnated onto zeolite AZM9 powder at a ratio of 0.35 g solution per g dry powder. With a density of 1.12 SG this corresponds to a volume ratio of 0.3125 mL solution per g powder. Due to the cost of palladium a mimic fluid of aqueous rhodamine 6G was used in place of the palladium nitrate solution, this is a bright pink fluid, used to give good contrast between wet and non-wet powder. A similar approach has been used to study the mechanics of spray driers, with rhodamine used as a dye to allow measurement with a spectrophotometer (Francia *et al.* 2015).

The pore volume of AZM9, measured by nitrogen physisorption, was found to be 0.3 mL g^{-1}, therefore the industrial recipe calls for liquid addition of 106 % of the pore volume. When using the mimic fluid, with a density of 1 SG, 0.3125 mL solution was added per g of powder to maintain this ratio.

The rhodamine dye solution was prepared by dissolving 0.5 g of rhodamine 6G per litre of deionised water. In all mixers this solution was sprayed onto the powder surface whilst the powder was agitated.

6.2.2. Mixers

Three different mixers were compared: a double bowl blender (DBB) (Forberg, Norway), a ribbon blender (RB) (WAM Group, Italy), and a Vrieco-Nauta mixer (Nauta) (Hosokawa, Netherlands). Both the DBB and RB were available for study at JMTC and so detailed experimental designs were possible. However, no Nauta was available at JMTC so trials were run at the vendor's site, limiting the extent to which detailed trials could be run.

Each mixer studied allowed different process variables to be controlled for optimisation studies. The independent variables used as process parameters, controlled variables kept constant, and disturbance variables measured for each type of mixer are described in the design of experiments section below.

6.2.3. Nozzles

For the IWI process, a spray nozzle is used to deliver the impregnating liquid into the mixer and is a key selection variable. Selection of an appropriate nozzle depends on the application, and requires consideration of target droplet size, boundary operating conditions, desired spray pattern, spray volume, and nozzle discharge, amongst others. The most commonly used nozzle spray patterns include: fan, hollow cone and full-cone.

Fan nozzles generate a tapered-edge, flat-fan spray pattern. These nozzles are typically the first choice for washing a product on a conveyor or rinsing a cake on filter belts. Many flat fan nozzle designs have tapered or parabolic distribution. It means that more of the spray is concentrated in the middle of the fan than the edges (Figure 6-3), this is deliberate when sprays are overlapped (Lechler 2017).

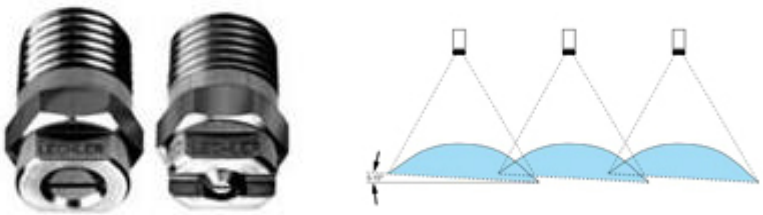

Figure 6-3: Fan nozzles from Lechler, overlapped layout

Spray-drop size an important factor affecting the spraying efficiency, from here it is important to assess its influence on incipient wetness impregnation. Fine droplets provide better coverage; however, they are also more prone to settling on the walls of the equipment, which can cause powder to adhere to the wall and become stuck, reducing product yield. A droplet size spectrum

is provided by BETE, where misting and fog nozzles are capable of generating droplet sizes between 1 to 100 µm (BETE 2017). BETE produce a range of nozzles, denoted “PJ”, and shown in Figure 6-4. Flow rates can be adjusted by changing the pressure applied to the nozzle or increasing/decreasing the nozzle aperture.

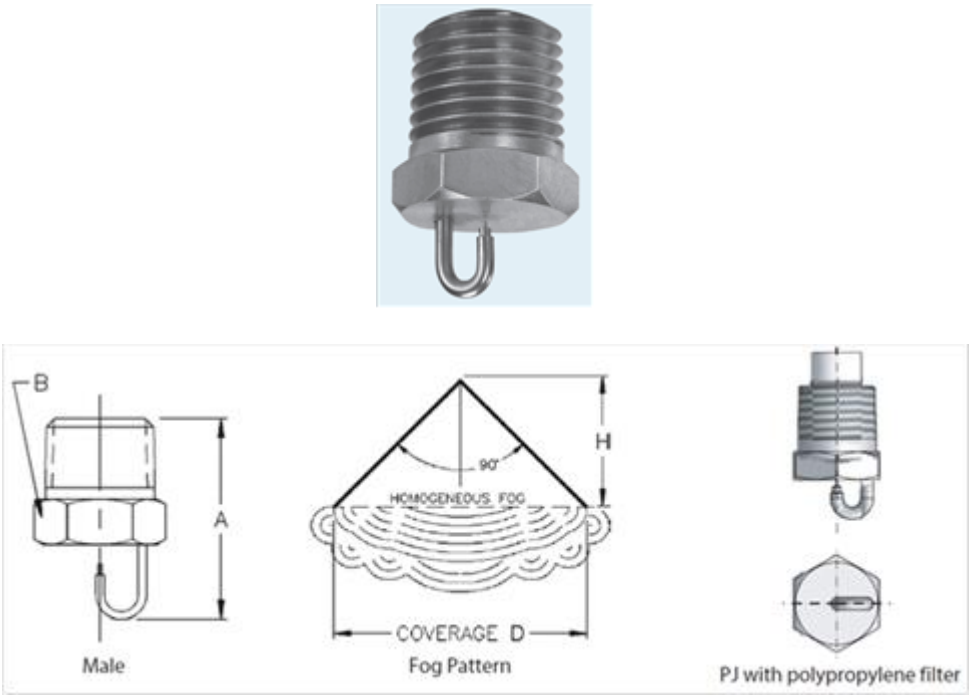

Figure 6-4: BETE - PJ nozzle 90^{o} coverage

Three PJ nozzles were selected for this study; PJ6, PJ10, and PJ20, specifications of the BETE PJ nozzles are shown in Figure 6-5 (BETE 2018).

Male Pipe Size	Nozzle Number	K Factor	GALLONS PER MINUTE @ PSI								Approx. Orifice Dia. (in.)	Approx. Coverage (inches) D	Approx. Spray Height H (in.)	Pipe Size	Approx. Dim. (in.) A	Approx. Dim. (in.) B	Wt. (oz.) Metal
			10 PSI	30 PSI	40 PSI	50 PSI	60 PSI	80 PSI	100 PSI	200 PSI	400 PSI							
1/8 OR	PJ6	0.00095				0.006	0.007	0.008	0.010	0.013	0.019	0.006	10	5	1/8	0.75	0.44	0.25
	PJ8	0.00180				0.013	0.014	0.016	0.018	0.025	0.036	0.008	10	5				
	PJ10	0.00269			**0.017**	0.019	0.021	0.024	0.027	0.038	0.054	0.010	10	5				
	PJ12	0.00364			**0.023**	0.026	0.028	0.033	0.036	0.051	0.073	0.012	10	5				
	PJ15	0.00585		0.032	**0.037**	0.041	0.045	0.052	0.059	0.083	0.117	0.015	10	5				
	PJ20	0.0106	0.034	0.058	**0.067**	0.075	0.082	0.095	0.11	0.15	0.21	0.020	12	6	1/4	0.97	0.56	
	PJ24	0.0158	0.050	0.087	**0.10**	0.11	0.12	0.14	0.16	0.22	0.32	0.024	16	8				
	PJ28	0.0206	0.065	0.11	**0.13**	0.15	0.16	0.18	0.21	0.29	0.41	0.028	18	9				
1/4	PJ32	0.0285	0.090	0.16	**0.18**	0.20	0.22	0.25	0.28	0.40	0.57	0.032	22	11				
	PJ40	0.0443	0.14	0.24	**0.28**	0.31	0.34	0.40	0.44	0.63	0.89	0.040	24	12				

Figure 6-5: PJ nozzle specifications (BETE, 2018)

6.2.4. Experimental Procedure

For all mixers the same experimental procedure was followed. Initially the mixer was filled to the desired fill level. This was done by measuring the required mass of powder to give the desired fill volume. The density conversion was based on the poured density of the zeolite powder of 450 kg m^{-3}, the same zeolite powder as used for slurryability validation trials in Chapter 4. The desired volume of pre-prepared rhodamine dye solution was measured into the liquid spray chamber for the mixer being studied. Both the DBB and RB had built in spray systems. For the Nauta a measuring cylinder was used. For the DBB and RB mixers the nozzle was positioned at the desired study height at this point.

To start the experiment the mixer was switched on at the desired rotation speed for three minutes prior to liquid addition to stabilise the system and remove any processing history from the powder. The liquid addition was then switched on and allowed to run for the specified time and flowrate for each experimental trial. The time required to add the liquid was measured in case it was different to the calculated time based on calibrated flowrate. This was important as occasionally the liquid addition system tended to partially block, increasing the addition time. This was more frequent for the DBB.

Following the final addition of the powder the mixer was run for five further minutes before the outlet was opened. After opening the outlet product was collected in a large vessel for five minutes as the mixer emptied with the mixer still rotating. Five minutes was generally longer than required for the product to flow out of the mixer but allowed a fixed time, universal across all trials, in case some powder stuck to moving parts was recovered in this time.

The collected product was then analysed for yield, homogeneity, and lumps as described in the output measurements section below.

6.2.5. Output Measurements

6.2.5.1. Flowable yield

The most significant critical to quality attribute highlighted for an industrial IWI process is the recovery of material. The high value of the raw materials in catalyst manufacture mean that any residual material left in mixers or other process equipment following manufacture adds significantly to the operating costs of that process. Therefore, the key dependent variable for optimisation to consider is the yield of flowable product, i.e. the ratio of product that freely flows from the mixer with no operator intervention (henceforth referred to as flowable yield). For all mixers studied this was simply the mass of powder recoverable after spraying with liquid when the mixer outlet was opened and agitation continued until no further powder flowed from the mixer. The flowable yield was calculated as:

$$Yield\ (\%) = \frac{M_{out}}{M_{in}} * 100 \qquad (24)$$

where M is the total mass (powder and liquid) added to or removed from the mixer during the course of the experiment

6.2.5.2. Homogeneity

A second critical to quality attribute of any industrial IWI process is the homogeneity of the final impregnated powder. As the liquid sprayed was a distinctive colour (pink versus the original white powder) optical visualisation through image analysis was used to give a measure of the homogeneity of the mixer product.

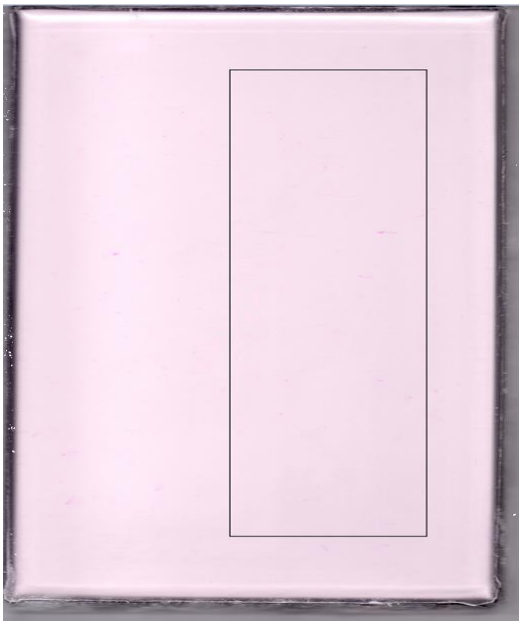

Figure 6-6: Example image from scanner demonstrating the interrogation area analysed by the MATLAB script

Images were taken as part of the DoE using a flatbed document scanner and a clear Perspex sample trough in which some of the flowable mixer product was placed. This provided a very constant and reliable light source on a prepared perfectly flat sample of powder bed. These images were then read into MATLAB to be analysed numerically based on pixel values throughout the image.

Initial observations of the image showed a constant issue with reflection in the same section of every image taken. This is likely to be the effect of external lighting as it is on the side of the scanned image facing the outside of the scanner. This is shown on the left-hand side of an example image in Figure 6-6. To overcome this problem, the script was written to only interrogate the right hand side of the images, and also cropped to well inside the edges of the bed to avoid effects from the container edges.

6.2.5.2.1. Analysis Approach

Two approaches were used to assess the homogeneity within the images. The first approach was simply to consider the spread of pixel values within individual images, as shown in Figure 6-7. This

can be expressed numerically as the standard deviation or coefficient of variance (CoV) within each image in all three of red, green, and blue dimensions.

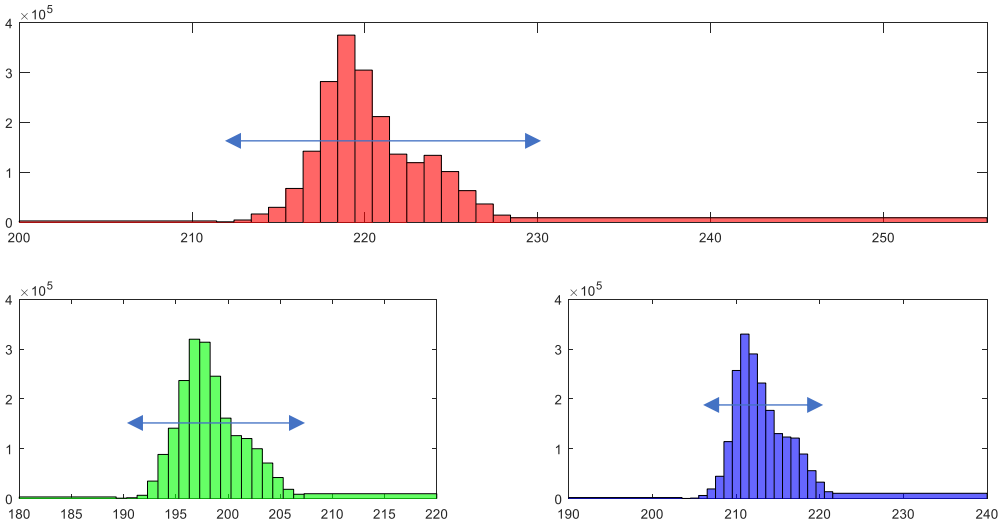

Figure 6-7: Example image broken down into red, green, and blue pixel value probability density functions

CoV is calculated as:

$$CoV = \frac{\sigma}{\bar{G}} \tag{25}$$

$$\sigma = \sqrt{\frac{1}{N-1}\sum_{i=1}^{N}(G_i - \bar{G})^2} \tag{26}$$

where N is the number of pixels interrogated in the image and G is the value of an individual pixel in each colour domain. This was also performed for greyscale images where conversion from RGB to grayscale was performed using the MATLAB command rgb2gray.

The second approach aimed to use calibration information to find pixel values corresponding to the concentration of dye according to the Beer-Lambert law. This calibration would then be used to predict a 'perfectly mixed' pixel value within an image. Thresholds can then be set above and

below this value, outside of which that pixel is deemed unmixed, whereas if the value falls inside these thresholds it is mixed. This is demonstrated for a single probability density function (PDF) in Figure 6-9. Unfortunately, the different batches of powder used proved to be different initial colours, as shown in Figure 6-8, and so a universal calibration was not possible. Therefore, the image mean was used as the central well mixed pixel value for each image, as successfully demonstrated for powder mixing by (Realpe and Velazquez 2003).

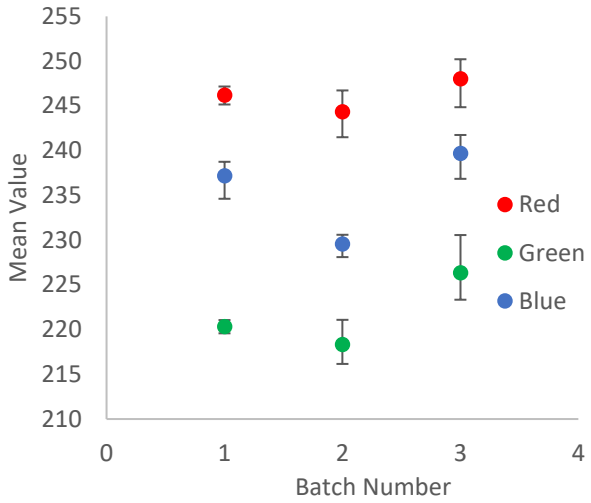

Figure 6-8: Comparison of mean image red, green and blue pixel values against the sample batch number

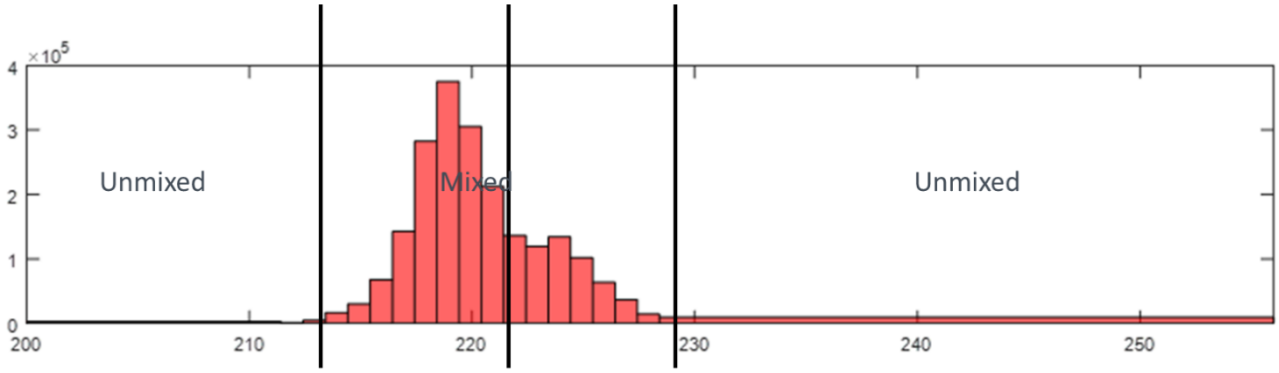

Figure 6-9: Example of thresholding used in image analysis

Anything unmixed is then given the pixel value 1 and anything mixed the value 0. This is done for all three colour dimensions, which are then summed and any non-zero pixel is set to the value 1.

A new image is then created where 0 = black and 1 = white. An example is shown right in Figure 6-10.

A homogeneity performance is then calculated as:

$$Homogeneity\ (\%) = \frac{\#\ of\ black\ pixels}{Total\ number\ of\ pixels} * 100 \qquad (27)$$

Figure 6-10: Example thresholded image

6.2.5.3. Lump Size

Subsequent process stages after IWI in the preparation of catalysts required lump free powder as an inlet. This meant that production of large, hard lumps during the IWI process would cause problems downstream. Hard lumps were defined as any that would not break during a gentle hand sieving action. Therefore, to measure the mass of lumps formed, 1.5 kg of the flowable product was passed through 3.35 mm and 1.17 mm sieves, agitated gently by hand. The mass of powder remaining in each sieve following this process was recorded, with minimal powder the target optimisation criterion.

6.2.6. Design of Experiments

Traditionally, experiments and simulations are often carried out using a "one-at-a-time" type approach, whereby one parameter is varied and the others are kept constant to establish the effect of that parameter. Not only is this very time and resource consuming due to the increased number of experiments, it also does not completely cover the experimental space. This results in a sub-optimal solution and lack of information regarding interactions between the different parameters.

The design of experiments (DoE) approach covers all of the experimental space using a minimum number of experimental points, maximising orthogonal variance (Figure 6-11), and thus producing a robust dataset for multivariate analysis. This in turn allows assessment of interactions between parameters and their effects on the experimental output.

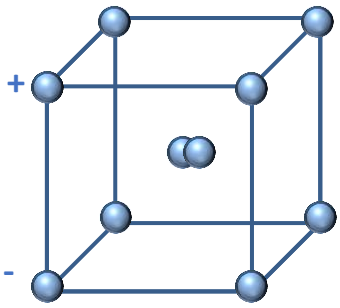

Figure 6-11: Orthogonal design of experiments

Therefore, a DoE approach can be used to produce a relatively small set of trials to fully "map" the experimental space and understand how the parameters interact with each other.

One of the most familiar designs is the factorial design, whereby all variables are altered at often 2 different levels in all possible combinations, or a subset of these combinations, altering many variables at once. This allows evaluation of all of the variables, as well as the interactions between them, but traditional factorial designs can often yield a high number of experiments.

Fractional factorials can vastly reduce the number of required trials, but at a detriment to the amount of information yielded.

The design used for this work uses a d-optimal approach, which aims to vary the experimental parameters in the most efficient manner possible in the least amount of experiments. A d-optimal approach often gives a non-orthogonal set of experiments, which are optimized to give maximal d-optimisation values for a given number of trials (Welch 1982). It is important to note that by reducing the number of trials in this manner the level of information it is possible to glean is diminished. In this study quadratic effects cannot be assessed, and so the level of linearity of response to specific variables will be unknown. However, full details on main effects and interactions can be assessed.

The selection of variables is important to consider as each additional variable has the potential to double the amount of experiments (in factorial designs), or to significantly increase the number. On the other hand, it is important to ensure that all important variables are included. Variables which are not included as parameters in the experimental design should still be measured and recorded, as all useful information will be included in the subsequent modelling/analysis.

The variables under consideration for the optimisation of the IWI process are detailed in the following sections pertaining to the double bowl and ribbon blenders. All of the DoE designs and subsequent analysis have been created in JMP 13 software (© SAS Institute Inc.).

When looking to optimise the IWI process inside each mixer a number of operating parameters were available to study their effect on process performance. Since each mixer has a different design, the parameters and values it was possible to modify for each were different and so each is described separately.

6.2.6.1. Double Bowl Blender

The main process parameters it was possible to change in the DBB included the quantity of powder added to the mixer prior to the start of the experiment (termed the fill level of the mixer). This was stated as a function of the maximum operating volume of the mixer of 20 L, described by the manufacturer.

The impeller speed could also be changed through a potentiometer with integer settings from 1-10. Previous trials on the mixer had shown that speed settings >7 caused excessive dust to be released from the mixer and so a maximum setting of 7 was used for the initial DoE.

The liquid flowrate was controlled by applying a pressure in the head space of the liquid storage vessel with the nozzle open. The maximum available pressure was 6 bar.

The distance from the nozzle to the top of the mixer paddle was changed using extension pieces to the pipework that fed the nozzle. The spray height is quoted as a percentage of the minimum height required for a full fog to be developed, as described in the nozzles section above.

Finally the type of nozzle could be changed, using both the PJ10 and PJ20 nozzles. A combination of the nozzle size and pressure applied to the liquid gave different liquid flowrates which were calibrated for all possible combinations prior to the start of experiments by spraying liquid into a measuring cylinder for a known time and measuring the volume delivered. However, the liquid addition rate itself is not taken as a process parameter due to the partial blocking that was described above, rather it is a dependent variable, measured for each experiment. To study these five parameters a custom design in JMP was used to create a d-optimal design resulting in 18 trials (16 trials including replicates, plus 2 centre points to establish linearity). Table 6-1 shows the variables and their levels.

Table 6-1: DoE table for double bowl blender trials

DoE Run Number	DoE Parameters (x-block)				
	Fill Level (%)	Speed (setting)	Pressure (bar)	Spray Height (%)	Nozzle
1	50%	7	2	90	PJ10
2	50%	7	2	130	PJ10
3	100%	3	2	90	PJ20
4	100%	7	6	130	PJ10
5	100%	3	2	90	PJ20
6	100%	7	6	130	PJ20
7	50%	3	2	130	PJ10
8	100%	7	2	90	PJ10
9	50%	7	6	90	PJ20
10	100%	3	6	90	PJ10
11	50%	3	6	130	PJ20
12	100%	7	2	130	PJ20
13	50%	3	6	90	PJ10
14	100%	3	6	130	PJ10
15	50%	7	6	90	PJ20
16	50%	3	2	130	PJ20
17	75%	5	4	110	PJ20
18	75%	5	4	110	PJ10

6.2.6.2. Ribbon Blender

In the ribbon blender the same set of parameters were studied. However, the nozzle location could not be varied and so spray height was not considered as a process parameter for this mixer. The maximum fill level of this mixer was 12 L. However, unlike the DBB, there is no room inside the RB to allow for volume expansion of the powder. Therefore, a maximum initial fill of 65 % was possible. Due to the smaller scale than the DBB it also was not possible to use the larger nozzle (PJ20) as this gave a spray pattern too large for the mixing chamber. Instead the two nozzles studied were the PJ6 and PJ10.

Table 6-2 shows the shows the 12 trials (10, plus two centre points) used to evaluate the RB, again using a d-optimal design.

Table 6-2: DoE table for ribbon blender trials

DoE Run Number	DoE Parameters (x-block)				
	Fill Level (%)	**Speed (RPM)**	**Pressure (bar)**	**Spray height**	**Nozzle**
1	35%	110	6	Fixed	PJ10
2	35%	200	2		PJ6
3	65%	200	6		PJ10
4	65%	110	2		PJ10
5	50%	155	4		PJ6
6	35%	200	2		PJ10
7	35%	110	2		PJ10
8	35%	110	6		PJ6
9	65%	200	6		PJ10
10	50%	155	4		PJ6
11	65%	200	6		PJ6
12	65%	110	2		PJ6

6.2.6.3. Nauta

As there was not a Nauta available for testing at JMTC it was not possible to run detailed optimisation design of experiments. Instead a set of scoping trials were carried out on a 5 L Nauta mixer at Johnson Matthey Process Technologies with Peter Johnson. Following the success of these scoping trials vendor trials were carried out at 20 L scale at the manufacturer's pilot facility.

6.2.6.3.1. Small Scale Scoping Trials

The scoping trials aimed to mimic the recipe used in the DoE for other two mixers, using an impregnation of water and dye solution on this zeolite at a concentration of 0.3125 mL solution per gram of solid. This is intended to include moisture already present inside the solid. However, to run at slightly more strenuous conditions to ensure the mixer would work beyond this value, the amount of liquid added was as if there was no moisture present in the solid.

Two different operating conditions were considered to aim for good and poor mixing, as shown in Table 6-3. This was to be controlled through varying the liquid addition technique. Poor addition

essentially involved dumping all 500 mL of solution onto the powder bed before switching the mixer on. Good mixing divided the solution into 10 50 mL aliquots, which were more carefully poured into the middle of the powder bed and then mixed for 30 seconds before the next aliquot was added. It is worth highlighting that this is still a very crude way of adding liquid and could be significantly improved, especially with increasing scale mixers.

After three minutes of mixing in both trials (so 30 seconds after the final addition in trial 2) the mixer was stopped and the temperature of the powder bed was measured with a mercury thermometer.

Following this, the bed was mixed for a further seven minutes to give ten minutes total mixing time for both trials. The mixer was then switched off and free flowing powder was removed into a product bucket. Once all free flowing powder was removed the walls and screw were scraped into a separate bucket, this material was deemed heels and not included in the product.

Table 6-3: 5L Nauta trial summary

Trial #	Mass Solid (kg)	Mass liquid (kg)	Liquid addition rate
1	2	500	All at once
2	2	500	10 50 mL aliquots

6.2.6.3.2. Large Scale Vendor Trials

Two mixers were tested, both designed and made by Hosokawa at a large range of scales. These mixers were a Vrieco Nauta conical screw mixer (Nauta) and a conical paddle mixer (CPM), shown in Figure 6-12. Both mixers studied were at approximately 20 L scale.

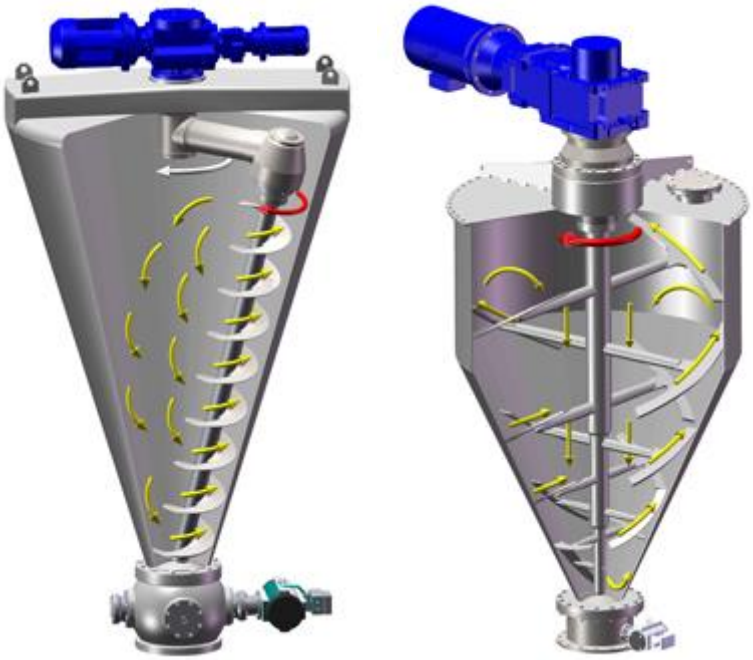

Figure 6-12: Schematic of Vrieco Nauta (left) and conical paddle (right) mixers (from Hosokawa website)

The mixers were filled with zeolite prior to beginning the addition of liquid. The volume of powder used was designed to ensure the top turn of the screw was just above the top of the powder bed at the highest point. This was an estimate for the first trial until the operators had seen the extent of the volume expansion with addition of liquid. The mass of powder used was recorded for each trial.

Three methods of liquid addition were tested; through a spray nozzle at a flow rate of 12 L hour^{-1}, through a straight hose at a flowrate of 16 L hour^{-1} and simply through pouring through a funnel with a hose into the centre of the powder bed. When using the funnel, liquid was added in 10 aliquots, with the mixer run for 1 minute between additions. The first two approaches were tested in both the Nauta and the CPM, whereas the last method was used in the Nauta only.

In trials 5 and 6 the Nauta was heated using the jacket on the vessel and a heated water bath and pump circulation loop.

In all trials on each mixer the rotation rate of the screw or paddles was kept constant at about 15 RPM in the Nauta and 36 in the CPM, the recommended operating speeds of each of the two mixers. A full list of trials is shown in Table 6-4.

Table 6-4: List of trials at Hosokawa to study large scale Nauta and CPM mixers

Trial #	Mixer	Liquid Addition	N (RPM)	Set Impregnation Temperature	Additional Tests
1	Nauta	Nozzle – 12 L hr^{-1}	15	Ambient	
2	CPM	Nozzle – 12 L hr^{-1}	36	Ambient	
3	CPM	Hose – 16 L hr^{-1}	36	Ambient	
4	Nauta	Hose - 16 L hr^{-1}	15	Ambient	
5	Nauta	Poured – 10 additions	15	30°C	1 hr drying @ 100°C
6	Nauta	Poured – 10 additions	15	65°C	

6.2.7. Multivariate Analysis

Many processes are not easily explained by simple trends with one variable alone affecting the quality or quantity of the output. In fact, a complex combination of factors may affect the output of interest, and first principles models or understanding may not be available. Therefore, it is useful to model the system empirically using observational data and statistical analysis.

Multivariate analysis is simply the application of statistical techniques to large datasets, consisting of many variables and outputs. The goal is to look for, and assess, any underlying correlations between variables and outputs, and gain a measure of which variables are key in the process. The stages involved in multivariate modelling generally fall into the following categories;

- Data pre-treatment – the raw data needs treating before optimal results are obtained from modelling. This involves getting the data into a useable format, and also pre-analysis treatments such as mean centring and auto scaling to ensure equal weighting of the parameters in the model.
- Pattern recognition – a major example of this is principal component analysis, or PCA,

which recognises co-variance in the data, and results in reduction of dimensionality and data compression. This can also be used to identify key correlations between variables and is one of the most widely used MVA techniques.

- Calibration – this is the building and testing of predictive models through a variety of methods, including multiple linear regression (MLR), principal component regression (PCR), and partial least squares (PLS). This is the extension of regression to a multivariate approach, regressing multiple variables against one or more output (or "y") variables. In this case, a mixture of standard and partial least squares modelling was used to predict the process outputs from the controlled and measured IWI variables.
- Validation – by using data not included in calibration of the model, the predictive ability of the model can be tested by looking at root mean square errors of cross validation and prediction (RMSECV and RMSEP respectively), which look at the deviation of predicted values from the actual values. This can be achieved by cross validation (leaving out random samples during calibration, and projecting those samples through the model), or by exposing the model to new information to test the predictive ability. Both types of validation were used for the models in this report.

PLS is a powerful technique and extremely useful in highlighting important patterns within datasets, this is very useful during R&D projects where probing into PLS models can help deliver understanding as to what is occurring within a process. It is also a powerful technique in that it can deal with highly co-correlated x variables. However, PLS may be less effective for predicting future performance than more tradition predictive regression techniques, such as least squares modelling due to the fact the models incorporate many variables that would be impractical to measure outside of an R&D setting (such as external disturbance variables).

More detailed descriptions of both PCA and PLS modelling are given in Chapter 4.

6.3. Results

6.3.1. Double Bowl Blender

6.3.1.1. Experimental Observations

After every experiment, a picture was taken from the top of the mixer for observation. Repeats show similar outcomes, for example experiment 3 and 5 show similar visual performance (Figure 6-13). The pictures also show traces of over wetted zones on the mixer walls.

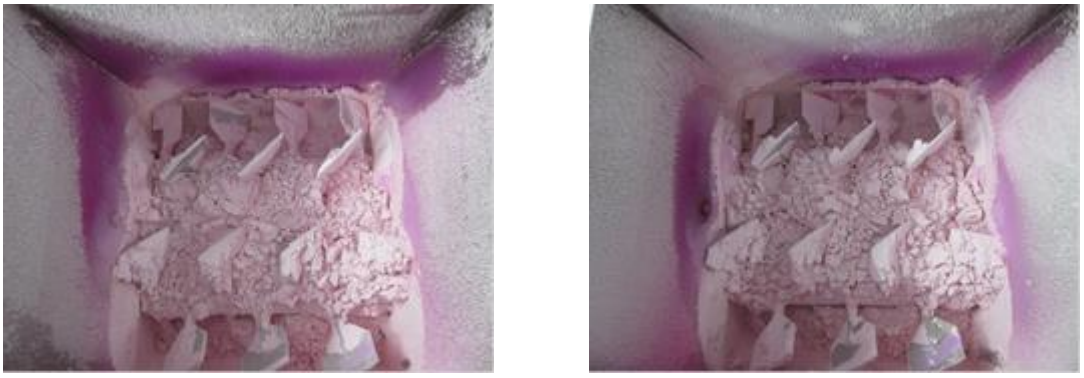

Figure 6-13: Status of mixer after trials 3 (left) and 5 (right)

An additional observation was made studying the liquid spray behaviour. As expected, liquid flow rate increases when spraying pressure is increased and formation of fog is more uniform. However, at low pressure the formation of fog is not consistent. This inconsistency is caused by the coalescence of fog on the nozzle surface; bigger drops form: which then drop from the nozzle into the powder bed.

Table 6-5 shows the flowable yield values for each of the trials in the DBB experimental design. The highest yields of 90.3 % and 89.9 % were seen in trials 8 and 4 respectively. The lowest yields were found in trials 9 and 11 of 63.2 % and 63 % respectively.

Table 6-5: Double bowl blender flowable yield values

Exp	Zeolite (kg)	Liquid (l)	Flowable mass out (kg)	Flowable Yield (%)
1	5.040	0.855	5.16	87.5%
2	5.030	0.658	3.87	68.0%
3	8.617	1.660	8.19	79.7%
4	9.579	1.502	9.96	89.9%
5	8.617	1.660	8.48	82.5%
6	9.819	1.398	9.66	86.1%
7	5.030	0.658	3.99	70.1%
8	8.793	1.687	9.46	90.3%
9	4.468	0.861	3.37	63.2%
10	8.793	1.687	8.86	84.5%
11	4.615	0.849	3.45	63.0%
12	9.137	1.465	9.26	87.3%
13	4.900	0.832	4.16	72.6%
14	9.229	1.699	8.98	82.2%
15	4.468	0.861	3.48	65.3%
16	4.910	0.699	3.76	66.9%
17	6.853	1.099	6.26	78.7%
18	6.897	1.159	6.86	85.2%

6.3.1.2. Principal Component Analysis

Figure 6-14 shows a colour map demonstrating correlations and interactions between variables (both input and output variables). Here, red shows a strong positive correlation, and blue a strong negative correlation. Grey-ish squares show little-to-no correlation. For example, as the experiments have been planned using an orthogonal design, you can expect to see no correlation between input parameters (asides from speed and RPM); indeed, correlation here would be detrimental. Unwanted correlations in input parameters is known as aliasing, or confounding, and is often an issue with one-at-a-time experimentation or incorrect experimental design.

There are a great many interactions between the variables and it would be impractical to list them all. However, the key correlations were between fill level variables (the weights of zeolite/water added), and with the yield variables. It also identified a potential aliasing between batch of zeolite used and the spray height of the nozzle due to lack of experimental randomisation. Many other correlations are visible to differing degrees, showing that the process is quite complex.

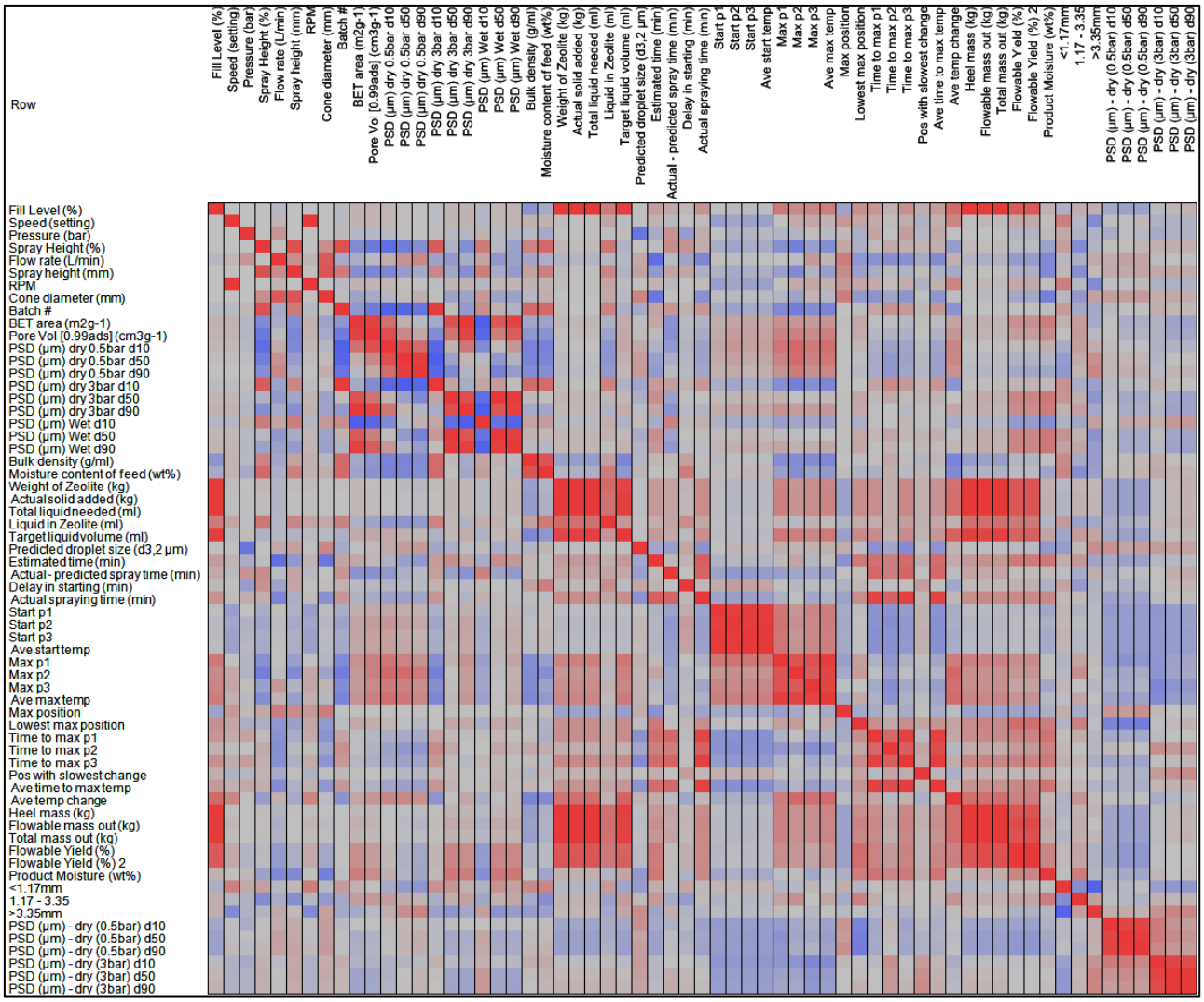

Figure 6-14: PCA colour map of variable correlation

6.3.1.3. Multivariate Modelling

6.3.1.3.1. Yield

Table 6-6 shows the VIP scores for factors most strongly affecting the product yield shows that fill level related variables (including material inputs and weights) are the bulk of the significant variables. This essentially amounts to the statement that *the more material is loaded into the system, the more flowable yield*. The same relationship held true through a few quick investigations into using a y-variable consisting of a fill level-normalised yield.

One of the other key variables was the length of impregnation, best indicated by the average time to max temperature. It should also be noted that one of these points giving high yield was produced by a nozzle malfunction (possible blockage) resulting in an impregnation length of twice the predicted value.

Table 6-6: Double bowl blender PLS significant VIP scores

X	VIP
Weight of Zeolite (kg)	1.8136
Actual solid added (kg)	1.8033
Total liquid needed (ml)	1.8033
Fill Level (%)	1.7409
Target liquid volume (ml)	1.6459
Liquid in Zeolite (ml)	1.3596
Estimated time (min)	1.2783
PSD (µm) dry 3bar d50	1.1327
PSD (µm) Wet d50	1.1224
PSD (µm) Wet d90	1.1189
PSD (µm) Wet d10	1.0226
PSD (µm) dry 3bar d90	1.0226

The prediction performance is shown in Figure 6-15. The model shows good predictive performance with 91 % of the y block variation described by 38 % of the x block variation in three latent variables.

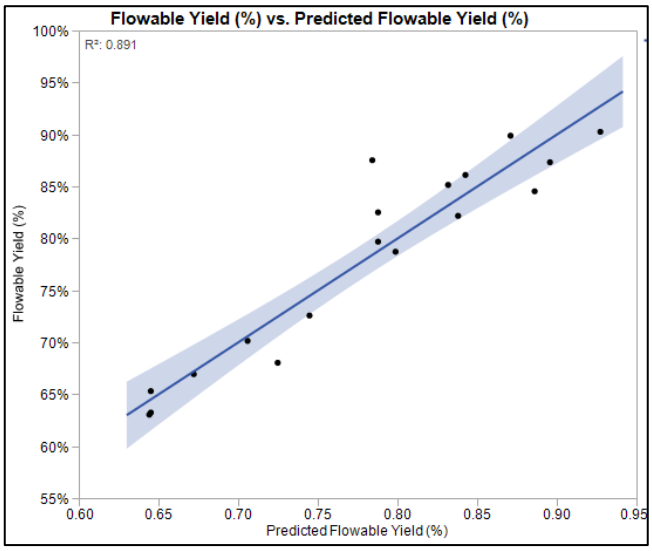

Figure 6-15: Double bowl blender flowable yield PLS predictions with three latent variables

6.3.1.3.2. Homogeneity

Table 6-7 shows the parameters that most strongly affect the mixing performance are the height of the spray system, the mixer speed, and many of the initial conditions, including initial moisture, initial temperature, and batch number.

Table 6-7: VIP Scores for CoV PLS analysis of homogeneity for double bowl blender

X	VIP
Spray height (mm)	1.7245
RPM	1.6208
Speed (setting)	1.6208
Cone diameter (mm)	1.6135
Spray Height (%)	1.4771
Liquid in Zeolite (ml)	1.4026
Start p1	1.4018
Ave start temp	1.3637
Start p2	1.3558
Predicted droplet size (d3,2 µm)	1.3212
Start p3	1.3064
PSD (µm) dry 0.5bar d10	1.2094
Batch #	1.1769
Actual - predicted spray time (min)	1.1595
PSD (µm) dry 3bar d10	1.0866
Pore Vol [0.99ads] (cm3g-1)	1.0841
Flow rate (L/min)	1.0449
Max position	1.0323
Pressure (bar)	1.0196
PSD (µm) dry 0.5bar d50	1.0082
Max p2	0.9963

Although these scores show the variables are significant they don't show in which direction they will affect mixing and so, as an example, a univariate plot of CoV vs mixer speed is shown in Figure 6-16; from which we can see that increasing the mixer speed reduces the image CoV and so improves mixing performance. However, this is clearly not a perfect correlation as other factors are also important.

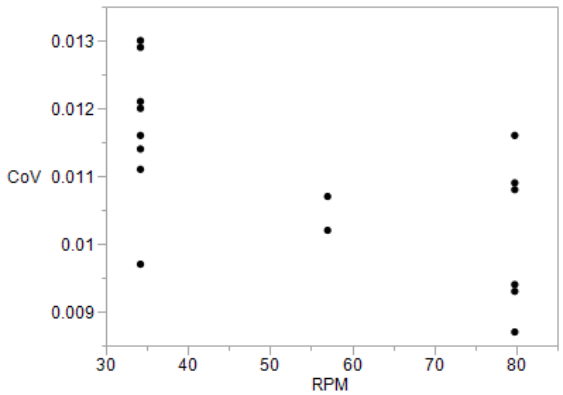

Figure 6-16: Univariate plot of CoV vs mixer speed for double bowl blender

This model can then be tested by seeing how well it predicts the points used to build it. This is shown below in Figure 6-17 and shows decent performance of the model with an $R^2 = 0.869$. This model explains 86.9% of variation in CoV using 50% of input variation.

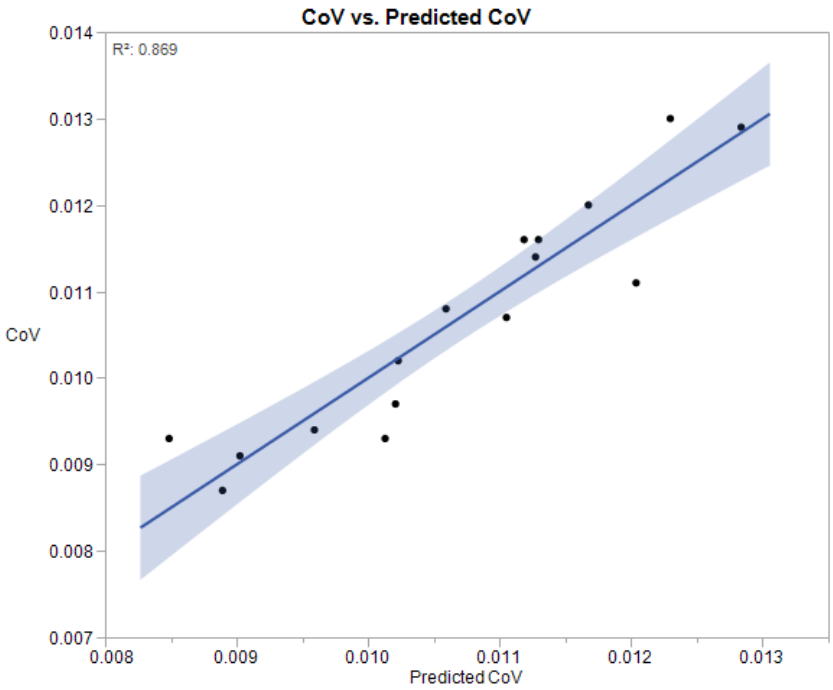

Figure 6-17: Predicted CoV from PLS model vs measured CoV for double bowl blender with three latent variables

6.3.1.3.3. Area Analysis

A similar approach to above was used but looking at the image as a whole, and binary gating it using the thresholding technique described above to produce binary images.

Although the order and exact VIP scores have changed slightly compared to the CoV model we see the same set of significant parameters for the model, shown in Table 6-8.

Table 6-8: PLS significant VIP scores for image area analysis for double bowl blender

X	VIP
RPM	1.9405
Speed (setting)	1.9405
Spray height (mm)	1.7381
Cone diameter (mm)	1.6005
Spray Height (%)	1.4347
Predicted droplet size (d3,2 µm)	1.4281
Liquid in Zeolite (ml)	1.4149
Start p1	1.2968
Max position	1.2544
Ave start temp	1.2308
Start p2	1.1973
Moisture content of feed (wt%)	1.1725
Start p3	1.1715
PSD (µm) dry 0.5bar d10	1.1131
Actual - predicted spray time (min)	1.1045
Flow rate (L/min)	1.0902
Batch #	1.0615
Pressure (bar)	1.0468
Pore Vol [0.99ads] (cm3g-1)	1.0431

Once again mixer speed and spray height are the two most significant parameters in the model with the same set of initial conditions also significant, but slightly less so. Again, the predictive model shows decent fit, with an R^2 of 0.889, as shown in Figure 6-18. Similarly, to the CoV model this one explains 88.87% of variation in y explained using 48% of variation in x.

It is possible to refine this model by removing all factors deemed insignificant based on their VIP scores and building a new model, this is shown in Figure 6-19. This increases the fit of the model to $R^2 = 0.95$ whilst increasing the y variation explained to 95% whilst using 83% of the smaller list of x variation, as shown in Figure 6-19.

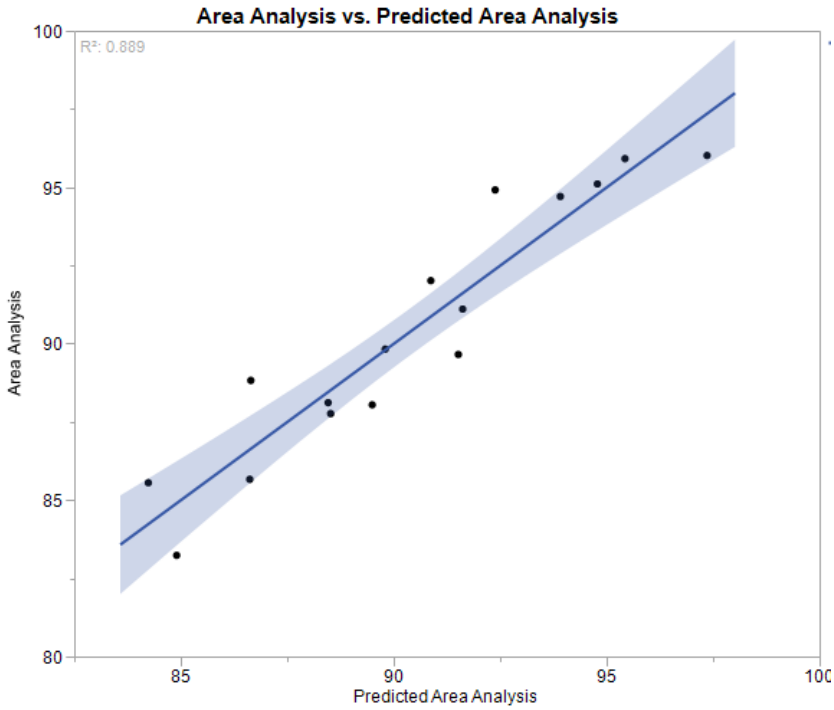

Figure 6-18: Predicted area mixed from PLS model vs measured mixing for double bowl blender with three latent variables

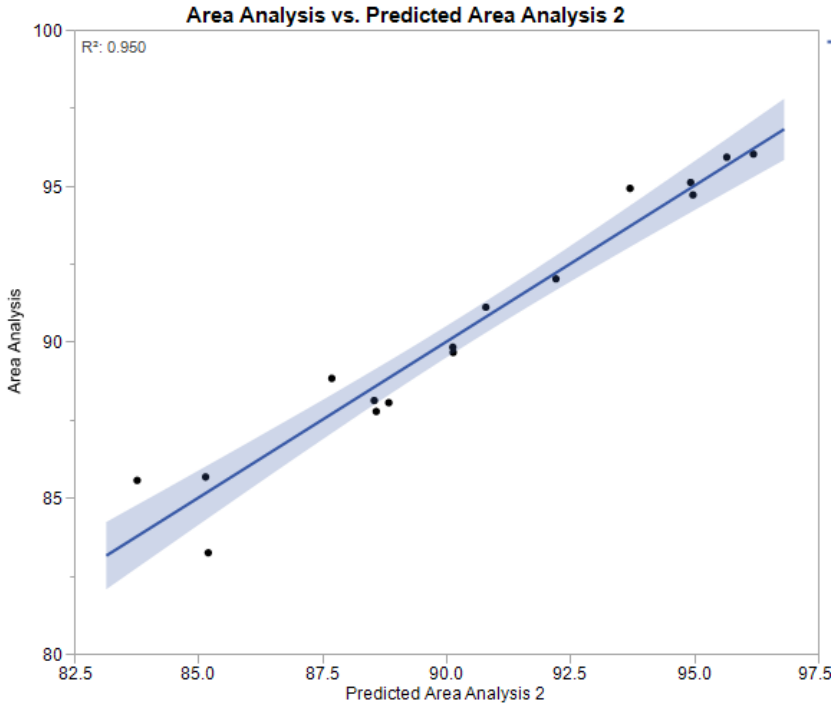

Figure 6-19: Predicted area mixed from refined PLS model vs measured mixing for double bowl blender with three latent variables

6.3.1.3.4. Lumps

Very few lumps were formed in any of the double bowl blender trials, with the highest mass of powder contained in lumps bigger than 3.35 mm less than 0.3 % of the recoverable powder. The most important variables with respect to agglomerate formation were speed and raw material properties, especially particle sizes, as shown in Table 6-9. A very good model was achieved using PLS, with an R^2 of prediction of 0.995 (Figure 6-20). It is worth noting this model includes a large number of significant VIP scores.

Table 6-9: PLS significant VIP scores for double bowl blender agglomerates

X	VIP
Speed (setting)	1.9191
RPM	1.9191
PSD (µm) Wet d50	1.7095
PSD (µm) dry 0.5bar d90	1.6869
PSD (µm) dry 3bar d50	1.6454
PSD (µm) Wet d90	1.4428
PSD (µm) dry 0.5bar d50	1.4037
Predicted droplet size (d3,2 µm)	1.3619
Bulk density (g/ml)	1.2710
PSD (µm) dry 3bar d10	1.2374
Moisture content of feed (wt%)	1.2098
Estimated time (min)	1.1543
PSD (µm) Wet d10	1.1190
PSD (µm) dry 3bar d90	1.1190
BET area (m2g-1)	1.0596
Max p3	1.0116
Liquid in Zeolite (ml)	1.0056

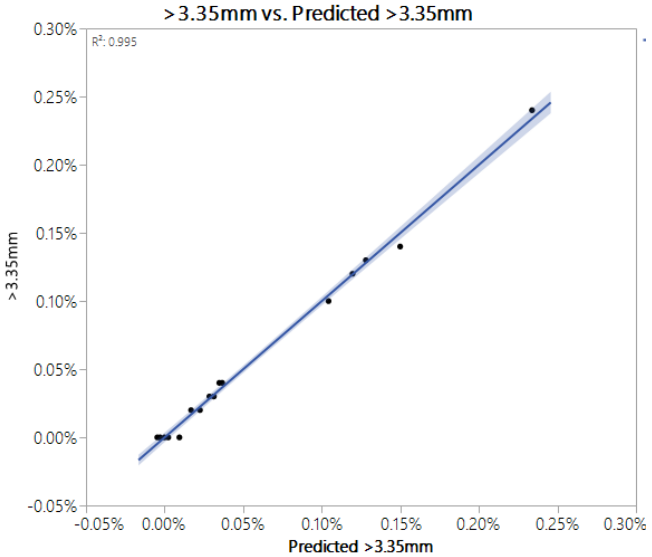

Figure 6-20: DBB agglomerate formation as a function of recoverable product PLS model predictions with three latent variables

6.3.1.4. Conclusions

The highest yields measured in the DBB were around 90 % in trials 4 and 8. These trials both contained high fill levels and the smaller of the two nozzles studied (PJ10). The lowest yields measured were 63 % in trials 11 and 15.

Flowable yield and material homogeneity were evaluated independently. Flowable yield mainly depends on parameters such as fill level (higher is better), liquid addition rate (lower flow rates are better) and batch of raw material (effect is variable). Product homogeneity mainly depends on the spraying system (further from bed is better), shaft rotation speed (higher is better) and initial moisture content of raw material. Both, flowable yield and homogeneity, are dependent parameters of raw material, which indicates the importance of a standard raw material feeding.

Formation of lumps was very low in all trials. However, it was found that high impeller speeds gave the lowest of any lumps measured.

6.3.2. Ribbon Blender

6.3.2.1. Experimental Observations

The biggest loss in flowable yield was seen when significant amounts of powder stuck to the moving parts of the ribbon, as shown in Figure 6-21 for trial 1 of the DoE.

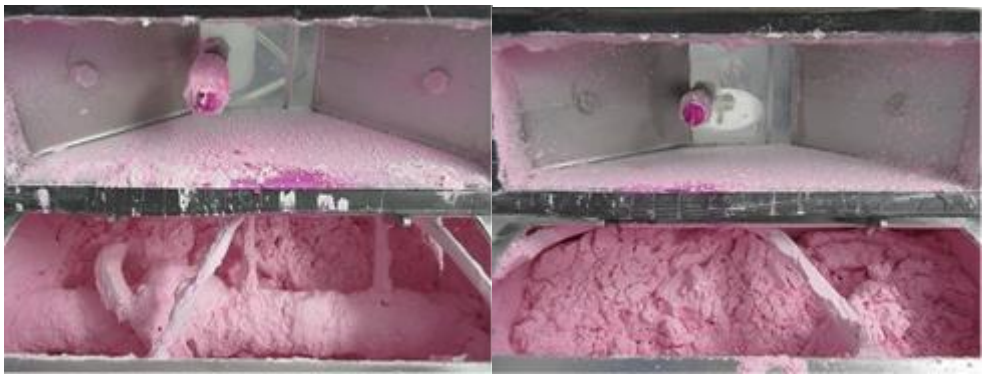

Figure 6-21: State of ribbon blender after emptying showing poor yield in trial 1 (left) and good yield in trial 12 (right)

Table 6-10 shows the flowable yield for each of the trials performed in the RB. Trials 12, 10, and 4 gave the highest yields of 94 %+. Most trials in the RB gave yields above 90 %, with only trials 1, 2, 7, and 8 giving yields less than this.

Table 6-10: Ribbon blender flowable yield values

Run	Zeolite (kg)	Liquid (L)	Flowable mass out (kg)	Flowable yield (%)
1	1.90	0.378	1.94	85
2	1.90	0.378	2.00	88
3	3.54	0.702	3.96	93
4	3.49	0.589	3.85	94
5	2.74	0.542	3.01	92
6	1.90	0.372	2.08	91
7	1.90	0.372	1.99	87
8	1.91	0.372	2.02	89
9	3.54	0.691	3.89	92
10	2.79	0.560	3.17	94
11	3.53	0.682	3.91	93
12	3.53	0.682	4.02	96

6.3.2.2. Principal Component Analysis

Figure 6-22 shows a PCA colour map of interactions and correlations between all input and output variables considered for the RB. Again, red denotes anti-correlation, blue is correlation, and grey shows no correlation between those two variables. Again, there are too many interactions to list individually However, again the batch number of powder used is correlated with many input parameters and so is potentially having a large disturbance effect on the measurements.

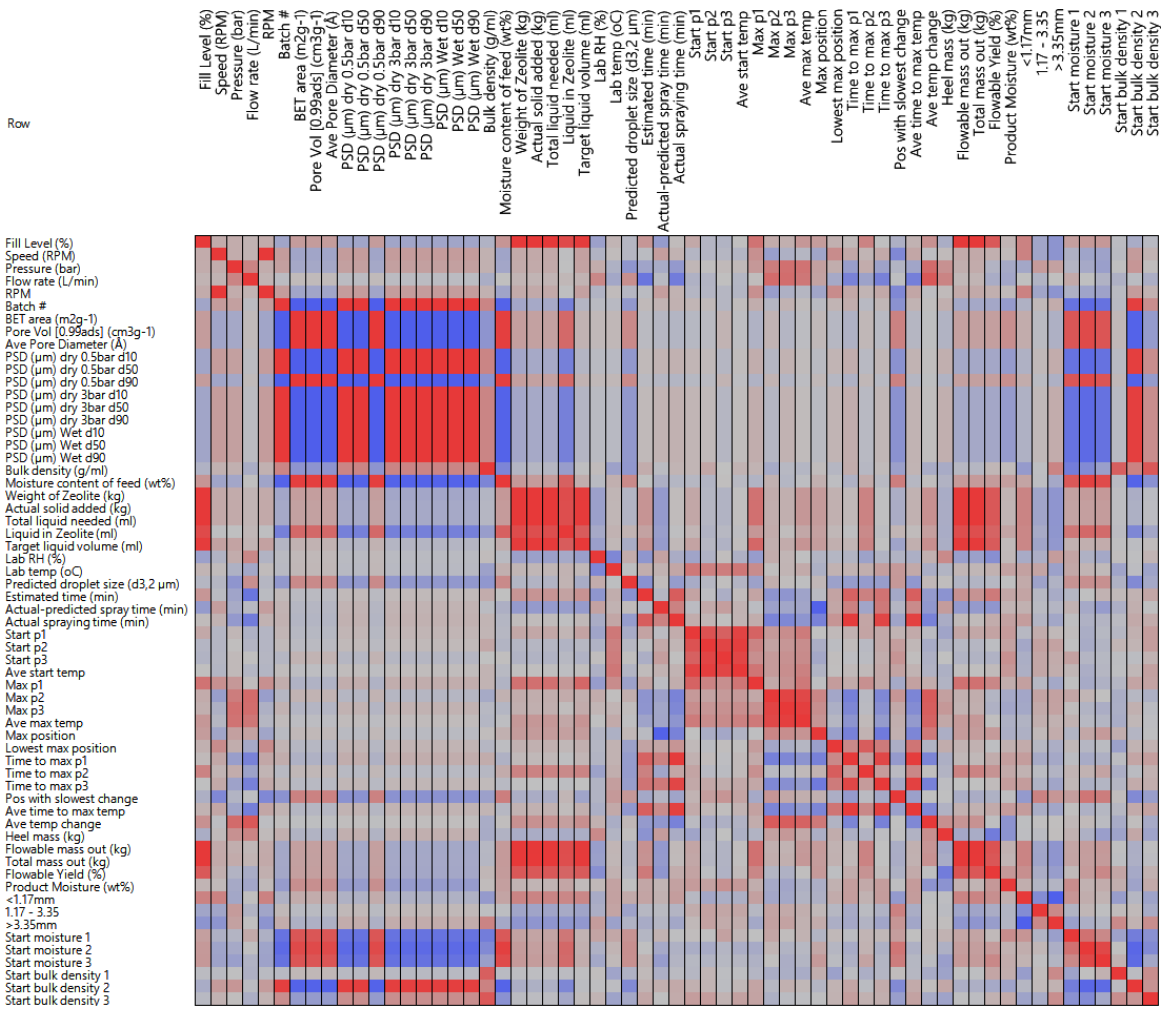

Figure 6-22: PCA colour map of correlations between variables for ribbon blender

6.3.2.3. Multivariate Modelling

6.3.2.3.1. Yield

The PLS model for flowable yield from the RB was reasonably complex, requiring 5 latent variables (LVs) to explain the variance in the model. Of which, 81% of the x-block was explained and 97% of the y-block. This resulted in a good fit to the model, with a R^2 of prediction of 0.969 (see Figure 6-24). The significant parameters, as shown by a VIP score of > 1 in Table 6-11, are mostly related to material in the mixer, the length of impregnation, and, interestingly, lab relative humidity (RH). This measurement was not available during the DBB trials, so will be assessed included in the confirmation trials.

Table 6-11: PLS significant VIP scores for ribbon blender flowable yield

X	VIP
Weight of Zeolite (kg)	1.6634
Actual solid added (kg)	1.6627
Total liquid needed (ml)	1.6627
Fill Level (%)	1.6289
Target liquid volume (ml)	1.6201
Liquid in Zeolite (ml)	1.4193
Actual-predicted spray time (min)	1.3677
Max p1	1.2991
Estimated time (min)	1.2355
Lab RH (%)	1.2080
Actual spraying time (min)	1.1696
Speed (RPM)	1.1057
RPM	1.1057
Time to max p1	1.0525
Ave time to max temp	1.0501
Time to max p2	1.0475
Start time (HH:MM)	1.0263
End time (HH:MM)	1.0196
Max p2	1.0010

Additionally, a least squares model was fit to just the DoE altered parameters, excluding the extra measurement data. This produced a regression equation linking the DoE parameters to allow optimal settings to be found for the confirmation trials. Figure 6-23 shows the least squares fit.

The benefit of the extra measurements in addition to the DoE parameters is clear and is illustrated by Figure 6-24 which shows the ability of the model using only the DoE parameters; the R^2 is far lower than the total model, at 0.79 compared to 0.97.

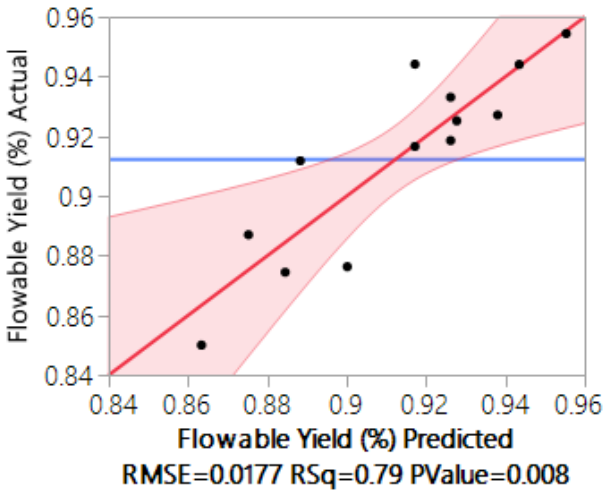

Figure 6-23: Least Squares prediction fit and expression for ribbon blender DoE trials

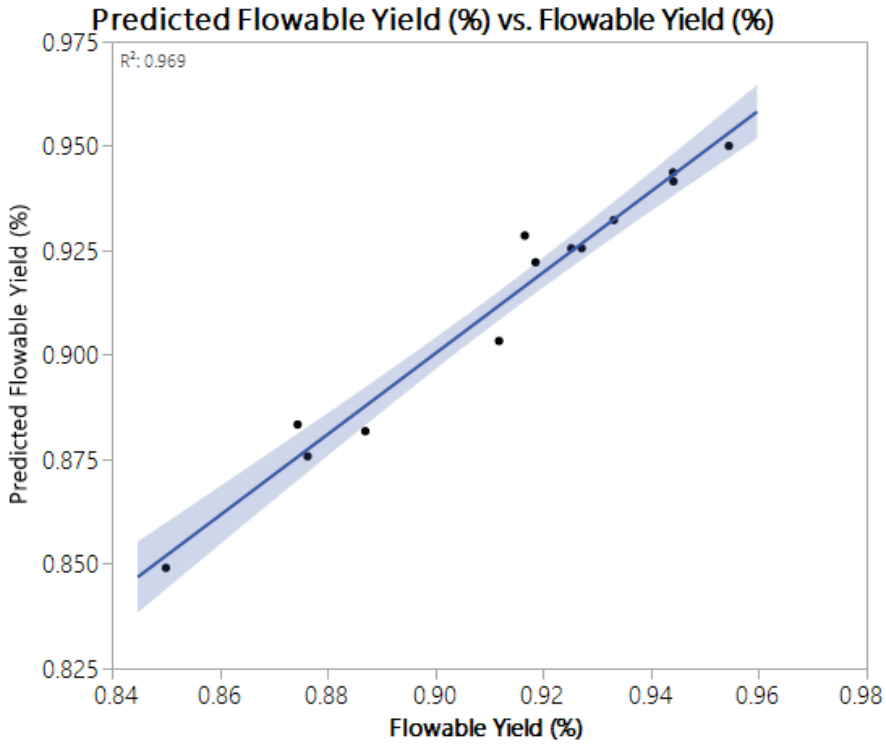

Figure 6-24: Ribbon blender flowable yield PLS model predictions with three latent variables

6.3.2.3.2. Homogeneity

Table 6-12 shows the VIP scores for all factors measured when running trials in the ribbon blender for the PLS model built based on the output of the image analysis measurements. It shows a completely different set of important parameters to those in the model for the DBB. The most significant parameters are external and initial conditions such as ambient relative humidity and the batch and initial moisture of the powder. However, it is worth noting from Figure 6-25 that the model produced is not particularly reliable. This is most likely because the samples from the RB show considerably higher homogeneity than those produced in the DBB, with higher total homogeneity values and a lower spread of values.

Table 6-12: PLS significant VIP Scores for ribbon blender homogeneity

X	VIP
Lab RH (%)	1.8440
Batch #	1.7147
Product Moisture (wt%)	1.6289
Moisture content of feed (wt%)	1.5052
Predicted droplet size (d3,2 µm)	1.2839
Lab temp (oC)	1.2576
Pressure (bar)	1.1913
Bulk density (g/ml)	1.1854
Time to max p3	1.1616
Pos with slowest change	1.1597
Time to max p1	1.0940
Nozzle	1.0801
Ave time to max temp	1.0486
Actual spraying time (min)	1.0482
Speed (RPM)	1.0391
RPM	1.0391
Max p1	1.0312
Max p2	1.0150
Ave temp change	0.9659
Start p2	0.9493
Liquid in Zeolite (ml)	0.9479
Start p1	0.9366
Flow rate (L/min)	0.9361
Max p3	0.9323
Ave start temp	0.8832
Lowest max position	0.8700
Max position	0.8697
Ave max temp	0.8642
Estimated time (min)	0.8058
Start p3	0.7976
Heel mass (kg)	0.7970
Actual-predicted spray time (min)	0.7872

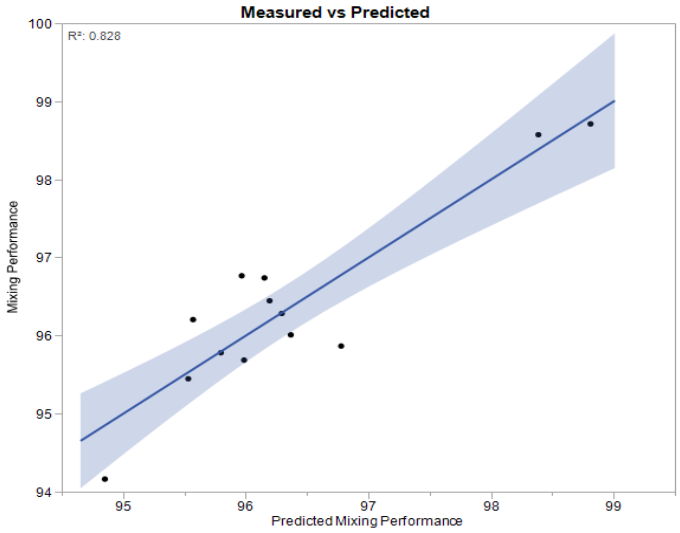

Figure 6-25: PLS model for ribbon blender homogeneity with four latent variables

6.3.2.3.3. Lumps

As noted previously, lump formation can be an issue in the RB, however the underlying factors causing the formation of lumps are complex and likely to be non-linear, as can be seen from the reasonably poor model performance seen in Figure 6-26. However, the key variables here are related to fill level, and again relative humidity (RH) shows significance. Here, speed is also a factor. Table 6-13 shows that the amount of material inside the mixer was the most significant factor in determining whether lumps formed or not.

Table 6-13: PLS significant VIP scores for ribbon blender agglomerates

X	VIP
Fill Level (%)	1.8158
Weight of Zeolite (kg)	1.7749
Actual solid added (kg)	1.7609
Total liquid needed (ml)	1.7609
Liquid in Zeolite (ml)	1.6650
End time (HH:MM)	1.6488
Target liquid volume (ml)	1.6392
Start time (HH:MM)	1.6151
Lab temp (oC)	1.5140
Bulk density (g/ml)	1.4978
Max p1	1.2244
Speed (RPM)	1.2158
RPM	1.2158
Lab RH (%)	1.1996
Moisture content of feed (wt%)	1.0011

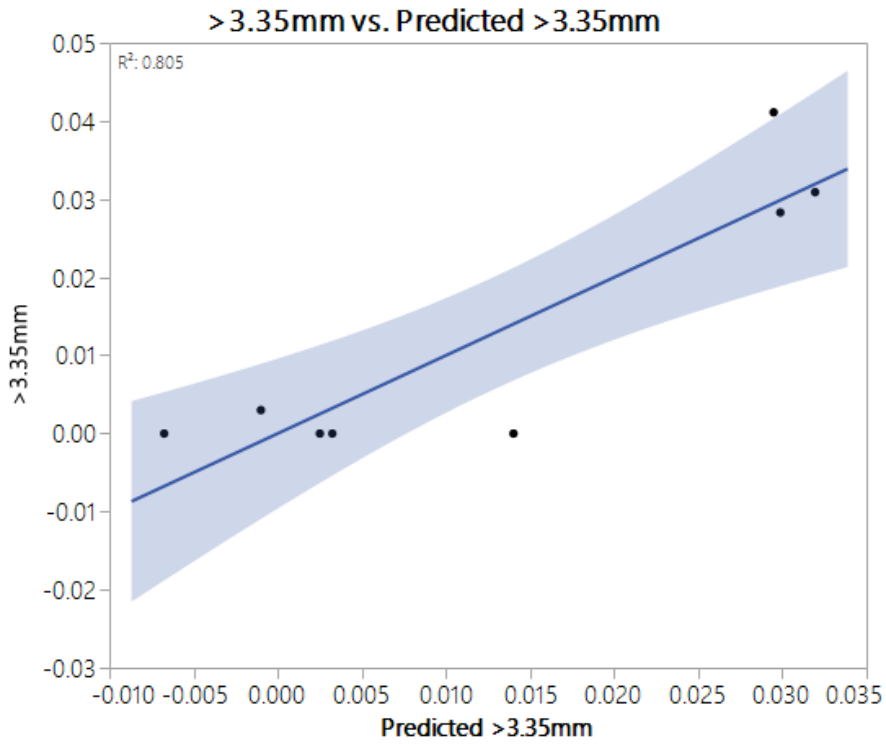

Figure 6-26: Ribbon blender agglomerate formation as a function of recoverable PLS model predictions with three latent variables

6.3.2.4. Conclusions

The best performance using the ribbon blender achieved a flowable yield of 95.8% with no lump formation and good homogeneity in trial 12. During this trial the fill level was 65%, rotation speed was 155 RPM, and liquid flow rate was 22 mL min^{-1} at 2 bar of pressure through PJ6 nozzle. The poorest performance saw a flowable yield of 82.1% and some lump formation, the fill level was 35%, the rotation speed 110 RPM, and the liquid flow rate was 106 mL min^{-1} at 6 bar of pressure through PJ10 nozzle.

Multivariate analysis showed the influence of external variables such as ambient relative humidity, initial moisture content and batch of bare zeolite, on the consistency of the product. However, the limited variation in homogeneity resulted in a reasonably poor model; generally, all results were homogenous. The most significant variables with respect to yield and product

moisture were related to fill level, in that higher mixer fill generally resulted in better yields and product moisture. Additionally, for flowable yield, having a longer more gradual impregnation was beneficial.

Formation of lumps was low in all trials. However, it was found that low fill levels gave the lowest level of lump formation.

6.3.3. Nauta Mixer

6.3.3.1. Initial scoping Trials

6.3.3.1.1. Experimental Observations

Table 6-14 shows the headline mass balance of the 5 L trials, considering the mass of product material as a proportion of total material added. As expected, trial 2 with the slower liquid addition rate gave a higher product yield. This was because there was considerably more over wet material stuck to the wall in trial 1, especially around the point the liquid was added and towards the bottom of the mixer. In trial 2 there was much less material stuck to the wall, but what was there was also around the point of liquid addition. This suggests the yield could be increased further through design of a suitable liquid addition system, minimizing the amount of liquid near the vessel walls, with a minimum possible yield of 90%.

Table 6-14: Headline mass balance

Mass Balance	Total Mass in	Product Mass (kg)	Heels (kg)	Yield (%)
1	2.50	2.25	0.22	90.1%
2	2.50	2.41	0.06	96.4%

It is also worth noting, larger models of Nauta mixers can rotate the screw in the opposite direction, diving powder out of the mixer, which would also increase product yield. However, this feature is not possible on the small scale model available.

Table 6-15: Total component mass balance

Trial	Total Mass in	Total Solid In (kg)	Total Liquid In (kg)	Total Mass Out (kg)	Mass Loss (kg)	Mass Loss (%)	Solid Out (kg)	Liquid Out (kg)	Solid Loss (kg)	Solid Loss (%)	Liquid Loss (kg)	Liquid Loss (%)
1	2.5	1.90	0.60	2.48	0.02	0.95%	1.89	0.59	0.02	0.89%	0.01	1.16%
2	2.5	1.92	0.58	2.47	0.03	1.20%	1.90	0.57	0.02	1.02%	0.01	1.78%

From the total component mass balance in Table 6-18 we see that in both cases, approximately 1% of the total mass added was lost during the course of the trials. This mass loss can be seen in both a loss in solid and liquid. In both trials more liquid is lost than solid. This is likely due to evaporation as the maximum temperature reached was around 55°C. Some dust was lost out of the top of the mixer and there are inevitably residues that aren't removed and measured as product or heels. The higher mass loss in trial 2 could well be due to the mixer being opened more frequently to add liquid in more additions, as seen by the higher percentage loss of liquid, or it could simply be within the experimental error. Repeats would be needed to assess this if deemed significant.

6.3.3.1.1.1. Temperature

As stated above, there was a significant temperature increase in both trials as shown in Table 6-16 below.

Table 6-16: Temperature Measurements

Trial	T_0 (°C)	T_{end} (°C)
1	21	54
2	20	53

Both powder beds increased in temperature by approximately 33°C. Since the mixer is a very low shear/low power mixer, this is likely to be almost entirely down to the exotherm as the zeolite becomes wet.

6.3.3.1.1.2. Sieving

For each trial three 500 g samples were taken from the product bed at random and sieved, first through a 3.35mm sieve and then a 1.7mm sieve. The results of sieving are shown in Figure 6-27.

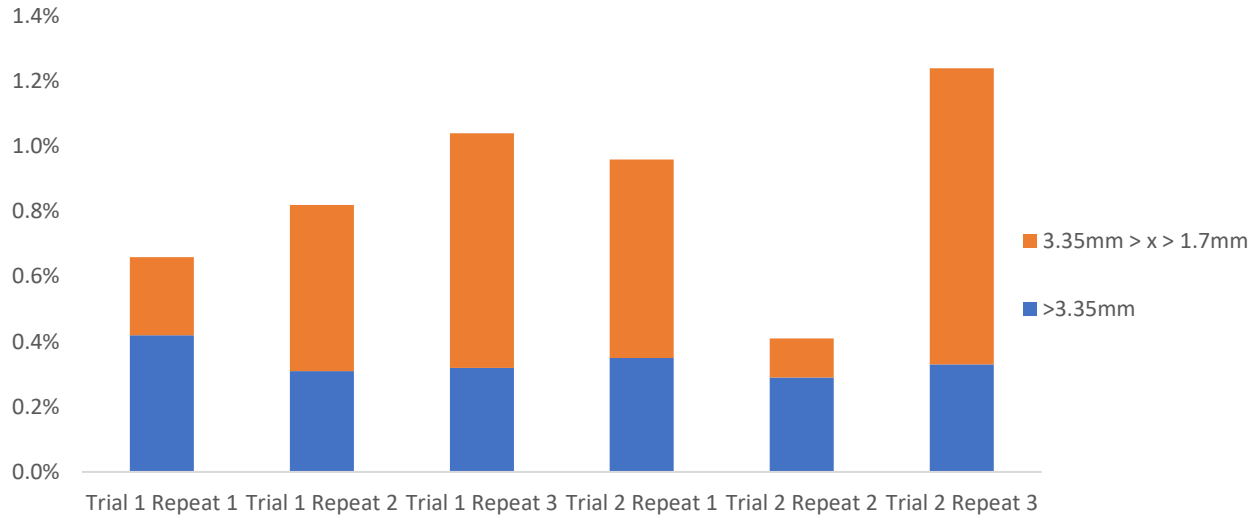

Figure 6-27: Agglomerate size fractions

No significant agglomerates produced during mixing larger than 1.7 mm capable of surviving the sieving process.

6.3.3.1.1.3. Homogeneity

Image analysis was done on five samples taken from each of the trials for the Nauta. The homogeneity of these is shown against the DBB and RB samples below in Figure 6-28. We see the samples did not appear as homogenous as those from the ribbon but still towards the upper end of samples from the DBB.

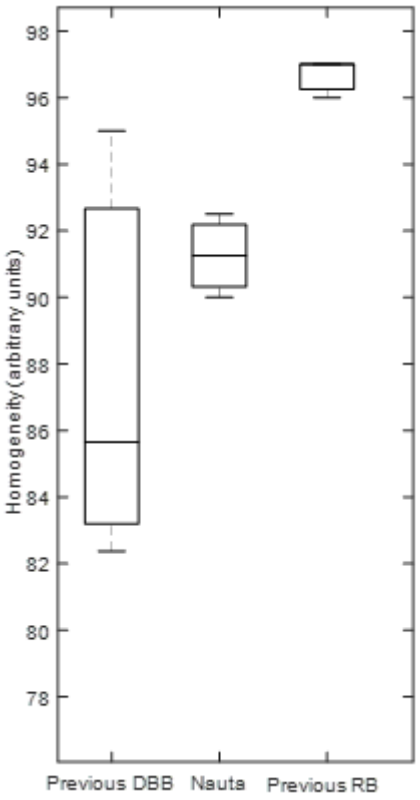

Figure 6-28: Homogeneity of Nauta samples compared to DBB and RB

6.3.3.2. Vendor trials

6.3.3.2.1. Experimental Observations

6.3.3.2.1.1. Trial 1 – Initial Vrieco Nauta Mixer Test

Mixing within the vessel was very effective, with colour quickly homogenising through the bed as it was sprayed. The mechanism is very gentle with very little movement of powder outside the bed and so little mass lost as dust. The vessel emptied by itself, however, the discharge was extremely slow, taking approximately an hour and a half to fully empty the mixer. All product discharged was extremely homogenous and free of agglomerates to eye.

Figure 6-29: Nauta mixer before addition of liquid with layer pressed between screw and wall highlighted

The temperature of the bed increased to approximately 40°C from an ambient temperature of 18°C, with the gentle mixing mechanism this is likely to be entirely heat of reaction as the powder is wet. This is in line with the expected adiabatic temperature rise on wetting of around 20°C.

A thick layer of powder formed at the edge of the mixer, as shown in Figure 6-29 and Figure 6-30. This layer started forming before any liquid was even added to the vessel but became thicker as more liquid was added. By the end of the trial this layer was compressed smooth to the wall of the vessel and could not be removed by agitation of the screw alone. There was relatively very

little material stuck to the screw at the end of the trial once the vessel was empty compared to that on the walls, as shown in Figure 6-31.

Figure 6-30: Nauta mixer after final addition of liquid with layer pressed between screw and wall highlighted

Figure 6-31: Nauta mixer after emptying in trial 1

6.3.3.2.1.2. Trial 2 – Initial Conical Paddle Mixer Test

This mixer involved significantly more power than the Nauta, with significantly more movement of powder inside the vessel. On emptying the discharge was extremely quick with all recoverable product emptying within 1 minute. It is worth noting this is most likely because the CPM has a

significantly larger orifice at the bottom than the Nauta, and so powder flows much more freely through it.

Figure 6-32: Powder stuck to CPM shaft

There was a noticeably higher amount of heat generated in the CPM, with obvious condensation from evaporation. The powder bed was measured at the end of impregnation at approximately 55°C. The extra heat in the CPM compared to the Nauta was expected by the operators and put down to the more violent mixing mechanism generating more heat through friction.

After emptying the vessel, the walls were free of powder. However, the large amount of moving parts inside the vessel were covered in stuck powder, this was especially true on the central shaft, as shown in Figure 6-32. This material remained stuck to the shaft and could not be removed by agitation alone.

6.3.3.2.1.3. Trial 3 – 'Improved' CPM Test

The idea behind this trial was to reduce the spray area of liquid by employing a 'hose' nozzle as shown in Figure 6-33, reducing the chance of liquid contact with the shaft, reducing the amount of material that got stuck.

Figure 6-33: 'Hose' nozzle

There was a slight improvement, with slightly less stuck material and no change in temperature or emptying behaviour. However, there was still a significant amount stuck to the shaft and relatively little on the wall.

6.3.3.2.1.4. Trial 4 – 'Improved' Nauta Test

After seeing the slight improvement in trial 3 over trial 2 the same modification was tested in the Nauta. There was very little change compared to trial 1, with the same layer forming between the screw and the wall even before liquid was added.

6.3.3.2.1.5. Trial 5 – Nauta Drying

The idea to attempt to dry the powder inside the mixer was suggested. To do this the Nauta was set up with a water bath to fill the jacket around the mixer. The impregnation was carried out at 30^{o}C (although the powder bed temperature still rose due to the reaction on wetting). After impregnation was complete the layer of compressed material between the screw and the wall, as previously noted, was obvious and very similar to trials 1 and 4.

Figure 6-34: Nauta mixer after impregnation with wall > 60oC after stuck layer collapsed

Following impregnation, the water bath temperature was set to 100°C with the mixer still turning as the temperature increased. It was noticed that when the current temperature in the water bath read 57°C the layer between the screw and the Nauta wall collapsed into the bulk and began moving with the powder bed, as shown in Figure 6-34. This continued up to 100°C.

The Nauta was left mixing at 100°C for one hour to partially dry the powder bed before discharge. When the bottom valve was opened powder flowed out of the mixer considerably faster than in trials 1 and 4, fully emptying the mixer within five minutes. There was also no layer left between the screw and the wall, meaning significantly more powder was available as product. The only powder remaining stuck to the wall was at the back of the mixer, away from the opening at the

front, where there was the highest level of condensation dripping down the mixer wall, as shown in Figure 6-35.

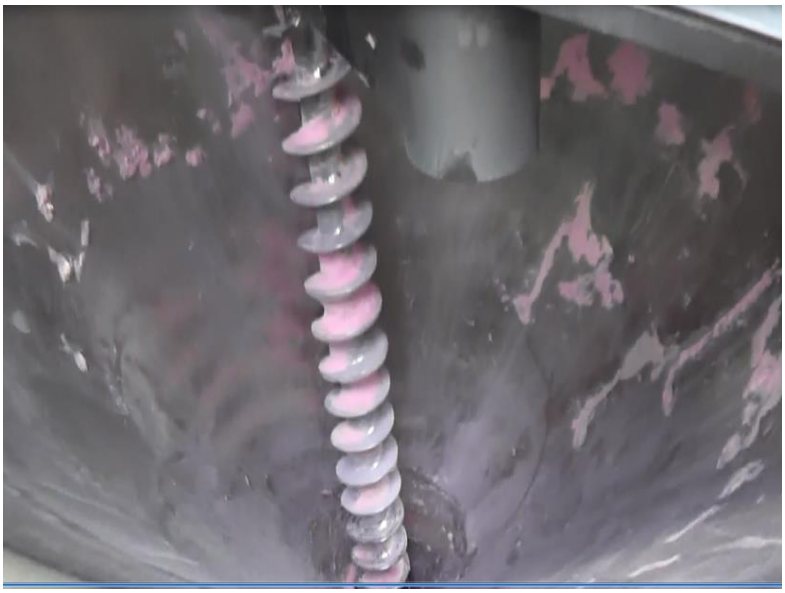

Figure 6-35: Nauta mixer after emptying at high temperature

The total yield (recoverable mass out/total mass in) in this trial is artificially low as there was considerable evaporation over the drying time. There was only 70 g of heels irrecoverably stuck to either the mixer walls or shaft compared to 7.5kg of recoverable product.

6.3.3.2.1.6. Trial 6 – Heated Nauta

The final trial was designed to see whether the improved yield in trial 5 was caused by drying the powder or simply the increased temperature of the mixer wall. The water bath temperature was set to 65^{o}C prior to adding the powder. After powder was added it was immediately obvious that the layer between the screw and the wall never formed. This allowed very high amount of product to be recovered, with approximately 70g of heels remaining in the mixer, again mostly from condensation.

6.3.3.2.2. Yield

Table 6-17: Headline mass balance

Trial #	Solid mass in (kg)	Liquid mass in (kg)	Total mass in (kg)	Recoverable mass out (kg)	Heels (kg)	Mass loss (kg)	Recoverable yield	Yield excluding mass loss
1	4	1.4	5.4	4.5	0.7	0.2	83.3%	86.5%
2	7	2.4	9.4	7.4	1.6	0.4	78.7%	82.2%
3	6.2	2.2	8.4	6.9	1.5	0	82.1%	82.1%
4	5.6	2	7.6	6.5	0.81	0.29	85.5%	88.9%
5	6	2.1	8.1	7.5	0.07	0.53	92.6%	99.1%
6	5.7	2	7.7	7.4	0.07	0.23	96.1%	99.1%

As noted in observations the build-up obviously caused a significant drop in product yield. When the build-up was prevented (trials 5 and 6) there was a significantly higher yield. It is worth noting that the yields in both trials 5 and 6 are artificially low. In trial 5 this is because the product was intentionally dried at 100^{o}C for one hour, this will have evaporated considerable amounts of water, reducing the mass of product removed from the mixer. In trial 6 discharge was very slow (taking approximately 1.5 hours) at 65^{o}C, again this will have caused a not insignificant amount of evaporation, lowering the mass of the product recovered. This is shown in Table 6-18. This slow discharge is specifically a problem at small scale and will become less of a problem as the mixer (and so the orifice at the bottom) becomes larger. If needed it can also be designed out by having a side discharge from the mixer. This is something done regularly by Hosokawa.

Table 6-18: Component mass balance for Hosokawa trials

Trial	Initial moisture	Solid added (kg)	Solid present (kg)	Liquid added (%)	Liquid present (kg)	No loss moisture	Actual moisture	Moisture loss (kg)	Yield loss due to evaporation
1	4.1%	4.0	3.84	1.4	1.56	29.0%	26.9%	0.11	2.1%
2	4.1%	7.0	6.71	2.4	2.69	28.6%	26.7%	0.18	1.3%
3	4.1%	6.2	5.95	2.2	2.45	29.2%	27.9%	0.11	1.3%
4	4.1%	5.6	5.37	2.0	2.23	29.3%	27.1%	0.17	2.2%
5	4.1%	6.0	5.75	2.1	2.35	29.0%	23.1%	0.47	5.9%
6	4.1%	5.7	5.47	2.0	2.23	29.0%	26.5%	0.19	2.5%

From Table 6-18 we see that the majority of material loss from both the Nauta and CPM was due to liquid loss. This liquid loss is assumed to be from evaporation. It is worth noting evaporation was considerably lower in the CPM trials than the Nauta. This is likely to be because the Nauta took a long time to discharge and the surface is exposed, whereas the CPM discharged very quickly and had a lid. By minimising evaporation through fast discharge it is likely that this yield loss could be largely negated, allowing possible yields of 99%+.

6.3.3.2.3. Homogeneity

Observationally at the time; the product discharged from either mixer looked completely homogenous and lump free, as shown in Figure 6-36 for the discharge from the Nauta. This was confirmed through images taken after the samples arrived at JMTC, showing homogeneity values of 85-95, similar to that seen on the 5 L scale. However, it is worth noting that the sample bags had to be agitated by hand to mix liquid back into powder that seemed to have migrated during transport and storage. This clearly adds a non-representative step to the product processing history.

Figure 6-36: Discharge of Nauta mixer after trial 6

6.3.3.3. Conclusions

Both the Nauta and CPM mixers showed significant levels of build up when run at room temperature. However, increasing the temperature of the wall above 60^{o}C, through a heated water jacket, of the Nauta mixer prevented build up on the wall allowing very high product yields, up to 96% measured at the time. However, this is likely to be conservative as discharge from the mixer was slow and so there will have been a significant amount of evaporation. With a suitable product discharge system, reducing evaporation, it is conceivable to achieve yields of >98%. Without heating or when running in the CPM the yield was considerably lower; with 78.8% the lowest seen in the CPM and 82.1% in the Nauta.

Discharge from the Nauta mixer was very slow (except with the dried product) this is essentially caused by the scale of operation as the orifice at the bottom of the 20L mixer is very small. As you go up in scale the orifice also becomes larger, preventing the slow discharge seen at this scale. The CPM, with a larger orifice, gave very quick discharge.

Liquid addition technique seemed to have minimal impact on either the homogeneity of the product or the yield.

Drying inside the mixer also seemed feasible through use of the jacket. Drying could be further improved by the design of the mixer as Hosokawa have designs with lids that are capable of drawing a light vacuum, this would help prevent condensation and remove water vapor, increasing the drying rate.

It is not possible to assess the effect of moisture content as all trials were run targeting 26% or higher moisture, the highest used in any of the mixers and was not detrimental to yield or mixing. No lumps were formed in either mixer.

There are several recommendations and observations from trials on the Nauta for development of a production scale process:

- Scale-up
    - Nauta mixers scale easily. Hosokawa have a large range of sizes they produce mixers at and claim mixing performance is consistent across scales (up to 18m^3). This is consistent with experience within JM from Peter Johnston.
    - Increasing the scale will improve discharge performance with a larger orifice.
- Side discharge
    - Increase discharge rate
    - Less evaporation due to slow discharge
- Dry in place
    - 1 hour at 100°C (trial 5) dried off 300g more water than the 1.5 hour discharge at 65°C in trial 6.
    - Suggests drying is possible inside mixer
    - Can also get mixers with rounded lids and capable of drawing light vacuum to accelerate drying and minimise condensation

6.3.4. Overall Results

6.3.4.1. Effect of raw material batch

6.3.4.1.1. Flowable yield and raw material moisture

Over the course of the DoE, and vendor trials in 4 different mixers, it became apparent that the choice of raw zeolite batch had an effect on the process. This was visible in a number of ways and was perhaps most significant when looking at the moisture content/uptake of the raw material. Before each trial, a sample of the raw material was analysed for moisture content.

Figure 6-37 shows the distribution of these data. Batches 1 and 5 did not have enough trials to form a conclusion based on spread (consistency) of raw material moisture content, however it does appear that raw material does have an effect on moisture uptake of the feed. Generally,

batch 4 was the most consistent, with a lower moisture content, whereas batch 3 was far more variable. Batch 5 was the lowest, however it is hard to confirm that with only two measurements.

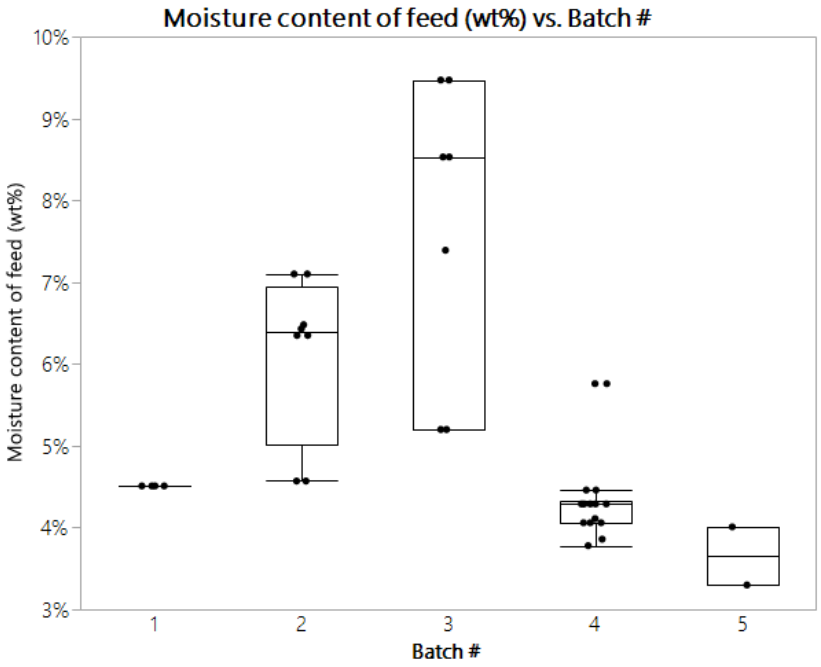

Figure 6-37: Moisture content in raw zeolite material batches

An additional effect of batch may be present in the flowable yield, however there are many confounding factors here, most significantly the variation in process parameters and mixer selection. The spread of results for the DBB and RB can be assessed (Figure 6-38), confirming that batch 4 looks more consistent.

As previously mentioned, the confounding effect of experimental parameter changes and mixer geometries make it difficult to properly assess the effect of batch on yield. A robust investigation would involve a larger number of batches being assessed across different mixers using comparable conditions and product moisture contents.

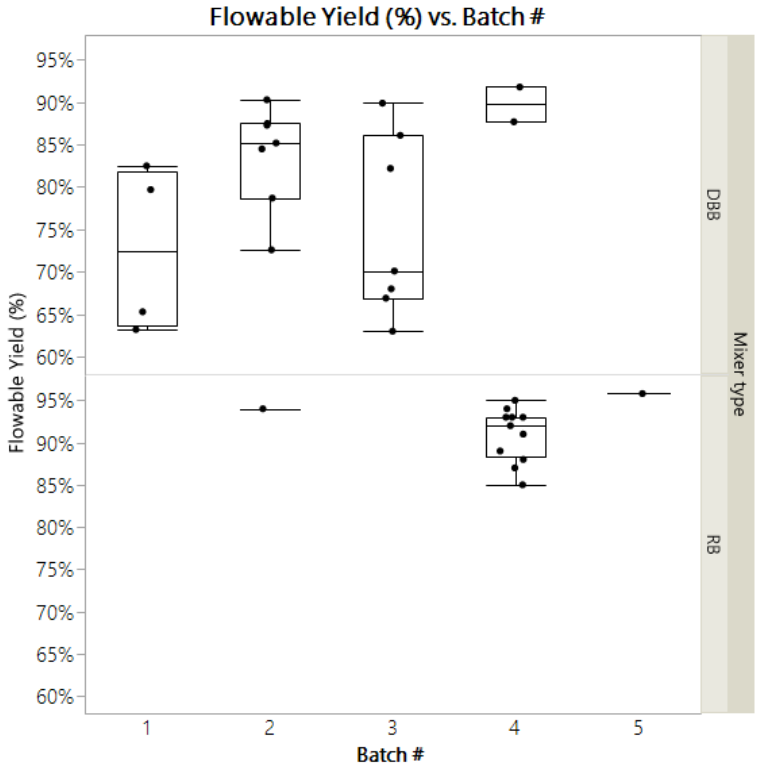

Figure 6-38: Flowable yield across different material batches, at 20% target product moisture for the RB and DBB

Clearly, batch is contributing something to the yield, as can be seen from Figure 6-39. Here two least squares models were built using only the DoE parameters; one included batch number and one did not. The increase of model predictive ability is clear, with an increase in R^2 from 0.96 to 1.00. This is only a minor increase, and least squares models (as opposed to PLS) can be subject to overfitting, however there is some useful variation that batch is bringing to the model.

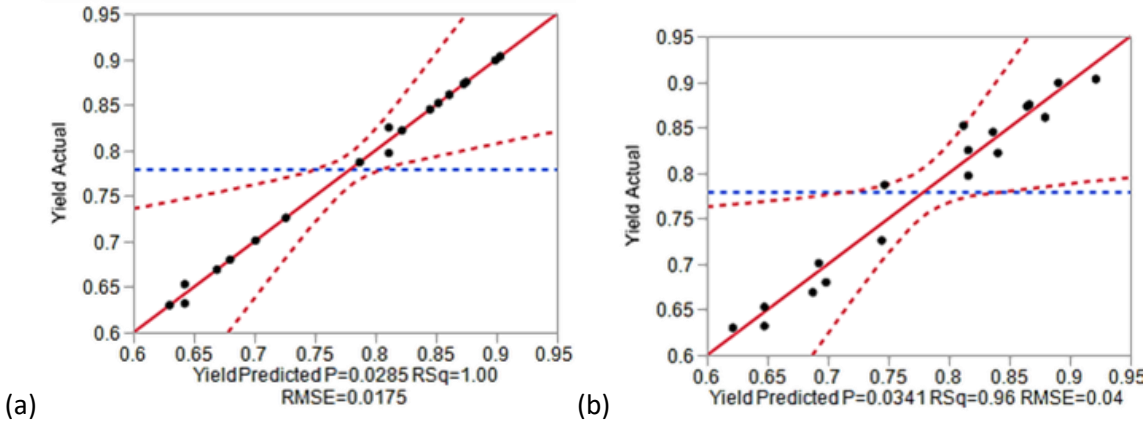

Figure 6-39: Flowable Yield predictions using DoE parameters in the DBB (a) with and (b) without batch number

6.3.4.1.2. Raw material properties

To assess the importance of the measured raw material properties on the outputs (yield, homogeneity, etc.), PCA can be used to calculate correlations between each set of variables. The colour map in Figure 6-40 shows the strength of these correlations, where red is positively correlated, blue is negatively correlated, and grey has no correlation. The following can be surmised from the PCA;

- There are no consistent univariate trends between powder properties of each batch (orange) and their resultant process outputs (green).
- Effect of batch properties is likely to be complex combination of factors.
- This PCA was performed with DBB data only (3 batches), as PSD data was not taken for other trials.

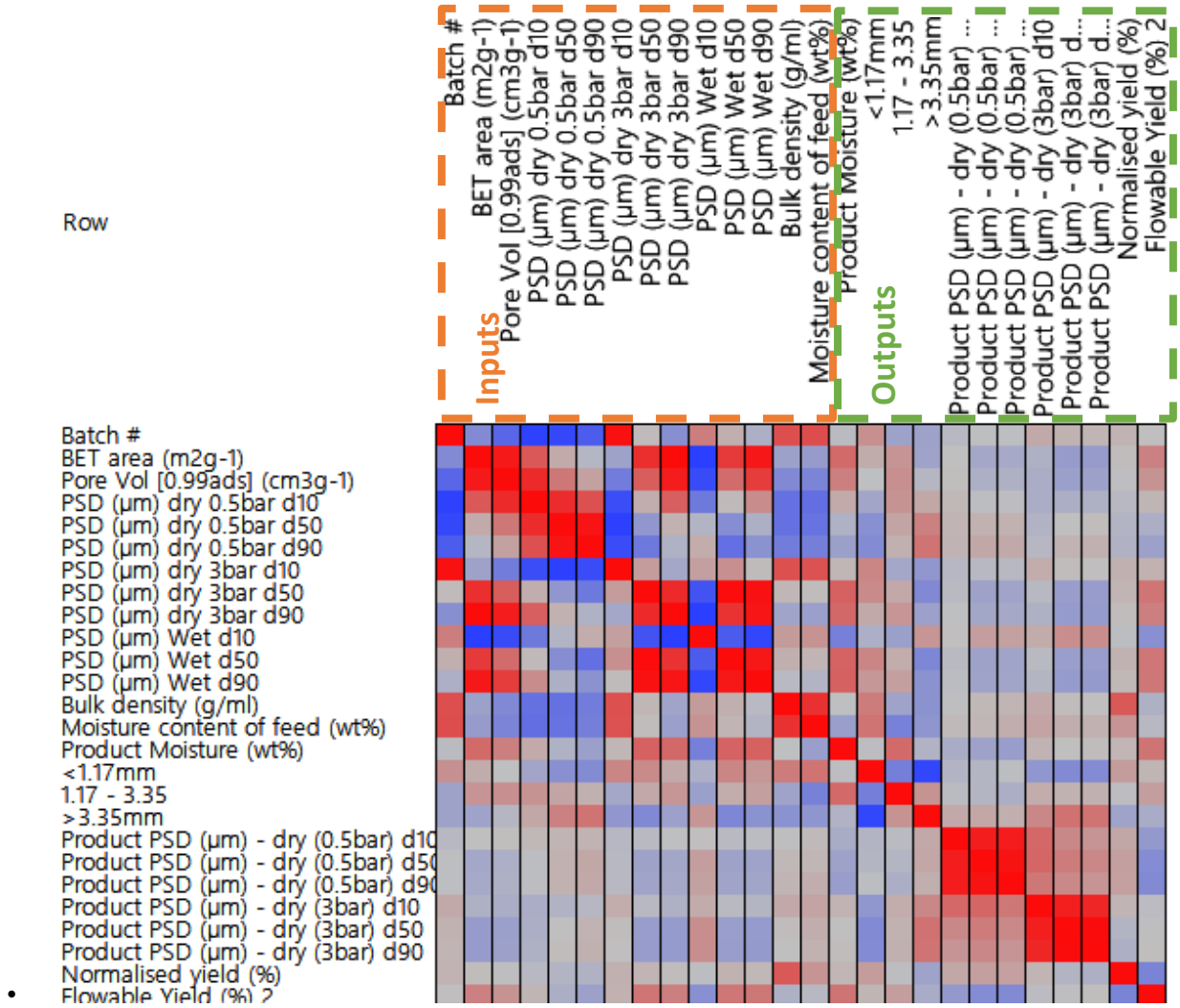

Figure 6-40: PCA correlations colour map for raw material properties and output parameters

6.3.4.2. Mixer comparisons

When comparing the DBB and RB results for product moisture and yield, it can be seen that the results are higher and far more consistent for the RB (Figure 83 c). However, this could be due to the use of mostly batch 4 for the RB trials which had a tighter distribution of raw zeolite moisture content. That being said, one of the runs in the RB was using batch 2, and this resulted in one of the best RB results.

One of the observations from the RB DoE trials was the formation of lumps, which appears to be a more significant issue than with the DBB, or with the Nauta/CPM mixers where there were no lumps formed. This can be seen in Figure 6-41, where a number of trials (generally those with low fill levels and low speeds) have significant lump formation. However, the key variables in lump formation were also shown to be fill level, speed, and flowrate/nozzle choice. Thus, reduction in lump formation should be possible by running the RB at the following conditions (as predicted by the RB DoE model): fill level 65%, speed 155 RPM, pressure 2 bar, PJ6 nozzle.

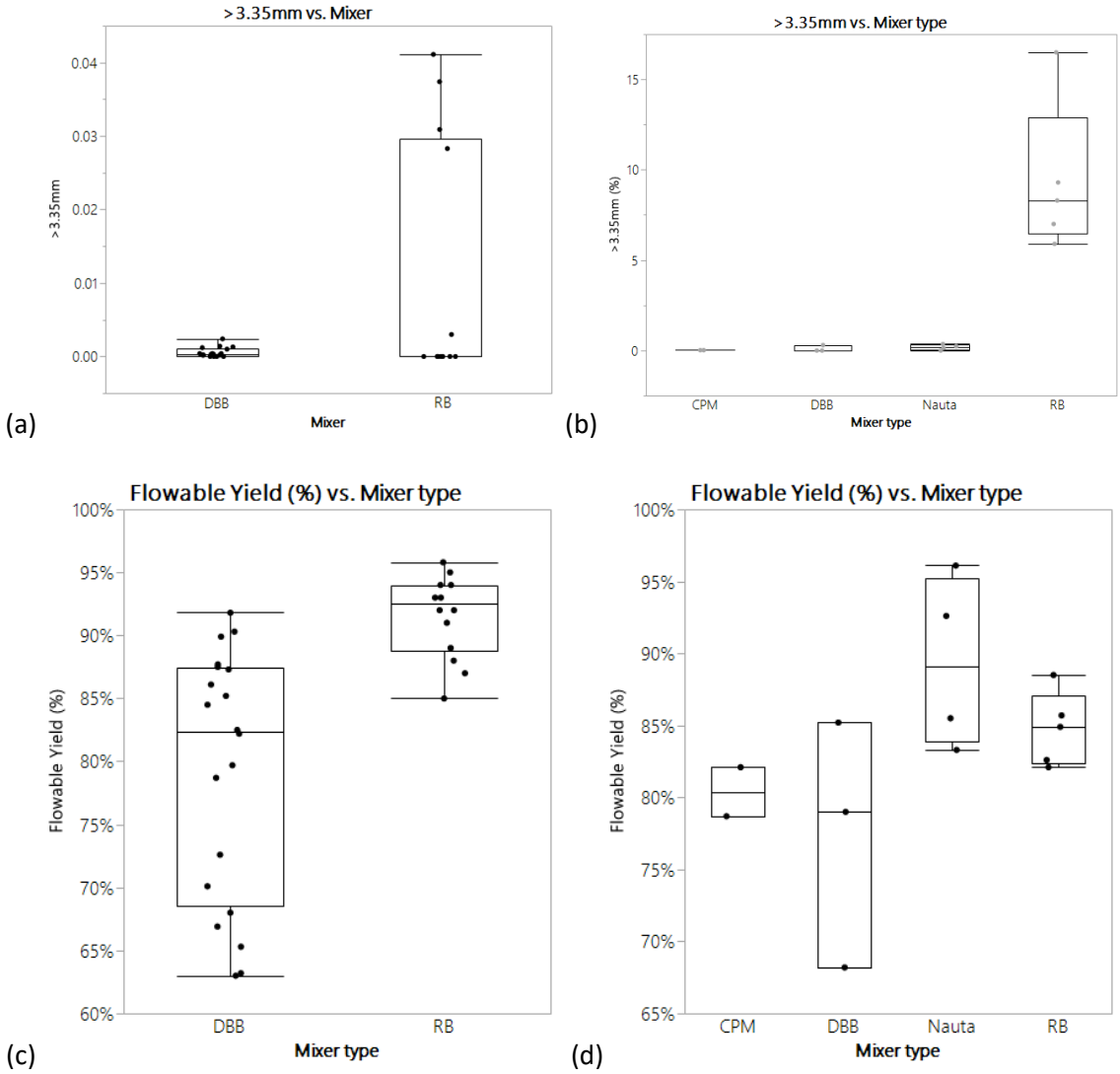

Figure 6-41: Comparison between mixers at 20% (a + c) and 26% product moisture (b + d), in terms of (a + b) sieving/lumps and (c + d) flowable yield.

With a limited number of trials able to run on the Nauta mixer it was not possible to 'optimise' the addition process. However, both the 5L and 20L Nauta showed 96%+ yields without any optimisation required. In both cases the majority of the mass lost was water due to evaporation as at these small scales discharge is very slow. Running at larger scale and rotating the screw downwards to drive the powder out of the mixer is likely to increase the yield even higher as it will minimise time for evaporation to occur.

6.3.4.3. Homogeneity

The difference in homogeneity values is shown clearly in Figure 6-42 which compares all image analysis measurements for all 18 DBB trials, 13 RB trials and 2 5L Nauta trials. From this we can see that the ribbon seems to produce consistently more homogenous product, with significantly less impact from external variables on the product quality.

In conclusion, the image analysis technique is useful to compare poorly mixed and well mixed samples. However, it is not a sufficiently robust technique to differentiate between two well mixed samples.

In terms of homogeneity of the dyed product the ribbon produced consistently good product whereas, the DBB was much more susceptible to operating condition causing poor mixing.

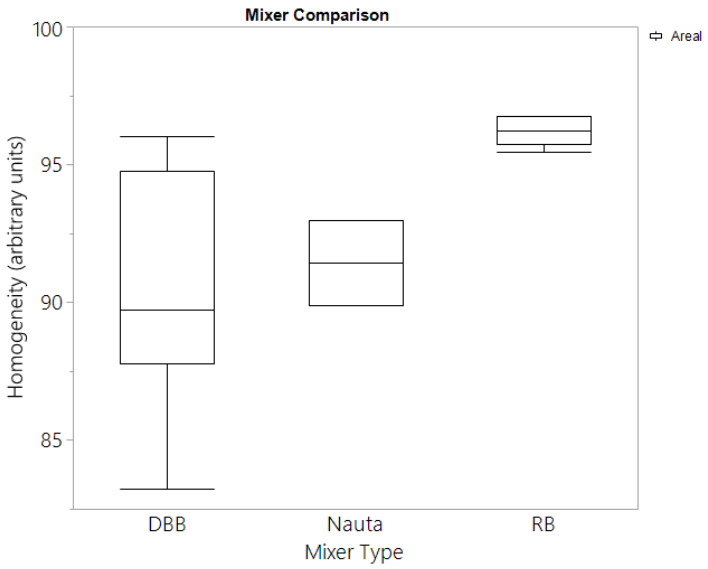

Figure 6-42: Comparison of homogeneity of product from DBB, RB, and Nauta trials

6.3.4.4. Model Comparison

For the double bowl blender two models were produced, one for homogeneity and one for yield. These models did not show conflicting variable dependencies and so it was possible to optimise for both outputs, as done for the 'best' and 'optimum' subsequent trials.

For the ribbon blender the homogeneity model was not useful as all trials showed very similar levels of homogeneity. Therefore, the only optimisation needed was done using the yield model.

6.4. Conclusions

All mixers studied, except for the CPM, were able to achieve > 90% yield, as shown in Table 6-19. The Vrieco-Nauta mixer showed the highest yield at over 96%. It is likely that at larger scales the Nauta would achieve even higher yields as the majority of lost material was due to evaporation during slow discharge, a problem that would become less severe at larger scale where the mixer orifice was larger. The double bowl showed the highest susceptibility to operating conditions; ranging from 63% - 91%. Whereas, the ribbon blender showed the most resilience to other factors affecting the yield with the smallest range; from 82% - 95%.

Table 6-19: Headline minimum and maximum yields for each mixer studied

	DBB	RB	CPM	Nauta 5L	Nauta 20L
Maximum Yield (%)	91.8%	95.8%	82.1%	96.4%	96.1%
Minimum Yield (%)	63.3%	82.1%	78.7%	90.1%	82.1%

The robust statistical design of experiments for both the ribbon and double bowl blenders allowed full process mapping and comparisons between the mixers. Optimal conditions within those spaces were determined, and the effect of the parameters on the process outputs evaluated. Specifically, fill level was the most significant variable for both the DBB and RB in terms of yield, in that higher fill levels equated to better flowable yields. It was also seen that longer, more gradual impregnations were beneficial in both mixers. For homogeneity and lump formation, RPM and raw material properties were key; higher speeds resulted in better homogeneity generally. Reasonably high quality, robust models were produced for all output parameters (e.g. yield, homogeneity, etc.), showing a good link between the chosen and measured variables and the process performances.

The high yield from the Nauta suggests that it is not affected by moisture content, with evaporation being the largest contributor to drop in yield. It is not possible to ascertain the effect of moisture content on CPM operability.

No lumps were seen in product from the DBB, Nauta or the CPM mixers at low or high moisture content. However, the ribbon blender showed significant lump formation with both ribbon and paddle shafts.

Specific batch number may well have affected the results, especially within the DBB DoE. However, it difficult to properly assess the effect of batch on yield. A robust investigation would involve a larger number of batches being assessed across different mixers using comparable conditions and product moisture contents. Different batches were found to be different colours when 'raw'. This prevented a universal calibration for the image analysis technique, making it less useful than it could have been if all initial material were the same.

The image analysis technique proved to be effective at comparing cases of poor mixing to cases of good mixing, such as across the scope of the DBB DoE. However, the technique cannot effectively compare between cases of good mixing, with all RB DoE trials essentially showing the same homogeneity within experimental error. One of the biggest challenges to this technique was the different starting colour of different batches. This meant external calibration, such as Beer-Lambert Law style plots of dye concentration vs colour, were not possible for comparisons between trials run with different batches. This is a problem with the technique, however, it can partially be overcome using internal calibration within each image.

7.

Overall Conclusions

The central objective of this thesis was to deliver fundamental engineering understanding of processes occurring during the wetting of porous catalyst support powders and use this knowledge to drive process improvements. Four major studies formed the basis of this thesis: understanding and optimising batch drawdown and incorporation processes, design of a continuous incorporation process, understanding what aspects of particulate solids determine their ease of incorporation into slurry, and optimisation of an incipient wetness impregnation process.

In this Chapter the outcomes of each of these studies, and the thesis as a whole, are discussed with respect to the primary aims of the thesis set out in Chapter 1. This thesis describes optimum conditions for both a batch drawdown process and an incipient wetness impregnation process, as well as a full, proven, manufacturing scale design of a continuous powder incorporation process. Finally, future possibilities for this work are discussed.

7.1. Reflection on Project Aims

- **To use experimental techniques to deliver scientific understanding of powder incorporation processes. Including:**
    - ***Understanding of how changes in the slurry affect processing as the slurry becomes more concentrated***

This thesis demonstrates the effect of high solid content systems on the drawdown and incorporation of floating solids in stirred vessels. At low solid contents mixed flow impellers out performed either radial or axial flow impellers tested. This is true for the entire range of solid contents studied (up to 50 % by weight). However, at the very highest solid contents (40 %+) the mechanism of powder incorporation changed: The central vortex collapses at this point such that solid is no longer brought directly to the impeller. Instead clumps of semi-wetted powder tend to form into agglomerates and then sink below the surface as fluid motion wets them to a sufficient density to overcome buoyancy forces on them. At this point the sawtooth impellers studied went from being the worst impeller at low solids to one of the better performing ones, this suggests that high shear is beneficial in achieving very high solid contents.

    - ***How powder drawdown and incorporation scales from the laboratory to production scale in stirred vessels***

Scaling on a constant N^3D is found to predict most accurately the scale up from a 5 L vessel to 25 L with geometric similarity for both up and down pumping PBTs up to around 40 % by weight solid content. This was the maximum concentration before the vortex collapsed in all systems tested and coincides with a constant Reynolds Number better predicting the change in impeller speed required to maintain drawdown. This concentration, approximately 40 % by weight solids for this specific powder, is also where a flow transition from turbulent (or constant power number) to laminar seems to occur, which has been demonstrated by analysis of the apparent power number

of the impeller at that point, which shows very little transitional flow behaviour. At solid contents higher than this scaling on a constant Reynolds number (constant ND^2) from the transition point most accurately predicts behaviour across scales.

- ***Understanding of how various powder properties affect their behaviour when being wet.***

The ease with which a powder is incorporated into a slurry is defined in this thesis as the *slurryability* of the powder and is measured in three distinct ways: The time required to achieve a 50 wt% solid content slurry in a fixed vessel geometry configuration, the energy required to achieve the same, and a threshold slurry concentration at which it requires more than 1 kJ to increase the solid content by a further 1 % in the vessel studied.

Partial least squares models are built which predict the slurryability of a powder based on its key properties. The most significant properties, based on variable importance in projection scores, are:

- Particle pore volume
- Pressure drop result of the Freeman FT4 powder rheometer permeability test
- Powder aeration energy measured on the Freeman FT4 powder rheometer
- Powder tapped density
- Powder poured density
- D_{50} particle size of the powder

By measuring these six properties it is shown to be possible to predict the slurryability of two validation powders, not present in the original training dataset, to an error in threshold concentration of ±10 %.

- ***Deliver a step change in manufacturing processing to increase the output of powder incorporation processes.***

A fully continuous process has been designed and tested for the incorporation of powders into concentrated slurries. This process has been validated at production scale for a number of different products including alumina, zeolite, and mixed oxide slurries for catalyst support applications.

This system was also expanded to be relevant to business units within the sponsor company beyond the original partner. These other applications included preparation of a high concentrated ink slurry formulation for automotive glass and pre-heated magnesia slurries for fluid catalytic cracking catalyst production.

All applications tested on this design functioned to specification at full production rates. The designed process resulting from this thesis was advanced within the sponsor company through Hansard Study 3 and detailed design for implementation on plant.

- **Describe the design space and optimisation criteria for a range of powder wetting processes, including an understanding of scale up from laboratory to manufacturing scale.**
    - ***Powder drawdown and incorporation in stirred vessels***

The impeller speed and power required to just drawdown and incorporate a fixed mass of powder was defined as the *just incorporation* condition. Minimising this condition was used as an optimisation criterion for studies of a batch incorporation process.

Both scoping one-at-a-time and Design of Experiments approaches were used throughout this thesis to find an optimal geometric configuration for drawdown and incorporation in stirred vessels. The impact of solid concentration was found to significantly impact the optimal

geometry, with this most obviously shown by the effect of baffles within the vessel. At low solid concentration, baffles reduced full body rotation of the fluid, increasing the power performance of the impeller and improved drawdown performance. However, above 10 wt% solid concentration the baffles began to inhibit drawdown, preventing further powder being incorporated into slurry.

The optimum impeller configuration was found to be a down pumping pitched blade turbine with a large diameter (50 % of the tank diameter). This was optimally placed at around half the vessel diameter above the bottom of the vessel, when the initial liquid height was equal to the vessel diameter. Further improvements were made by either tilting and/or moving the impeller eccentric by 10^{o} and 10 % of the vessel diameter respectively.

Combined, this optimised geometry showed a significant performance improvement over a standard impeller configuration, reducing the time required to prepare a 50 wt% slurry by two thirds.

- ***Incipient wetness impregnation of dry powder with catalyst solution***

An image analysis technique was designed to allow measurement of homogeneity in powder processed through an incipient wetness impregnation. This, along with the product yield from the mixer, was used as optimisation criteria for the process.

Three separate mixers were studied for their suitability for incipient wetness impregnation processes. The Nauta mixer showed the best product yield, despite being the least studied of the mixers and so not fully optimised. A key learning from the Nauta was that heating the walls above $50^{o}C$ prevented material from sticking, greatly increasing the possible yield.

Full optimal conditions were found for both a ribbon blender and a double bowl blender. Of all three mixers the ribbon blender showed the most homogeneous product and an intermediate

yield. The double bowl blender showed the lowest yield and least homogeneity. It also showed the most fragility to changes in process parameters and disturbance variables.

7.2. Context and Future Work

Implementation of scale-up to larger scales:

The scale up study presented in Chapter 2 shows scaling rules between 5 and 25 L, where a constant N^3D most reliably predicts the just incorporation condition between scales below the transition concentration, and constant Reynolds number above. It would be interesting to increase the size of vessels studied further to show whether the predictive performance of these scaling rules is maintained between larger scale differences.

The next stage for Johnson Matthey is to implement the optimal designs found in Chapters 2 and 3 at pilot scale to test their efficacy for drawdown of various production powders.

Combining slurryability and stirred vessel optimisation:

The optimal stirred vessel geometry found in Chapters 2 and 3 was based on studies using a single powder, that was found to have a high slurryability in Chapter 5. It would make an interesting study to see how the optimisation changes when studying less slurryable powders, when the transition from turbulent mixing to apparently laminar flow occurs at lower solid concentrations. This would be a particularly useful study for industry as it would allow determination of ideal mixing configurations for specific powders and specification solid concentrations.

Implementation of continuous incorporation process

A fully designed continuous powder incorporation process is described in this thesis in Chapter 4. The final remaining technical risk highlighted throughout the project that Johnson Matthey does not have sufficient data to answer is to ascertain the level of wear on the moving parts of the continuous mixer. The next stage of this project required to answer this risk is to build a pilot or

production scale line and operate for 1000+ hours. This was unfeasible at JMTC due to the amount of slurry that would be required to be produced.

Extending Slurryability Study

In Chapter 5 predictive PLS models are built to predict the slurryability of support material powders based on six fundamental properties. These models are built on a training dataset of thirteen powders and over 40 measured properties. These models are shown to predict the slurryability of two powders not included in the training dataset within an error of ±10 %. This study could be further improved by adding more powders and more properties to the training dataset. For example there are relatively few powders studied at low slurryability, giving the model less discrimination in this range. Therefore, adding more powders to the training dataset with low slurryabilities is likely to improve the model prediction performance.

Although the effect of interfacial tension was shown to have little correlation with a powders slurryability it would be interesting to probe this further by measuring the solid surface free energy, using the Owens Wendt Rabel and Kaelble method described in Chapter 5. This would enable measurement of the solid material property, rather than simply its apparent contact angle with water.

Heating Surfaces of other mixers for IWI

It was found during trials on the Vrieco-Nauta mixer that heating the vessel walls prevented a static layer of moist powder becoming irretrievably stuck to the wall, dramatically reducing the effective yield from the process. Neither the DBB or RB mixers tested were capable of heating the vessel walls. However, an interesting study would be to modify these existing mixers to allow a water jacket to be used, heating the walls to investigate whether the yield from these mixers could be improved.

8.

References

A. Alzaydi, A. (1975). Flow of Gases through Porous Media.

Acres, G.J.K. and Harrison, B. (2004). The Development of Catalysts for Emission Control from Motor Vehicles: Early Research at Johnson Matthey. *Topics in Catalysis* **28**(1–4):3–11. doi: https://doi.org/10.1023/B:TOCA.0000024329.85506.94.

Adegbite, S. (2010). *COATING OF CATALYST SUPPORTS: LINKS BETWEEN SLURRY CHARACTERISTICS, COATING PROCESS AND FINAL COATING QUALITY*. PhD, University of Birmingham.

Adrian, R.J. and Westerweel, J. (2011). *Particle Image Velocimetry*. Cambridge University Press.

Agashe, null and Regalbuto, null (1997). A Revised Physical Theory for Adsorption of Metal Complexes at Oxide Surfaces. *Journal of Colloid and Interface Science* **185**(1):174–189.

Agrafiotis, C. and Tsetsekou, A. (2000). The effect of processing parameters on the properties of γ-alumina washcoats deposited on ceramic honeycombs. *Journal of Materials Science* **35**(4):951–960. doi: https://doi.org/10.1023/A:1004762827623.

Agrafiotis, C., Tsetsekou, A. and Ekonomakou, A. (1999). The effect of particle size on the adhesion properties of oxide washcoats on cordierite honeycombs. *Journal of Materials Science Letters* **18**(17):1421–1424. doi: https://doi.org/10.1023/A:1006675524692.

Agrawal, Y.K. (2016). *Towards Turbulence Modulation in Concentrated Solid-Liquid Flows*. Master's, University of Alberta.

Akarachantachote, N., Chadcham, S. and Saithanu, K. (2014). Cutoff threshold of variable importance in projection for variable selection. *International Journal of Pure and Apllied Mathematics* **94**. doi: https://doi.org/10.12732/ijpam.v94i3.2.

Ammarcha, C., Gatumel, C., Dirion, J.L., Cabassud, M. and Berthiaux, H. (2017). Continuous powder mixing of segregating mixtures under steady and unsteady state regimes: Homogeneity assessment by real-time on-line image analysis. *Powder Technology* **315**:39–52. doi: https://doi.org/10.1016/j.powtec.2017.02.010.

Anderson, N.G. (2001). Practical Use of Continuous Processing in Developing and Scaling Up Laboratory Processes. *Organic Process Research & Development* **5**(6):613–621. doi: https://doi.org/10.1021/op0100605.

Andersson, J.M. (2005). *Controlling the Formation and Stability of Alumina Phases*. Ph.D, Linköping University.

Ansorena, D. (Diana), Peña, M.P. (María P. de, Astiasarán, I. (Iciar) and Bello, J. (José) (1997). Colour evaluation of chorizo de Pamplona, a Spanish dry fermented sausage: Comparison between the CIE L(∗)a(∗)b(∗) and the Hunter lab systems with illuminants D65 and C.

Avila, P., Montes, M. and Miró, E.E. (2005). Monolithic reactors for environmental applications: A review on preparation technologies. *Chemical Engineering Journal* **109**(1):11–36. doi: https://doi.org/10.1016/j.cej.2005.02.025.

Badman, C. and Trout, B.L. (2015). Achieving Continuous Manufacturing May 20–21 2014 Continuous Manufacturing Symposium. *Journal of Pharmaceutical Sciences* **104**(3):779–780. doi: https://doi.org/10.1002/jps.24246.

Basinskas, G. and Sakai, M. (2016). Numerical study of the mixing efficiency of a ribbon mixer using the discrete element method. *Powder Technology* **287**:380–394. doi: https://doi.org/10.1016/j.powtec.2015.10.017.

Benson, T. (2009). *Surfance Oil Flow*. Available at: http://www.grc.nasa.gov/WWW/k-12/airplane/tunvoil.html [Accessed: 4 April 2014].

BETE (2017). BETE Nozzles. *BETE Brochures*.

BETE (2018). *Fine Fog Nozzles | PJ Series Impingement Nozzles*. Available at: https://www.bete.com/products/pj [Accessed: 15 August 2018].

Bharadwaj, R., Ketterhagen, W.R. and Hancock, B.C. (2010). Discrete element simulation study of a Freeman powder rheometer. *Chemical Engineering Science* **65**(21):5747–5756. doi: https://doi.org/10.1016/j.ces.2010.04.002.

Binks, B.P. and Whitby, C.P. (2005). Nanoparticle silica-stabilised oil-in-water emulsions: improving emulsion stability. *Colloids and Surfaces A: Physicochemical and Engineering Aspects* **253**(1):105–115. doi: https://doi.org/10.1016/j.colsurfa.2004.10.116.

Bodke, A.S., Bharadwaj, S.S. and Schmidt, L.D. (1998). The Effect of Ceramic Supports on Partial Oxidation of Hydrocarbons over Noble Metal Coated Monoliths. *Journal of Catalysis* **179**(1):138–149. doi: https://doi.org/10.1006/jcat.1998.2224.

Bohidar, N.R., Restaino, F.A. and Schwartz, J.B. (1975). Selecting key parameters in pharmaceutical formulations by principal component analysis. *Journal of Pharmaceutical Sciences* **64**(6):966–969. doi: https://doi.org/10.1002/jps.2600640615.

Bontha, J.R., Colton, N.G., Daymo, E.A., Hylton, T.D., Bayne, C.K. and May, T.H. (2000). *Qualification of the Lasentec M600P Particle Size Analyzer and the Red Valve Model 1151 Pressure Sensor*. Pacific Northwest National Lab., Richland, WA (US).

Bowker, M., Nuhu, A. and Soares, J. (2007). High activity supported gold catalysts by incipient wetness impregnation. *Catalysis Today* **122**(3):245–247. doi: https://doi.org/10.1016/j.cattod.2007.01.021.

Braun, J.H., Baidins, A. and Marganski, R.E. (1992). TiO2 pigment technology: a review. *Progress in Organic Coatings* **20**(2):105–138. doi: https://doi.org/10.1016/0033-0655(92)80001-D.

Bridgwater, J. (1976). Fundamental powder mixing mechanisms. *Powder Technology* **15**(2):215–236. doi: https://doi.org/10.1016/0032-5910(76)80051-4.

Brookfield Ametek (2018). What is Powder Flow Analysis?

Brown, G.E., Henrich, V.E., Casey, W.H., Clark, D.L., Eggleston, C., Felmy, A., … Zachara, J.M. (1999). Metal Oxide Surfaces and Their Interactions with Aqueous Solutions and Microbial Organisms. *Chemical Reviews* **99**(1):77–174. doi: https://doi.org/10.1021/cr980011z.

Brunelle, J.P. (1979). Preparation of Catalysts by Adsorption of Metal Complexes on Mineral Oxides**Published in Pure Appl. Chem., 50, 9-10 (1978), p. 1211. In: Delmon, B., Grange, P., Jacobs, P. and Poncelet, G. (eds.). *Studies in Surface Science and Catalysis*. Elsevier, pp. 211–232.

Buckton, G. (1988). The assessment, and pharmaceutical importance, of the solid/liquid and the solid/vapour interface: a review with respect to powders. *International Journal of Pharmaceutics* **44**(1):1–8. doi: https://doi.org/10.1016/0378-5173(88)90093-2.

Cabaret, F., Bonnot, S., Fradette, L. and Tanguy, P.A. (2007). Mixing Time Analysis Using Colorimetric Methods and Image Processing. *Industrial & Engineering Chemistry Research* **46**(14):5032–5042. doi: https://doi.org/10.1021/ie0613265.

Calabrese, G.S. and Pissavini, S. (2011). From batch to continuous flow processing in chemicals manufacturing. *AIChE Journal* **57**(4):828–834. doi: https://doi.org/10.1002/aic.12598.

Caporaso, N., Whitworth, M.B., Fowler, M.S. and Fisk, I.D. (2018). Hyperspectral imaging for non-destructive prediction of fermentation index, polyphenol content and antioxidant activity in single cocoa beans. *Food Chemistry* **258**:343–351. doi: https://doi.org/10.1016/j.foodchem.2018.03.039.

Carman, P.C. (1938). The determination of the specific surface of powders. *J. Soc. Chem. Ind.* **57**:225–234.

Carr, R.L. (1965). Evaluating flow properties of solids.

Carter, P.A., Rowley, G., Fletcher, E.J. and Hill, E.A. (1992). An experimental investigation of triboelectrification in cohesive and non-cohesive pharmaceutical powders. *Drug Development and Industrial Pharmacy* **18**(14):1505–1526. doi: https://doi.org/10.3109/03639049209040855.

Chandratilleke, G.R., Dong, K.J. and Shen, Y.S. (2018). DEM study of the effect of blade-support spokes on mixing performance in a ribbon mixer. *Powder Technology* **326**:123–136. doi: https://doi.org/10.1016/j.powtec.2017.12.055.

Chang, F.-W., Kuo, M.-S., Tsay, M.-T. and Hsieh, M.-C. (2003). Hydrogenation of CO2 over nickel catalysts on rice husk ash-alumina prepared by incipient wetness impregnation. *Applied Catalysis A: General* **247**(2):309–320. doi: https://doi.org/10.1016/S0926-860X(03)00181-9.

Chapple, D., Kresta, S.M., Wall, A. and Afacan, A. (2002). The Effect of Impeller and Tank Geometry on Power Number for a Pitched Blade Turbine. *Chemical Engineering Research and Design* **80**(4):364–372. doi: https://doi.org/10.1205/026387602317446407.

Chauruka, S.R., Hassanpour, A., Brydson, R., Roberts, K.J., Ghadiri, M. and Stitt, H. (2015). Effect of mill type on the size reduction and phase transformation of gamma alumina. *Chemical Engineering Science* **134**:774–783. doi: https://doi.org/10.1016/j.ces.2015.06.004.

Chilekar, V.P., Schaaf, J. van der, Kuster, B.F.M., Tinge, J.T. and Schouten, J.C. (2009). Influence of elevated pressure and particle lyophobicity on hydrodynamics and gas–liquid mass transfer in slurry bubble columns. *AIChE Journal* **56**(3):584–596. doi: https://doi.org/10.1002/aic.11987.

Chou, K.-S. and Lee, L.-J. (2005). Effect of Dispersants on the Rheological Properties and Slip Casting of Concentrated Alumina Slurry. *Journal of the American Ceramic Society* **72**(9):1622–1627. doi: https://doi.org/10.1111/j.1151-2916.1989.tb06293.x.

Chung, K.H.K. (2008). *MIXING IN HIGH THROUGHPUT EXPERIMENTATION REACTORS*. PhD, University of Birmingham.

Cooper, B.J. (1983). *Durability of Platinum-Containing Automotive Exhaust Control Catalysts*. Available at: https://www.ingentaconnect.com/content/matthey/pmr/1983/00000027/00000004/art00001 [Accessed: 15 August 2018].

Cybulski, A. and Moulijn, J.A. (2005). *Structured Catalysts and Reactors*. CRC Press.

Dang Vu, T. and Jan, H. (2005). Characterization of porous materials by capillary rise method. *Physicochemical Problems of Mineral Processing* **39**.

Dickinson, E. (2010). Food emulsions and foams: Stabilization by particles. *Current Opinion in Colloid & Interface Science* **15**(1):40–49. doi: https://doi.org/10.1016/j.cocis.2009.11.001.

Dickinson, E. (2012). Use of nanoparticles and microparticles in the formation and stabilization of food emulsions. *Trends in Food Science & Technology* **24**(1):4–12. doi: https://doi.org/10.1016/j.tifs.2011.09.006.

Drelich, J., Miller, J.D. and Hupka, J. (1993). The Effect of Drop Size on Contact Angle over a Wide Range of Drop Volumes. *Journal of Colloid and Interface Science* **155**(2):379–385. doi: https://doi.org/10.1006/jcis.1993.1050.

Einstein, A. (1906). Eine neue Bestimmung der Moleküldimensionen. *Annalen der Physik* **324**(2):289–306. doi: https://doi.org/10.1002/andp.19063240204.

Eshel, G., Levy, G.J., Mingelgrin, U. and Singer, M.J. (2004). Critical Evaluation of the Use of Laser Diffraction for Particle-Size Distribution Analysis. *Soil Science Society of America Journal* **68**(3):736–743. doi: https://doi.org/10.2136/sssaj2004.7360.

Espinoza, C.J.U., Simmons, M.J.H., Alberini, F., Mihailova, O., Rothman, D. and Kowalski, A.J. (2018). Flow studies in an in-line Silverson 150/250 high shear mixer using PIV. *Chemical Engineering Research and Design* **132**:989–1004. doi: https://doi.org/10.1016/j.cherd.2018.01.028.

European Commission (2012). *Commission Regulation (EU) No 459/2012 of 29 May 2012 Amending Regulation (EC) No 715/2007 of the European Parliament and of the Council and Commission Regulation (EC) No 692/2008 as Regards Emissions from Light Passenger and Commercial Vehicles (Euro 6) Text with EEA Relevance*.

Fleming, S.E., Sosulski, F.W., Kilara, A. and Humbert, E.S. (2006). Viscosity and Water Absorption Charactercstics of Slurries of Sunflower and Soybean Flours, Concentrates and Isolates. *Journal of Food Science* **39**(1):188–192. doi: https://doi.org/10.1111/j.1365-2621.1974.tb01019.x.

Francia, V., Martín, L., Bayly, A.E. and Simmons, M.J.H. (2015). The role of wall deposition and re-entrainment in swirl spray dryers. *AIChE Journal* **61**(6):1804–1821. doi: https://doi.org/10.1002/aic.14767.

Freudig, B., Hogekamp, S. and Schubert, H. (1999). Dispersion of powders in liquids in a stirred vessel. *Chemical Engineering and Processing: Process Intensification* **38**(4–6):525–532. doi: https://doi.org/10.1016/S0255-2701(99)00049-5.

Gabriele, A., Tsoligkas, A.N., Kings, I.N. and Simmons, M.J.H. (2011). Use of PIV to measure turbulence modulation in a high throughput stirred vessel with the addition of high Stokes number particles for both up- and down-pumping configurations. *Chemical Engineering Science* **66**(23):5862–5874. doi: https://doi.org/10.1016/j.ces.2011.08.007.

Galet, L., Patry, S. and Dodds, J. (2010). Determination of the wettability of powders by the Washburn capillary rise method with bed preparation by a centrifugal packing technique. *Journal of Colloid and Interface Science* **346**(2):470–475. doi: https://doi.org/10.1016/j.jcis.2010.02.051.

Germani, G., Stefanescu, A., Schuurman, Y. and van Veen, A.C. (2007). Preparation and characterization of porous alumina-based catalyst coatings in microchannels. *Chemical Engineering Science* **62**(18):5084–5091. doi: https://doi.org/10.1016/j.ces.2007.02.034.

Gonnissen, Y., Gonçalves, S.I.V., De Geest, B.G., Remon, J.P. and Vervaet, C. (2008). Process design applied to optimise a directly compressible powder produced via a continuous manufacturing process. *European Journal of Pharmaceutics and Biopharmaceutics* **68**(3):760–770. doi: https://doi.org/10.1016/j.ejpb.2007.09.007.

Gore, R.A. and Crowe, C.T. (1989). Effect of particle size on modulating turbulent intensity. *International Journal of Multiphase Flow* **15**(2):279–285. doi: https://doi.org/10.1016/0301-9322(89)90076-1.

Gulicovski, J.J., Čerović, L.S. and Milonjić, S.K. (2008). Point of Zero Charge and Isoelectric Point of Alumina. *Materials and Manufacturing Processes* **23**(6):615–619. doi: https://doi.org/10.1080/10426910802160668.

Gurden, S.P., Martin, E.B. and Morris, A.J. (1998). The introduction of process chemometrics into an industrial pilot plant laboratory. *Chemometrics and Intelligent Laboratory Systems* **44**(1):319–330. doi: https://doi.org/10.1016/S0169-7439(98)00119-1.

Haaland, D.M. and Thomas, E.V. (1988). Partial least-squares methods for spectral analyses. 1. Relation to other quantitative calibration methods and the extraction of qualitative information. *Analytical Chemistry* **60**(11):1193–1202. doi: https://doi.org/10.1021/ac00162a020.

Halidan, M., Chandratilleke, G.R., Dong, K.J. and Yu, A.B. (2018). Mixing performance of ribbon mixers: Effects of operational parameters. *Powder Technology* **325**:92–106. doi: https://doi.org/10.1016/j.powtec.2017.11.009.

Hall, J.F., Barigou, M., Simmons, M.J.H. and Stitt, E.H. (2004). Mixing in Unbaffled High-Throughput Experimentation Reactors. *Industrial & Engineering Chemistry Research* **43**(15):4149–4158. doi: https://doi.org/10.1021/ie049872q.

Hall, J.R., Barigou, M., Simmons, M.J.H. and Stitt, E.H. (2005). A PIV study of hydrodynamics in gas-liquid high throughput experimentation (HTE) reactors with eccentric impeller configurations. *Chemical Engineering Science* **60**(22):6403–6413. doi: https://doi.org/10.1016/j.ces.2005.03.044.

Harnby, N., Edwards, M.F. and Nienow, A.W. (1997). *Mixing in the Process Industries: Second Edition*. 1st ed. Butterworth-Heinemann.

Harwood, C.F., Walanski, K., Luebcke, E. and Swanstrom, C. (1975). The performance of continuous mixers for dry powders. *Powder Technology* **11**(3):289–296. doi: https://doi.org/10.1016/0032-5910(75)80054-4.

Hausner, H.H. (1966). FRICTION CONDITIONS IN A MASS OF METAL POWDER. *Int. J. Powder Met., 3: No. 4, 7-13(Oct. 1967).*

Hemrajani, R.R. (1988). Suspending floating solids in stirred tanks: mixer design, scale-up and optimization. Pavia, Italy, pp. 259–265.

Hersey, J.A. (1975). Ordered mixing: A new concept in powder mixing practice. *Powder Technology* **11**(1):41–44. doi: https://doi.org/10.1016/0032-5910(75)80021-0.

Heymann, L., Peukert, S. and Aksel, N. (2002). On the solid-liquid transition of concentrated suspensions in transient shear flow. *Rheologica Acta* **41**(4):307–315. doi: https://doi.org/10.1007/s00397-002-0227-1.

Hirsch, R. (2004). *Exploring Colour Photography: A Complete Guide*. Laurence King.

Hunt, J.C.R., Abell, C.J., Peterka, J.A. and Woo, H. (1978). Kinematical studies of the flows around free or surface-mounted obstacles; applying topology to flow visualization. *Journal of Fluid Mechanics* **86**(1):179–200. doi: https://doi.org/10.1017/S0022112078001068.

Hunter, R.J. (2013). *Zeta Potential in Colloid Science: Principles and Applications*. Academic Press.

Hunter, R.S. (1958). Photoelectric Color Difference Meter*. *JOSA* **48**(12):985–995. doi: https://doi.org/10.1364/JOSA.48.000985.

IKA Process GmbH (2017). http://www.ikaprocess.com/ika/pdf/flyer-catalog/20161213_magic_LAB_brochure_IWS_EN_94000211_screen.pdf. *IKA MagicLAB Brochure*.

Ince, H. and Trafalis, T.B. (2007). Kernel principal component analysis and support vector machines for stock price prediction. *IIE Transactions* **39**(6):629–637. doi: https://doi.org/10.1080/07408170600897486.

Ionescu, A., Allouche, A., Aycard, J.-P., Rajzmann, M. and Hutschka, F. (2002). Study of γ-Alumina Surface Reactivity: Adsorption of Water and Hydrogen Sulfide on Octahedral Aluminum Sites. *The Journal of Physical Chemistry B* **106**(36):9359–9366. doi: https://doi.org/10.1021/jp020145n.

IPA (2014). *IPA - International Platinum Group Metals Association - Catalytic Converters*. Available at: https://ipa-news.com/index/pgm-applications/automotive/catalytic-converters/ [Accessed: 13 August 2018].

J Pierce, A., Lu, F., S Bryant, D. and Shih, Y. (2010). New Developments in Surface Oil Flow Visualization. *27th AIAA Aerodynamic Measurement Technology and Ground Testing Conference 2010*. doi: https://doi.org/10.2514/6.2010-4353.

Jia, L., Shen, M. and Wang, J. (2007). Preparation and characterization of dip-coated γ-alumina based ceramic materials on FeCrAl foils. *Surface and Coatings Technology* **201**(16):7159–7165. doi: https://doi.org/10.1016/j.surfcoat.2007.01.023.

Johnson Matthey (2018). *Annual Report 2018 | Johnson Matthey*. Available at: https://matthey.com/investors/report-archive/annual-report-2018 [Accessed: 12 August 2018].

Joosten, G.E.H., Schilder, J.G.M. and Broere, A.M. (1977). SUSPENSION OF FLOATING SOLIDS IN STIRRED VESSELS. *Transactions of the Institution of Chemical Engineers* **55**(3):220–222.

Kaelble, D.H. (1970). Dispersion-Polar Surface Tension Properties of Organic Solids. *The Journal of Adhesion* **2**(2):66–81. doi: https://doi.org/10.1080/0021846708544582.

Kanan, C. and Cottrell, G.W. (2012). Color-to-Grayscale: Does the Method Matter in Image Recognition? *PLOS ONE* **7**(1):e29740. doi: https://doi.org/10.1371/journal.pone.0029740.

Karcz, J. and Mackiewicz, B. (2009). Effects of vessel baffling on the drawdown of floating solids. *Chemical Papers* **63**(2):164–171. doi: https://doi.org/10.2478/s11696-009-0011-0.

Kemper, W.D. and Rosenau, R.C. (1986). Aggregate Stability and Size Distribution. *Methods of Soil Analysis, Part 1. Physical and Mineralogical Methods (2nd Edition)*. pp. 425–442.

Ketterhagen, W.R., Ende, M.T. am and Hancock, B.C. (2009). Process modeling in the pharmaceutical industry using the discrete element method. *Journal of Pharmaceutical Sciences* **98**(2):442–470. doi: https://doi.org/10.1002/jps.21466.

Khazam, O. and Kresta, S.M. (2008). Mechanisms of solids drawdown in stirred tanks. *The Canadian Journal of Chemical Engineering* **86**(4):622–634. doi: https://doi.org/10.1002/cjce.20077.

Khazam, O. and Kresta, S.M. (2009). A novel geometry for solids drawdown in stirred tanks. *Chemical Engineering Research and Design* **87**(3):280–290. doi: https://doi.org/10.1016/j.cherd.2008.09.013.

Kirchberg, S., Abdin, Y. and Ziegmann, G. (2011). Influence of particle shape and size on the wetting behavior of soft magnetic micropowders. *Powder Technology* **207**(1):311–317. doi: https://doi.org/10.1016/j.powtec.2010.11.012.

Kirdponpattara, S., Phisalaphong, M. and Newby, B.Z. (2013). Applicability of Washburn capillary rise for determining contact angles of powders/porous materials. *Journal of*

Colloid and Interface Science **397**:169–176. doi: https://doi.org/10.1016/j.jcis.2013.01.033.

Kiyohara, P.K., Santos, H.S., Coelho, A.C.V. and Santos, P.D.S. (2000). Structure, surface area and morphology of aluminas from thermal decomposition of Al(OH)(CH3COO)2 crystals. *Anais da Academia Brasileira de Ciências* **72**(4):471–495. doi: https://doi.org/10.1590/S0001-37652000000400003.

Koc, A., Silleli, H., Koc, C. and Dayioglu, M. (2007). Monitoring of Dry Powder Mixing With Real-Time Image Processing. *Journal of Applied Sciences*. doi: https://doi.org/10.3923/jas.2007.1218.1223.

Konstantinov, K.B. and Cooney, C.L. (2015). White Paper on Continuous Bioprocessing May 20–21 2014 Continuous Manufacturing Symposium. *Journal of Pharmaceutical Sciences* **104**(3):813–820. doi: https://doi.org/10.1002/jps.24268.

Koynov, S. (2015). *Using Statistical Methods to Optimize Powder Flow Measurements and to Predict Powder Processing Performance*. Rutgers University - Graduate School - New Brunswick.

Kranias, S. (2004). Effect of drop volume on static contact angles. *Kruus Application/Technical Notes*:2.

Kresta, S.M., III, A.W.E., Dickey, D.S., Atiemo-Obeng, V.A. and Forum, N.A.M. (eds.) (2015). *Advances in Industrial Mixing: A Companion to the Handbook of Industrial Mixing*. 2nd Revised ed. edition. Wiley-Blackwell.

Krieger, I.M. and Dougherty, T.J. (1959). A Mechanism for Non-Newtonian Flow in Suspensions of Rigid Spheres. *Transactions of the Society of Rheology* **3**:137–152.

Kukukova, A., Aubin, J. and Kresta, S.M. (2011). Measuring the scale of segregation in mixing data. *The Canadian Journal of Chemical Engineering* **89**(5):1122–1138. doi: https://doi.org/10.1002/cjce.20532.

Kumar, P., Kapur, P.C. and Saraf, D.N. (1975). Effect of zeta potential on apparent viscosity of settling suspensions. *Colloid and Polymer Science* **253**(9):738–743. doi: https://doi.org/10.1007/BF02464457.

Kumar, V., Taylor, M.K., Mehrotra, A. and Stagner, W.C. (2013). Real-Time Particle Size Analysis Using Focused Beam Reflectance Measurement as a Process Analytical Technology Tool for a Continuous Granulation–Drying–Milling Process. *AAPS PharmSciTech* **14**(2):523–530. doi: https://doi.org/10.1208/s12249-013-9934-4.

Lan, L.N., Kan, C.W., Yuen, M.C.W. and Lau, R.K.W. (2011). Study of the Correlation between Solid Colors Measured by Spectrophotometer and DigiEye. Thailand.

Laurent, B.F.C. and Bridgwater, J. (2002). Influence of agitator design on powder flow. *Chemical Engineering Science* **57**(18):3781–3793. doi: https://doi.org/10.1016/S0009-2509(02)00317-2.

Lechler (2017). Spray Nozzles and Systems – Creative Solutions in Spray Technology. *Lechler Brochures*.

Lemieux, M., Léonard, G., Doucet, J., Leclaire, L.-A., Viens, F., Chaouki, J. and Bertrand, F. (2008). Large-scale numerical investigation of solids mixing in a V-blender using the discrete element method. *Powder Technology* **181**(2):205–216. doi: https://doi.org/10.1016/j.powtec.2006.12.009.

Leturia, M., Benali, M., Lagarde, S., Ronga, I. and Saleh, K. (2014). Characterization of flow properties of cohesive powders: A comparative study of traditional and new testing methods. *Powder Technology* **253**:406–423. doi: https://doi.org/10.1016/j.powtec.2013.11.045.

Leyland, N.S., Evans, J.R.G. and Harrison, D.J. (2002). Lithographic printing of ceramics. *Journal of the European Ceramic Society* **22**(1):1–13. doi: https://doi.org/10.1016/S0955-2219(01)00247-3.

Lu, F.K. (2010). Surface oil flow visualization. *The European Physical Journal Special Topics* **182**(1):51–63. doi: https://doi.org/10.1140/epjst/e2010-01225-0.

Maciver, D.S., Tobin, H.H. and Barth, R.T. (1963). Catalytic aluminas I. Surface chemistry of eta and gamma alumina. *Journal of Catalysis* **2**(6):485–497. doi: https://doi.org/10.1016/0021-9517(63)90004-6.

Maltby, R.L., North Atlantic Treaty Organization, Advisory Group for Aeronautical Research and Development and Royal Aircraft Establishment (Great Britain) (1962). *Flow Visualization in Wind Tunnels Using Indicators,*. Parism: North Atlantic Treaty Organization, Advisory Group for Aeronautical Research and Development.

Mandø, M., Lightstone, M.F., Rosendahl, L., Yin, C. and Sørensen, H. (2009). Turbulence modulation in dilute particle-laden flow. *International Journal of Heat and Fluid Flow* **30**(2):331–338. doi: https://doi.org/10.1016/j.ijheatfluidflow.2008.12.005.

Marmur, A. (1996). Equilibrium contact angles: theory and measurement. *Colloids and Surfaces A: Physicochemical and Engineering Aspects* **116**(1–2):55–61. doi: https://doi.org/10.1016/0927-7757(96)03585-6.

McCarty, J.G., Gusman, M., Lowe, D.M., Hildenbrand, D.L. and Lau, K.N. (1999). Stability of supported metal and supported metal oxide combustion catalysts. *Catalysis Today* **47**(1):5–17. doi: https://doi.org/10.1016/S0920-5861(98)00279-X.

Melling, A. (1997). Tracer particles and seeding for particle image velocimetry. *Measurement Science and Technology* **8**(12):1406. doi: https://doi.org/10.1088/0957-0233/8/12/005.

Metzner, A.B. and Otto, R.E. (1957). Agitation of non-Newtonian fluids. *AIChE Journal* **3**(1):3–10. doi: https://doi.org/10.1002/aic.690030103.

Mewes, D. (2015). Visualization Techniques in Process Engineering. *chemanager online*.

Meyer, R.R. (1985). *In-Flight Surface Oil-Flow Photographs with Comparisons to Pressure Distribution and Boundary-Layer Data*.

Middleton, J.C. (1992). Gas Liquid Dispersion and Mixing. *Harnby N., Edwards M. F. and Nienow A. W.: Mixing in the Process Industries*. 2nd ed. Butterworth-Heinemann, pp. 322–363.

Milne, A.A. (1928). *The House at Pooh Corner*. Reissue edition. New York: Puffin.

Mogalicherla, A.K. and Kunzru, D. (2011). The Effect of Prewetting on the Loading of γ-Alumina Washcoated Cordierite Monolith. *International Journal of Applied Ceramic Technology* **8**(2):430–436. doi: https://doi.org/10.1111/j.1744-7402.2009.02441.x.

Montgomery, D.C. (2012). *Design and Analysis of Experiments*. 8th Edition edition. Hoboken, NJ: John Wiley & Sons.

Mueller, S., Llewellin, E.W. and Mader, H.M. (2010). The rheology of suspensions of solid particles. *Proceedings of the Royal Society of London A: Mathematical, Physical and Engineering Sciences* **466**(2116):1201–1228. doi: https://doi.org/10.1098/rspa.2009.0445.

Munnik, P., de Jongh, P.E. and de Jong, K.P. (2015). Recent Developments in the Synthesis of Supported Catalysts. *Chemical Reviews* **115**(14):6687–6718. doi: https://doi.org/10.1021/cr500486u.

Musha, H., Dong, K., Chandratilleke, G.R., Bridgwater, J. and Yu, A.B. (2013). Mixing behaviour of cohesive and non-cohesive particle mixtures in a ribbon mixer. pp. 731–734.

Musil, J., Blažek, J., Zeman, P., Prokšová, Š., Šašek, M. and Čerstvý, R. (2010). Thermal stability of alumina thin films containing γ-Al2O3 phase prepared by reactive magnetron sputtering. *Applied Surface Science* **257**(3):1058–1062. doi: https://doi.org/10.1016/j.apsusc.2010.07.107.

Muzzio, F.J., Llusa, M., Goodridge, C.L., Duong, N.-H. and Shen, E. (2008). Evaluating the mixing performance of a ribbon blender. *Powder Technology* **186**(3):247–254. doi: https://doi.org/10.1016/j.powtec.2007.12.013.

Naidu, D.V. and Raol, J.R. (2008). Pixel-level Image Fusion using Wavelets and Principal Component Analysis. *Defence Science Journal* **58**. doi: https://doi.org/10.14429/dsj.58.1653.

Nam, K., Lim, S., Kim, S.-K., Peck, D. and Jung, D. (2011). Mechanical milling of catalyst support for enhancing the performance in fuel cells. *Powder Technology - POWDER TECHNOL* **214**:423–430. doi: https://doi.org/10.1016/j.powtec.2011.08.041.

Nienow, A.W., Edwards, M.F. and Harnby, N. (1997). *Mixing in the Process Industries: Second Edition*. Butterworth-Heinemann.

Nowak, E., Combes, G., Stitt, E.H. and Pacek, A.W. (2013). A comparison of contact angle measurement techniques applied to highly porous catalyst supports. *Powder Technology* **233**:52–64. doi: https://doi.org/10.1016/j.powtec.2012.08.032.

Nowak, E., Robbins, P., Combes, G., Stitt, E.H. and Pacek, A.W. (2013). Measurements of contact angle between fine, non-porous particles with varying hydrophobicity and water and non-polar liquids of different viscosities. *Powder Technology* **250**:21–32. doi: https://doi.org/10.1016/j.powtec.2013.09.001.

Owens, D.K. and Wendt, R.C. (2003). Estimation of the surface free energy of polymers. *Journal of Applied Polymer Science* **13**(8):1741–1747. doi: https://doi.org/10.1002/app.1969.070130815.

Özcan-Taşkin, G. (2006). Effect of scale on the draw down of floating solids. *Chemical Engineering Science* **61**(9):2871–2879. doi: https://doi.org/10.1016/j.ces.2005.10.061.

Özcan-Taşkin, G. and McGrath, G. (2001). Draw Down of Light Particles in Stirred Tanks. *Chemical Engineering Research and Design* **79**(7):789–794. doi: https://doi.org/10.1205/026387601753191966.

Özcan-Taşkin, G. and Wei, H. (2003). The effect of impeller-to-tank diameter ratio on draw down of solids. *Chemical Engineering Science* **58**(10):2011–2022. doi: https://doi.org/10.1016/S0009-2509(03)00024-1.

Özcan-Taşkın, G.N. (2012). INCORPORATION OF NANOPARTICLE CLUSTERS INTO A LIQUID USING A PROPRIETARY DESIGN MIXER- YTRON Y JET. Warszawa, pp. 347–352.

Park, J. and Regalbuto, J.R. (1995). A Simple, Accurate Determination of Oxide PZC and the Strong Buffering Effect of Oxide Surfaces at Incipient Wetness. *Journal of Colloid and Interface Science* **175**(1):239–252. doi: https://doi.org/10.1006/jcis.1995.1452.

Pavlik, M. (2011). *The Dependence of Suspension Viscosity on Particle Size, Shear Rate, and Solvent Viscosity*. DePaul University.

Pearson, K. (1901). LIII. On lines and planes of closest fit to systems of points in space. *The London, Edinburgh, and Dublin Philosophical Magazine and Journal of Science* **2**(11):559–572. doi: https://doi.org/10.1080/14786440109462720.

Pernenkil, L. and Cooney, C.L. (2006). A review on the continuous blending of powders. *Chemical Engineering Science* **61**(2):720–742. doi: https://doi.org/10.1016/j.ces.2005.06.016.

Pitts, K.L. and Fenech, M. (2013). Micro-particle Image Velocimetry for Velocity Profile Measurements of Micro Blood Flows. *Journal of Visualized Experiments : JoVE*(74). doi: https://doi.org/10.3791/50314.

Plumb, K. (2005). Continuous Processing in the Pharmaceutical Industry: Changing the Mind Set. *Chemical Engineering Research and Design* **83**(6):730–738. doi: https://doi.org/10.1205/cherd.04359.

Poechlauer, P., Colberg, J., Fisher, E., Jansen, M., Johnson, M.D., Koenig, S.G., … O'Kearney-McMullan, A. (2013). Pharmaceutical Roundtable Study Demonstrates the Value of Continuous Manufacturing in the Design of Greener Processes. *Organic Process Research & Development* **17**(12):1472–1478. doi: https://doi.org/10.1021/op400245s.

Poechlauer, P., Manley, J., Broxterman, R., Gregertsen, B. and Ridemark, M. (2012). Continuous Processing in the Manufacture of Active Pharmaceutical Ingredients and Finished Dosage Forms: An Industry Perspective. *Organic Process Research & Development* **16**(10):1586–1590. doi: https://doi.org/10.1021/op300159y.

Portillo, P.M., Ierapetritou, M.G. and Muzzio, F.J. (2008). Characterization of continuous convective powder mixing processes. *Powder Technology* **182**(3):368–378. doi: https://doi.org/10.1016/j.powtec.2007.06.024.

Post Mixing Optimizations and Solutions (2017). *Impellers*. Available at: http://www.postmixing.com/mixing%20forum/impellers/impellers.htm.

Prescott, J.K. and Barnum, R.A. (2000). On powder flowability. *Pharmaceutical Technology* **24**:60–85.

Rabel, W. (1971). Einige Aspekte der Benetzungstheorie und ihre Anwendung auf die Untersuchung und Veränderung der Oberflächeneigenschaften von Polymeren. *Farbe und Lacke* **77**(10):997–1005.

Raffel, M., Willert, C.E., Wereley, S.T. and Kompenhans, J. (2007). *Particle Image Velocimetry: A Practical Guide*. Springer.

Ramsay, J., Simmons, M.J.H., Ingram, A. and Stitt, E.H. (2016). Mixing of Newtonian and viscoelastic fluids using "butterfly" impellers. *Chemical Engineering Science* **139**:125–141. doi: https://doi.org/10.1016/j.ces.2015.09.026.

Realpe, A. and Velazquez, C. (2003). Image processing and analysis for determination of concentration of powder mixtures. *Powder Technology* **134**:193. doi: https://doi.org/10.1016/S0032-5910(03)00138-4.

Remy, B., Khinast, J.G. and Glasser, B.J. (2009). Discrete element simulation of free flowing grains in a four-bladed mixer. *AIChE Journal* **55**(8):2035–2048. doi: https://doi.org/10.1002/aic.11876.

Rouquerol, J., Rouquerol, F., Llewellyn, P., Maurin, G. and Sing, K.S.W. (2013). *Adsorption by Powders and Porous Solids: Principles, Methodology and Applications*. Academic Press.

Rushton, J.H., Costich, E.W. and Everett, H.J. (1950). Power characteristics of mixing impeller I and II. *Chem. Eng. Prog.* **46**(8):395.

Ruthiya, K.C., van der Schaaf, J., Kuster, B.F.M. and Schouten, J.C. (2005). Similar effect of carbon and silica catalyst support on the hydrogenation reaction rate in organic slurry reactors. *Chemical Engineering Science* **60**(22):6492–6503. doi: https://doi.org/10.1016/j.ces.2005.03.034.

Samain, L., Jaworski, A., Edén, M., Ladd, D.M., Seo, D.-K., Javier Garcia-Garcia, F. and Häussermann, U. (2014). Structural analysis of highly porous γ-Al2O3. *Journal of Solid State Chemistry* **217**:1–8. doi: https://doi.org/10.1016/j.jssc.2014.05.004.

Sandler, N., Reiche, K., Heinämäki, J. and Yliruusi, J. (2010). Effect of Moisture on Powder Flow Properties of Theophylline. *Pharmaceutics* **2**(3):275–290. doi: https://doi.org/10.3390/pharmaceutics2030275.

Schröder, A. and Willert, C.E. (eds.) (2008). *Particle Image Velocimetry: New Developments and Recent Applications*. Berlin Heidelberg: Springer-Verlag.

Schulze, D. (2008). Powders and Bulk Solids.

Sharp, K.V. and Adrian, R.J. (2001). PIV study of small-scale flow structure around a Rushton turbine. *AIChE Journal* **47**(4):766–778. doi: https://doi.org/10.1002/aic.690470403.

Sherritt, R.G., Chaouki, J., Mehrotra, A.K. and Behie, L.A. (2003). Axial dispersion in the three-dimensional mixing of particles in a rotating drum reactor. *Chemical Engineering Science* **58**(2):401–415. doi: https://doi.org/10.1016/S0009-2509(02)00551-1.

Siddiqui, H. (1993). Mixing technology for buoyant solids in a nonstandard vessel. *AIChE Journal* **39**(3):505–509. doi: https://doi.org/10.1002/aic.690390312.

e Silva, J.P.S., Splendor, D., Gonçalves, I.M.B., Costa, P. and Sousa Lobo, J.M. (2013). Note on the Measurement of Bulk Density and Tapped Density of Powders According to the European Pharmacopeia. *AAPS PharmSciTech* **14**(3):1098–1100. doi: https://doi.org/10.1208/s12249-013-9994-5.

Silverson Machines Inc. (2018). Silverson Powder/Liquid Mixers.

Sjöblom, J., Svensson, O., Josefson, M., Kullberg, H. and Wold, S. (1998). An evaluation of orthogonal signal correction applied to calibration transfer of near infrared spectra. *Chemometrics and Intelligent Laboratory Systems* **44**(1):229–244. doi: https://doi.org/10.1016/S0169-7439(98)00112-9.

Smith, P.G. and Merritt, G.M. (2002). *Proactive Risk Management: Controlling Uncertainty in Product Development*. 1 edition. New York, NY: Productivity Press.

Spieker, W.A. and Regalbuto, J.R. (2001). A fundamental model of platinum impregnation onto alumina. *Chemical Engineering Science* **56**(11):3491–3504. doi: https://doi.org/10.1016/S0009-2509(01)00052-5.

Stitt, E.H. (2014). *Managing Technical Risk in Innovative & Capital Projects*. Johnson Matthey.

Stitt, E.H. (2016). Models of Good Behaviour. *The Chemical Engineer*:33–36.

Svanberg, S. (2003). *Atomic and Molecular Spectroscopy: Basic Aspects and Practical Applications*. 4th ed. 2004. Springer.

Takahashi, K. and Sasaki, S. (1999). Complete Drawdown and Dispersion of Floating Solids in Agitated Vessel Equipped with Ordinary Impellers. *Journal of Chemical Engineering of Japan* **32**(1):40–44. doi: https://doi.org/10.1252/jcej.32.40.

Thring, R.W. and Edwards, M.F. (1990). An experimental investigation into the complete suspension of floating solids in an agitated tank. *Industrial & Engineering Chemistry Research* **29**(4):676–682. doi: https://doi.org/10.1021/ie00100a029.

Tran, T.N., Afanador, N.L., Buydens, L.M.C. and Blanchet, L. (2014). Interpretation of variable importance in Partial Least Squares with Significance Multivariate Correlation (sMC). *Chemometrics and Intelligent Laboratory Systems* **138**:153–160. doi: https://doi.org/10.1016/j.chemolab.2014.08.005.

Twigg, M.V. (2007). Progress and future challenges in controlling automotive exhaust gas emissions. *Applied Catalysis B: Environmental* **70**(1):2–15. doi: https://doi.org/10.1016/j.apcatb.2006.02.029.

Twigg, M.V. (2015). Urea-SCR Technology for deNOx After Treatment of Diesel Exhausts. *Johnson Matthey Technology Review* **59**(3):221.

Unadkat, H., Nagy, Z.K. and Rielly, C.D. (2013). Investigation of turbulence modulation in solid–liquid suspensions using parallel competing reactions as probes for micro-mixing efficiency. *Chemical Engineering Research and Design* **91**(11):2179–2189. doi: https://doi.org/10.1016/j.cherd.2013.05.005.

Vanarase, A.U. (2011). *Design, Modeling and Real-Time Monitoring of Continuous Powder Mixing Processes*. Rutgers University - Graduate School - New Brunswick.

Vanarase, A.U., Osorio, J.G. and Muzzio, F.J. (2013). Effects of powder flow properties and shear environment on the performance of continuous mixing of pharmaceutical powders. *Powder Technology* **246**:63–72. doi: https://doi.org/10.1016/j.powtec.2013.05.002.

Vasilenko, A., Glasser, B.J. and Muzzio, F.J. (2011). Shear and flow behavior of pharmaceutical blends — Method comparison study. *Powder Technology* **208**(3):628–636. doi: https://doi.org/10.1016/j.powtec.2010.12.031.

Voelkel, A., Strzemiecka, B., Adamska, K. and Milczewska, K. (2009). Inverse gas chromatography as a source of physiochemical data. *Journal of Chromatography A* **1216**(10):1551–1566. doi: https://doi.org/10.1016/j.chroma.2008.10.096.

Waghmare, Y., Falk, R., Graham, L. and Koganti, V. (2011). Drawdown of floating solids in stirred tanks: Scale-up study using CFD modeling. *International Journal of Pharmaceutics* **418**(2):243–253. doi: https://doi.org/10.1016/j.ijpharm.2011.05.039.

Wang, Y., Li, T., Muzzio, F.J. and Glasser, B.J. (2017a). Predicting feeder performance based on material flow properties. *Powder Technology* **308**:135–148. doi: https://doi.org/10.1016/j.powtec.2016.12.010.

Wangler, J. and Kohlus, R. (2017). Dynamics of Capillary Wetting of Biopolymer Powders. *Chemical Engineering & Technology* **40**(9):1552–1560. doi: https://doi.org/10.1002/ceat.201600607.

Washburn, E.W. (1921). The Dynamics of Capillary Flow. *Physical Review* **17**(3):273–283. doi: https://doi.org/10.1103/PhysRev.17.273.

Weinekötter, R. and Gericke, H. (2006). *Mixing of Solids*. 1st ed. 2000. Corr. 2nd printing 2006 edition. Dordrecht: Springer.

Welch, W.J. (1982). Branch-and-Bound Search for Experimental Designs Based on D Optimality and Other Criteria. *Technometrics* **24**(1):41–48. doi: https://doi.org/10.1080/00401706.1982.10487707.

Williams, J.L. (2001). Monolith structures, materials, properties and uses. *Catalysis Today* **69**(1):3–9. doi: https://doi.org/10.1016/S0920-5861(01)00348-0.

Wise, B.M. and Gallagher, N.B. (1996). The process chemometrics approach to process monitoring and fault detection. *Journal of Process Control* **6**(6):329–348. doi: https://doi.org/10.1016/0959-1524(96)00009-1.

Wold, S., Sjöström, M. and Eriksson, L. (2001). PLS-regression: a basic tool of chemometrics. *Chemometrics and Intelligent Laboratory Systems* **58**(2):109–130. doi: https://doi.org/10.1016/S0169-7439(01)00155-1.

Wood, T., Simmons, M.J.H., Greenwood, R.W. and Stitt, E.H. (2018). Concentrated slurry formation via drawdown and incorporation of wettable solids in a mechanically agitated vessel. *AIChE Journal* **64**(5):1885–1895. doi: https://doi.org/10.1002/aic.16121.

Wood, T., Simmons, M.J.H. and Stitt, E.H. (2018). Optimisation of stirred vessel geometry for the drawdown and incorporation of floating solids to prepare concentrated slurries.

Chemical Engineering Research and Design **133**:70–78. doi: https://doi.org/10.1016/j.cherd.2018.03.002.

Xie, L., Rielly, C.D., Eagles, W. and Özcan-Taşkin, G. (2007). Dispersion of Nano-Particle Clusters Using Mixed Flow and High Shear Impellers in Stirred Tanks. *Chemical Engineering Research and Design* **85**(5):676–684. doi: https://doi.org/10.1205/cherd06195.

Yan, N., Maham, Y., Masliyah, J.H., Gray, M.R. and Mather, A.E. (2000). Measurement of Contact Angles for Fumed Silica Nanospheres Using Enthalpy of Immersion Data. *Journal of Colloid and Interface Science* **228**(1):1–6. doi: https://doi.org/10.1006/jcis.2000.6856.

Yang, Y., Zhang, S., Wang, S., Zhang, K., Wang, H., Huang, J., … Yu, G. (2015). Ball Milling Synthesized MnOx as Highly Active Catalyst for Gaseous POPs Removal: Significance of Mechanochemically Induced Oxygen Vacancies. *Environmental Science & Technology* **49**(7):4473–4480. doi: https://doi.org/10.1021/es505232f.

Yeow, S.T., Shahar, A., Aziz, N.A., Anuar, M.S., Yusof, Y.A. and Taip, F.S. (2011). The influence of operational parameters and feed preparation in a convective batch ribbon powder mixer. *Drug Design, Development and Therapy* **5**:465–469. doi: https://doi.org/10.2147/DDDT.S25047.

Yokosawa, M.M., Pandolfelli, V.C. and Frollini, E. (2002). Influence of pH and Time on the Stability of Aqueous Alumina Suspensions Containing Sodium Polyacrylates: A Revisited Process. *Journal of Dispersion Science and Technology* **23**(6):827–836. doi: https://doi.org/10.1081/DIS-120015979.

Young, T. (1805). An Essay on the Cohesion of Fluids. *Philosophical Transactions of the Royal Society of London* **95**:65–87.

Yousif, M.Y., Holdsworth, D.W. and Poepping, T.L. (2009). Deriving a blood-mimicking fluid for particle image velocimetry in Sylgard-184 vascular models. *Conference proceedings: ... Annual International Conference of the IEEE Engineering in Medicine and Biology Society. IEEE Engineering in Medicine and Biology Society. Annual Conference* **2009**:1412–1415. doi: https://doi.org/10.1109/IEMBS.2009.5334175.

YTRON Process Technology GmbH (2018). *YTRON ZC Powder Disperser*. Available at: http://www.ytron.com/en/products/ytron-zc-powder-disperser/.

Zwietering, T.N. (1958). Suspending of solid particles in liquid by agitators. *Chemical Engineering Science* **8**(3–4):244–253. doi: https://doi.org/10.1016/0009-2509(58)85031-9.

Appendix 1 – Pump Calibration

The peristaltic pump used in Chapter 4 was calibrated by recording the mass of liquid delivered in one minute at a series of pump settings. This was repeated five times at each pump setting. A linear regression was then fit through these data to give the mass delivery rate from the pump as a function of the pump setting. The calibration plot is shown in Figure 9-1.

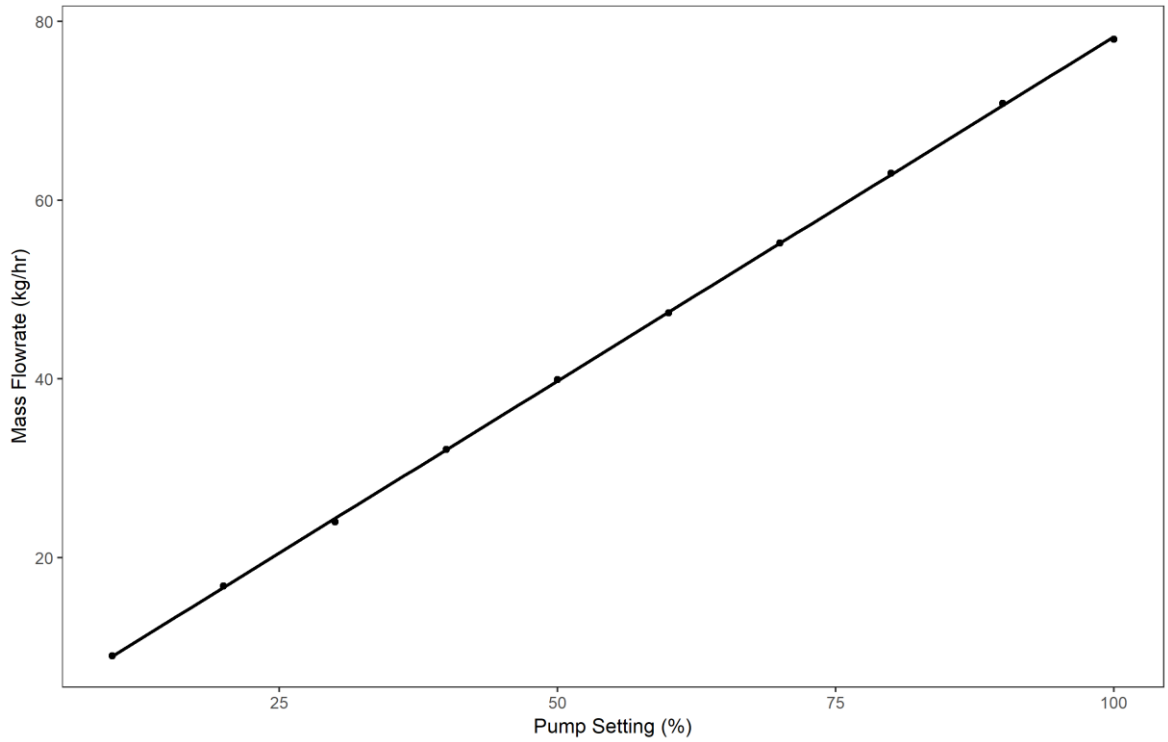

Figure 9-1: Example pump calibration curve for peristaltic pump used in Chapter 4